Following Neuropeptide Secretion

Puntman, Daniël Chris

2022

document version
Publisher's PDF, also known as Version of record

Following neuropeptide secretion:

Role of SM-proteins in neuropeptide secretion from

DENSE CORE VESICLES

Daniël Puntman

Following Neuropeptide Secretion

The role of SM-proteins in Dense Core Vesicle exocytosis

Daniël Puntman

Colophon
Following Neuropeptide Secretion
The role of SM proteins in Dense Core Vesicle exocytosis
Daniël C. Puntman

The research described in this thesis was conducted at the department of Functional Genomics, Center for Neurogenomics and Cognitive Research, Neuroscience Campus Amsterdam, VU University Amsterdam, The Netherlands.

Illustrations by dr. Sanne Remmelzwaal
Printed by Ridderprint | www.ridderprint.nl

VRIJE UNIVERSITEIT

Following Neuropeptide Secretion
The role of SM proteins in Dense Core vesicle exocytosis

ACADEMISCH PROEFSCHRIFT

ter verkrijging van de graad Doctor of Philosophy
aan de Vrije Universiteit Amsterdam,
op gezag van de rector magnificus
prof.dr. J.J.G. Geurts,
in het openbaar te verdedigen
ten overstaan van de promotiecommissie
van de Faculteit der Bètawetenschappen
op vrijdag 16 september 2022 om 11.45 uur
in een bijeenkomst van de universiteit,
De Boelelaan 1105

door

Daniël Chris Puntman

geboren te Deventer

promotor:	prof.dr. M. Verhage
copromotor:	dr. R.F.G. Toonen
promotiecommissie:	prof.dr. D. Thurmond prof.dr. C.A. Lohmann dr. W. Scheper dr. H.D. MacGillavry prof.dr. S.E. La Fleur

Table of contents

Chapter 1

Introduction

For proper brain function, neuronal communication is driven by secretion and subjected to profound regulation. Fast transmission of information between neurons occurs via neurotransmitters at specialized compartments called synapses. To build, maintain and support synaptic transmission, many factors are regulated, including the extracellular matrix for plasticity, energy homeostasis and insertion of neurotransmitter receptors and cell adhesion molecules into the plasma membrane. An additional level of regulation is managed by neuropeptide signaling, which modulates synaptic transmission and neuronal activity. Neuropeptides control diverse brain functions such as memory, appetite and mood (Cropper *et al.*, 2018; Comeras, Herzog and Tasan, 2019; Miranda *et al.*, 2019), but the mechanisms that drive neuropeptide release from dense core vesicles (DCVs) remain incompletely understood.

1.1 Secretion drives Neuronal communication

Neurons are far from unique in their ability to secrete substances. In fact, all cells have some version of secretion and many cell types are specialized herein. A first distinction is made between constitutive and regulated secretion. Constitutive secretion is driven by an ongoing stream of vesicles that come from the Golgi and undergo exocytosis whenever they reach the plasma membrane (For a review see: Ponnambalam and Baldwin, 2003). Regulated secretion is an umbrella definition that covers all types of exocytosis that require a certain trigger. Often regulated secretion depends on calcium signaling, but especially neurons have several parallel pathways of regulated secretion which all react differently to triggers. Here, the regulated secretion pathways in neurons are introduced.

1.1.1. Synaptic transmission

Making up the basis for neuronal communication, synaptic transmission is evolved to be fast, efficient and tightly regulated. Neurotransmitter release from synaptic vesicles already occurs upon a single action potential, but higher quantities are released during burst-firing (Watanabe et al., 2013; Williams and Stuart, 1999). In contrast to many other secretory vesicles, synaptic vesicles (SVs) are locally generated and recycled many times via membrane reuptake and reloading with neurotransmitters (For a review see: Hannah et al., 1999). SVs release their cargo (mainly neurotransmitters such as glutamate or GABA; γ-Aminobutyric acid) in the synaptic cleft, where a high concentration of neurotransmitters builds-up and is readily detected by postsynaptic ionotropic receptors.

Based on high-pressure freezing electron microscopy (EM) findings, it is proposed that upon exocytosis of SVs, immediate reuptake of synaptic membrane (ultra-fast endocytosis) occurs in order to recycle the vesicles, but also to keep the synaptic plasma membrane tight for efficient secretion (Watanabe et al., 2013, 2018). The newly endocytosed membrane may be directed to a structure named the ''synaptic endosome'', from which clathrin-dependent budding generates new SVs (Watanabe et al., 2014). The clathrin coats readily fall off before SVs arrive at the active zone. This proposed mechanism explains how the readily releasable SV pool may be efficiently recycled, which is sufficient to support normal synaptic transmission.

Alternatively, recycling of SVs may occur via incomplete exocytosis via so called ''kiss-and-run'' events, which were often observed in non-neuronal secretory cells (Alés et al., 1999; for a review see: Burgoyne et al., 2001). Several observations also indicate the occurrence of SV kiss-and-run events in mammalian synapses (Qi et al., 2009; Stevens and Williams, 2000; for a review see: Chanaday et al., 2019), however, due to the sporadic nature of these observations, it remains uncertain whether these events play a major role in SV recycling. Upon higher activity, SVs from the reserve pool additionally participate in exocytosis. These are then refilled via a much slower form of endocytosis: clathrin dependent bulk endocytosis (Clayton et al., 2008; Granseth et al., 2006). These tight regulations enable fast and efficient secretion of neurotransmitters, with minimal loss of specialized membrane. Other secretion pathways help regulating or supporting neurotransmission as will be discussed below.

1.1.2. Neuropeptide signaling

Neuropeptide signaling is a common widespread system in which most, if not all, neurons are participating. Neurons in the central nervous system (CNS) express many neuropeptides and neuropeptide receptors. Just based on expression of 47 neuropeptide signaling genes measured via single cell RNA sequencing, mouse CNS neurons can be grouped together per neuron subtype (Smith et al., 2019). This reveals extensive neuropeptide signaling networks in the brain, with each neuron type having its own hallmark of expressed neuropeptide and receptor genes.

Most receptors activated by neuropeptides are G-protein coupled receptors (GPCRs) (For reviews see: Hoyer and Bartfai, 2012; Krishnan and Schiöth, 2015; van den Pol, 2012). Many GPCRs have not yet been identified. In general, ligand binding to GPCRs leads to second messenger cascades directing various quick cellular responses (via kinases etc.), but also mediating slower responses via changes in transcription (For a review see: Hamm, 1998). In this way, neuropeptide secretion supports many brain functions. For example, NPY secretion regulates appetite, stress and supports neural proliferation and outgrowth, via interaction with several GPCRs called Y receptors (For reviews see: Comeras et al., 2019; Hansel et al., 2001; Reichmann and Holzer, 2016). In addition, endogenous opioid proteins such as enkephalins, endorphins and dynorphins bind act via specific GPCRs called opioid receptors and regulate pain (For reviews see: Brownstein, 1993; Elphick et al., 2018; Jékely, 2013; Stein, 2016). Brain derived neurotrophic growth factor (BDNF) acts on a different type of receptor: the tropomyosin kinase B (TrkB) receptor, via which BDNF stimulates neural growth and differentiation, and regulates synaptic plasticity (Kowiański et al., 2018). More specifically, many neuropeptides regulate neurotransmission, as for example NPY has an inhibiting effect on synaptic transmission and BDNF a stimulating effect (Collin et al., 2001; Raposinho et al., 1999; Shinoda et al., 2014; Tartaglia et al., 2001; Tschenett et al., 2003; Tyler and Pozzo-Miller, 2001). Therefore, neuropeptides modulate synaptic transmission in acute and sustained ways.

1.1.3 Other pathways supporting or exhibiting neuronal signaling

Exocytosis of glutamate receptors and glucose transporter 4 supports synaptic transmission

Several other secretion pathways are also important to support or modulate synaptic transmission. AMPA and NMDA receptors are inserted in the postsynaptic plasma membrane via exocytosis of endosomal organelles, or removed via endocytosis, which alters the postsynaptic response to glutamate (Derkach et al., 2007; Rao and Finkbeiner,

2007). Upon repeated firing, presynapses have to meet an increasing energy demand. The increased exocytosis and endocytosis costs energy, but especially the refilling of recycled SVs with neurotransmitters via V-ATPases requires many ATP molecules. In order to support these energy demands, neurons may increase glucose transporter 4 (GLUT4) insertion into the presynaptic plasma membrane by exocytosis of GLUT4 vesicles (Ashrafi et al., 2017). Without GLUT4, neurons fail to support SV recycling during sustained firing.

Lysosomal exocytosis supports synaptic plasticity

Lysosomes may have a role in synaptic plasticity by secretion of extracellular matrix (ECM) modulating factors. Dendritic lysosomes in hippocampal pyramidal neurons responded to back-propagating action potentials by undergoing exocytosis at dendritic spines (Padamsey et al., 2017). The resulting secretion of Cathepsin B increases activity of matrix metalloproteinase 9 (MMP-9) and leads to degradation of the ECM, which supports structural synaptic changes. A different study in cerebellar granule cells also shows activity dependent exocytosis of axonal lysosomes (Ibata et al., 2019). These lysosomes release Cathepsin B and additionally co-release synaptic organizer Cbln1, which binds to presynaptic neurexin and postsynaptic δ2 glutamate receptors. Overexpression of lysosomal exocytosis inhibitors Neu1 and Cathepsin A decrease secretion of Cathepsin B and Cbln1, and reduce axonal bouton formation. Therefore, activity dependent lysosomal exocytosis at dendrites and axons may support both presynaptic and postsynaptic structural changes that occur during synaptic plasticity.

Exosome release from Multivesicular bodies

In addition to these secretion pathways to mediate and support synaptic transmission, neurons may also transfer information in a different way via exosomes (Smalheiser, 2007). Exosomes originate from Multivesicular bodies (MVBs), which are organelles that form from endosomes when these internalize vesicles containing cytoplasm. When these MVBs undergo exocytosis, the cytoplasm containing vesicles called exosomes are secreted. Alternatively, exosomes may directly form from the plasma membrane. Exosomes contain all kinds of proteins and RNAs originating from the cytoplasm and can transfer these to other cells, in that way changing their internal milieu (For a review on exosome biogenesis and secretion see: Colombo et al., 2014). Especially RNAs have the potential to regulate many processes in the receiving cell by changing protein expression. Although regulated MVB exocytosis has not been shown yet in neurons, this type of secretion occurs in response to stimulation of the histamine H1 receptor in Hela cells (Verweij et al., 2018). Therefore, MVB exocytosis is potentially a powerful way of cell to cell signaling without requiring receptors and having a different mode of action.

Non-vesicular neuronal signaling pathways

In addition to these secretion pathways, neuronal signaling may occur in various other ways. Some neurons are connected via gap junctions, resulting in direct electrical coupling due to direct passing of electrons and ions from cell to cell, which helps to synchronize activity (Bennett and Zukin, 2004). Signaling can also occur via cell to cell interactions, which are amongst others mediated by synaptic cell adhesion molecules (i.e. integrins, neurexin/neuroligin, N-cadherin) and are important for correct synaptic assembly of the brain during development (For reviews see: Missler et al., 2012; Park and Goda, 2016; De Wit and Ghosh, 2016). Other signaling pathways in the brain may rely on membrane permeable metabolites such as endocannabinoids (For a review

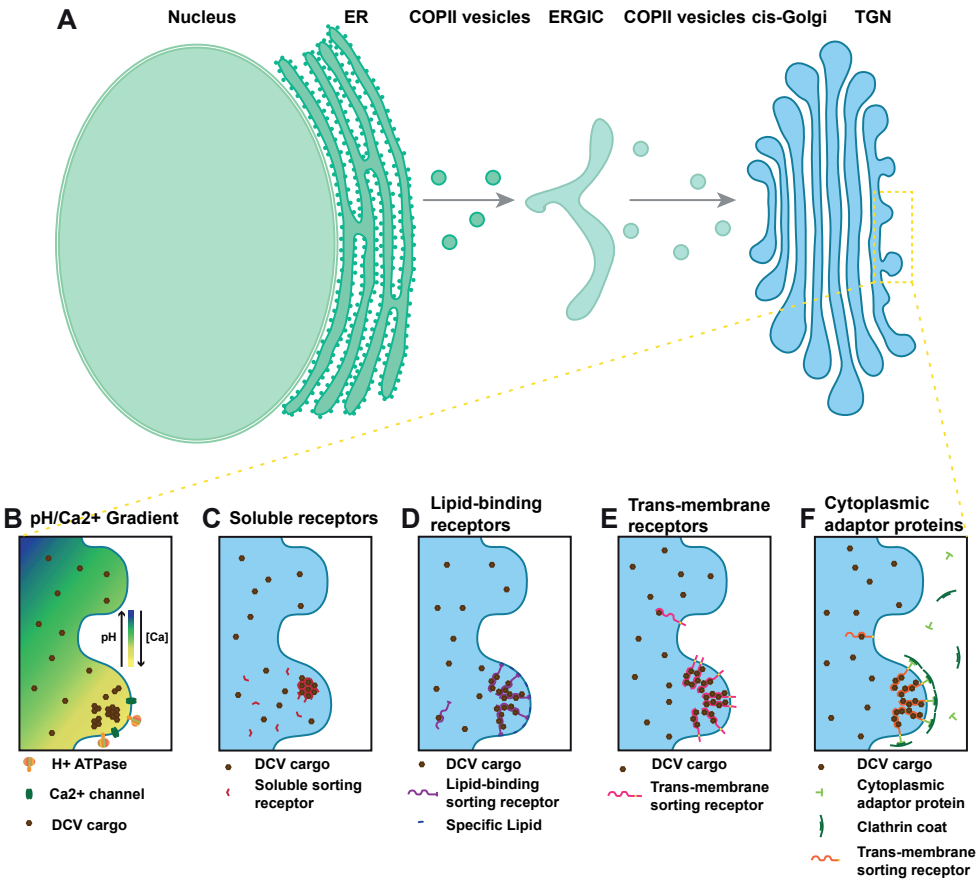

Figure 1. The route of newly synthesized DCV cargo from ER to TGN. (**A**) Depicted from left to right, the organelles through which DCV cargo and precursors travel during DCV biogenesis. DCV cargo genes are transcribed in the nucleus, their mRNA is translated in the ER, from where the newly synthesized pre-pro-neuropeptides exit via COPII vesicles after cleavage of the pre-part. From there, cargo travels via the ERGIC and again COPII vesicles to the cis-Golgi and travels through the Golgi Apparatus to the TGN, where cargo sorting occurs. (**B**) Insert shows zoom of TGN with the low-pH, high-calcium sorting model for DCV cargo, where H+ ATPases and Calcium channels locally elevate calcium and proton concentration, initiating DCV cargo aggregation and formation of a new DCV. (**C**) Insert shows soluble cargo receptors as a model for aggregating DCV cargo. (**D**) Insert shows lipid-binding DCV cargo receptors as a model for accumulating/aggregating DCV cargo and initiating budding from the TGN. (**E**) Insert shows Trans-membrane DCV cargo receptors as a model for accumulation and aggregation of DCV cargo and initiation of DCV budding from the TGN. (**F**) Insert shows a model for DCV cargo accumulation/aggregation and budding from the TGN where cytoplasmic adaptor proteins form a clathrin coat and bind to TGN trans-membrane proteins, thereby linking vesicular budding to aggregation/accumulation of the content.

see: Lovinger, 2007) or NO (Park et al., 1998) to target receptors from nearby neurons. However, this thesis will further focus on the neuropeptide secretion pathway.

Neuromodulation via neuropeptide secretion is involved in brain functions such as: sleep, fear, memory, appetite, cognition and mood (Cropper *et al.*, 2018; Comeras, Herzog and Tasan, 2019; Miranda *et al.*, 2019). In addition, neuropeptide genes are linked to several neurological and psychiatric diseases, including depression, schizophrenia and epilepsy (For reviews see: Griebel and Holsboer, 2012; Nestor et al., 2019; Werner and Coveñas, 2010). Despite the importance of neuropeptide secretion, many basic questions about the generation and exocytosis of neuropeptide vesicles remain unanswered. Below,

the current working models about the generation and exocytosis of neuropeptide vesicles, as well as the steps in between, will be discussed. Additionally, the function of SM-proteins, one of the core secretory proteins, will be specifically introduced and discussed.

1.2 DCV biogenesis

To regulate neuropeptide secretion apart from synaptic transmission and other signaling pathways, neurons package neuropeptides in dense core vesicles (DCVs). These vesicles are ~70nm in diameter and are recognized by their dense core in electron microscopy (EM). Secretion from DCVs is highly regulated and mainly occurs upon prolonged electrical activity. Vesicles from other secretory cells with similar dense cores and cargo containing peptides and hormones are here referred to as secretory granules (SGs). Most studies on biogenesis focus on SGs in non-neuronal cell-types. This section describes DCV biogenesis by summarizing the route of newly synthesized DCV/SG cargo from the ER, through the Golgi apparatus to the TGN and sorting mechanisms at the TGN, and describes DCV maturation by focusing on post-TGN changes to the vesicles.

1.2.1 The route of newly synthesized neuropeptides from ER to TGN

The first step in the biogenesis of new DCVs is neuropeptide gene transcription. Translation of these mRNAs occurs at the ER, where the newly synthesized pre-pro-neuropeptides are internalized and only exit after cleavage of the ER retention signal (pre- part). The pro-neuropeptides then translocate via COPII (protein complex II) vesicles to the ERGIC (ER-Golgi intermediate compartment), where ER-resident proteins are sorted away (Fig. 1A). Secretory cargo including pro-neuropeptides travels further via COPII vesicles to the cis Golgi, a polarized structure consisting of flattened cisternae that are interconnected (for reviews on ER to Golgi trafficking see: Brandizzi and Barlowe, 2013; Zanetti et al., 2012) (Fig. 1A). This newly synthesized cargo undergoes posttranslational modifications (such as glycosylation, ubiquitination) that support correct protein folding and functionality, while translocating through the Golgi to the TGN (for reviews on modifications see: Fisher and Ungar, 2016; De Graffenried and Bertozzi, 2004). At the TGN, secretory cargo is separated and pro-neuropeptides are sorted and packaged into SGs or DCVs (For reviews see: Dikeakos and Reudelhuber, 2007; Kim et al., 2006), while other cargo is directed to endosomes, lysosomes or the plasma membrane (For reviews see: Boncompain and Perez, 2013; Bonnemaison et al., 2013).

1.2.2. TGN acidity and calcium support SG cargo aggregation

The cargo sorting step from the TGN to the corresponding vesicles is referred to as ''Sorting by entry''. Several factors may be important for sorting by entry, including TGN pH and calcium (Fig. 1B), and the presence of sorting receptors (For reviews see: Bonnemaison et al., 2013; Kim et al., 2006). Sorting receptors are luminal/soluble (Fig. 1C), lipid binding (Fig. 1D) or transmembrane proteins (Fig. 1E) that bind secretory cargo and that cluster and select for the appropriate secretion pathway. Within single neurons, multiple neuropeptides are expressed, of which it is currently unknown whether they are sorted to different DCVs, or packaged together. However, it is clear that

cargo sorting between secretory pathways at the TGN is essential for neurons, since many secretory pathways are active simultaneously. Here, different modes of cargo sorting at the TGN are introduced.

Cargo sorting may depend on TGN pH and calcium

The acidic pH (~6,8) and high calcium concentration in the TGN are thought to help secretory cargo aggregation into newly budding vesicles. Evidence for a role of TGN acidity came from a mouse pituitary line, where neutralizing intracellular pH diverts ACTH from a regulated to a constitutive secretory pathway (Moore et al., 1983). Vice versa, human Secretogranin II aggregates *in vitro* at a low pH and high calcium concentration, suggesting that granulation may be supported by the TGN internal milieu (Gerdes et al., 1989). Furthermore, lowering the pH or calcium in permeabilized PC12 cells causes Chromogranin B and Secretogranin II aggregation already in the ER (Chanat and Huttner, 1991). Similarly, a low pH in permeabilized PC12 cells inhibits SgII release from the TGN (Carnell and Moore, 1994). However, specific depletion of calcium from the TGN has no such effect, raising the question whether calcium in the TGN is important for granulation. Nonetheless, most findings point to roles of both the pH and calcium in the TGN in supporting granular formation (Fig. 1B).

HID1 is involved in SG biogenesis

A recent study showed that *HID1* KO in PC12 cells impairs SgII secretion, reduces SG core size and decreases the total number of SGs, while constitutive secretion remains unaltered (Hummer et al., 2017). In addition, the authors find that HID1 KO elevates the TGN pH, albeit with a small effect size (from 6.6 to 6.9). Furthermore, sucrose fractioning shows mislocalization of the V-ATPase subunit isoform a2. However, the authors do not show whether HID1 KO cells has normal Golgi morphology, allowing for alternative explanation of the impaired SG biogenesis. These findings suggest that HID1 is an important player in SG biogenesis, perhaps by regulating the pH to support sorting by entry. Alternatively, the role of HID1 in SG biogenesis may be explained via maintaining proper Golgi morphology.

Cab45 is a soluble calcium dependent sorting receptor in the TGN for constitutive secretion

A possible mechanism for how calcium may promote granulation comes from constitutive secretion in HeLa cells. Here, secretory pathway calcium ATPase 1 (SPCA1) interacts with actin depolymerizer ADF/cofilin and knock-down of either decreases TGN calcium uptake and causes missorting of constitutive secretory cargo (von Blume et al., 2011). The proposed candidate downstream target is Cab45 (Calcium binding protein 45), a soluble protein that expresses at the TGN lumen in micro domains with secretory proteins and SPCA1 (Crevenna et al., 2016). siRNA against Cab45 or SPCA1 hampers exit of secretory cargos from the TGN and leads to missorting and incomplete processing of several secretory proteins (von Blume et al., 2012). The authors propose that Cab45 may act as a soluble sorting receptor (Fig. 1C), as it assembles into oligomers with secretory cargo (COMP, LysC) in a calcium dependent way, while mutations in the Cab45 calcium binding sites prevent oligomerization, as well as COMP and LysC sorting. Together, these findings provide a sorting mechanism where factors from outside the TGN (ADF/Cofilin) determine sites for cargo build-up, by severing of actin filaments, activating SPCA1, inducing calcium influx and causing soluble sorting receptor Cab45 to aggregate with secretory cargo, inducing secretory vesicle generation. However, whether such a system may also sort regulated secretion cargo is currently unknown.

1.2.3. Sorting by entry: receptors and cytosolic adaptor proteins

Studies on secretory cells lead to the proposal of many sorting receptors. Besides Cab45 as an example of a soluble sorting receptor (Fig. 1C), two other types of receptors have been proposed: (1) Lipid-binding sorting receptors locate to microdomains in the TGN through interaction with specific lipids such as cholesterol (Fig. 1D). (2) Transmembrane receptors may directly accumulate cargo (Fig. 1E) or connect to cytosolic adaptor proteins, thereby linking cargo accumulation to clathrin and other budding factors (Fig. 1F). Below, evidence for both is summarized.

Lipid binding SG cargo receptors

Some SG proteins directly bind specific lipids in the TGN, which helps to sort them into SGs. These include prohormone convertases 1/3 & 2 (PC1/3 & PC2), which interact with lipid rafts, and secretogranin III (SGIII), which binds to cholesterol (Blázquez et al., 2000; Bonnemaison et al., 2013; Dikeakos et al., 2009; Hosaka et al., 2004). SGIII may additionally function as a sorting receptor, as it interacts at the TGN with Chromogranin A, which is known to support prohormone aggregation (Hosaka and Watanabe, 2010; Hosaka et al., 2004). Indeed, disrupting the interaction of Chromogranin A with SGIII leads to missorting of Chromogranin A (Hosaka et al., 2002).

Carboxypeptidase E (CPE) is a prohormone processing enzyme located at the TGN and is associated with lipid rafts in a cholesterol-dependent manner (For reviews see: Dhanvantari et al., 2002; Dikeakos and Reudelhuber, 2007). CPE is required for processing of proinsulin and pro-gonadotropin releasing hormone (Irminger et al., 1997; Srinivasan et al., 2004) and is proposed as a sorting receptor, since it interacts with the sorting domain (N-terminal region) of POMC (proopiomelanocortin) and CPE^{fat} mutant mouse pituitary cells that lack CPE miss sort POMC to the constitutive secretion pathway (Cool et al., 1997). This was called into question by the finding that CPE is not essential for proinsulin, luteinizing hormone, or follicle stimulating hormone sorting to the regulated secretion pathway (Irminger et al., 1997). However, recent evidence shows that CPE supports pro-glucagon sorting into secretory vesicles (McGirr et al., 2013). Additionally, CPE may act as a sorting receptor for BDNF, as a sorting motif in BDNF interacts with CPE and mutation herein lead to missorting of pro-BDNF to the constitutive pathway in AtT-20 cells (Lou et al., 2005). Consistent with this, CPE knock-out in mice ablates activity-dependent ^{35}S labeled BDNF secretion from anterior pituitary cells and cortical neurons. Therefore, CPE may function as a sorting receptor in a subset of secretory pathways by associating with both cargo proteins and TGN lipids. This may provide an example of how similar proteins could help sorting secretory cargo.

Transmembrane sorting receptors at the TGN

Several transmembrane proteins in the TGN are sorted into SGs and could potentially serve as sorting receptors. These include Phogrin (mentioned above), VMATs (Vesicular monoamine transporters), Sortilin, PAM-1 (Peptidylglycine α-amidating monooxygenase 1), MPRs (Mannose 6-phosphate receptors), Furin and CPD (Carboxypeptidase D). Some of these associate with cytosolic adaptor proteins that are involved in build-up of the clathrin coat and vesicular budding. For most of these proteins, their sorting is well-documented, but whether they serve as sorting receptors themselves remains unclear (For a review on sorting receptors see: Bonnemaison et al., 2013). One exception is Sortilin, a type I transmembrane protein. In neurons, Sortilin binds the pro-region of DCV cargos BDNF (Brain-derived neurotrophic factor), NGF

(Neural growth factor) and Neurotensin (Chen et al., 2005; Munck Petersen et al., 1999; Nykjaer et al., 2004). Truncation or siRNA interference of Sortilin leads to a switch from regulated to constitutive secretion of BDNF, suggesting that Sortilin is required for the correct sorting of BDNF (Chen et al., 2005). Although direct evidence is scarce, it is likely that many of the above mentioned TGN transmembrane proteins may serve as sorting receptors.

Cytosolic adaptor proteins may link cargo sorting to vesicular budding at the TGN

Although there are indications that soluble sorting receptors such as the Chromogranins may initiate budding via aggregation-induced TGN membrane curvature (Kim et al., 2006), mounting evidence points at a role for cytosolic adaptor proteins. An indication for role of cytosolic adaptor proteins in SG cargo sorting and budding at the TGN comes from the requirement of cytosolic domains in many SG proteins (*i.e.* phogrin, PAM-1, VMAT2, VAChT and MPR) (For a review see: Bonnemaison et al., 2013). Indeed, several cytosolic adaptor proteins associate with clathrin and clathrin-mediated endocytosis is involved in secretory cargo sorting. For example GGA3 (Golgi-localized coat protein, γ-adaptin ear containing, Arf-binding 3) recruits clathrin to the TGN, which is required for TGN to endosome transport (Puertollano et al., 2001). Furthermore, GGAs support processing and sorting of SG cargo in cell lines and chromaffin cells (Asensio et al., 2010; Kakhlon et al., 2006; Sirkis et al., 2013). Another cytosolic adaptor protein is ADP-ribosylation factor 1 (Arf1) of the ADP-ribosylation family, which recruits AP-1A (adaptor protein 1A) to membranes (Austin et al., 2000; Dittié et al., 1996). In cell-free systems derived from PC12 or GH_3 cells, Arf1 enhances formation of both SGs and constitutive vesicles (Barr and Huttner, 1996; Chen and Shields, 1996). PACS-1 (Phosphofurin Acidic Cluster Sorting protein 1), another AP-1A interactor, interacts with the acidic clusters of cytosolic domains from SG transmembrane cargo proteins (For a review see: Bonnemaison et al., 2013). PICK1 colocalizes with the immature granule marker syntaxin-6 in chromaffin cells, regulates chromaffin SG number and cargo filling, requiring its membrane binding and PDZ binding domain (Pinheiro et al., 2014). Together, these cytosolic adaptor proteins set-up clathrin coats via AP-1A and in this way may contribute to the budding of SGs and other vesicles from the TGN (Fig. 1F). However, it remains unclear if these actions occur at the TGN or downstream in secretory routes, in so called maturation processes which will be discussed below.

1.2.4 Post TGN sorting and processing: Maturation

After budding from the TGN, the newly generated SGs/DCVs may not be ready for exocytosis yet. Several lines of evidence suggest that additional steps are required in order to prepare these vesicles and their cargo for regulated exocytosis, which will be discussed in more detail below. In short, a gradual increase in luminal acidity (& calcium ion influx) of secretory vesicles supports enzymatic processing and crystallization of the cargo. Additionally, SG to SG (or DCV to DCV) fusion may help to increase vesicular size and cargo content in a process called ''homotypic fusion''. Finally, many studies point towards a ''Sorting by retention'' mechanism, that may supplement (or replace) sorting by entry at the TGN. Sorting by retention involves removal (fission) of cargo/membrane proteins destined for other pathways from immature secretory vesicles. This helps to purify the cargo, but also to prevent membrane proteins that regulate internal membrane trafficking from interfering with final steps of regulated exocytosis. Multiple of these mechanisms may contribute together to generate fully mature SGs/DCVs (For the models see: Fig. 2).

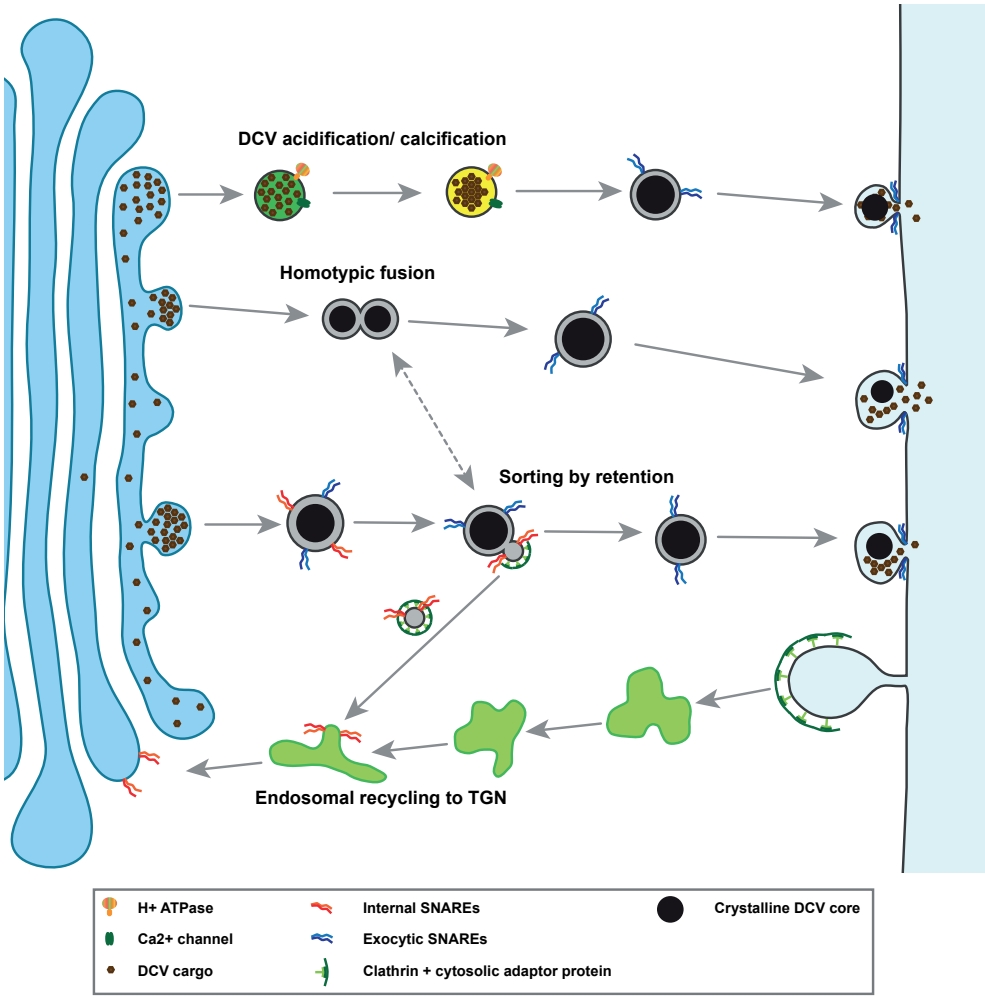

Figure 2. Models for DCV maturation. At the top, DCV acidification and calcification is depicted in newly budded DCVs that travel from the TGN (left) to their secretion site (right). Below that, homotypic fusion is shown by the membrane and core fusion of two small immature DCVs (left) that recently budded from the TGN (far left), to yield a larger mature DCV with a larger crystalline core (right), which may undergo exocytosis (far right). Below that, sorting by retention is depicted, where unnecessary cargo and membrane proteins (such as SNAREs for internal membrane trafficking) are removed via clathrin-dependent fission (middle) of the immature DCV that came directly from the TGN (left), or from a homotypic fusion reaction (above). The remaining vesicle (right) contains only the specific SNAREs and membrane proteins required for exocytosis, giving maturity to the DCV (often also in terms of acidification/calcification such as depicted on top) and enables it to fuse with the plasma membrane (far right). The small vesicle that emerged from membrane/cargo fission off the immature DCV may join the endosomal pathway directed to the TGN (below), which in that way recycles TGN specific membrane proteins and SNAREs for internal membrane trafficking, and restricts these largely to the TGN and immature DCVs.

Luminal acidification and calcification drive SG maturation

Newly generated DCVs/SGs may not have completely aggregated and crystallized cargo upon budding from the TGN (For a review see: Bonnemaison et al., 2013). In secretory cells, the next step involves tightly clustering of the SG cores during a crystallization

process, while many cargo peptides and proteins are still being processed. This evolutionary well-conserved maturation process requires an increase in SG luminal calcium and proton concentration. The calcium concentration becomes elevated by the calcium ATPase pump SPCA (Shull et al., 2003) and SG luminal acidity is increased to a pH of ~5.5 by proton pumping activity of vesicular ATPases (V/H+ ATPases) (Casey et al., 2010; Wu et al., 2001), indicating post-TGN roles for both these pumps. The increased SG luminal calcium concentration and acidity both promote aggregation of the cargo peptides and proteins into a crystal-like core. Additionally, the increased acidity supports activity of convertases, which most efficiently cleave pro-neuropeptides and proteins at a pH of ~5.5 (For a review on the chromaffin cell DCV internal milieu see: Borges et al., 2010), as was also recently shown (Jiang et al., 2021). Therefore, calcium and proton pumps have an essential role in SG maturation, while defects in their function may indicate improper SG biogenesis or maturation.

Homotypic fusion of SGs to increase size and cargo

Newly generated immature SGs (iSGs) may not have the size or amount of content that mature SGs have (Du et al., 2016; Tooze et al., 1991; Urbé et al., 1998). One way to enlarge iSGs or built-up more cargo after budding from the TGN, is iSG to iSG fusion or ''homotypic fusion''. Evidence for this type of fusion mainly comes from non-neuronal secretory cells and cell-free assays. In these assays membrane and content mixing of identical SGs is detected *in vitro* via enzymatic activity (Tooze and Huttner, 1990; Urbé et al., 1998). Candidate proteins for homotypic fusion found using these assays include Synaptotagmin-4 and Syntaxin-6 (Ahras et al., 2006; Wendler et al., 2001). Additional evidence for homotypic fusion comes from an EM study on pancreatic β-cells, which reveals that insulin granules in the cell periphery have larger sizes than those adjacent to the Golgi (Du et al., 2016). The same authors suggest that HID1 (high-temperature-induced dauer formation 1) supports homotypic fusion of immature insulin granules. Genetic HID1 inactivation reduces homotypic fusion of insulin granules *in vitro* and decreases insulin granule size in the cell periphery. In addition, it hampers processing of proinsulin to insulin and granule acidification (Du et al., 2016). These findings show that homotypic fusion can be detected *in vitro* and provide evidence for SG size increases through maturation. However, they do not prove that homotypic fusion happens *in vivo*, leaving room for alternative explanations of how SGs may increase their size.

Sorting by retention

Many proteins are specifically retained at the TGN and iSGs, but do not localize to mature SGs, including several of the TGN/SG membrane proteins discussed above, as well as VAMP4, syntaxin-6 and Syt-4. This suggests that during the course of maturation, many SG membrane proteins are sorted away from iSGs, indicating a membrane remodeling step. Cargo that is not sorted away is retained, hence the term ''sorting by retention''. For example MRP, VAMP4, Syntaxin-6 and Syt-4 are located to the TGN and immature SGs, but are readily removed before maturation, likely via GGA (Kakhlon et al., 2006), AP-1A and clathrin-mediated fission (For reviews see: Bonnemaison et al., 2013; Eaton et al., 2000. In addition, VAMP4 may be directly involved in this process by recruiting AP-1 (Hinners et al., 2003). VAMP4 is furthermore known to cycle from the cell surface to the TGN (Tran et al., 2007), suggesting a potential link between iSG membrane remodeling and the endocytic pathway. The proposed roles of Syt-4 and Syntaxin-6 in homotypic fusion and/or SG maturation suggest that they have to exert these functions before such a clathrin-dependent membrane remodeling step. However, the timing and mechanisms of these events have not been directly tested.

Rab2 and interacting proteins CCCP-1 and RUND1 may function in such a sorting by retention mechanism for SG and neuronal DCV maturation. In *C. elegans Rab2 null* mutants, soluble and membrane DCV cargo is missorted to early endosomes (via a PI(3) P-dependent trafficking pathway), while aggregated neuropeptides remains in DCVs (Edwards et al., 2009). Similarly, *CCCP-1* and *RUND1 null* mutants in *C. elegans* reduce soluble and transmembrane cargo of neuronal DCVs (Ailion et al., 2014), and CCCP-1 knock-out in rat insulinoma cells reduces SG cargo expression and localization (Cattin-Ortolá et al., 2017). Additionally, knock-down of Rab2a or Noc2 in rat/mouse insulinoma cells impairs cargo processing from proinsulin to insulin (Matsunaga et al., 2017). These findings suggest that RAB2 and interacting proteins are involved in a membrane remodeling step during SG and DCV maturation, where soluble and membrane cargo can be sorted away, but aggregated cargo cannot be redistributed.

TGN and iSG resident proteins that are sorted away during maturation may be not directly trafficked to the Golgi, but join the endocytic pathway, as was suggested by the VAMP4 and RAB2 studies above. Additional evidence for this route involves the role of the EARP (endosome-associated recycling protein) complex in SG/DCV maturation. This multi-subunit tethering complex is known for its involvement in endocytic recycling (Schindler et al., 2015). EARP members VPS-50-54 affect axonal DCV cargo expression in *C. elegans* when mutated (Topalidou et al., 2016). The same study shows that EIPR1 (EARP complex and GARP complex interacting protein 1) associats with the EARP complex and is also required for axonal DCV cargo expression. In insulinoma cells, EIPR1 is required for the processing and expression of insulin and CPE in mature SGs, but not for TGN exit of these cargos (Topalidou et al., 2020), suggesting a role in granular maturation. Similarly, VPS-50 may also be involved in DCV maturation, as it controls DCV and SV acidification in *C. elegans* (Paquin et al., 2016). Furthermore, cargo processing is reduced in *VPS-50 null*, in line with these defects in acidification. Since VPS-50 interacts with V-ATPase subunit VHA-15, it is tempting to speculate that it controls vesicle acidification and cargo processing via this interaction. While *VPS-50 null* mutants show increased synaptic neuropeptide levels, secretion (measured from coelomocytes) is severely reduced. This suggests that failure to remove cargo/membrane proteins destined for other pathways interferes with the exocytosis of DCVs. Together, these findings support a sorting by retention model, where unwanted cargo is sorted away via the endocytic pathway, and the remaining DCV is allowed to further mature.

The above findings reveal possible mechanisms and working models for SG biogenesis and maturation. However, biogenesis and maturation of neuronal DCVs is a virtually unexplored territory. Many basic questions herein remain unanswered, including: (1) What is the DCV production rate in neurons? And: (2) How long does it take until newly generated DCVs are ready to undergo regulated exocytosis? However, to answer these questions, new pulse chase techniques complemented with fluorescent live imaging are required. A recently developed fluorescent pulse chase technique called SNAP-cell may be such a promising tool, as it was used to label different age-populations of insulin granules and allows for both live and fixed imaging (Ivanova et al., 2013). In this thesis (Chapter 5), these techniques will be explored with the purpose of answering these questions in the future.

1.3 Transport

Neurons are highly polarized and compartmentalized cells, which heavily depend on their cytoskeletal buildup to support the special needs of each sub region. DCVs travel through neurons using motor proteins that walk along the cytoskeletal network. Two components of the cytoskeleton form the cellular highways (microtubules) and the B-roads (actin). Microtubules grow only from their dynamic plus-end, and are all plus-end out orientated in axons, but mixed in dendrites. These orientations, in combination with post-translational modifications, allow different motor proteins to bind and travel (For a review see: Kapitein and Hoogenraad, 2011). Members of the kinesin protein family and dynein are the motor proteins that travel on microtubules, with different affinity and direction, and bind to various different organelles and vesicles via adaptor proteins, to enable fast transport (For review see: Hirokawa et al., 2009; Reck-Peterson et al., 2018). The actin cytoskeleton encompasses many different structures, including filamentous actin and more branched actin. Members of the myosin protein family bind and walk onto actin, mediating slow transport (For a review see: Kneussel and Wagner, 2013). All motor proteins use ATP as an energy source to drive the conformational changes that translocate them along the cytoskeleton. Below, the principles of DCV transport in neurons are summarized.

DCV trafficking depends on motor proteins

Long-range fast transport of DCVs is driven by kinesins and dynein via microtubules. The primary kinesins that drive DCV transport are KIF1A (kinesin-3) and KIF5C (kinesin-1). KIF1A knock-down in primary hippocampal neurons blocks most axonal and dendritic transport of DCVs (Lo et al., 2011; Stucchi et al., 2018). In addition, doublecortin-like kinase 1 (DCLK1) is required for KIF1-dependent DCV transport into dendrites (Lipka et al., 2016). In Drosophila, anterograde neuropeptide transport is mediated by kinesin-1 & kinesin 3 (KIF5 & KIF1) as well (Barkus et al., 2007; Lim et al., 2017) and in *C. elegans*, KIF1A specifically mediates anterograde axonal transport of DCVs (Zahn et al., 2004). No convincing evidence for dynein as a DCV motor protein has been shown yet. However, DCVs do travel retrogradely in *Drosophila* axons (Shakiryanova et al., 2006) and mammalian axons (Knabbe et al., 2018; Lo et al., 2011), and generally this type of transport is dynein-mediated (For a review see: Kapitein and Hoogenraad, 2011). Myosin-based trafficking of DCVs is not well documented, but overexpression of the dominant-negative tail of myosin Va impairs retrograde axonal transport of DCVs, while not affecting anterograde trafficking (Bittins et al., 2010), suggesting that DCVs may traffic along the actin cytoskeleton as well.

Adaptor proteins link DCVs to motor proteins

DCVs associate with motor proteins by binding to adaptor proteins. A family of adaptor proteins are the RAB proteins, which alternate between a GDP and GTP bound state. This switches their affinity for target membranes and their association to motor proteins (Jordens et al., 2005). In addition to having a role in DCV maturation via sorting by retention, RAB2 may be important for bidirectional axonal transport of DCVs. *Rab2* mutation in *Drosophila* larvae blocks most axonal DCV transport, with the largest effect on distally retrograde traveling DCVs (Lund et al., 2020). Surprisingly, neuropeptide release and replenishment after activity remains unaffected, which is opposite to the RAB2 findings described above at DCV maturation. Furthermore, RAB2 associates with KIF1A *in situ* (Lund et al., 2020). Therefore, RAB2 may be an adaptor protein that links

DCVs to KIF1A motor proteins. This proposed transporting role for RAB2 may be an alternative for its proposed role in DCV maturation, or supplements it. However, this should be further explored in mammalian neurons. Other RAB proteins are also found on DCVs, including RAB6, which additionally labels other vesicle types (Gumy et al., 2017). This suggests that RAB6 is a more generic adaptor protein. DCV transport into the axon may depend on adaptor protein ARL8. In *Drosophila Arl8* mutants, DCVs build-up in the soma, are unable to enter the axon and have a generally reduced trafficking speed (Lund et al., 2020). In the same study, ARL8 localizes to DCVs. Similarly, in primary hippocampal neurons ARL8 is required for axonal entry of piccolo-bassoon vesicles (Vukoja et al., 2018). Therefore, ARL8 likely functions as an adaptor protein for DCVs to a kinesin. ARL8 is also required for lysosomal exit from the soma and it supports axonal transport of presynaptic cargo (Klassen et al., 2010; Nakae et al., 2010; Rosa-Ferreira and Munro, 2011). Therefore, RAB2 and ARL8 may be important adaptor proteins for DCV transport, while ARL8 function is not restricted to DCVs only.

DCV arrival at secretion sites

To allow exocytosis, DCVs may need to abandon motor-protein mediated trafficking, detach from the microtubules and be captured by specific molecules at DCV release zones. This so called ''DCV capture'' was first found in *Drosophila* neuromuscular junctions (Shakiryanova et al., 2006; Wong et al., 2012) where it is enhanced upon activity (Cavolo et al., 2016). However, the mechanism is as yet incompletely understood. Currently, it is being investigated as it provides opportunities for neurons to regulate location and quantity of neuropeptide secretion. One capture mechanism may include KIF1A detachment from microtubule plus ends, which locate most frequently at mammalian presynaptic boutons (Guedes-Dias et al., 2018). This is facilitated by the intrinsic low affinity of KIF1A to Tubulin. Furthermore, the authors show that traveling synaptophysin puncta (representing SVs) stop more frequently near presynaptic boutons. A different mechanism for DCV capture was proposed for postsynaptic sites. In dendrites, calcium activated Calmodulin (CaM) increases KIF1A binding to and motility of DCVs. Subsequently, dendritic DCVs may be captured by liprin-α and TANC2 (tetratricopeptide repeat, ankyrin repeat, and coiled coil containing 2) (Stucchi et al., 2018). A third mechanism may be capture via myosin or actin, since expression of a dominant-negative tail of myosin Va enhances DCV exocytosis in primary neurons (Bittins et al., 2009). Therefore, capture of DCVs prior to exocytosis may occur via one or multiple of these mechanisms, but it is not excluded that DCVs may undergo exocytosis without such a capturing step.

1.4 DCV exocytosis

Both mobile and stationary DCVs can be triggered into exocytosis (Farina et al., 2015). While the mechanisms and requirements of DCV capture are poorly understood, many components of the DCV exocytosis machinery have recently been identified. They show surprisingly high overlap with the machinery required for neurotransmitter secretion, which is better characterized and has been serving as a working model for the mechanisms of neuropeptide release (For reviews see: Rizo and Xu, 2015; Südhof, 2013). Yet, despite these similarities, DCVs require many more action potentials to

trigger exocytosis compared to SVs and they additionally secrete at other locations than the presynapses.

1.4.1. The exocytic machinery of DCVs

The components required for SV and DCV release can be roughly subdivided into three roles: (1) the Soluble N-Ethylmaleimide-Sensitive Factor Attachment Protein Receptor (SNARE) and assessor proteins, (2) (functional) homologs of the yeast exocyst complex and (3) calcium sensors (For a simplified model on DCV exocytosis see: Fig. 3). Together, these groups encompass the proteins that mediate vesicular fusion to the plasma membrane.

Four essential core components are highly conserved

The principles of secretory vesicle exocytosis are well conserved and were first characterized in yeast (Aalto et al., 1993; Novick and Schekman, 1979; Novick et al., 1980, 1981; Protopopov et al., 1993). Four canonical components appear to be essential in all types of regulated exocytosis: three SNARE proteins, of the (i) /SEC9/SNAP (Soluble N-Ethylmaleimide-Sensitive Factor Attachment Protein) family, (ii) the SNC/synaptobrevin/VAMP (Vesicle Associated Membrane Protein) family, and (iii) the SSO1/2 /syntaxin family; and (iv) a SEC1/MUNC18 (SM) protein (Jahn and Scheller, 2006; Kaeser and Regehr, 2014; Südhof and Rothman, 2009; Toonen and Verhage, 2003, 2007). Indeed, synaptic transmission also relies on these components, with SNAP25, VAMP2, Syntaxin-1 and MUNC18-1 all having an important role in SV exocytosis (Jahn and Fasshauer, 2012; Rizo and Xu, 2015; Südhof, 2013). While two of these canonical components (SNAP25/47 and VAMP2) have recently been identified for DCV exocytosis in mammalian neurons (Arora et al., 2017; Hoogstraaten et al., 2020; Shimojo et al., 2015), the participation of syntaxin/SSO1/2 and an SM-protein has remained elusive (Fig. 3).

Functional conservation of the exocyst complex in mammalian DCV exocytosis

In addition to the four canonical components (the SNARE proteins and an SM-protein), another protein complex is essential for yeast exocytosis as well: the exocyst complex. This complex consists of the SEC3-6, 8, 10, & 15 proteins, together with EXO70 and EXO84 (Bowser et al., 1992; Guo et al., 1999; TerBush and Novick, 1995; TerBush et al., 1996). Mammalian homologs of these proteins, including RAB3 (homologous to SEC4), have so far no important roles in SV secretion (Mehta et al., 2005; Murthy et al., 2003; Schlüter et al., 2004, 2006; Schwenger and Kuner, 2010). Other proteins, not homologous to the exocyst complex, do have important roles in neurotransmitter secretion, including CAPS, Synaptotagmin-1 and Synaptotagmin-7 (calcium sensors), MUNC13 (calcium sensor & essential priming factor), complexin (priming factor for SNARE complexes) and RIM1 (Active zone component and tethers calcium channels) (Südhof, 2013) (Fig. 3). However, our lab recently showed that mammalian SEC4 homolog RAB3 is essential for neuropeptide secretion (Persoon et al., 2019). In addition, RIM1/2 is also required for DCV exocytosis, more specifically the N-terminal RAB3- and MUNC13-binding domains are sufficient to support secretion (Persoon et al., 2019). MUNC13 is also known to support neuropeptide secretion, controlling the location of release (van de Bospoort et al., 2012). This suggests that RAB3/RIM/MUN13 may provide a mammalian substitute for the yeast exocyst complex in DCV exocytosis. In chromaffin cells, E466K mutation in MUNC18-1 increased interaction with RAB3A and enhanced LDCV exocytosis (Graham et al., 2008). This suggests that MUNC18-1

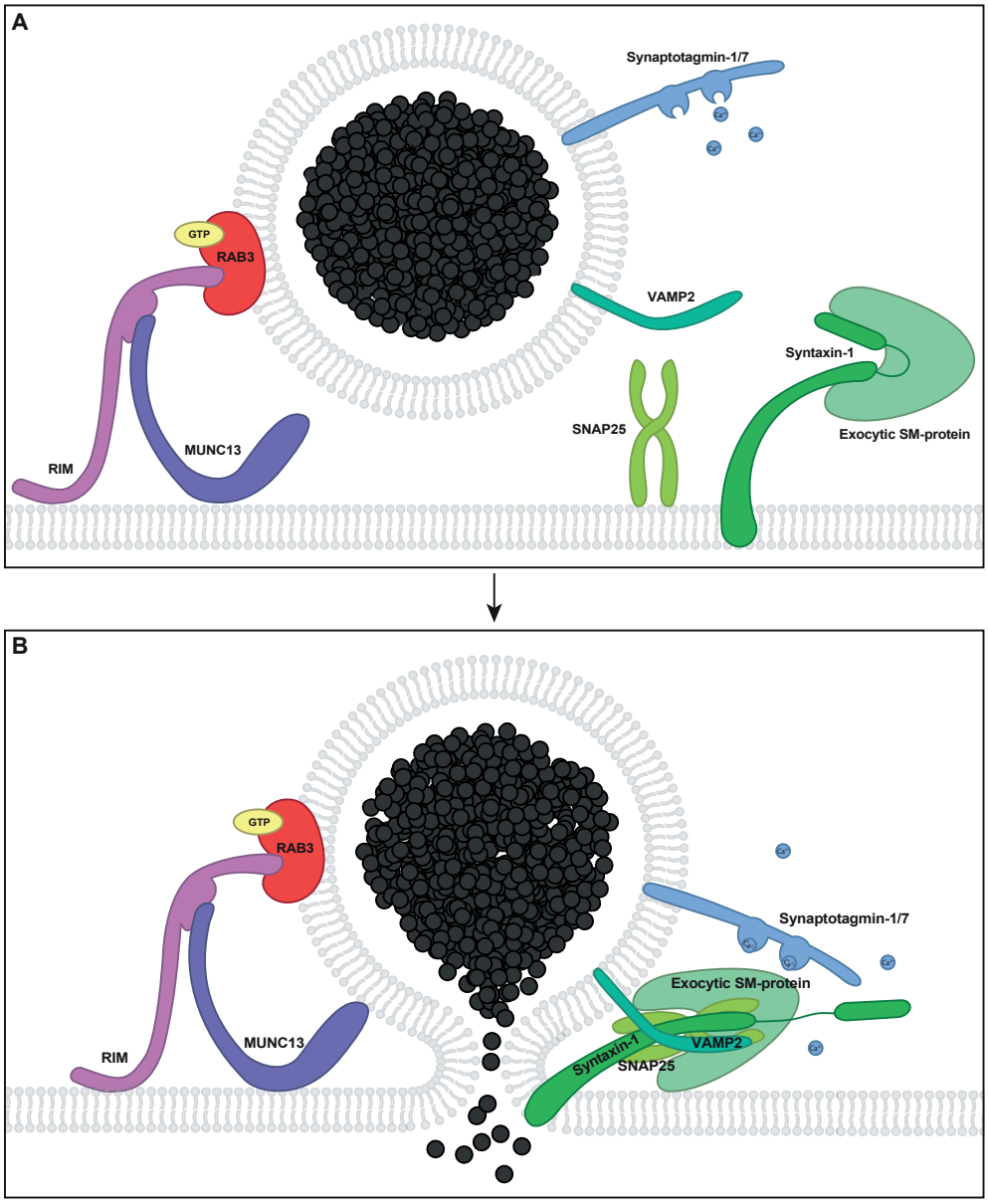

Figure 3. Model of DCV exocytosis machinery. (**A**) DCVs are tethered (but not docked) via the RIM-RAB3-MUNC13 module, which is (functionally) homologous to the yeast exocyst complex. Prior to docking, Syntaxin-1 resides in the plasma membrane and is locked in an auto-inhibitory state by binding of an exocytic SM-protein. In addition, at that moment SNAP25 is associated with the plasma membrane and VAMP2 is located on the DCV. Calcium sensors Synaptotagmin-1 & -7 may be on the DCV or plasma membrane. (**B**) To fuse the DCV with the plasma membrane, the SNARE domains of Syntaxin-1, SNAP25 and VAMP2 zipper together, with the help of MUNC18-1. Other exocytic proteins (MUNC13, Synaptotagmin-1/7) help SNARE zippering, or stimulate membrane future after this step. All depicted proteins have been shown to play key roles in DCV exocytosis. However, the role of an exocytic SM-protein has not been elucidated yet.

interacts not only with the core SNAREs for exocytosis, but also with RAB3, perhaps bridging these two modules of exocytosis machinery.

Roles of Calcium sensors in DCV exocytosis

Regulated secretion in mammals is often triggered by calcium influx. Calcium sensors involved in synaptic transmission are Synaptotagmin-1/2, Synaptotagmin-7/12, Doc2, MUNC13 and CAPS (Südhof, 2013). Roles of Synaptotagmin-1, Synaptotagmin-7, MUNC13 and CAPS have also been identified for DCV exocytosis (van de Bospoort et al., 2012; Farina et al., 2015; Westen et al., 2021). CAPS1/2 is similarly important for DCV and SV exocytosis. Therefore, striking similarities have been shown between the SV and DCV exocytosis machinery. However, not all of these proteins are as essential for DCV exocytosis as for neurotransmitter secretion. MUNC13 for example is essential for synaptic transmission (Augustin et al., 1999; Betz et al., 2001; Rosenmund et al., 2002), while neurons lacking MUNC13 still have 40% remaining neuropeptide secretion (van de Bospoort et al., 2012). Therefore, the DCV and SV exocytosis machineries are highly similar, albeit with a few exceptions.

1.4.2. Triggers and locations of DCV exocytosis

Despite the similarities between the underlying molecular mechanisms of DCV and SV exocytosis, two properties of neuropeptide secretion differ extensively from neurotransmission: the locations where DCVs can undergo exocytosis and the number of action potentials required to trigger neuropeptide release. Both these properties will be discussed below.

Locations of exocytosis

Locations of neuropeptide release are in part separated from neurotransmitter secretion. SVs undergo exocytosis within the active zone (AZ), a highly specialized protein-lipid structure, composed of many factors essential for membrane fusion and structural support (Südhof, 2012). DCVs secrete their content from presynapses as well (~65% of the events), but additionally release neuropeptides from extra-synaptic locations, including dendrites (van de Bospoort et al., 2012; Farina et al., 2015; Persoon et al., 2018). Many exocytic components are highly enriched within presynapses, including MUNC13-1/2, which specifically supports presynaptic neuropeptide release (van de Bospoort et al., 2012). This suggests that extra-synaptic DCV exocytosis may occur in a MUNC13-1/2 independent manner (van de Bospoort et al., 2012). Other presynaptic resident proteins RAB3, RIM1/2 and CAPS-1 co-traffic with DCVs when overexpressed, suggesting that they could support extra-synaptic DCV exocytosis. Indeed, CAPS-1 supports both presynaptic and extra-synaptic neuropeptide release (Farina et al., 2015) and the nearly absent secretion in *Rab3*, *RIM1/2* or *SNAP25 null* neurons suggests that these proteins support DCV exocytosis from all subcellular locations as well (Arora et al., 2017; Persoon et al., 2019). Therefore, extra-synaptic neuropeptide secretion requires at least in part the same exocytosis machinery as synaptic DCV exocytosis. Within the presynapse, neuropeptide release may also occur at a different location than SV exocytosis, as DCV exocytic profiles in EM were exclusively present outside of AZs (Zhu et al., 1986) and most DCVs were located outside of the SV cluster that is adjacent to the AZ (Verhage et al., 1991). Even more so, *C. elegans* DCVs do not cluster at the AZ, while the docked DCVs are excluded from the AZ, suggesting that DCVs have different secretion sites than SVs (Hammarlund et al., 2008). Therefore, DCVs may altogether undergo exocytosis at different locations than SVs.

Triggers for exocytosis

Neuropeptide secretion requires many more action potentials as a trigger than neurotransmitter release. On average, one action potential triggers exocytosis of 1-2 SVs (Watanabe et al., 2013, 2014, 2018), whereas robust DCV exocytosis requires high-frequency burst-firing (Persoon et al., 2018). In general, exocytosis is triggered by calcium, which appears to have a similarly important role for DCV exocytosis as for neurotransmitter secretion. Low calcium media and knock-out of calcium sensors impact both types of release (Augustin et al., 1999; Balkowiec et al., 2000; Betz et al., 2001; van de Bospoort et al., 2012; Farina et al., 2015; Hartmann et al., 2001; Jockusch et al., 2007; Katz and Miledi, 1970; Rosenmund et al., 2002; De Wit et al., 2009), although ionomycin (a calcium ionophore) inefficiently triggered DCV or SV exocytosis (Capogna et al., 1996; Persoon et al., 2018). cAMP may also trigger exocytosis, as SV and DCV exocytic could be triggered by cAMP uncaging in *C. elegans* (Steuer Costa et al., 2017). However, elevating cAMP levels via forskolin treatment in mossy fiber synapses however did not affect SV docking, while the number of docked DCVs was increased (Maus et al., 2020). Therefore, the types of triggers for SV or DCV exocytosis are very similar, while the required quantity differs.

With this very different response to action potentials and different locations of secretion, it is striking how similar the DCV and SV exocytosis machineries are. Perhaps the location of exocytosis helps explaining this difference, as SVs lie ready for fusion at the AZ, while DCVs may still need to undergo all the docking and priming steps at the moment of stimulation. Furthermore, the DCV exocytosis machinery is yet incompletely characterized.

2.1 SM-proteins are essential for regulated secretion

One of the core components required for neuronal DCV exocytosis has not been identified yet: The role of an SM-protein in neuropeptide secretion. The SM-proteins expressed in mammalian neurons are mSly1, VPS33A & B, and VPS45, which have roles in intracellular membrane trafficking, and the exocytic SM-proteins MUNC18-1, MUNC18-2 and MUNC18-3 (Yue et al., 2014; Zeisel et al., 2015; For a review see: Toonen and Verhage, 2003). MUNC18 proteins are highly conserved across *Metazoa* and *Choanoflagellata*, with similar structure and molecular interactions (Burkhardt et al., 2011). Two gene duplications found in all vertebrates gave rise to paralogs MUNC18-1, MUNC18-2 and MUNC18-3, of which the latter have respectively 62% and 52% homology to MUNC18-1 (Toonen and Verhage, 2003). Each cell type expresses one or multiple of these MUNC18 paralogs, which are essential for many regulated secretion pathways. Underlining their crucial role in secretion, null mutations in each *Munc18* paralog result in embryonal lethal or still-born mice (Gutierrez et al., 2018; Oh et al., 2005, 2012; Verhage et al., 2000). So far, functions in the brain are mainly observed for paralog MUNC18-1, as it is essential for neuronal viability and synaptic transmission, while mutations in the human gene cause neurodevelopmental disorders.

2.1.1 SM-proteins are important for regulated secretion in many cell types

Regulated secretion from many different cell types depends on one or multiple MUNC18 proteins. Here, the role of MUNC18 proteins in secretion of several frequently

investigated cell types will be addressed, including blood, immune, pancreatic, adipose and chromaffin cells. MUNC18 proteins have a U-, or arch-shaped structure, containing a binding groove for a Syntaxin family protein (Archbold et al., 2014; Hackmann et al., 2013; Hu et al., 2007; Misura et al., 2000). *In vitro,* MUNC18-1 and -2 both bind to Syntaxin-1, -2 and -3, albeit with different affinities, whereas MUNC18-3 mainly binds Syntaxin-2 and -4 (Hata and Südhof, 1995; Peng et al., 2010; Tamori et al., 1998). To support exocytosis, MUNC18 proteins bind syntaxins (Bin et al., 2013; Burkhardt et al., 2008; Dulubova et al., 2007; Kauppi et al., 2002; Misura et al., 2000; Thurmond et al., 1998), promote docking of secretory vesicles (Bouwman et al., 2004; Oh and Thurmond, 2009; Oh et al., 2012; Voets et al., 2001; de Wit et al., 2009) and probably serve as a template for SNARE-complex assembly, which drives exocytosis (André et al., 2020; Jiao et al., 2018; Meijer et al., 2018; Parisotto et al., 2014; Peng et al., 2010; Sitarska et al., 2017; Wang et al., 2019).

Secretion from blood/immune cells requires MUNC18-2.

To prevent excessive bleeding, blood platelets are activated by extracellular matrix components to secrete a plethora of factors via exocytosis of multiple granule types to form a thrombus (For a review see: Golebiewska and Poole, 2014). Platelets express all three MUNC18 paralogs (Cardenas et al., 2019; Houng et al., 2003; Schraw et al., 2003). Early studies found that platelet exocytosis is decreased via interfering with MUNC18-1 or MUNC18-3 derived peptides, but that peptide or antibody interference with MUNC18-3-Syntaxin-4 complexes increases platelet exocytosis (Houng et al., 2003; Schraw et al., 2003). Analysis of platelets from patients with biallelic mutations in STXBP2 (*Munc18-2*) shows that MUNC18-2 and also syntaxin-11 levels are drastically reduced and secretion is profoundly affected (Hawas et al., 2012), suggesting a central role of MUNC18-2 in platelet exocytosis. Recently, a genetic study using conditional *Munc18-1, -2* or *-3 null* mice shows that alpha, dense, and lysosomal granule exocytosis from platelets is ablated by *Munc18-2* conditional knock-out (cKO), but not affected by *Munc18-1* or *Munc18-3* cKO (Cardenas et al., 2019). Therefore, MUNC18-2 is the SM-protein required for blood platelet secretion.

Mast cells are immune cells important to detect intruders. When activated, they degranulate, secreting chemo-attractants for white blood cells. All three Munc18 paralogs are expressed in mast cells (Gutierrez et al., 2018; Nigam et al., 2005). Munc18-2 knock-down (KD) decreases secretion in rat RBL cells (a cell line similar to mast cells) (Bin et al., 2013; Brochetta et al., 2014; Tadokoro et al., 2007) and primary mast cells (Brochetta et al., 2014), suggesting that MUNC18-2 supports mast cell degranulation. Reducing MUNC18-2 expression by single allelic (heterozygous; HZ) *Munc18-2* inactivation also reduces mast cell degranulation and secretion (Kim et al., 2012). Conversely, *Munc18-1 null* mast cells shows normal secretion (Wu et al., 2013). Recently, a study on conditional *Munc18-1, -2 or -3 null* mice showed that only *Munc18-2 cKO* mast cells have severe defects in compound and single-vesicle-regulated exocytosis, whereas *Munc18-1 cKO* or *Munc18-3 cKO* cells are unaffected (Gutierrez et al., 2018). Therefore, mast cell secretion is also exclusively mediated by MUNC18-2, despite expression of all MUNC18 paralogs.

Mutations in STXBP2 (human gene encoding MUNC18-2 protein) cause FHL5 (familial hemophagocytic lymphohistiocytosis 5), which further demonstrates the important role of Munc18-2 in several cell types (Cetica et al., 2010; Côte et al., 2009). FHL may be caused by mutations in STXBP2 (FHL5), syntaxin 11 (FHL4), Munc13-4 (FHL3) or perforin-1 (FHL2), and these patients have severe immune deficiency (Cetica et al., 2010; Côte

et al., 2009; Feldmann et al., 2003; Meeths et al., 2010; Zur Stadt et al., 2006; Stepp et al., 1999). FHL5 patients have symptoms that frequently include severe diarrhea, often abnormal bleeding and sometimes sensorineural hearing deficits (Pagel et al., 2012). These hint that MUNC18-2 may have functions besides its role in blood and immune cells, for example perhaps in some neuron types and in the intestine. The FHL5 causing mutations in STXBP2 are located at the syntaxin-11 binding region and lead to reduced syntaxin-11 protein levels (Hackmann et al., 2013; zur Stadt et al., 2009). Syntaxin-11 and MUNC18-2 facilitate cytolytic granule release by cytotoxic T lymphocytes and natural killer cells (Luzio et al., 2014; De Saint Basile et al., 2010). A new study using a lipid mixing assay shows that syntaxin-11 supports lipid hemifusion together with its cognate SNARE protein partners, while MUNC18-2 addition stimulated full membrane fusion, suggesting that MUNC18-2 is required for the core fusion machinery in cytotoxic T lymphocytes and natural killer cells (Spessott et al., 2017). These findings on STXBP2 patient mutations reveal roles of MUNC18-2 in several blood and immune cells (i.e. lymphocytes, macrophages and blood platelets), where MUNC18-2 is important for secretion via its interaction with syntaxin-11.

Insulin secretion from β-cells is mediated by all three MUNC18 paralogs

Pancreatic β-cells regulate blood glucose levels by secreting insulin in response to high blood sugar, causing glucose uptake from the blood by many cell types. Insulin secretion in response to hyperglycemia generally comes in two phases: a first phase of acute high insulin secretion and a second phase of longer sustained secretion. In *Munc18-1 null* and HZ mouse islets, first-phase insulin secretion is reduced, while overexpression of MUNC18-1 increases secretion during this phase (Oh et al., 2012). Insulin secretion during the sustained phase, but not the first phase, is reduced in mouse *Munc18-3* HZ islets and in MIN6 cells expressing Munc18-3 siRNA (Oh and Thurmond, 2009). In human beta-cells however, Munc18-3 knock-down decreases both phases of insulin secretion (Zhu et al., 2015), showing that perhaps human and mouse insulin secretion are differentially regulated by MUNC18-3. Munc18-2 KD in rat pancreatic islets decreases insulin secretion during all phases (Lam et al., 2013). In this study, siRNA interference also specifically reduces compound secretion, visualized as sequential exocytosis using TIRF imaging. In line with mouse islets, Munc18-2 overexpression in β-cells from human type 2 diabetes patients increases both phases of insulin secretion (Qin et al., 2017). Taken together, these findings point out that all 3 MUNC18 paralogs are important for glucose stimulated insulin secretion, albeit during different phases. Interestingly, human diabetes type 2 beta cells, which are deficient in insulin secretion, have drastically decreased expression levels of the SNARE and SM-proteins required for exocytosis (Ostenson et al., 2006; Qin et al., 2017).

MUNC18 dependent secretion in lung and other epithelial cells

Lung mucus consists of mucin and helps to trap inhaled particles, pathogens and toxicants. Lung epithelial cells secrete mucin at a basal constant rate, but also boost this secretion upon an extracellular trigger. Both types of secretion require an SM-protein, as basal secretion is decreased in *Munc18-1 null* cells and ATP-stimulated secretion is defective in *Munc18-2 null* cells (Jaramillo et al., 2019; Kim et al., 2012). MUNC18-2 also seems to drive secretion in other epithelial cells, as cultured Munc18-2-KD parietal cells secrete less acid (Liu et al., 2007) and *Munc18-2 null* intestinal organoids fail to correctly organize their brush border due to cell-polarity defects (Mosa et al., 2018). In line with this function of MUNC18-2 in the intestine are the intestinal problems that sometimes occur in FHL5 patients (Pagel et al., 2012). This was replicated in vitro as

FHL5 causing mutations in Munc18-2 cause enteropathy in intestinal organoids (Vogel et al., 2017). Therefore, MUNC18-2 may be involved in cell-polarity of the intestine, but more evidence is required to determine whether these defects have arisen directly via Munc18-2 and its role in secretion. Together, these findings suggest an important role for MUNC18-2 in secretion from several epithelial cells.

Adipocyte MUNC18-3 is involved in GLUT4 exocytosis in response to insulin

Insulin-dependent glucose uptake from the blood by adipocytes is mediated by glucose transporter 4 (GLUT4) insertion into the plasma membrane (Dugani and Klip, 2005). Viral overexpression of Munc18-3 in 3T3-L1 cells (a mouse adipocyte cell-line) inhibited insulin-stimulated GLUT4 translocation the plasma membrane and limited glucose uptake (Tamori et al., 1998; Thurmond et al., 1998). Conversely, overexpression of Munc18-2 does not affect GLUT4 expression at the plasma membrane. In line with these findings, mouse *Munc18-3 null* adipocytes show= enhanced insulin-stimulated glucose uptake (Kanda et al., 2005), suggesting that MUNC18-3 inhibits GLUT4 vesicle exocytosis. Similar to adipocytes, skeletal muscle cells show more insulin-stimulated GLUT4 plasma membrane insertion upon inactivation of Munc18-3 (Jain et al., 2012). However, Munc18-3 KD decreases insulin-mediated GLUT4 insertion in the plasma membrane of adipocytes (Jewell et al., 2011). This suggests that MUNC18-3 supports insulin-stimulates GLUT4 insertion into the plasma membrane. The same study shows that Insulin Receptors bind to, and phosphorylate Y219 and Y521 residues on Munc18-3, which is required for insulin-mediated dissociation of MUNC18-3 from syntaxin-4. Overexpression of WT or phospho-mimetic Munc18-3 mutants increased insulin stimulates GLUT4 expression at the plasma membrane, while phospho-defective mutants decrease this (Jewell et al., 2011). Perhaps after MUNC18-3 dissociates from closed-state syntaxin-4, it allows syntaxin-4 to open up and is still present to bind syntaxin-4 in open-state and set-up the SNARE complex with VAMP2 and SNAP23, as was shown in a liposome fusion assay (Yu et al., 2013). However, the precise involvement of Munc18-3 in GLUT4 vesicle exocytosis remains enigmatic.

MUNC18-1 mediates chromaffin cell secretion

MUNC18-1 is essential for docking and exocytosis of secretory granules in chromaffin cells (Gulyás-Kovács et al., 2007; Toonen et al., 2006a; Voets et al., 2001). In addition, *Munc18-1 null* chromaffin cells show a thickened actin layer at the cell cortex (Kurps and De Wit, 2012; Toonen et al., 2006a), which was proposed to form a barrier for secretion (Papadopulos et al., 2015). However, colleagues recently showed that this forms no rate-limiting factor for granular secretion (Pons-Vizcarra et al., 2019). Different from neurons, ectopic expression of MUNC18-2 in *Munc18-1 null* chromaffin cells rescues secretory granule docking and to some extend exocytosis (Gulyás-Kovács et al., 2007). This suggests that neurotransmitter secretion in neurons may be a more specialized pathway than chromaffin cell secretion, which could be beneficial for neurons as they require tight regulation of neurotransmitter secretion in parallel with neuropeptide secretion and perhaps other pathways.

2.1.2 MUNC18-1 is essential in the brain

The main exocytic SM-protein expressed in the brain is MUNC18-1. Extensive research described its role in synaptic transmission, but also in neuronal viability and neurodevelopmental disorders, which all will be discussed here.

Munc18-1 is essential for neuronal viability.

Two decades ago, MUNC18-1 was identified as the SM-protein responsible for synaptic transmission (Verhage et al., 2000). *Munc18-1* null brains develop normally, with formed, albeit functionally silent, synaptic connections. However, *Munc18-1 null* mice shortly die after birth and structural analysis reveals that many nuclei in the brain were already degenerating upon birth (Law et al., 2016; Verhage et al., 2000). The stage of degeneration follows the order of development, with early developed brain areas having the most severe degeneration. Primary neurons from *Munc18-1 null* mice also die shortly (3-4 days) after culturing, which can be delayed via application of neurotrophic factors BDNF and insulin (Heeroma et al., 2004). Viral expression of MUNC18-1, but also MUNC18-2 or MUNC18-3, supports normal viability in *Munc18-1 null* primary neurons (He et al., 2017; Santos et al., 2017), suggesting functional redundancy between these paralogs. To the best of our knowledge, neurons are the only cell-type that depend on MUNC18 for their survival, while the mechanisms that induce neuronal death in *Munc18-1 null* neurons have remained enigmatic.

MUNC18-1 has a core function in synaptic transmission

MUNC18-1 is essential for chromaffin cell secretion and synaptic transmission (Verhage et al., 2000; Voets et al., 2001). In chromaffin cells, it is well-established that MUNC18-1 is crucial for docking of the vesicle to the plasma membrane and in both systems MUNC18-1 supports the steps after (Bouwman et al., 2004; Heeroma et al., 2003; Smyth et al., 2013; Toonen et al., 2006a; Voets et al., 2001; Weimer et al., 2003). MUNC18-1 binds syntaxin-1 in a closed configuration that prevents SNARE-complex formation (Misura et al., 2000). At the same time this configuration acts as the nucleation-point for SNARE complex assembly in which MUNC18-1 acts as template for interaction of the v-SNARE VAMP2 with syntaxin-1 and SNAP-25 upon disinhibition of the Syntaxin-1-Munc18-1 complex by Munc13-1 (Dulubova et al., 2007; Jiao et al., 2018; Ma et al., 2011; Meijer et al., 2018; Shen et al., 2007; Sitarska et al., 2017; Wang et al., 2019), revealing a post-docking role of MUNC18-1. In addition, recent work shows that Munc18-1 prevents de-priming by inhibiting NSF (He et al., 2017; Prinslow et al., 2019; Stepien et al., 2019). Although MUNC18-2 or -3 overexpression in *Munc18-1 null* neurons support viability, both do not support normal synaptic transmission (He et al., 2017; Santos et al., 2017). This suggests that the role of MUNC18-1 in SV exocytosis is highly specialized. However, which SM-protein is involved in neuropeptide release remains unknown.

2.1.3 Reduced MUNC18-1 levels in STXBP1 syndrome may affect synaptic transmission

Mutations in STXBP1 (the human gene encoding MUNC18-1) cause STXBP1 encephalopathy (Saitsu et al., 2008), characterized by developmental delay, intellectual disability, epilepsy, autism spectrum disorders and involuntary movements (spasms and jerks) (Gburek-Augustat et al., 2016; Hamdan et al., 2011). This disease was recently termed STXBP1 syndrome (Verhage and Sørensen, 2020). The current working model for STXBP1 syndrome is that mutations in STXBP1 cause haploinsufficiency. Ectopic expression of STXBP1 disease variants in mouse *Munc18-1 null* neurons largely support synaptic transmission to a variable extent, but severely decrease MUNC18-1 protein levels (Kovačević et al., 2018). Several disease-linked missense mutations result in destabilization and perhaps aggregation of the mutant and wild-type protein, decreasing MUNC18-1 protein levels (Guiberson et al., 2018). Therefore, reduced

MUNC18-1 protein levels are considered the main cause for the symptoms of STXBP1 syndrome.

Since decreased MUNC18-1 protein levels seem causal for STXBP1 syndrome, *Munc18-1* HZ mice are often used as a model system for this disease. *Munc18-1* HZ neurons have approximately 50% reduced MUNC18-1 protein expression compared to WT, mimicking the reduced levels in STXBP1 syndrome (Chen et al., 2020; Kovačević et al., 2018; Miyamoto et al., 2019; Toonen et al., 2005, 2006b; Verhage et al., 2000). In addition, *Munc18-1* HZ mice recapitulate many of the behavioral and neurodevelopmental features seen in patients. For instance, EEG measurements show similar spike wave discharges and epileptic features (Chen et al., 2020; Kovačević et al., 2018; Miyamoto et al., 2019; Ohtahara and Yamatogi, 2006) and harbor many of the other symptoms often seen in patients, including cognitive impairments, hyperactivity and anxiety-like behavior. These studies on disease mechanisms in mice mainly focused on synaptic transmission.

Two studies show that specific synaptic connections are affected in *Munc18-1* HZ mice. First, neurotransmission from cortical to striatal fast spiking interneurons is reduced, but synaptic transmission from cortical to striatal medium spiny neurons (MSNs) is unaffected (Miyamoto et al., 2019). Second, synaptic transmission from PV interneurons to layer 2/3 pyramidal neurons in the somatosensory cortex is decreased, but neurotransmission from Somatostatin interneurons to the same pyramidal neurons is normal (Chen et al., 2020). Cultured mouse neurons also show some defects in synaptic transmission, including reduced SV docking and decreased transmission upon prolonged stimulation, but the first evoked response is normal (Toonen et al., 2006b). Therefore, reduced expression of MUNC18-1 seems to impact synaptic transmission in a different way for each synapse type. Recently, human studies on MUNC18-1 emerge, including one on *STXBP1* HZ IPSC-derived human neurons where MUNC18-1 expression is decreased and evoked EPSC amplitude and miniature EPSC frequency is hampered (Patzke et al., 2015). Neuropeptide secretion has not been assessed yet in this type of human neurons, and any effects of reduced MUNC18-1 levels on DCV exocytosis in mouse or human neurons has not been studied yet either. Therefore, neuropeptide secretion could be an overlooked aspect of STXBP1 syndrome that might contribute to the neurodevelopmental and cognitive aspects of this disease.

3.1 Aim of the Thesis

The role of SM-proteins in DCV exocytosis has remained elusive. In addition, it is unknown if DCV exocytosis principles found in mice generalize to human neurons. Furthermore, the upstream mechanisms required to produce DCVs and prepare them for exocytosis are poorly understood.

The first aim of this thesis is to contribute to our understanding of these pressing outstanding questions in the field. In **chapter 2** we use a genetic approach in combination with live DCV exocytosis reporters to test which SM-protein is required for DCV exocytosis in mouse hippocampal neurons. We identify MUNC18-1 as the main paralog essential for DCV exocytosis, while replacement of MUNC18-1 with MUNC18-2 or -3 does not support DCV exocytosis. In addition, we discover that inactivation of a single

Munc18-1 allele (*Munc18-1* HZ) reduces DCV exocytosis, suggesting that impaired DCV exocytosis may contribute to the neurodevelopmental, behavioral and cognitive defects displayed in *Munc18-1* HZ mice. In **chapter 3**, IPSC derived neurons are used to test the role of STXBP1 (human MUNC18-1) and the effect of STXBP1 patient mutations in DCV exocytosis from human neurons. We show that similar to mouse neurons, STXBP1 is essential for DCV exocytosis in human IPSC derived neurons. In addition, we find that one patient-associated mutation (D207G) in STXBP1 hampers DCV exocytosis, while DCV exocytosis in STXBP1 HZ neurons is unaffected. Therefore, we propose a central role for MUNC18-1/STXBP1 in mouse and human DCV exocytosis, including a possible contribution to the neurodevelopmental and cognitive defects of STXBP1 syndrome.

In **chapter 4**, we investigate the role of MUNC18-2 in neuronal secretion pathways. We show that MUNC18-2 is not required for DCV exocytosis or synaptic transmission. Furthermore, we test GLUT4 vesicle exocytosis in response to different stimulations and show that MUNC18-2 is also not required for this secretion pathway. To investigate the upstream mechanisms required for DCV exocytosis, we develop new assays to study DCV biogenesis and maturation processes in **chapter 5**. We test SNAP-Cell for pulse-chase labeling and show that DCVs in NPY-SNAPtag expressing neurons are only sporadically labeled by this technique. Using time-controlled induction of NPY-pHluorin expression, we find that primary hippocampal mouse neurons have different DCV biogenesis rates ranging from 0 to 1637 DCVs produced after 30 hours, which can largely not be explained by viral load. We conclude that DCV production depends on cell-intrinsic properties and may be affected by neuronal activity. In **chapter 6**, the main findings from each chapter are summarized and placed in context with published literature.

References

Aalto, M.K., Ronne, H., and Keranen, S. (1993). Yeast syntaxins Sso1p and Sso2p belong to a family of related membrane proteins that function in vesicular transport. EMBO J. *12*, 4095–4104.

Ahras, M., Otto, G.P., and Tooze, S.A. (2006). Synaptotagmin IV is necessary for the maturation of secretory granules in PC12 cells. J. Cell Biol. *173*, 241–251.

Ailion, M., Hannemann, M., Dalton, S., Pappas, A., Watanabe, S., Hegermann, J., Liu, Q., Han, H.F., Gu, M., Goulding, M.Q., et al. (2014). Two Rab2 interactors regulate dense-core vesicle maturation. Neuron *82*, 167–180.

Alés, E., Tabares, L., Poyato, J.M., Valero, V., Lindau, M., and De Toledo, G.A. (1999). High calcium concentrations shift the mode of exocytosis to the kiss-and-run mechanism. Nat. Cell Biol. *1*, 40–44.

André, T., Classen, J., Brenner, P., Betts, M.J., Dörr, B., Kreye, S., Zuidinga, B., Meijer, M., Russell, R.B., Verhage, M., et al. (2020). The Interaction of Munc18-1 Helix 11 and 12 with the Central Region of the VAMP2 SNARE Motif Is Essential for SNARE Templating and Synaptic Transmission. ENeuro *7*, 1–15.

Archbold, J.K., Whitten, A.E., Hu, S.-H., Collins, B.M., and Martin, J.L. (2014). SNARE-ing the structures of Sec1/Munc18 proteins. Curr. Opin. Struct. Biol. *29*, 44–51.

Arora, S., Saarloos, I., Kooistra, R., van de Bospoort, R., Verhage, M., and Toonen, R.F. (2017). SNAP-25 gene family members differentially support secretory vesicle fusion. J. Cell Sci. *130*, 1877– 1889.

Asensio, C.S., Sirkis, D.W., and Edwards, R.H. (2010). RNAi screen identifies a role for adaptor protein AP-3 in sorting to the regulated secretory pathway. J. Cell Biol. *191*, 1173–1187.

Ashrafi, G., Wu, Z., Farrell, R.J., and Ryan, T.A. (2017). GLUT4 Mobilization Supports Energetic Demands of Active Synapses. Neuron *93*, 606-615.e3.

Augustin, I., Rosenmund, C., Südhof, T.C., and Brose, N. (1999). Munc13-1 is essential for fusion competence of glutamatergic synaptic vesicles. Nature *400*, 457–461.

Austin, C., Hinners, I., and Tooze, S.A. (2000). Direct and GTP-dependent interaction of ADP-ribosylation factor 1 with clathrin adaptor protein AP-1 on immature secretory granules. J. Biol. Chem. *275*, 21862–21869.

Balkowiec, A., Katz, D.M., and Verhage, M. (2000). Activity-dependent release of endogenous brain-derived neurotrophic factor from primary sensory neurons detected by ELISA in situ. J. Neurosci. *20*, 7417–7423.

Barkus, R. V., Klyachko, O., Horiuchi, D., Dickson, B.J., and Saxton, W.M. (2007). Diacylglycerol Is Required for the Formation of COPI Vesicles in the Golgi-to-ER Transport Pathway. Mol. Biol. Cell *18*, 3250–3263.

Barr, F.A., and Huttner, W.B. (1996). A role for ADP-ribosylation factor 1, but not cop 1, in secretory vesicle biogenesis from the trans-Golgi network. FEBS Lett. *384*, 65–70.

Bennett, M.V.L., and Zukin, R.S. (2004). Electrical Coupling and Neuronal Synchronization in the Mammalian Brain. Neuron *41*, 495–511.

Betz, A., Thakur, P., Junge, H.J., Ashery, U., Rhee, J.S., Scheuss, V., Rosenmund, C., Rettig, J., and Brose, N. (2001). Functional interaction of the active zone proteins Munc13-1 and RIM1 in synaptic vesicle priming. Neuron *30*, 183–196.

Bin, N.R., Jung, C.H., Piggott, C., and Sugita, S. (2013). Crucial role of the hydrophobic pocket region of Munc18 protein in mast cell degranulation. Proc. Natl. Acad. Sci. U. S. A. *110*, 4610–4615.

Bittins, C.M., Eichler, T.W., and Gerdes, H.H. (2009). Expression of the dominant-negative tail of myosin va enhances exocytosis of large dense core vesicles in neurons. Cell. Mol. Neurobiol. *29*, 597–608.

Bittins, C.M., Eichler, T.W., Hammer, J.A., and Gerdes, H.H. (2010). Dominant-negative myosin Va impairs retrograde but not anterograde axonal transport of large dense core vesicles. Cell. Mol. Neurobiol. *30*, 369–379.

Blázquez, M., Thiele, C., Huttner, W.B., Docherty, K., and Shennan, K.I.J. (2000). Involvement of the membrane lipid bilayer in sorting prohormone convertase 2 into the regulated secretory pathway. Biochem. J. *349*, 843–852.

von Blume, J., Alleaume, A.M., Cantero-Recasens, G., Curwin, A., Carreras-Sureda, A., Zimmermann, T., van Galen, J., Wakana, Y., Valverde, M.A., and Malhotra, V. (2011). ADF/cofilin regulates secretory cargo sorting at the TGN via the Ca2+ ATPase SPCA1. Dev. Cell *20*, 652–662.

von Blume, J., Alleaume, A.M., Kienzle, C., Carreras-Sureda, A., Valverde, M., and Malhotra, V. (2012). Cab45 is required for Ca2+;-dependent secretory cargo sorting at the trans-Golgi network. J. Cell Biol. *199*, 1057–1066.

Boncompain, G., and Perez, F. (2013). The many routes of Golgi-dependent trafficking. Histochem. Cell Biol. *140*, 251–260.

Bonnemaison, M.L., Eipper, B.A., and Mains, R.E. (2013). Role of adaptor proteins in secretory granule biogenesis and maturation. Front. Endocrinol. (Lausanne). *4*, 1–17.

Borges, R., Pereda, D., Beltrán, B., Prunell, M., Rodríguez, M., and MacHado, J.D. (2010). Intravesicular factors controlling exocytosis in chromaffin cells. Cell. Mol. Neurobiol. *30*, 1359–1364.

van de Bospoort, R., Farina, M., Schmitz, S.K., de Jong, A., de Wit, H., Verhage, M., and Toonen, R.F. (2012). Munc13 controls the location and efficiency of dense-core vesicle release in neurons. J. Cell Biol. *199*, 883–891.

Bouwman, J., Maia, A.S., Camoletto, P.G., Posthuma, G., Roubos, E.W., Oorschot, V.M.J., Klumperman, J., and Verhage, M. (2004). Quantification of synapse formation and maintenance in vivo in the absence of synaptic release. Neuroscience *126*, 115–126.

Bowser, R., Muller, H., Govindan, B., and Novick, P. (1992). Sec8p and Sec15p are components of a plasma membrane-associated 19.5S particle that may function downstream of Sec4p to control exocytosis. J. Cell Biol. *118*, 1041–1056.

Brandizzi, F., and Barlowe, C. (2013). Organization of the ER-Golgi interface for membrane traffic control. Nat. Rev. Mol. Cell Biol. *14*, 382–392.

Brochetta, C., Suzuki, R., Vita, F., Soranzo, M.R., Claver, J., Madjene, L.C., Attout, T., Vitte, J., Varin-Blank, N., Zabucchi, G., et al. (2014). Munc18-2 and Syntaxin 3 Control Distinct Essential Steps in Mast Cell Degranulation. J. Immunol. *192*, 41–51.

Brownstein, M.J. (1993). A brief history of opiates, opioid peptides, and opioid receptors. Proc. Natl. Acad. Sci. U. S. A. *90*, 5391–5393.

Burgoyne, R.D., Fisher, R.J., and Graham, M.E. (2001). Regulation of kiss-and-run exocytosis. Trends Cell Biol. *11*, 404–405.

Burkhardt, P., Hattendorf, D.A., Weis, W.I., and Fasshauer, D. (2008). Munc18a controls SNARE assembly through its interaction with the syntaxin N-peptide. EMBO J. *27*, 923–933.

Burkhardt, P., Stegmann, C.M., Cooper, B., Kloepper, T.H., Imig, C., Varoqueaux, F., Wahl, M.C., and Fasshauer, D. (2011). Primordial neurosecretory apparatus identified in the choanoflagellate Monosiga brevicollis. Proc. Natl. Acad. Sci. U. S. A. *108*, 15264–15269.

Capogna, M., Gähwiler, B.H., and Thompson, S.M. (1996). Presynaptic inhibition of calcium-dependent and -independent release elicited with ionomycin, gadolinium, and α-latrotoxin in the hippocampus. J. Neurophysiol. *75*, 2017–2028.

Cardenas, E.I., Gonzalez, R., Breaux, K., Da, Q., Gutierrez, B.A., Ramos, M.A., Cardenas, R.A., Burns, A.R., Rumbaut, R.E., and Adachi, R. (2019). Munc18-2, but not Munc18-1 or Munc18-3, regulates platelet exocytosis, hemostasis, and thrombosis. J. Biol. Chem. *294*, 4784–4792.

Carnell, L., and Moore, H.P.H. (1994). Transport via the regulated secretory pathway in semi-intact PC12 cells: Role of intra-cisternal calcium and pH in the transport and sorting of secretogranin II. J. Cell Biol. *127*, 693–705.

Casey, J.R., Grinstein, S., and Orlowski, J. (2010). Sensors and regulators of intracellular pH. Nat. Rev. Mol. Cell Biol. *11*, 50–61.

Cattin-Ortolá, J., Topalidou, I., Dosey, A., Merz, A.J., and Ailion, M. (2017). The dense-core vesicle maturation protein CCCP-1 binds RAB-2 and membranes through its C-terminal domain. Traffic *18*, 720–732.

Cavolo, S.L., Bulgari, D., Deitcher, D.L., and Levitan, E.S. (2016). Activity Induces Fmr1-Sensitive Synaptic Capture of Anterograde Circulating Neuropeptide Vesicles. J. Neurosci. *36*, 11781–11787.

Cetica, V., Santoro, A., Gilmour, K.C., Sieni, E., Beutel, K., Pende, D., Marcenaro, S., Koch, F., Grieve, S., Wheeler, R., et al. (2010). STXBP2 mutations in children with familial haemophagocytic lymphohistiocytosis type 5. J. Med. Genet. *47*, 595–600.

Chanaday, N.L., Cousin, M.A., Milosevic, I., Watanabe, S., and Morgan, J.R. (2019). The synaptic vesicle cycle revisited: New insights into the modes and mechanisms. J. Neurosci. *39*, 8209–8216.

Chanat, E., and Huttner, W.B. (1991). Milieu-induced, selective aggregation of regulated secretory proteins in the trans-Golgi network. J. Cell Biol. *115*, 1505–1519.

Chen, Y.G., and Shields, D. (1996). ADP-ribosylation factor-1 stimulates formation of nascent secretory vesicles from the trans-Golgi network of endocrine cells. J. Biol. Chem. *271*, 5297–5300.

Chen, W., Cai, Z.-L., Chao, E.S., Chen, H., Longley, C.M., Hao, S., Chao, H.-T., Kim, J.H., Messier, J.E., Zoghbi, H.Y., et al. (2020). Stxbp1/Munc18-1 haploinsufficiency impairs inhibition and mediates key neurological features of STXBP1 encephalopathy. Elife *9*, 1–33.

Chen, Z.-Y., Ieraci, A., Teng, H., Dall, H., Meng, C.-X., Herrera, D.G., Nykjaer, A., Hempstead, B.L., and Lee, F.S. (2005). Sortilin Controls Intracellular Sorting of Brain-Derived Neurotrophic Factor to the Regulated Secretory Pathway. J. Neurosci. *25*, 6156–6166.

Clayton, E.L., Evans, G.J.O., and Cousin, M.A. (2008). Bulk synaptic vesicle endocytosis is rapidly triggered during strong stimulation. J. Neurosci. *28*, 6627–6632.

Collin, C., Vicario-Abejon, C., Rubio, M.E., Wenthold, R.J., McKay, R.D.G., and Segal, M. (2001). Neurotrophins act at presynaptic terminals to activate synapses among cultured hippocampal neurons. Eur. J. Neurosci. *13*, 1273–1282.

Colombo, M., Raposo, G., and Théry, C. (2014). Biogenesis, secretion, and intercellular interactions of exosomes and other extracellular vesicles. Annu. Rev. Cell Dev. Biol. *30*, 255–289.

Comeras, L.B., Herzog, H., and Tasan, R.O. (2019). Neuropeptides at the crossroad of fear and hunger: A special focus on neuropeptide y. In Annals of the New York Academy of Sciences, (John Wiley & Sons, Ltd (10.1111)), pp. 59–80.

Cool, D.R., Normant, E., Shen, F.S., Chen, H.C., Pannell, L., Zhang, Y., and Loh, Y.P. (1997). Carboxypeptidase E is a regulated secretory pathway sorting receptor: Genetic obliteration leads to endocrine disorders in Cpe(fat) mice. Cell *88*, 73–83.

Côte, M., Ménager, M.M., Burgess, A., Mahlaoui, N., Picard, C., Schaffner, C., Al-Manjomi, F., Al-Harbi, M., Alangari, A., Le Deist, F., et al. (2009). Munc18-2 deficiency causes familial hemophagocytic lymphohistiocytosis type 5 and impairs cytotoxic granule exocytosis in patient NK cells. J. Clin. Invest. *119*, 3765–3773.

Crevenna, A.H., Blank, B., Maiser, A., Emin, D., Prescher, J., Beck, G., Kienzle, C., Bartnik, K., Habermann, B., Pakde, M., et al. (2016). Secretory cargo sorting by Ca2+-dependent Cab45 oligomerization at the trans-Golgi network. J. Cell Biol. *213*, 305–314.

Derkach, V.A., Oh, M.C., Guire, E.S., and Soderling, T.R. (2007). Regulatory mechanisms of AMPA receptors in synaptic plasticity. Nat. Rev. Neurosci. *8*, 101–113.

Dhanvantari, S., Arnaoutova, I., Snell, C.R., Steinbach, P.J., Hammond, K., Caputo, G.A., London, E., and Loh, Y.P. (2002). Carboxypeptidase E, a prohormone sorting receptor, is anchored to secretory granules via a C-terminal transmembrane insertion. Biochemistry *41*, 52–60.

Dikeakos, J.D., and Reudelhuber, T.L. (2007). Sending proteins to dense core secretory granules: Still a lot to sort out. J. Cell Biol. *177*, 191–196.

Dikeakos, J.D., Lello, P. Di, Lacombe, M.J., Ghirlando, R., Legault, P., Reudelhuber, T.L., and Omichinski, J.G. (2009). Functional and structural characterization of a dense core secretory granule sorting domain from the PC1/3 protease. Proc. Natl. Acad. Sci. U. S. A. *106*, 7408–7413.

Dittié, A.S., Hajibagheri, N., and Tooze, S.A. (1996). The AP-1 adaptor complex binds to immature secretory granules from PC12 cells, and is regulated by ADP-ribosylation factor. J. Cell Biol. *132*, 523–536.

Du, W., Zhou, M., Zhao, W., Cheng, D., Wang, L., Lu, J., Song, E., Feng, W., Xue, Y., Xu, P., et al. (2016). HID-1 is required for homotypic fusion of immature secretory granules during maturation. Elife *5*, 1–22.

Dugani, C.B., and Klip, A. (2005). Glucose transporter 4: Cycling, compartments and controversies. EMBO Rep. *6*, 1137–1142.

Dulubova, I., Khvotchev, M., Liu, S., Huryeva, I., Südhof, T.C., and Rizo, J. (2007). Munc18-1 binds directly to the neuronal SNARE complex. Proc. Natl. Acad. Sci. U. S. A. *104*, 2697–2702.

Eaton, B.A., Haugwitz, M., Lau, D., and Moore, H.P.H. (2000). Biogenesis of regulated exocytotic carriers in neuroendocrine cells. J. Neurosci. *20*, 7334–7344.

Edwards, S.L., Charlie, N.K., Richmond, J.E., Hegermann, J., Eimer, S., and Miller, K.G. (2009). Impaired dense core vesicle maturation in Caenorhabditis elegans mutants lacking Rab2. J. Cell Biol. *186*, 881–895.

Elphick, M.R., Mirabeau, O., and Larhammar, D. (2018). Correction: Evolution of neuropeptide signalling systems (Journal of Experimental Biology (2018) 221 (jeb151092) DOI: 10.1242/jeb.151092). J. Exp. Biol. *221*.

Farina, M., van de Bospoort, R., He, E., Persoon, C.M., van Weering, J.R.T., Broeke, J.H., Verhage, M., Toonen, R.F., Alabi, A., Tsien, R., et al. (2015). CAPS-1 promotes fusion competence of stationary dense-core vesicles in presynaptic terminals of mammalian neurons. Elife *4*, 393–422.

Feldmann, J., Callebaut, I., Raposo, G., Certain, S., Bacq, D., Dumont, C., Lambert, N., Ouachée-Chardin, M., Chedeville, G., Tamary, H., et al. (2003). Munc13-4 Is Essential for Cytolytic Granules Fusion and Is Mutated in a Form of Familial Hemophagocytic Lymphohistiocytosis (FHL3). Cell *115*, 461–473.

Fisher, P., and Ungar, D. (2016). Bridging the gap between glycosylation and vesicle traffic. Front. Cell Dev. Biol. *4*, 1–12.

Gburek-Augustat, J., Beck-Woedl, S., Tzschach, A., Bauer, P., Schoening, M., and Riess, A. (2016). Epilepsy is not a mandatory feature of STXBP1 associated ataxia-tremor-retardation syndrome. Eur. J. Paediatr. Neurol. *20*, 661–665.

Gerdes, H.H., Rosa, P., Phillips, E., Baeuerle, P.A., Frank, R., Argos, P., and Huttner, W.B. (1989). The primary structure of human secretogranin II, a widespread tyrosine-sulfated secretory granule protein that exhibits low pH- and calcium-induced aggregation. J. Biol. Chem. *264*, 12009–12015.

Golebiewska, E.M., and Poole, A.W. (2014). Secrets of platelet exocytosis - what do we really know about platelet secretion mechanisms? Br. J. Haematol. *165*, 204–216.

De Graffenried, C.L., and Bertozzi, C.R. (2004). The roles of enzyme localisation and complex formation in glycan assembly within the Golgi apparatus. Curr. Opin. Cell Biol. *16*, 356–363.

Graham, M.E., Handley, M.T.W., Barclay, J.W., Ciufo, L.F., Barrow, S.L., Morgan, A., and Burgoyne, R.D. (2008). A gain-of-function mutant of Munc18-1 stimulates secretory granule recruitment and exocytosis and reveals a direct interaction of Munc18-1 with Rab3. Biochem. J *409*, 407–416.

Granseth, B., Odermatt, B., Royle, S.J.J., and Lagnado, L. (2006). Clathrin-Mediated Endocytosis Is the Dominant Mechanism of Vesicle Retrieval at Hippocampal Synapses. Neuron *51*, 773–786.

Griebel, G., and Holsboer, F. (2012). Neuropeptide receptor ligands as drugs for psychiatric diseases: The end of the beginning? Nat. Rev. Drug Discov. *11*, 462–478.

Guedes-Dias, P., Nirschl, J.J., Abreu, N., Tokito, M.K., Janke, C., Magiera, M.M., Correspondence, E.L.F.H., and Holzbaur, E.L.F. (2018). Kinesin-3 Responds to Local Microtubule Dynamics to Target Synaptic Cargo Delivery to the Presynapse. Curr. Biol. *29*, 1–15.

Guiberson, N.G.L., Pineda, A., Abramov, D., Kharel, P., Carnazza, K.E., Wragg, R.T., Dittman, J.S., and Burré, J. (2018). Mechanism-based rescue of Munc18-1 dysfunction in varied encephalopathies by chemical chaperones. Nat. Commun. *9*.

Gulyás-Kovács, A., De Wit, H., Milosevic, I., Kochubey, O., Toonen, R., Klingauf, J., Verhage, M., and Sørensen, J.B. (2007). Munc18-1: Sequential interactions with the fusion machinery stimulate vesicle docking and priming. J. Neurosci. *27*, 8676–8686.

Gumy, L.F., Katrukha, E.A., Grigoriev, I., Jaarsma, D., Kapitein, L.C., Akhmanova, A., Hoogenraad, C.C., Gumy, L.F., Katrukha, E.A., Grigoriev, I., et al. (2017). MAP2 Defines a Pre-axonal Filtering Zone to Regulate KIF1- versus KIF5-Dependent Cargo Transport in Sensory Neurons. Neuron *94*, 347- 362.e7.

Guo, W., Roth, D., Walch-Solimena, C., and Novick, P. (1999). The exocyst is an effector for Sec4P, targeting secretory vesicles to sites of exocytosis. EMBO J. *18*, 1071–1080.

Gutierrez, B.A., Chavez, M.A., Rodarte, A.I., Ramos, M.A., Dominguez, A., Petrova, Y., Davalos, A.J., Costa, R.M., Elizondo, R., Tuvim, M.J., et al. (2018). Munc18-2, but not Munc18-1 or Munc18-3, controls compound and single-vesicle–regulated exocytosis in mast cells. J. Biol. Chem. *293*, 7148–7159.

Hackmann, Y., Graham, S.C., Ehl, S., Höning, S., Lehmberg, K., Aricó, M., Owen, D.J., and Griffiths, G.M. (2013). Syntaxin binding mechanism and disease-causing mutations in Munc18-2. Proc. Natl. Acad. Sci. U. S. A. *110*, E4482-91.

Hamdan, F.F., Gauthier, J., Dobrzeniecka, S., Lortie, A., Mottron, L., Vanasse, M., D'Anjou, G., Lacaille, J.C., Rouleau, G.A., and Michaud, J.L. (2011). Intellectual disability without epilepsy associated with STXBP1 disruption. Eur. J. Hum. Genet. *19*, 607–609.

Hamm, H.E. (1998). The many faces of G protein signaling. J. Biol. Chem. *273*, 669–672.

Hammarlund, M., Watanabe, S., Schuske, K., and Jorgensen, E.M. (2008). CAPS and syntaxin dock dense core vesicles to the plasma membrane in neurons. J. Cell Biol. *180*, 483–491.

Hannah, M.J., Schmidt, A. a, and Huttner, W.B. (1999). Synaptic Vesicle Biogenesis. Machinery.

Hansel, D.E., Eipper, B.A., and Ronnett, G. V. (2001). Neuropeptide Y functions as a neuroproliferative factor. Nature *410*, 940–944.

Hartmann, M., Heumann, R., and Lessmann, V. (2001). Synaptic secretion of BDNF after high-frequency stimulation of glutamatergic synapses. EMBO J. *20*, 5887–5897.

Hata, Y., and Südhof, T.C. (1995). A novel ubiquitous form of Munc-18 interacts with multiple syntaxins. Use of the yeast two-hybrid system to study interactions between proteins involved in membrane traffic. J. Biol. Chem. *270*, 13022–13028.

Hawas, R. Al, Ren, Q., Ye, S., Karim, Z.A., Filipovich, A.H., and Whiteheart, S.W. (2012). Munc18b/STXBP2 is required for platelet secretion. Blood *120*, 2493–2500.

He, E., Wierda, K., Van Westen, R., Broeke, J.H., Toonen, R.F., Cornelisse, L.N., and Verhage, M. (2017). Munc13-1 and Munc18-1 together prevent NSF-dependent de-priming of synaptic vesicles. Nat. Commun. *8*.

Heeroma, J.H., Plomp, J.J., Roubos, E.W., and Verhage, M. (2003). Development of the mouse neuromuscular junction in the absence of regulated secretion. Neuroscience *120*, 733–744.

Heeroma, J.H., Roelandse, M., Wierda, K., Van Aerde, K.I., Toonen, R.F.G., Hensbroek, R.A., Brussaard, A., Matus, A., and Verhage, M. (2004). Trophic support delays but not prevent cell-intrinsic degeneration of neurons deficient for munc18-1. Eur. J. Neurosci. *20*, 623–634.

Hinners, I., Wendler, F., Fei, H., Thomas, L., Thomas, G., and Tooze, S.A. (2003). AP-1 recruitment to VAMP4 is modulated by phosphorylation-dependent binding of PACS-1. EMBO Rep. *4*, 1182–1189.

Hirokawa, N., Noda, Y., Tanaka, Y., and Niwa, S. (2009). Kinesin superfamily motor proteins and intracellular transport. Nat. Rev. Mol. Cell Biol. *10*, 682–696.

Hoogstraaten, R.I., Keimpema, L. Van, Toonen, R.F., and Verhage, M. (2020). Tetanus insensitive VAMP2 differentially restores synaptic and dense core vesicle fusion in tetanus neurotoxin treated neurons. Sci. Rep. 1–14.

Hosaka, M., and Watanabe, T. (2010). Secretogranin III: a bridge between core hormone aggregates and the Secretory granule membrane.

Hosaka, M., Watanabe, T., Sakai, Y., Uchiyama, Y., and Takeuchi, T. (2002). Identification of a Chromogranin A Domain That Mediates Binding to Secretogranin III and Targeting to Secretory Granules in Pituitary Cells and Pancreatic $^{\alpha}_{\beta}$-Cells. Mol. Biol. Cell *13*, 1977–2000.

Hosaka, M., Suda, M., Sakai, Y., Izumi, T., Watanabe, T., and Takeuchi, T. (2004). Secretogranin III Binds to Cholesterol in the Secretory Granule Membrane as an Adapter for Chromogranin A. J. Biol. Chem. *279*, 3627–3634.

Houng, A., Polgar, J., and Reed, G.L. (2003). Munc18-syntaxin complexes and exocytosis in human platelets. J. Biol. Chem. *278*, 19627–19633.

Hoyer, D., and Bartfai, T. (2012). Neuropeptides and Neuropeptide Receptors : Drug Targets, and Peptide and Non-Peptide Ligands : a Tribute to Prof . Dieter Seebach are to be cleaved and often post-translationally modified . The first neuropeptide and Gaddum in 1931 . Its sequence was onl. Chem. Biodivers. *9*, 2367–2387.

Hu, S.H., Latham, C.F., Gee, C.L., James, D.E., and Martin, J.L. (2007). Structure of the Munc18c/Syntaxin4 N-peptide complex defines universal features of the N-peptide binding mode of Sec1/Munc18 proteins. Proc. Natl. Acad. Sci. U. S. A. *104*, 8773–8778.

Hummer, B.H., de Leeuw, N.F., Hosford, B., Burns, C., Joens, M.S., Fitzpatrick, J.A.J., and Asensio, C.S. (2017). HID-1 controls cargo sorting and dense core formation by influencing trans- Golgi network acidification in neuroendocrine cells. Mol. Biol. Cell *28*.

Ibata, K., Kono, M., Narumi, S., Motohashi, J., Kakegawa, W., Kohda, K., and Yuzaki, M. (2019). Activity-Dependent Secretion of Synaptic Organizer Cbln1 from Lysosomes in Granule Cell Axons. Neuron 1–15.

Irminger, J.C., Verchere, C.B., Meyer, K., and Halban, P.A. (1997). Proinsulin targeting to the regulated pathway is not impaired in carboxypeptidase E-deficient Cpe(fat)/Cpe(fat) mice. J. Biol. Chem. *272*, 27532–27534.

Ivanova, A., Kalaidzidis, Y., Dirkx, R., Sarov, M., Gerlach, M., Schroth-Diez, B., Müller, A., Liu, Y., Andree, C., Mulligan, B., et al. (2013). Age-dependent labeling and imaging of insulin secretory granules. Diabetes *62*, 3687–3696.

Jahn, R., and Fasshauer, D. (2012). Molecular machines governing exocytosis of synaptic vesicles. Nature *490*, 201–207.

Jahn, R., and Scheller, R.H. (2006). SNAREs - Engines for membrane fusion. Nat. Rev. Mol. Cell Biol. *7*, 631–643.

Jain, S.S., Snook, L.A., Glatz, J.F.C., Luiken, J.J.F.P., Holloway, G.P., Thurmond, D.C., and Bonen, A. (2012). Munc18c provides stimulus-selective regulation of GLUT4 but not fatty acid transporter trafficking in skeletal muscle. FEBS Lett. *586*, 2428–2435.

Jaramillo, A.M., Piccotti, L., Velasco, W. V., Delgado, A.S.H., Azzegagh, Z., Chung, F., Nazeer, U., Farooq, J., Brenner, J., Parker-Thornburg, J., et al. (2019). Different Munc18 proteins mediate baseline and stimulated airway mucin secretion. JCI Insight *4*.

Jékely, G. (2013). Global view of the evolution and diversity of metazoan neuropeptide signaling. Proc. Natl. Acad. Sci. U. S. A. *110*, 8702–8707.

Jewell, J.L., Oh, E., Ramalingam, L., Kalwat, M.A., Tagliabracci, V.S., Tackett, L., Elmendorf, J.S., and Thurmond, D.C. (2011). Munc18c phosphorylation by the insulin receptor links cell signaling directly to SNARE exocytosis. J. Cell Biol. *193*, 185–199.

Jiang, Z., Lietz, C.B., Podvin, S., Yoon, M.C., Toneff, T., Hook, V., and O'Donoghue, A.J. (2021). Differential Neuropeptidomes of Dense Core Secretory Vesicles (DCSV) Produced at Intravesicular and Extracellular pH Conditions by Proteolytic Processing. ACS Chem. Neurosci. *12*, 2385–2398.

Jiao, J., He, M., Port, S.A., Baker, R.W., Xu, Y., Qu, H., Xiong, Y., Wang, Y., Jin, H., Eisemann, T.J., et al. (2018). Munc18-1 catalyzes neuronal SNARE assembly by templating SNARE association. Elife *7*, 1–32.

Jockusch, W.J., Speidel, D., Sigler, A., Sørensen, J.B., Varoqueaux, F., Rhee, J.S., and Brose, N. (2007). CAPS-1 and CAPS-2 Are Essential Synaptic Vesicle Priming Proteins. Cell *131*, 796–808.

Jordens, I., Marsman, M., Kuijl, C., and Neefjes, J. (2005). Rab proteins, connecting transport and vesicle fusion. Traffic *6*, 1070–1077.

Kaeser, P.S., and Regehr, W.G. (2014). Molecular mechanisms for synchronous, asynchronous, and spontaneous neurotransmitter release. Annu. Rev. Physiol. *76*, 333–363.

Kakhlon, O., Sakya, P., Larijani, B., Watson, R., and Tooze, S.A. (2006). GGA function is required for maturation of neuroendocrine secretory granules. EMBO J. *25*, 1590–1602.

Kanda, H., Tamori, Y., Shinoda, H., Yoshikawa, M., Sakaue, M., Udagawa, J., Otani, H., Tashiro, F., Miyazaki, J.I., and Kasuga, M. (2005). Adipocytes from Munc18c-null mice show increased sensitivity to insulin-stimulated GLUT4 externalization. J. Clin. Invest. *115*, 291–301.

Kapitein, L.C., and Hoogenraad, C.C. (2011). Which way to go? Cytoskeletal organization and polarized transport in neurons. Mol. Cell. Neurosci. *46*, 9–20.

Katz, B., and Miledi, R. (1970). Further study of the role of calcium in synaptic transmission. J. Physiol. *207*, 789–801.

Kauppi, M., Wohlfahrt, G., and Olkkonen, V.M. (2002). Analysis of the Munc18b-syntaxin binding interface. Use of a mutant Munc18b to dissect the functions of syntaxins 2 and 3. J. Biol. Chem. *277*, 43973–43979.

Kim, K., Petrova, Y.M., Scott, B.L., Nigam, R., Agrawal, A., Evans, C.M., Azzegagh, Z., Gomez, A., Rodarte, E.M., Olkkonen, V.M., et al. (2012). Munc18b is an essential gene in mice whose expression is limiting for secretion by airway epithelial and mast cells. Biochem. J. *446*, 383–394.

Kim, T., Gondré-Lewis, M.C., Arnaoutova, I., and Loh, Y.P. (2006). Dense-core secretory granule biogenesis. Physiology *21*, 124–133.

Klassen, M.P., Wu, Y.E., Maeder, C.I., Nakae, I., Cueva, J.G., Lehrman, E.K., Tada, M., Gengyo-Ando, K., Wang, G.J., Goodman, M., et al. (2010). An Arf-like Small G Protein, ARL-8, Promotes the Axonal Transport of Presynaptic Cargoes by Suppressing Vesicle Aggregation. Neuron *66*, 710–723.

Klumperman, J. (2011). Architecture of the mammalian Golgi. Cold Spring Harb. Perspect. Biol. *3*, 1–19.

Knabbe, J., Nassal, J.P., Verhage, M., and Kuner, T. (2018). Secretory vesicle trafficking in awake and anaesthetized mice: differential speeds in axons versus synapses. J. Physiol. *596*, 3759–3773.

Kneussel, M., and Wagner, W. (2013). Myosin motors at neuronal synapses: drivers of membrane transport and actin dynamics. Nat. Rev. Neurosci. *14*.

Kovačević, J., Maroteaux, G., Schut, D., Loos, M., Dubey, M., Pitsch, J., Remmelink, E., Koopmans, B., Crowley, J., Cornelisse, L.N., et al. (2018). Protein instability, haploinsufficiency, and cortical hyper-excitability underlie STXBP1 encephalopathy. Brain *141*, 1350–1374.

Kowiański, P., Lietzau, G., Czuba, E., Waśkow, M., Steliga, A., and Moryś, J. (2018). BDNF: A Key Factor with Multipotent Impact on Brain Signaling and Synaptic Plasticity. Cell. Mol. Neurobiol. *38*, 579–593.

Krishnan, A., and Schiöth, H.B. (2015). The role of G protein-coupled receptors in the early evolution of neurotransmission and the nervous system. J. Exp. Biol. *218*, 562–571.

Kurps, J., and De Wit, H. (2012). The role of Munc18-1 and its orthologs in modulation of cortical F-actin in chromaffin cells. In Journal of Molecular Neuroscience, pp. 339–346.

Lam, P.P.L., Ohno, M., Dolai, S., He, Y., Qin, T., Liang, T., Zhu, D., Kang, Y., Liu, Y., Kauppi, M., et al. (2013). Munc18b is a major mediator of insulin exocytosis in rat pancreatic b-Cells. Diabetes *62*, 2416–2428.

Larhammar, D., and Salaneck, E. (2004). Molecular evolution of NPY receptor subtypes. Neuropeptides *38*, 141–151.

Law, C., Schaan Profes, M., Levesque, M., Kaltschmidt, J.A., Verhage, M., and Kania, A. (2016). Normal Molecular Specification and Neurodegenerative Disease-Like Death of Spinal Neurons Lacking the SNARE-Associated Synaptic Protein Munc18-1. J. Neurosci. *36*, 561–576.

Lim, A., Rechtsteiner, A., and Saxton, W.M. (2017). Two kinesins drive anterograde neuropeptide transport. Mol. Biol. Cell *28*, 3542–3553.

Lipka, J., Kapitein, L.C., Jaworski, J., and Hoogenraad, C.C. (2016). Microtubule-binding protein doublecortin-like kinase 1 (DCLK1) guides kinesin-3-mediated cargo transport to dendrites. Embo J. *1*, 1–17.

Liu, Y., Ding, X., Wang, D., Deng, H., Feng, M., Wang, M., Yu, X., Jiang, K., Ward, T., Aikhionbare, F., et al. (2007). A mechanism of Munc18b-syntaxin 3-SANP25 complex assembly in regulated epithelial secretion. FEBS Lett. *581*, 4318–4324.

Lo, K.Y., Kuzmin, A., Unger, S.M., Petersen, J.D., and Silverman, M.A. (2011). KIF1A is the primary anterograde motor protein required for the axonal transport of dense-core vesicles in cultured hippocampal neurons. Neurosci. Lett. *491*, 168–173.

Lou, H., Kim, S.K., Zaitsev, E., Snell, C.R., Lu, B., and Loh, Y.P. (2005). Sorting and activity-dependent secretion of BDNF require interaction of a specific motif with the sorting receptor carboxypeptidase E. Neuron *45*, 245–255.

Lovinger, D.M. (2007). Endocannabinoid liberation from neurons in transsynaptic signaling. J. Mol. Neurosci. *33*, 87–93.

Lund, V.K., Lycas, M.D., Schack, A., Andersen, R.C., and Gether, U. (2020). Rab2 drives axonal transport of dense core vesicles and lysosomal organelles. 1–52.

Luzio, J.P., Hackmann, Y., Dieckmann, N.M.G., and Griffiths, G.M. (2014). The biogenesis of lysosomes and lysosome-related organelles. Cold Spring Harb. Perspect. Biol. *6*, 1–18.

Ma, C., Li, W., Xu, Y., and Rizo, J. (2011). Munc13 mediates the transition from the closed syntaxin-Munc18 complex to the SNARE complex. Nat. Struct. Mol. Biol. *18*, 542–549.

Matsunaga, K., Taoka, M., Isobe, T., and Izumi, T. (2017). Rab2a and Rab27a cooperatively regulate the transition from granule maturation to exocytosis through the dual effector Noc2. J. Cell Sci. *130*, 541–550.

Maus, L., Lee, C.K., Altas, B., Sertel, S.M., Weyand, K., Rizzoli, S.O., Rhee, J.S., Brose, N., Imig, C., and Cooper, B.H. (2020). Ultrastructural Correlates of Presynaptic Functional Heterogeneity in Hippocampal Synapses. Cell Rep. *30*, 3632-3643.e8.

McGirr, R., Guizzetti, L., and Dhanvantari, S. (2013). The sorting of proglucagon to secretory granules is mediated by carboxypeptidase E and intrinsic sorting signals. J. Endocrinol. *217*, 229–240.

Meeths, M., Entesarian, M., Al-Herz, W., Chiang, S.C.C., Wood, S.M., Al-Ateeqi, W., Almazan, F., Boelens, J.J., Hasle, H., Ifversen, M., et al. (2010). Spectrum of clinical presentations in familial hemophagocytic lymphohistiocytosis type 5 patients with mutations in STXBP2. Blood *116*, 2635–2643.

Mehta, S.Q., Hiesinger, P.R., Beronja, S., Zhai, R.G., Schulze, K.L., Verstreken, P., Cao, Y., Zhou, Y., Tepass, U., Crair, M.C., et al. (2005). Mutations in Drosophila sec15 reveal a function in neuronal targeting for a subset of exocyst components. Neuron *46*, 219–232.

Meijer, M., Dörr, B., Lammertse, H.C., Blithikioti, C., Weering, J.R., Toonen, R.F., Söllner, T.H., and Verhage, M. (2018). Tyrosine phosphorylation of Munc18-1 inhibits synaptic transmission by preventing SNARE assembly . EMBO J. *37*, 300–320.

Missler, M., Südhof, T.C., and Biederer, T. (2012). Synaptic cell adhesion. Cold Spring Harb. Perspect. Biol. *4*.

Misura, K.M.S., Scheller, R.H., and Weis, W.I. (2000). Three-dimensional structure of the neuronal-Sec1-syntaxin 1a complex. Nature *404*, 355–362.

Miyamoto, H., Tatsukawa, T., Shimohata, A., Yamagata, T., Suzuki, T., Amano, K., Mazaki, E., Raveau, M., Ogiwara, I., Oba-Asaka, A., et al. (2019). Impaired cortico-striatal excitatory transmission triggers epilepsy. Nat. Commun. *10*, 1–13.

Moore, H.P., Gumbiner, B., and Kelly, R.B. (1983). Chloroquine diverts ACTH from a regulated to a constitutive secretory pathway in AtT-20 cells. Nature *302*, 434–436.

Mosa, M.H., Nicolle, O., Maschalidi, S., Sepulveda, F.E., Bidaud-Meynard, A., Menche, C., Michels, B.E., Michaux, G., de Saint Basile, G., and Farin, H.F. (2018). Dynamic formation of microvillus inclusions during enterocyte differentiation in Munc18-2 deficient intestinal organoids. Cell. Mol. Gastroenterol. Hepatol. *6*, 477-493.e1.

Munck Petersen, C., Nielsen, M.S., Jacobsen, C., Tauris, J., Jacobsen, L., Gliemann, J., Moestrup, S.K., and Madsen, P. (1999). Propeptide cleavage conditions sortilin/neurotensin receptor-3 for ligand binding. EMBO J. *18*, 595–604.

Murthy, M., Garza, D., Scheller, R.H., and Schwarz, T.L. (2003). Mutations in the Exocyst Component Sec5 Disrupt Neuronal Membrane Traffic, but Neurotransmitter Release Persists. Neuron *37*, 433–447.

Nakae, I., Fujino, T., Kobayashi, T., Sasaki, A., Kikko, Y., Fukuyama, M., Gengyo-Ando, K., Mitani, S., Kontani, K., and Katada, T. (2010). The Arf-like GTPase Arl8 Mediates Delivery of Endocytosed Macromolecules to Lysosomes in *Caenorhabditis elegans*. Mol. Biol. Cell *21*, 2434–2442.

Nestor, P.G., O'Donovan, K., Lapp, H.E., Hasler, V.C., Boodai, S.B., and Hunter, R. (2019). Risk and protective effects of serotonin and BDNF genes on stress-related adult psychiatric symptoms. Neurobiol. Stress *11*, 100186.

Nigam, R., Sepulveda, J., Tuvim, M., Petrova, Y., Adachi, R., Dickey, B.F., and Agrawal, A. (2005). Expression and transcriptional regulation of Munc18 isoforms in mast cells. Biochim. Biophys. Acta - Gene Struct. Expr. *1728*, 77–83.

Novick, P., and Schekman, R. (1979). Secretion and cell-surface growth are blocked in a temperature-sensitive mutant of Saccharomyces cerevisiae. Proc. Natl. Acad. Sci. U. S. A. *76*, 1858–1862.

Novick, P., Field, C., and Schekman, R. (1980). Identification of 23 Complementation Groups Required for Post-translational Events in the Yeast Secretory Pathway. Cell *21*, 205–221.

Novick, P., Ferro, S., and Schekman, R. (1981). Order of events in the yeast secretory pathway. Cell *25*, 461–469.

Nykjaer, A., Lee, R., Teng, K.K., Jansen, P., Madsen, P., Nielsen, M.S., Jacobsen, C., Kliemannel, M., Schwarz, E., Willnow, T.E., et al. (2004). Sortilin is essential for proNGF-induced neuronal cell death. Nature *427*, 843–848.

Oh, E., and Thurmond, D.C. (2009). Munc18c depletion selectively impairs the sustained phase of insulin release. Diabetes *58*, 1165–1174.

Oh, E., Spurlin, B.A., Pessin, J.E., and Thurmond, D.C. (2005). Munc18c heterozygous knockout mice display increased susceptibility for severe glucose intolerance. Diabetes *54*, 638–647.

Oh, E., Kalwat, M.A., Kim, M.J., Verhage, M., and Thurmond, D.C. (2012). Munc18-1 regulates first-phase insulin release by promoting granule docking to multiple syntaxin isoforms. J. Biol. Chem. *287*, 25821–25833.

Ohtahara, S., and Yamatogi, Y. (2006). Ohtahara syndrome: With special reference to its developmental aspects for differentiating from early myoclonic encephalopathy. Epilepsy Res. *70*, 58–67.

Ostenson, C.G., Gaisano, H., Sheu, L., Tibell, A., and Bartfai, T. (2006). Impaired gene and protein expression of exocytotic soluble N-ethylmaleimide attachment protein receptor complex proteins in pancreatic islets of type 2 diabetic patients. Diabetes *55*, 435–440.

Padamsey, Z., McGuinness, L., Bardo, S.J., Reinhart, M., Tong, R., Hedegaard, A., Hart, M.L., and Emptage, N.J. (2017). Activity-Dependent Exocytosis of Lysosomes Regulates the Structural Plasticity of Dendritic Spines. Neuron *93*, 132–146.

Pagel, J., Beutel, K., Lehmberg, K., Koch, F., Maul-Pavicic, A., Rohlfs, A.K., Al-Jefri, A., Beier, R., Ousager, L.B., Ehlert, K., et al. (2012). Distinct mutations in STXBP2 are associated with variable clinical presentations in patients with familial hemophagocytic lymphohistiocytosis type 5 (FHL5). Blood *119*, 6016–6024.

Papadopulos, A., Gomez, G.A., Martin, S., Jackson, J., Gormal, R.S., Keating, D.J., Yap, A.S., and Meunier, F.A. (2015). Activity-driven relaxation of the cortical actomyosin II network synchronizes Munc18-1-dependent neurosecretory vesicle docking. Nat. Commun. *6*.

Paquin, N., Murata, Y., Froehlich, A., Omura, D.T., Ailion, M., Pender, C.L., Constantine-Paton, M., and Horvitz, H.R. (2016). The Conserved VPS-50 Protein Functions in Dense-Core Vesicle Maturation and Acidification and Controls Animal Behavior. Curr. Biol. *26*, 862–871.

Parisotto, D., Pfau, M., Scheutzow, A., Wild, K., Mayer, M.P., Malsam, J., Sinning, I., and Söllner, T.H. (2014). An extended helical conformation in domain 3a of Munc18-1 provides a template for SNARE (soluble N-Ethylmaleimidesensitive factor attachment protein receptor) complex assembly. J. Biol. Chem. *289*, 9639–9650.

Park, Y.K., and Goda, Y. (2016). Integrins in synapse regulation. Nat. Rev. Neurosci. *17*, 745–756.

Park, J.H., Straub, V.A., and O'Shea, M. (1998). Anterograde signaling by nitric oxide: Characterization and in vitro reconstitution of an identified nitrergic synapse. J. Neurosci. *18*, 5463–5476.

Patzke, C., Han, Y., Covy, J., Yi, F., Maxeiner, S., Wernig, M., and Südhof, T.C. (2015). Analysis of conditional heterozygous STXBP1 mutations in human neurons. J. Clin. Invest. *125*, 3560–3571.

Peng, R.-W., Guetg, C., Abellan, E., and Fussenegger, M. (2010). Munc18b regulates core SNARE complex assembly and constitutive exocytosis by interacting with the N-peptide and the closed-conformation C-terminus of syntaxin 3. Biochem. J *431*, 353–361.

Persoon, C.M., Moro, A., Nassal, J.P., Farina, M., Broeke, J.H., Arora, S., Dominguez, N., Weering, J.R., Toonen, R.F., and Verhage, M. (2018). Pool size estimations for dense-core vesicles in mammalian CNS neurons. EMBO J. *37*, e99672.

Persoon, C.M., Hoogstraaten, R.I., Nassal, J.P., van Weering, J.R.T., Kaeser, P.S., Toonen, R.F., and Verhage, M. (2019). The RAB3-RIM Pathway Is Essential for the Release of Neuromodulators. Neuron *104*, 1065-1080.e12.

Pinheiro, P.S., Jansen, A.M., de Wit, H., Tawfik, B., Madsen, K.L., Verhage, M., Gether, U., and Sørensen, J.B. (2014). The BAR Domain Protein PICK1 Controls Vesicle Number and Size in Adrenal Chromaffin Cells. J. Neurosci. *34*, 10688–10700.

van den Pol, A.N. (2012). Neuropeptide Transmission in Brain Circuits. Neuron *76*, 98–115.

Ponnambalam, S., and Baldwin, S.A. (2003). Constitutive protein secretion from the trans-Golgi network to the plasma membrane. Mol. Membr. Biol. *20*, 129–139.

Pons-Vizcarra, M., Kurps, J., Tawfik, B., Sørensen, J.B., van Weering, J.R.T., and Verhage, M. (2019). MUNC18-1 regulates the submembrane F-actin network, independently of syntaxin1 targeting, via hydrophobicity in β-sheet 10. J. Cell Sci. *132*, jcs.234674.

Prinslow, E.A., Stepien, K.P., Pan, Y.Z., Xu, J., and Rizo, J. (2019). Multiple factors maintain assembled trans-SNARE complexes in the presence of NSF and αSNAP. Elife *8*, 1–29.

Protopopov, V., Govindan, B., Novick, P., and Gerst, J.E. (1993). Homologs of the synaptobrevin/VAMP family of synaptic vesicle proteins function on the late secretory pathway in S. cerevisiae. Cell *74*, 855–861.

Puertollano, R., Randazzo, P.A., Presley, J.F., Hartnell, L.M., and Bonifacino, J.S. (2001). The GGAs Promote ARF-Dependent Recruitment of Clathrin to the TGN coats containing GGAs, however, remains to be elucidated. The domain organization of the GGAs may hold clues. Cell *105*, 93–102.

Qi, Z., Li, Y., and Tsien, R.W. (2009). The dynamic control of kiss-and-run and vesicular reuse probed with single nanoparticles. Science (80-.). *325*, 1448–1454.

Qin, T., Liang, T., Zhu, D., Kang, Y., Xie, L., Dolai, S., Sugita, S., Takahashi, N., Ostenson, C.-G., Banks, K., et al. (2017). Munc18b Increases Insulin Granule Fusion, Restoring Deficient Insulin Secretion in Type-2 Diabetes Human and Goto-Kakizaki Rat Islets with Improvement in Glucose Homeostasis. EBioMedicine *16*, 262–274.

Rao, V.R., and Finkbeiner, S. (2007). NMDA and AMPA receptors: old channels, new tricks. Trends Neurosci. *30*, 284–291.

Raposinho, P.D., Broqua, P., Pierroz, D.D., Hayward, A., Dumont, Y., Quirion, R., Junien, J.L., and Aubert, M.L. (1999). Evidence that the inhibition of luteinizing hormone secretion exerted by central administration of neuropeptide Y (NPY) in the rat is predominantly mediated by the NPY-Y5 receptor subtype. Endocrinology *140*, 4046–4055.

Reck-Peterson, S.L., Redwine, W.B., Vale, R.D., and Carter, A.P. (2018). The cytoplasmic dynein transport machinery and its many cargoes. Nat. Rev. Mol. Cell Biol. *19*, 382–398.

Reichmann, F., and Holzer, P. (2016). Neuropeptide Y: A stressful review. Neuropeptides *55*, 99–109.

Rizo, J., and Xu, J. (2015). The Synaptic Vesicle Release Machinery. Annu. Rev. Biophys. *44*, 339–367.

Rosa-Ferreira, C., and Munro, S. (2011). Arl8 and SKIP Act Together to Link Lysosomes to Kinesin-1. Dev. Cell *21*, 1171–1178.

Rosenmund, C., Sigler, A., Augustin, I., Reim, K., Brose, N., and Rhee, J.S. (2002). Differential control of vesicle priming and short-term plasticity by Munc13 isoforms. Neuron *33*, 411–424.

De Saint Basile, G., Ménasché, G., and Fischer, A. (2010). Molecular mechanisms of biogenesis and exocytosis of cytotoxic granules. Nat. Rev. Immunol. *10*, 568–579.

Saitsu, H., Kato, M., Mizuguchi, T., Hamada, K., Osaka, H., Tohyama, J., Uruno, K., Kumada, S., Nishiyama, K., Nishimura, A., et al. (2008). De novo mutations in the gene encoding STXBP1 (MUNC18-1) cause early infantile epileptic encephalopathy. Nat. Genet. *40*, 782–788.

Santos, T.C., Wierda, K., Broeke, J.H., Toonen, R.F., and Verhage, M. (2017). Early Golgi Abnormalities and Neurodegeneration upon Loss of Presynaptic Proteins Munc18-1, Syntaxin-1, or SNAP-25. J. Neurosci. *37*, 4525–4539.

Schindler, C., Chen, Y., Pu, J., Guo, X., and Bonifacino, J.S. (2015). EARP is a multisubunit tethering complex involved in endocytic recycling. Nat. Cell Biol. *17*, 639–650.

Schlüter, O.M., Schmitz, F., Jahn, R., Rosenmund, C., and Südhof, T.C. (2004). A complete genetic analysis of neuronal Rab3 function. J. Neurosci. *24*, 6629–6637.

Schlüter, O.M., Basu, J., Südhof, T.C., and Rosenmund, C. (2006). Rab3 superprimes synaptic vesicles for release: Implications for short-term synaptic plasticity. J. Neurosci. *26*, 1239–1246.

Schraw, T.D., Lemons, P.P., Dean, W.L., and Whiteheart, S.W. (2003). A role for Sec1/Munc18 proteins in platelet exocytosis. Biochem. J *374*, 207–217.

Schwenger, D.B., and Kuner, T. (2010). Acute genetic perturbation of exocyst function in the rat calyx of Held impedes structural maturation, but spares synaptic transmission. Eur. J. Neurosci. *32*, 974–984.

Shakiryanova, D., Tully, A., and Levitan, E.S. (2006). Activity-dependent synaptic capture of transiting peptidergic vesicles. Nat. Neurosci. *9*, 896–900.

Shen, J., Tareste, D.C., Paumet, F., Rothman, J.E., and Melia, T.J. (2007). Selective Activation of Cognate SNAREpins by Sec1/Munc18 Proteins. Cell *128*, 183–195.

Shimojo, M., Courchet, J., Pieraut, S., Torabi-Rander, N., Sando, R., Polleux, F., and Maximov, A. (2015). SNAREs Controlling Vesicular Release of BDNF and Development of Callosal Axons. Cell Rep. *11*, 1054–1066.

Shinoda, Y., Ahmed, S., Ramachandran, B., Bharat, V., Brockelt, D., Altas, B., and Dean, C. (2014). BDNF enhances spontaneous and activity-dependent neurotransmitter release at excitatory terminals but not at inhibitory terminals in hippocampal neurons. Front. Synaptic Neurosci. *6*, 1–12.

Shull, G.E., Okunade, G., Liu, L.H., Kozel, P., Periasamy, M., Lorenz, J.N., and Prasad, V. (2003). Physiological Functions of Plasma Membrane and Intracellular Ca2+ Pumps Revealed by Analysis of Null Mutants. Ann. N.Y. Acad. Sci. *11*, 453–460.

Sirkis, D.W., Edwards, R.H., Asensio, C.S., Chandy, K., and Chow, R. (2013). Widespread Dysregulation of Peptide Hormone Release in Mice Lacking Adaptor Protein AP-3. PLoS Genet. *9*, e1003812.

Sitarska, E., Xu, J., Park, S., Liu, X., Quade, B., Stepien, K., Sugita, K., Brautigam, C.A., Sugita, S., and Rizo, J. (2017). Autoinhibition of munc18-1 modulates synaptobrevin binding and helps to enable munc13-dependent regulation of membrane fusion. Elife *6*, 1–24.

Smalheiser, N.R. (2007). Exosomal transfer of proteins and RNAs at synapses in the nervous system. Biol. Direct *2*, 1–15.

Smith, S.J., Smbül, U., Graybuck, L.T., Collman, F., Seshamani, S., Gala, R., Gliko, O., Elabbady, L., Miller, J.A., Bakken, T.E., et al. (2019). Single-cell transcriptomic evidence for dense intracortical neuropeptide networks. Elife *8*, 1–35.

Smyth, A.M., Yang, L., Martin, K.J., Hamilton, C., Lu, W., Cousin, M.A., Rickman, C., and Duncan, R.R. (2013). Munc18-1 protein molecules move between membrane molecular depots distinct from vesicle docking sites. J. Biol. Chem. *288*, 5102–5113.

Spessott, W.A., Sanmillan, M.L., McCormick, M.E., Kulkarni, V. V, and Giraudo, C.G. (2017). SM protein Munc18-2 facilitates transition of Syntaxin 11-mediated lipid mixing to complete fusion for T-lymphocyte cytotoxicity. Proc. Natl. Acad. Sci. U. S. A. *114*, E2176–E2185.

Srinivasan, S., Bunch, D.O., Feng, Y., Rodriguiz, R.M., Li, M., Ravenell, R.L., Luo, G.X., Arimura, A., Fricker, L.D., Eddy, E.M., et al. (2004). Deficits in reproduction and pro-gonadotropin-releasing hormone processing in male Cpefat mice. Endocrinology *145*, 2023–2034.

zur Stadt, U., Rohr, J., Seifert, W., Koch, F., Grieve, S., Pagel, J., Strauß, J., Kasper, B., Nürnberg, G., Becker, C., et al. (2009). Familial Hemophagocytic Lymphohistiocytosis Type 5 (FHL-5) Is Caused by Mutations in Munc18-2 and Impaired Binding to Syntaxin 11. Am. J. Hum. Genet. *85*, 482–492.

Zur Stadt, U., Beutel, K., Kolberg, S., Schneppenheim, R., Kabisch, H., Janka, G., and Hennies, H.C. (2006). Mutation Spectrum in Children With Primary Hemophagocytic Lymphohistiocytosis: Molecular and Functional Analyses of PRF1, UNC13D, STX11, and RAB27A. Hum Mutat. *27*, 62–68.

Stein, C. (2016). Opioid receptors. Annu. Rev. Med. *67*, 433–451.

Stepien, K.P., Prinslow, E.A., and Rizo, J. (2019). Munc18-1 is crucial to overcome the inhibition of synaptic vesicle fusion by αSNAP. Nat. Commun. *10*, 1–18.

Stepp, S.E., Dufourcq-Lagelouse, R., Le Deist, F., Bhawan, S., Certain, S., Mathew, P.A., Henter, J.I., Bennett, M., Fischer, A., De Saint Basile, G., et al. (1999). Perforin gene defects in familial hemophagocytic lymphohistiocytosis. Science (80-.). *286*, 1957–1959.

Steuer Costa, W., Yu, S., Liewald, J.F., and Gottschalk, A. (2017). Fast cAMP Modulation of Neurotransmission via Neuropeptide Signals and Vesicle Loading. Curr. Biol. *27*, 495–507.

Stevens, C.F., and Williams, J.H. (2000). "Kiss and run" exocytosis at hippocampal synapses. Proc. Natl. Acad. Sci. U. S. A. *97*, 12828–12833.

Stucchi, R., Plucińska, G., Hummel, J.J.A., Zahavi, E.E., Guerra San Juan, I., Klykov, O., Scheltema, R.A., Altelaar, A.F.M., and Hoogenraad, C.C. (2018). Regulation of KIF1A-Driven Dense Core Vesicle Transport: Ca 2+ /CaM Controls DCV Binding and Liprin-α/TANC2 Recruits DCVs to Postsynaptic Sites. Cell Rep. *24*, 685–700.

Südhof, T.C. (2012). The presynaptic active zone. Neuron *75*, 11–25.

Südhof, T.C. (2013). Neurotransmitter Release: The Last Millisecond in the Life of a Synaptic Vesicle. Neuron *80*, 675–690.

Südhof, T.C., and Rothman, J.E. (2009). Membrane fusion: Grappling with SNARE and SM proteins. Science (80-.). *323*, 474–477.

Tadokoro, S., Kurimoto, T., Nakanishi, M., and Hirashima, N. (2007). Munc18-2 regulates exocytotic membrane fusion positively interacting with syntaxin-3 in RBL-2H3 cells. Mol. Immunol. *44*, 3427–3433.

Tamori, Y., Kawanishi, M., Niki, T., Shinoda, H., Araki, S., Okazawa, H., and Kasuga, M. (1998). Inhibition of insulin-induced GLUT4 translocation by Munc18c through interaction with syntaxin4 in 3T3-L1 adipocytes. J. Biol. Chem. *273*, 19740–19746.

Tartaglia, N., Du, J., Tyler, W.J., Neale, E., Pozzo-Miller, L., and Lu, B. (2001). Protein Synthesis-dependent and -independent Regulation of Hippocampal Synapses by Brain-derived Neurotrophic Factor. J. Biol. Chem. *276*, 37585–37593.

TerBush, D.R., and Novick (1995). Sec6, Sec8, and Secl5 Are Components of a Multisubunit Complex Which Localizes to Small Bud Tips in Saccharomyces cerevisiae. J. Cell Biol. *130*, 299–312.

TerBush, D.R., Maurice, T., Roth, D., and Novick, P. (1996). The Exocyst is a multiprotein complex required for exocytosis in Saccharomyces cerevisiae. EMBO J. *15*, 6483–6494.

Thurmond, D.C., Ceresa, B.P., Okada, S., Elmendorf, J.S., Coker, K., and Pessin, J.E. (1998). Regulation of insulin-stimulated GLUT4 translocation by Munc18c in 3T3L1 adipocytes. J. Biol. Chem. *273*, 33876–33883.

Toonen, R.F.G., and Verhage, M. (2003). Vesicle trafficking: Pleasure and pain from SM genes. Trends Cell Biol. *13*, 177–186.

Toonen, R.F.G., and Verhage, M. (2007). Munc18-1 in secretion: lonely Munc joins SNARE team and takes control. Trends Neurosci. *30*, 564–572.

Toonen, R.F., Kochubey, O., De Wit, H., Gulyas-Kovacs, A., Konijnenburg, B., Sørensen, J.B., Klingauf, J., and Verhage, M. (2006a). Dissecting docking and tethering of secretory vesicles at the target membrane. EMBO J. *25*, 3725–3737.

Toonen, R.F.G., De Vries, K.J., Zalm, R., Südhof, T.C., and Verhage, M. (2005). Munc18-1 stabilizes syntaxin 1, but is not essential for syntaxin 1 targeting and SNARE complex formation. J. Neurochem. *93*, 1393–1400.

Toonen, R.F.G., Wierda, K., Sons, M.S., de Wit, H., Cornelisse, L.N., Brussaard, A., Plomp, J.J., and Verhage, M. (2006b). Munc18-1 expression levels control synapse recovery by regulating readily releasable pool size. Proc. Natl. Acad. Sci. *103*, 18332–18337.

Tooze, S.A., and Huttner, W.B. (1990). Cell-Free Protein Sorting to the Regulated and Constitutive Secretory Pathways. Cell *60*, 637–647.

Tooze, S.A., Flatmark, T., Tooze, J., and Huttner, W.B. (1991). Characterization of the immature secretory granule, an intermediate in granule biogenesis. J. Cell Biol. *115*, 1491–1503.

Topalidou, I., Cattin-Ortolá, J., Pappas, A.L., Cooper, K., Merrihew, G.E., MacCoss, M.J., and Ailion, M. (2016). The EARP Complex and Its Interactor EIPR-1 Are Required for Cargo Sorting to Dense-Core Vesicles. PLoS Genet. *12*.

Topalidou, I., Cattin-Ortolá, J., Hummer, B., Asensio, C.S., and Ailion, M. (2020). EIPR1 controls dense-core vesicle cargo retention and EARP complex localization in insulin-secreting cells. Mol. Biol. Cell *31*, 59–79.

Tran, T.H.T., Zeng, Q., and Hong, W. (2007). VAMP4 cycles from the cell surface to the trans-Golgi network via sorting and recycling endosomes. J. Cell Sci. *120*, 1028–1041.

Tschenett, A., Singewald, N., Carli, M., Balducci, C., Salchner, P., Vezzani, A., Herzog, H., and Sperk, G. (2003). Reduced anxiety and improved stress coping ability in mice lacking NPY-Y2 receptors. Eur. J. Neurosci. *18*, 143–148.

Tyler, W.J., and Pozzo-Miller, L.D. (2001). BDNF enhances quantal neurotransmitter release and increases the number of docked vesicles at the active zones of hippocampal excitatory synapses. J. Neurosci. *21*, 4249–4258.

Urbé, S., Page, L.J., and Tooze, S.A. (1998). Homotypic fusion of immature secretory granules during maturation in a cell-free assay. J. Cell Biol. *143*, 1831–1844.

Verhage, M., and Sørensen, J.B. (2020). SNAREopathies: Diversity in Mechanisms and Symptoms. Neuron *107*, 22–37.

Verhage, M., McMahon, H.T., Ghijsen, W.E.J.M., Boomsma, F., Scholten, G., Wiegant, V.M., and Nicholls, D.G. (1991). Differential release of amino acids, neuropeptides, and catecholamines from isolated nerve terminals. Neuron *6*, 517–524.

Verhage, M., Maia, A.S., Plomp, J.J., Brussaard, A.B., Heeroma, J.H., Vermeer, H., Toonen, R.F., Hammer, R.E., van den Berg, T.K., Missler, M., et al. (2000). Synaptic Assembly of the Brain in the Absence of Neurotransmitter Secretion. Science (80-.). *287*, 864–869.

Verweij, F.J., Bebelman, M.P., Jimenez, C.R., Garcia-Vallejo, J.J., Janssen, H., Neefjes, J., Knol, J.C., de Goeij-de Haas, R., Piersma, S.R., Baglio, S.R., et al. (2018). Quantifying exosome secretion from single cells reveals a modulatory role for GPCR signaling. J. Cell Biol. *217*, 1129–1142.

Voets, T., Toonen, R.F., Brian, E.C., De Wit, H., Moser, T., Rettig, J., Südhof, T.C., Neher, E., and Verhage, M. (2001). Munc18-1 promotes large dense-core vesicle docking. Neuron *31*, 581–592.

Vogel, G.F., Van Rijn, J.M., Krainer, I.M., Janecke, A.R., Posovzsky, C., Cohen, M., Searle, C., Jantchou, P., Escher, J.C., Patey, N., et al. (2017). Disrupted apical exocytosis of cargo vesicles causes enteropathy in FHL5 patients with Munc18-2 mutations. JCI Insight *2*.

Vukoja, A., Rey, U., Petzoldt, A.G., Ott, C., Vollweiter, D., Quentin, C., Puchkov, D., Reynolds, E., Lehmann, M., Hohensee, S., et al. (2018). Presynaptic Biogenesis Requires Axonal Transport of Lysosome-Related Vesicles. Neuron 1–17.

Wang, S., Li, Y., Gong, J., Ye, S., Yang, X., Zhang, R., and Ma, C. (2019). Munc18 and Munc13 serve as a functional template to orchestrate neuronal SNARE complex assembly. Nat. Commun. *10*, 69.

Watanabe, S., Rost, B.R., Camacho-Pérez, M., Davis, M.W., Söhl-Kielczynski, B., Rosenmund, C., and Jorgensen, E.M. (2013). Ultrafast endocytosis at mouse hippocampal synapses. Nature *504*, 242–247.

Watanabe, S., Trimbuch, T., Camacho-Pérez, M., Rost, B.R., Brokowski, B., Söhl-Kielczynski, B., Felies, A., Davis, M.W., Rosenmund, C., and Jorgensen, E.M. (2014). Clathrin regenerates synaptic vesicles from endosomes. Nature *515*, 228–233.

Watanabe, S., Mamer, L.E., Raychaudhuri, S., Luvsanjav, D., Eisen, J., Trimbuch, T., Söhl-Kielczynski, B., Fenske, P., Milosevic, I., Rosenmund, C., et al. (2018). Synaptojanin and Endophilin Mediate Neck Formation during Ultrafast Endocytosis. Neuron *98*, 1184-1197.e6.

Weimer, R.M., Richmond, J.E., Davis, W.S., Hadwiger, G., Nonet, M.L., and Jorgensen, E.M. (2003). Defects in synaptic vesicle docking in unc-18 mutants. Nat. Neurosci. *6*, 1023–1030.

Wendler, F., Page, L.J., Urbé, S., and Tooze, S.A. (2001). Homotypic Fusion of Immature Secretory Granules During Maturation Requires Syntaxin 6. J. Cell Biol. *143*, 1831–1844.

Werner, F.M., and Coveñas, R. (2010). Classical neurotransmitters and neuropeptides involved in major depression: A review. Int. J. Neurosci. *120*, 455–470.

Westen, R. Van, Poppinga, J., Díez, R., Toonen, R.F., and Verhage, M. (2021). Neuromodulator release in neurons requires two functionally redundant calcium sensors. PNAS *118*.

Williams, S.R., and Stuart, G.J. (1999). Mechanisms and consequences of action potential burst firing in rat neocortical pyramidal neurons. J. Physiol. *521*, 467–482.

de Wit, H., Walter, A.M., Milosevic, I., Gulyás-Kovács, A., Riedel, D., Sørensen, J.B., and Verhage, M. (2009). Synaptotagmin-1 Docks Secretory Vesicles to Syntaxin-1/SNAP-25 Acceptor Complexes. Cell *138*, 935–946.

De Wit, J., and Ghosh, A. (2016). Specification of synaptic connectivity by cell surface interactions. Nat. Rev. Neurosci. *17*, 22–35.

De Wit, J., Toonen, R.F., and Verhage, M. (2009). Matrix-Dependent Local Retention of Secretory Vesicle Cargo in Cortical Neurons. J. Neurosci. *29*, 23–37.

Wong, M.Y., Zhou, C., Shakiryanova, D., Lloyd, T.E., Deitcher, D.L., and Levitan, E.S. (2012). Neuropeptide delivery to synapses by long-range vesicle circulation and sporadic capture. Cell *148*, 1029–1038.

Wu, M.M., Grabe, M., Adams, S., Tsien, R.Y., Moore, H.P.H., and Machen, T.E. (2001). Mechanisms of pH Regulation in the Regulated Secretory Pathway. J. Biol. Chem. *276*, 33027–33035.

Wu, Z., Macneil, A.J., Berman, J.N., and Lin, T.-J. (2013). Syntaxin Binding Protein 1 Is Not Required for Allergic Inflammation via IgE-Mediated Mast Cell Activation. PLoS One *8*.

Yu, H., Rathore, S.S., Lopez, J.A., Davis, E.M., James, D.E., Martin, J.L., and Shen, J. (2013). Comparative studies of Munc18c and Munc18-1 reveal conserved and divergent mechanisms of Sec1/Munc18 proteins. Proc. Natl. Acad. Sci. U. S. A. *110*, E3271-80.

Yue, F., Cheng, Y., Breschi, A., Vierstra, J., Wu, W., Ryba, T., Sandstrom, R., Ma, Z., Davis, C., Pope, B.D., et al. (2014). A comparative encyclopedia of DNA elements in the mouse genome. Nature *515*, 355–364.

Zahn, T.R., Angleson, J.K., MacMorris, M.A., Domke, E., Hutton, J.F., Schwartz, C., and Hutton, J.C. (2004). Dense core vesicle dynamics in Caenorhabditis elegans neurons and the role of kinesin UNC-104. Traffic *5*, 544–559.

Zanetti, G., Pahuja, K.B., Studer, S., Shim, S., and Schekman, R. (2012). Erratum: COPII and the regulation of protein sorting in mammals (Nature Cell Biology (2012) 14 (20-28)). Nat. Cell Biol. *14*, 221.

Zeisel, A., M̂oz-Manchado, A.B., Codeluppi, S., Lönnerberg, P., Manno, G. La, Juréus, A., Marques, S., Munguba, H., He, L., Betsholtz, C., et al. (2015). Cell types in the mouse cortex and hippocampus revealed by single-cell RNA-seq. Science (80-.). *347*, 1138–1142.

Zhu, D., Xie, L., Karimian, N., Liang, T., Kang, Y., Huang, Y.-C., and Gaisano, H.Y. (2015). Munc18c mediates exocytosis of pre-docked and newcomer insulin granules underlying biphasic glucose stimulated insulin secretion in human pancreatic beta-cells. Mol. Metab. *4*, 418–426.

Zhu, P.C., Thureson-Klein, Å., and Klein, R.L. (1986). Exocytosis from large dense cored vesicles outside the active synaptic zones of terminals within the trigeminal subnucleus caudalis: A possible mechanism for neuropeptide release. Neuroscience *19*, 43–54.

Chapter 2

Munc18-1 is essential for neuropeptide secretion in neurons

Munc18-1 is essential for neuropeptide secretion

This chapter is published in the Journal of Neuroscience: 10.1523/jneurosci.3150-20.2021

Authors

Daniël C. Puntman[1], Swati Arora[2], Margherita Farina[1], Ruud F. Toonen[2*], Matthijs Verhage[1,2*]

Affiliations

[1] Section Functional genomics, Department of Clinical Genetics, Center for Neurogenomics and Cognitive Research (CNCR), UMC Amsterdam, The Netherlands

[2] Department of Functional Genomics, Center for Neurogenomics and Cognitive Research (CNCR), *Vrije* Universiteit (VU) Amsterdam, de Boelelaan 1087, 1081 HV Amsterdam, The Netherlands

Abstract

Neuropeptide secretion from dense-core vesicles (DCVs) controls many brain functions. Several components of the DCV exocytosis machinery have recently been identified, but the participation of a SEC1/MUNC18 (SM) protein has remained elusive. Here, we tested the ability of the three exocytic SM-proteins expressed in the mammalian brain, MUNC18-1/2/3, to support neuropeptide secretion. We quantified DCV exocytosis at a single vesicle resolution upon action potential train-stimulation in mouse CNS neurons (of unknown sex) using pHluorin- and/or mCherry-tagged Neuropeptide-Y (NPY) or Brain-Derived Neurotrophic Factor (BDNF). Conditional inactivation of *Munc18-1* abolished all DCV exocytosis. Expression of MUNC18-1, but not MUNC18-2 or MUNC18-3, supported DCV exocytosis in *Munc18-1 null* neurons. Heterozygous (HZ) inactivation of *Munc18-1,* as a model for reduced MUNC18-1 expression, impaired DCV exocytosis, especially during the initial phase of train-stimulation, when the release was maximal. These data show that neurons critically and selectively depend on MUNC18-1 for neuropeptide secretion. Impaired neuropeptide secretion may explain aspects of the behavioral and neurodevelopmental phenotypes that were observed in *Munc18-1* HZ mice.

Statement of significance

Neuropeptide secretion from dense-core vesicles (DCVs) modulates synaptic transmission, sleep, appetite, cognition and mood. However, the mechanisms of DCV exocytosis are poorly characterized. Here, we identify MUNC18-1 as an essential component for neuropeptide secretion from DCVs. Paralogs MUNC18-2 or -3 cannot compensate for MUNC18-1. MUNC18-1 is the first protein identified to be essential for both neuropeptide secretion and synaptic transmission. In heterozygous *Munc18-1* neurons, that have a 50% reduced MUNC18-1 expression and model the human STXBP1 syndrome, DCV exocytosis is impaired, especially during the initial phase of train-stimulation, when the release is maximal. These data show that MUNC18-1 is essential for neuropeptide secretion and that impaired neuropeptide secretion upon reduced MUNC18-1 expression may contribute to the symptoms of STXBP1 syndrome.

Introduction

Neuropeptides control diverse brain functions such as memory, appetite and mood (Cropper et al., 2018; Comeras et al., 2019; Miranda et al., 2019), but the mechanisms that drive neuropeptide release from dense core vesicles (DCVs) remain poorly understood. The principles of secretory vesicle exocytosis are well conserved and first characterized in yeast (Novick and Schekman, 1979; Novick et al., 1980, 1981; Aalto et al., 1993; Protopopov et al., 1993). Four canonical components appear to be essential in all types of regulated exocytosis: three SNARE proteins, of the (i) SNAP/SEC9 family, (ii) the synaptobrevin/VAMP/SNC family, and (iii) the syntaxin/ SSO1/2 family; and (iv) a SEC1/MUNC18 (SM) protein (Toonen and Verhage, 2003, 2007; Jahn and Scheller, 2006; Südhof and Rothman, 2009; Südhof, 2013; Kaeser and Regehr, 2014). While two of these canonical components have recently been identified for DCV exocytosis in mammalian neurons (Shimojo et al., 2015; Arora et al., 2017; Hoogstraaten et al., 2020), the participation of an SM-protein has remained elusive.

In mammals, 7 SM-proteins are expressed: mSly1, mVPS33A, mVPS33B, mVPS45, MUNC18-1, MUNC18-2 and MUNC18-3. The first four control internal membrane trafficking, while the three MUNC18 proteins control exocytosis (For a review see: Toonen and Verhage, 2003). MUNC18 proteins bind syntaxins (Thurmond et al., 1998; Misura et al., 2000; Kauppi et al., 2002; Dulubova et al., 2007; Burkhardt et al., 2008; Bin et al., 2013), promote docking of secretory vesicles (Voets et al., 2001; de Wit et al., 2009) and probably serve as a template for SNARE-complex assembly, which drives exocytosis (Parisotto et al., 2014; Sitarska et al., 2017; Jiao et al., 2018; Meijer et al., 2018; Wang et al., 2019; André et al., 2020). MUNC18-2 acts in blood platelets, cytotoxic T lymphocytes, natural killer cells and mast cells (Côte et al., 2009; Hackmann et al., 2013; Gutierrez et al., 2018; Cardenas et al., 2019); MUNC18-3 in adipocytes (Tamori et al., 1998; Thurmond et al., 2000); and MUNC18-1 in chromaffin cells and the posterior pituitary (Voets et al., 2001; Korteweg et al., 2005) and in synaptic vesicle exocytosis in neurons (Verhage et al., 2000). In other cell types, such as lung mucus cells and pancreatic beta-cells, multiple MUNC18 paralogs support different phases of secretion in the same pathway (Oh and Thurmond, 2009; Oh et al., 2012; Lam et al., 2013; Jaramillo et al., 2019). In neurons, all three MUNC18 paralogs are expressed, but MUNC18-1 has a ~10-fold higher expression and is the only paralog that supports neurotransmission (Verhage et al., 2000; Yue et al., 2014; Zeisel et al., 2015; He et al., 2017; Santos et al., 2017). Which SM-protein(s) support DCV exocytosis is unknown.

To identify which SM-protein(s) support DCV exocytosis in neurons, we analyzed DCV fusion with single vesicle resolution using three fluorescent DCV-fusion reporters in primary neurons from homozygous and heterozygous *Munc18-1 null* mutant mice. We found that *Munc18-1* inactivation abolished neuropeptide release and that expression of MUNC18-2 or MUNC18-3 did not restore DCV exocytosis. Heterozygous (HZ) *Munc18-1* inactivation reduced DCV exocytosis. We conclude that neurons critically and specifically depend on MUNC18-1 for neuropeptide secretion.

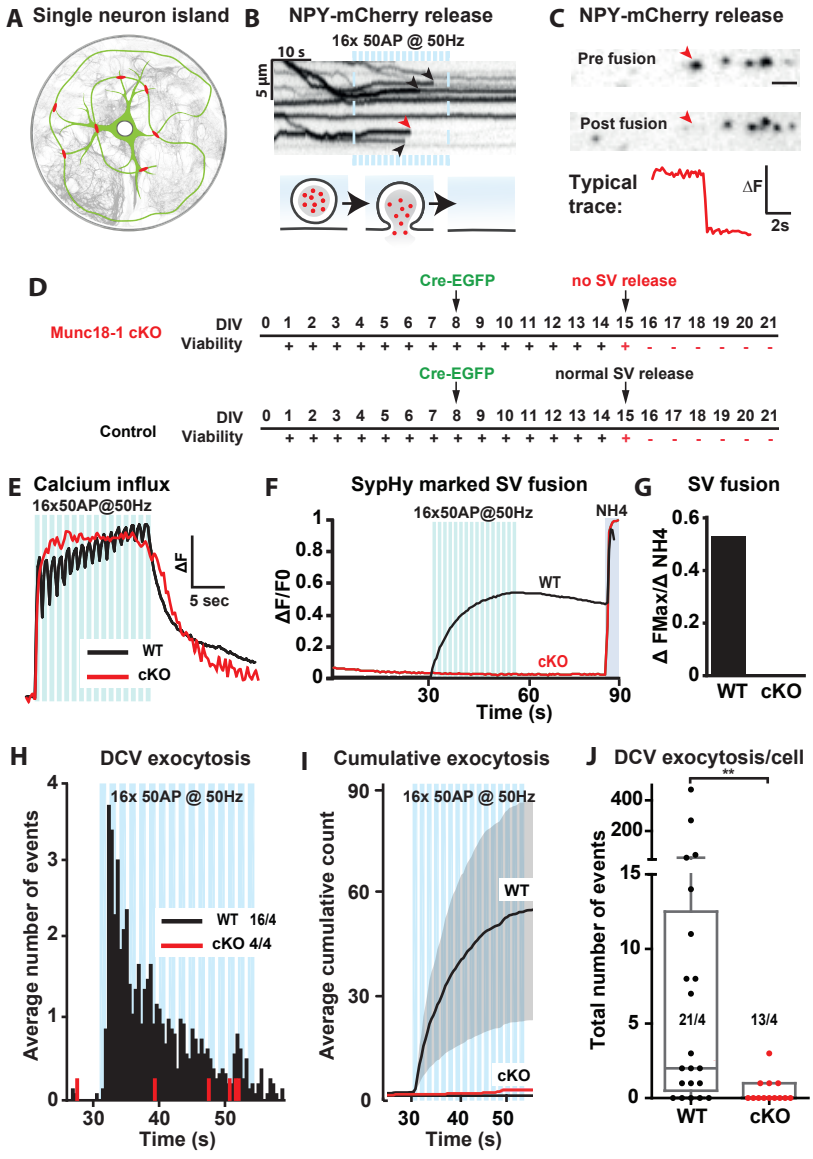

Figure 1: Munc18-1 is essential for DCV exocytosis in neurons. (**A**) Schematic representation of a primary mouse hippocampal neuron grown on a glia micro-island. (**B**) The kymograph shows NPY-mCherry fluorescence in an axonal stretch over time. During high-frequency train-stimulation indicated by blue bars (16 trains of 50 action potentials at 50 Hz), NPY-mCherry release events are visible as an abrupt termination of the line, marked by arrowheads. Below, a schematic model of an NPY-mCherry release event. (**C**) Disappearance of a NPY-mCherry punctum visualized by two still frames: one before and one after the indicated exocytosis event (red arrowhead, same event as in B). The typical trace shows the change in fluorescence (ΔF) over time measured from the indicated exocytosis event. (**D**) Isolated *Munc18-1* cKO and WT (Control) neurons infected at DIV8 with Cre-EGFP were tested for viability (+ = viable, - = non-viable) and for SV exocytosis using Synaptophysin-pHluorin. (**E**) Typical Ca^{2+} traces during high-frequency burst-stimulation (16 trains of 50 action potentials at 50 Hz, blue bars), obtained using Fluo5-AM, which increases fluorescence upon Ca2+ binding, in DIV14-15 *Munc18-1* cKO (+ Cre-EGFP) and WT (- Cre-EGFP) neurons. (**F**) Synaptic vesicle (SV) exocytosis assessed using Synaptophysin-pHluorin (SypHy) in *Munc18-1* cKO (+ Cre-EGFP) and WT (- Cre-EGFP) neurons. Fluorescence intensity increase reports SV exocytosis. NH_4^+ is superfused at second 85 (indicated by gray shading) to dequench SypHy fluorescence in all synaptic vesicles. (**G**) Quantification

of F: ΔFMax/Δ NH_4^+ of Synaptophysin-pHluorin in *Munc18-1* cKO and WT neurons. (**H**) Histogram of the average number of DCV exocytosis events over time from non-silent *Munc18-1* cKO neurons infected with ΔCre (WT) or Cre (cKO). The blue bars indicate the stimulation paradigm. Sample size excluding silent neurons is visualized as n/N. (**I**) Cumulative representation of the data in D. Error bars are SEM. (**J**) The Tukey/scatter plot shows that the total number of DCV exocytosis events per cell is severely reduced in *Munc18-1* cKO neurons (sample size is visualized as n/N). Mann Whitney-U test: ** $p < 0.01$.

Results

Munc18-1 is essential for DCV exocytosis in neurons.

To test which SM-protein(s) drives DCV exocytosis in mammalian neurons, we used hippocampal neurons from conditional *Munc18-1 null* (cKO) mice grown on pre-patterned glia micro-islands, each containing a single neuron infected with NPY-mCherry as a DCV exocytosis reporter (De Wit et al., 2009; Farina et al., 2015; Persoon et al., 2018) (Fig. 1A). Neurons were infected with EGFP-tagged Cre-recombinase at days in vitro (DIV) 8 to induce *Munc18-1 null*, or with ineffective deltaCre (WT) as control. DCV exocytosis was triggered by high-frequency burst-stimulation (16 x 50 AP at 50Hz) (Fig. 1B) and individual release events, marked as sudden disappearance of mCherry fluorescence, were quantified over time (Fig. 1C).

As MUNC18-1 is essential for synaptic vesicle (SV) exocytosis (Verhage et al., 2000), we used the fluorescent SV exocytosis reporter Synaptophysin-pHluorin (Granseth et al., 2006) to assess the Cre-dependent loss of MUNC18-1 protein in *Munc18-1* cKO neurons. SV exocytosis was marked as an increase in fluorescence during burst stimulation in control neurons at DIV15 and was blocked in *Munc18-1* cKO neurons that were infected 7 days earlier with Cre-EGFP, while calcium influx during stimulation was not significantly affected (Fig. 1D-G). In sister cultures at DIV15, control neurons showed NPY-mCherry release events throughout the 50Hz burst stimulation, with the highest rate during the first few bursts, as shown before (Fig. 1H,I; Farina et al., 2015; Persoon et al., 2018, 2019). In contrast, virtually no NPY-mCherry release events occurred in *Munc18-1* cKO neurons (Fig. 1H-J). Not a single release event was observed in 75% of these neurons (Fig. 1J). Hence, MUNC18-1 is essential for neuronal DCV exocytosis.

Expression of MUNC18-1, but not MUNC18-2 or -3, supports DCV exocytosis in *Munc18-1 null* neurons.

For independent confirmation of the DCV exocytosis defect in *Munc18-1* cKO neurons, we next used a different DCV exocytosis reporter in classical *Munc18-1 null* neurons. The pH-sensitive DCV exocytosis reporter NPY-pHluorin, which has low basal fluorescence due to quenching at the low pH inside DCVs, and detects DCV fusion pore opening (van de Bospoort et al., 2012; Farina et al., 2015; Persoon et al., 2018). During high-frequency burst-stimulation, NPY-pHluorin marks DCV exocytosis events by a sudden increase in fluorescence upon DCV fusion with the plasma membrane, followed by an immediate decrease (transient events representing fusion pore closure and vesicle reacidification or full cargo release) or delayed decrease (persistent events representing delayed reacidification or extracellular cargo deposition) (Fig. 2A,B). To visualize the total DCV pool, neurons were superfused with NH_4^+ at the end of each recording, de-quenching NPY-pHluorin in acidified compartments (Fig. 2A,B).

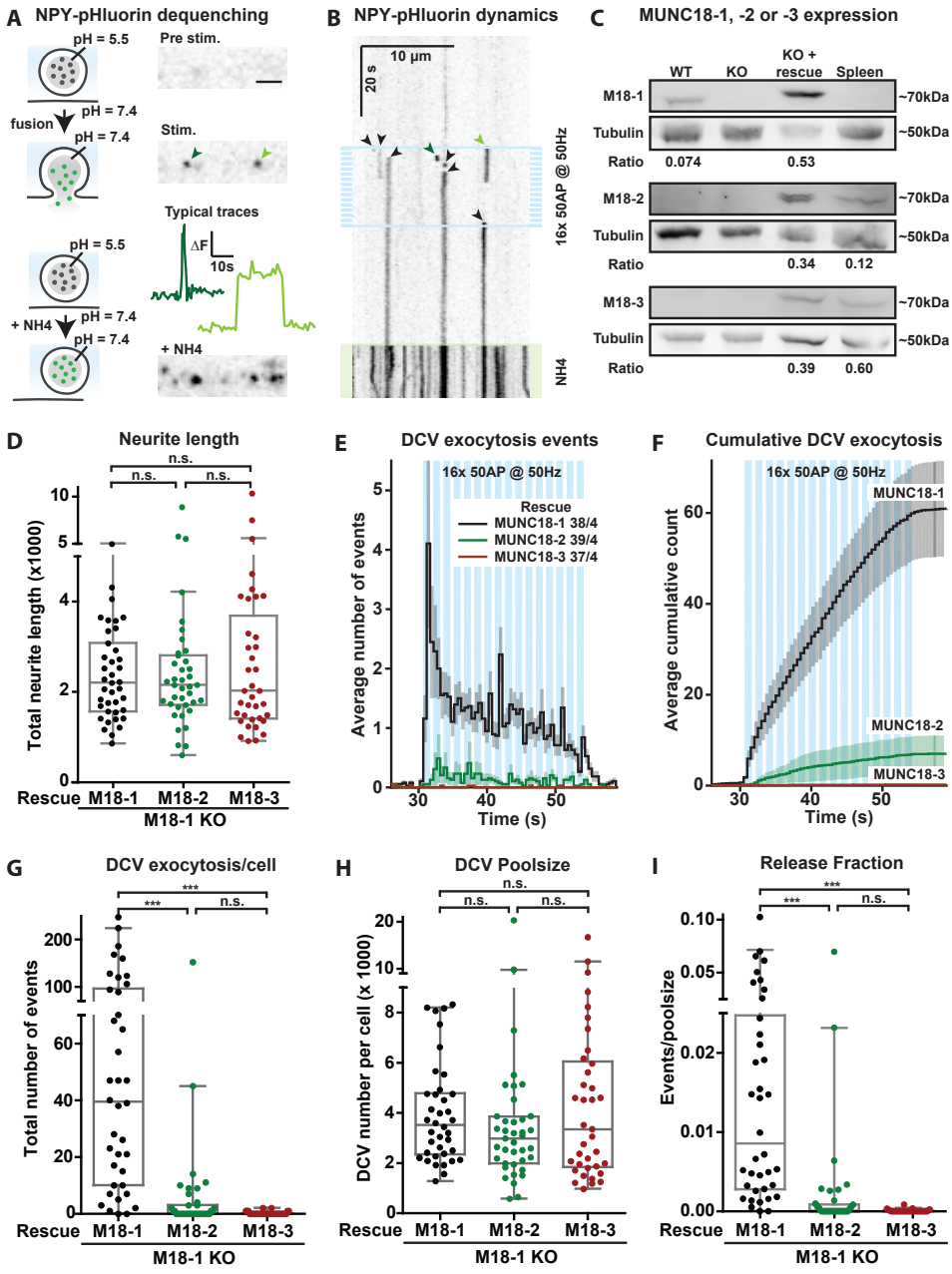

Figure 2: Expression of MUNC18-1, but not MUNC18-2 or -3, supports DCV exocytosis in *Munc18-1 null* neurons. (**A**) Left: model showing the DCV cargo NPY-pHluorin quenched at the low pH inside the vesicle, and de-quenched upon vesicular pH elevation during an exocytosis event or NH_4^+ application. Right: the still frames show an axonal stretch before and during stimulation, and during NH_4^+ perfusion. The line plots show changes in fluorescence (ΔF) over time measured from the exocytosis events indicated by the green arrows. Scale bar: 5µm. (**B**) The kymograph shows an axonal stretch over time, visualizing NPY-pHluorin de-quenching events (arrowheads), caused by DCV exocytosis, as well as de-quenching caused by NH_4^+ (depicted by green-shading at the bottom). High-frequency train-stimulation is indicated with blue bars. The green arrowheads indicate the same exocytosis events as in A. The black arrows indicate other visible exocytosis events. (**C**) Lysates of primary WT neurons, *Munc18-1 null*

(KO) neurons (DIV 14-18) or mouse spleen were separated via SDS-PAGE gel electrophoresis and immunoblotted for MUNC18-1 (M18-1), MUNC18-2 (M18-2) or MUNC18-3 (M18-3), and for γ-Tubulin (Tubulin) as loading control. Rescue of *Munc18-1* KO neurons (indicated with KO + rescue, 3rd lane) was done with Munc18-1 (top), Munc18-2 (middle) or Munc18-3 (bottom) containing lentivirus particles at DIV0. Ratio indicates intensity of MUNC18-1, -2 or -3 divided by tubulin, showing that MUNC18-1 rescue levels were higher than WT and that MUNC18-2 rescue levels were higher, while MUNC18-3 rescue levels were lower than endogenous levels in the spleen. (**D**) The Tukey/scatter plot shows that the total neurite length of *Munc18-1 null* neurons rescued with MUNC18-1, -2 or -3 is similar (Same data set as in Fig. 2). Kruskal-Wallis with Dunn's correction: n.s. = non-significant. (**E**) Histogram showing the average number of NPY-pHluorin labeled DCV exocytosis events in *Munc18-1 null* neurons rescued with MUNC18-1 (black), MUNC18-2 (green) or MUNC18-3 (brown). Sample size is indicated per condition as n/N. The blue bars indicate the stimulation paradigm. Error bars are SEM. (**F**) Cumulative representation of the data in D. Error bars are SEM. (**G**) The Tukey/scatter plot shows that *Munc18-1 null* neurons rescued with MUNC18-2 or MUNC18-3 have a strong reduction in the total number of DCV exocytosis events per cell compared to MUNC18-1 rescued neurons. Kruskal-Wallis with Dunn's correction: *** $p < 0.001$. n.s. = non-significant, $p > 0.05$. (**H**) The Tukey/scatter plot shows that the total pool of DCVs per cell, revealed by NH_4 application, is similar in *Munc18-1 null* neurons rescued with MUNC18-1, -2 or -3. Kruskal-Wallis with Dunn's correction: n.s. = non-significant. For neuronal length and normalized DCV exocytosis see Figure 2-3. (**I**) The Tukey/scatter plot shows that in MUNC18-2 or -3 rescued neurons, the number of DCV exocytosis events normalized by the poolsize (indicated as release fraction) is strongly reduced. Kruskal-Wallis with Dunn's correction: *** $p < 0.001$, n.s. = non-significant.

Munc18-1 null neurons degenerate *in vitro* and *in vivo*, which can be delayed by the trophic factors insulin and BDNF (Verhage et al., 2000; Heeroma et al., 2004). Viral expression of MUNC18-1, or its paralogs MUNC18-2 or MUNC18-3 completely rescues cell viability (He et al., 2017; Santos et al., 2017). To test which paralogs support DCV exocytosis, we expressed each paralog separately in *Munc18-1 null* neurons and quantified DCV exocytosis with NPY-pHluorin. All MUNC18 paralogs were detected on Western-blot, supported normal viability and neurons expressing any of these paralogs had a normal morphology, as reported before (Fig. 2C,D). Re-expression of MUNC18-1 in *Munc18-1 null* neurons resulted in robust DCV exocytosis upon high-frequency burst-stimulation (Fig. 2E-G), comparable to wild-type (WT) neurons (see below). However, DCV exocytosis was severely impaired upon expression of MUNC18-2 or MUNC18-3 (Fig. 2E-G). Not a single fusion event was observed in 56% (MUNC18-2) and 81% (MUNC18-3) of the neurons (Fig. 2G). The total number of DCVs per neuron (DCV poolsize) was similar in all three conditions (Fig. 2H). DCV exocytosis normalized to the poolsize (release fraction) was normal in *Munc18-1 null* neurons re-expressing MUNC18-1, but severely impaired in *Munc18-1 null* neurons expressing MUNC18-2 or MUNC18-3 (Fig. 2I). These data show that MUNC18-1 re-expression supports stimulus-evoked DCV exocytosis in *Munc18-1 null* neurons and that MUNC18-2 and MUNC18-3 do not support DCV exocytosis. In addition, MUNC18-1, -2 and -3 all support normal morphology and DCV biogenesis in *Munc18-1 null* neurons.

Reduced expression in *Munc18-1* HZ neurons leads to decreased DCV exocytosis

To characterize the role of MUNC18-1 in DCV exocytosis further, we quantified exocytosis events of NPY-pHluorin-labeled DCVs under conditions of reduced expression in *Munc18-1* HZ neurons, which are shown to have approximately 50% reduced MUNC18-1 expression levels (Toonen et al., 2006b; Kovačević et al., 2018). First, *Munc18-1* WT and *Munc18-1* HZ neurons were stimulated with a high-frequency burst-stimulation (16 x 50AP at 50Hz). *Munc18-1* HZ neurons showed a trend towards reduced DCV exocytosis, especially during the first two bursts (2 x 50 AP) (Fig. 3A,B). Post hoc analysis of this initial phase indicated a 61% reduction in initial DCV exocytosis in *Munc18-1* HZ neurons (Fig 3C,D). The median DCV exocytosis onset delay, defined as the duration from the start of the stimulation until 50% of the DCV exocytosis events have occurred, was increased in *Munc18-1* HZ (Fig. 3E). The total number of exocytosis events, the total DCV pool and release fraction were all not altered (Fig. 3F-H).

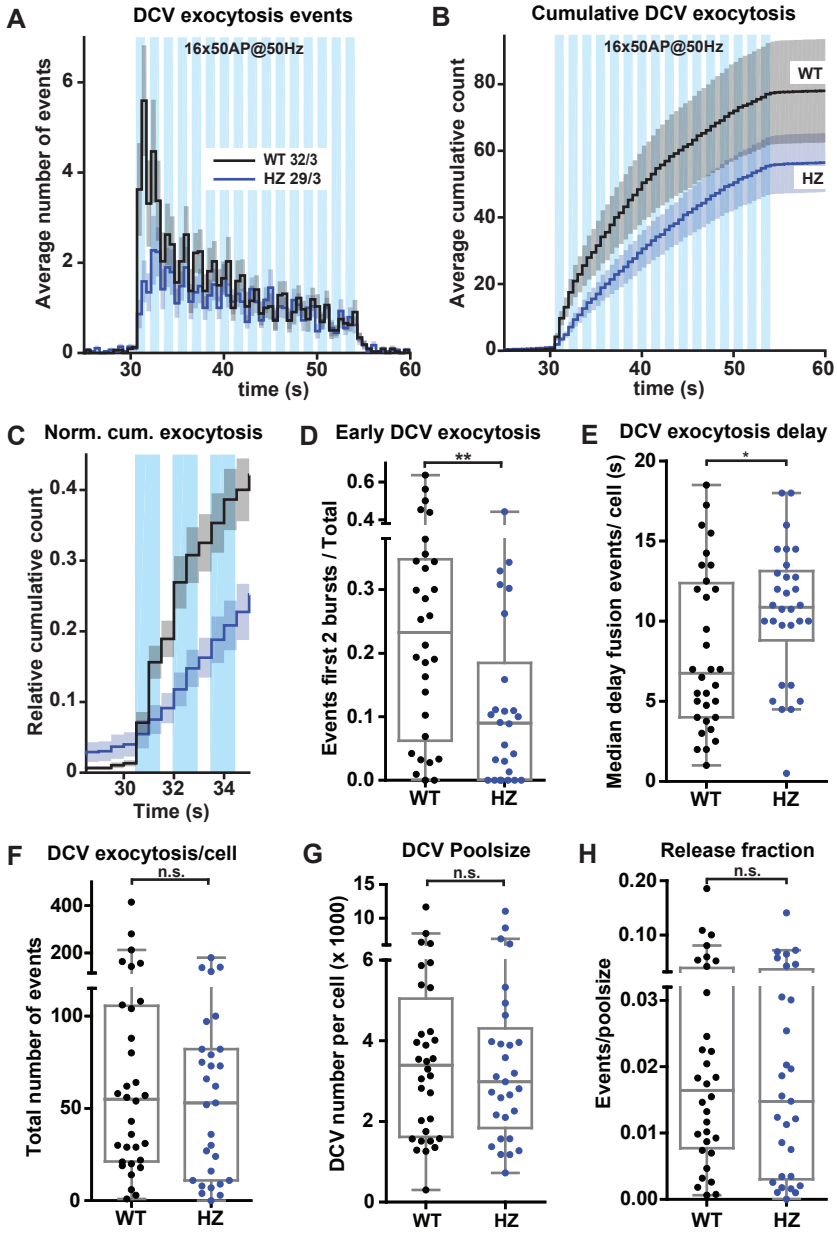

Figure 3: Reduced MUNC18-1 levels decrease DCV exocytosis during the first seconds of stimulation. (**A**) The histogram shows the average number of DCV exocytosis events for *Munc18-1* WT (black) and *Munc18-1* HZ (blue) neurons over time (sample size is indicated as n/N). Error bars are SEM. (**B**) Cumulative representation of the data in A. Error bars are SEM. WT exocytosis levels varied between experiments, probably due to changes in medium batches. (**C**) Normalized cumulative representation of the data in A during the first seconds of train-stimulation. Error bars are SEM. (**D**) The Tukey/scatter plot shows that the relative DCV exocytosis during the first two trains of stimulation is decreased in *Munc18-1* HZ neurons. This was calculated per cell by dividing the number of events during the first two seconds of stimulation by the total number of exocytosis events of that cell. Mann Whitney test: ** $p < 0.01$. (**E**) The Tukey/scatter plot shows that the median delay of DCV exocytosis events relative to the start of the

train-stimulation is larger in *Munc18-1* HZ neurons comparted to WT. Mann Whitney test: * $p < 0.05$. (**F**) The Tukey/scatter plot shows the number of DCV exocytosis events for *Munc18-1* WT and HZ neurons. Mann Whitney test: n.s. = non-significant. (**G**) The Tukey/scatter plot shows the total number of DCVs, extracted from NH_4^+ superfusion at the end of each recording, for *Munc18-1* WT and HZ neurons. Mann Whitney test: n.s. = non-significant. (**H**) The Tukey/scatter plot shows the number of DCV exocytosis events normalized by the poolsize (release fraction) for *Munc18-1* WT and HZ neurons. Mann Whitney test: n.s. = non-significant.

To seek independent confirmation of these effects, we stimulated *Munc18-1* WT and HZ neurons in a new series of experiments with half the number of bursts (8 instead of 16), the same number of action potentials per burst (50) and the same frequency (50Hz), followed by the same pattern 30 seconds later. DCV exocytosis in *Munc18-1* HZ neurons was reduced throughout the first 8-burst train-stimulation, by 79% (Fig. 4A-C, Movie 1,2). During this first 8-burst train-stimulation, the onset of exocytosis events was unaltered in *Munc18-1* HZ neurons compared to WT neurons (Fig 4A,B,D,E). During the subsequent (second) 8-burst train-stimulation, both *Munc18-1* WT and HZ neurons showed acceleration of DCV exocytosis compared with the first train-stimulation, indicated by a strong reduction in the median delay of DCV exocytosis relative to the start of the train-stimulation (Fig. 4A,B,D,E). DCV exocytosis was again reduced in HZ neurons during the second stimulation, with a smaller effect size than during the first stimulation (60% reduction, Fig. 4A,B,F, Movie 1,2), resulting in a median reduction of 69% over the two 8-trains. As a measure for potentiation of DCV exocytosis, the number of exocytosis events during the second stimulation was divided by the number of events during the first stimulation. DCV exocytosis in *Munc18-1* HZ neurons showed a potentiation effect during the second train-stimulation, whereas this was absent in WT neurons (Fig. 4G). The total DCV pool was similar between genotypes (Fig. 4H). Consequently, DCV exocytosis normalized by the poolsize was significantly reduced during both stimulations in *Munc18-1* HZ neurons (Fig. 4I,J).

To assess the overall effect of reduced MUNC18-1 expression on DCV exocytosis in both data sets (Figs. 3 & 4), we performed a meta-analysis combining the data of the first 8 bursts of 50 APs from both experiments. This analysis revealed that DCV exocytosis was reduced by 56% during the first 8 bursts of high-frequency stimulation (Fig. 5A-C). The total number of DCVs and the total neurite length were not altered, and as a consequence, DCV exocytosis normalized to the total DCV pool was reduced by 56% (Fig. 5D-F). Taken together, these data show that HZ inactivation of *Munc18-1* decreased DCV exocytosis, with a relatively stronger effect during the first stimulation, while acceleration of DCV exocytosis during the second stimulation stayed intact.

Finally, to test if the reduction of DCV exocytosis in *Munc18-1* HZ neurons generalizes to different DCV cargo types, we used the neurotrophin release reporter BDNF-pHluorin as an alternative DCV cargo. The total number of BDNF-pHluorin exocytosis events in both genotypes was at least twice as high as with NPY-pHluorin (Fig. 4A,B,C,F, 6A-D). *Munc18-1* HZ neurons expressing BDNF-pHluorin and stimulated with 2 episodes of 8-burst train-stimulation of 50 AP at 50Hz showed a 36% reduced DCV exocytosis during the first stimulation, with a similar, albeit smaller, effect during the second stimulation (Fig. 6A-D), resulting in a median reduction of 43% over the two 8-trains compared to WT. Exocytosis in *Munc18-1* HZ neurons was potentiated during the second train-stimulation, whereas this effect was absent in WT neurons (Fig. 6E). The acceleration of release during the second 8-train was similar to the previous experiment using NPY-pHluorin and similar for both genotypes (Fig 6F,G). The total DCV pool was again similar between experimental groups and consequently DCV exocytosis normalized to the total pool was reduced during the first stimulation, but less pronounced during the second stimulation (Fig. 6H-J). Hence, HZ inactivation of *Munc18-1* and a 50% reduced

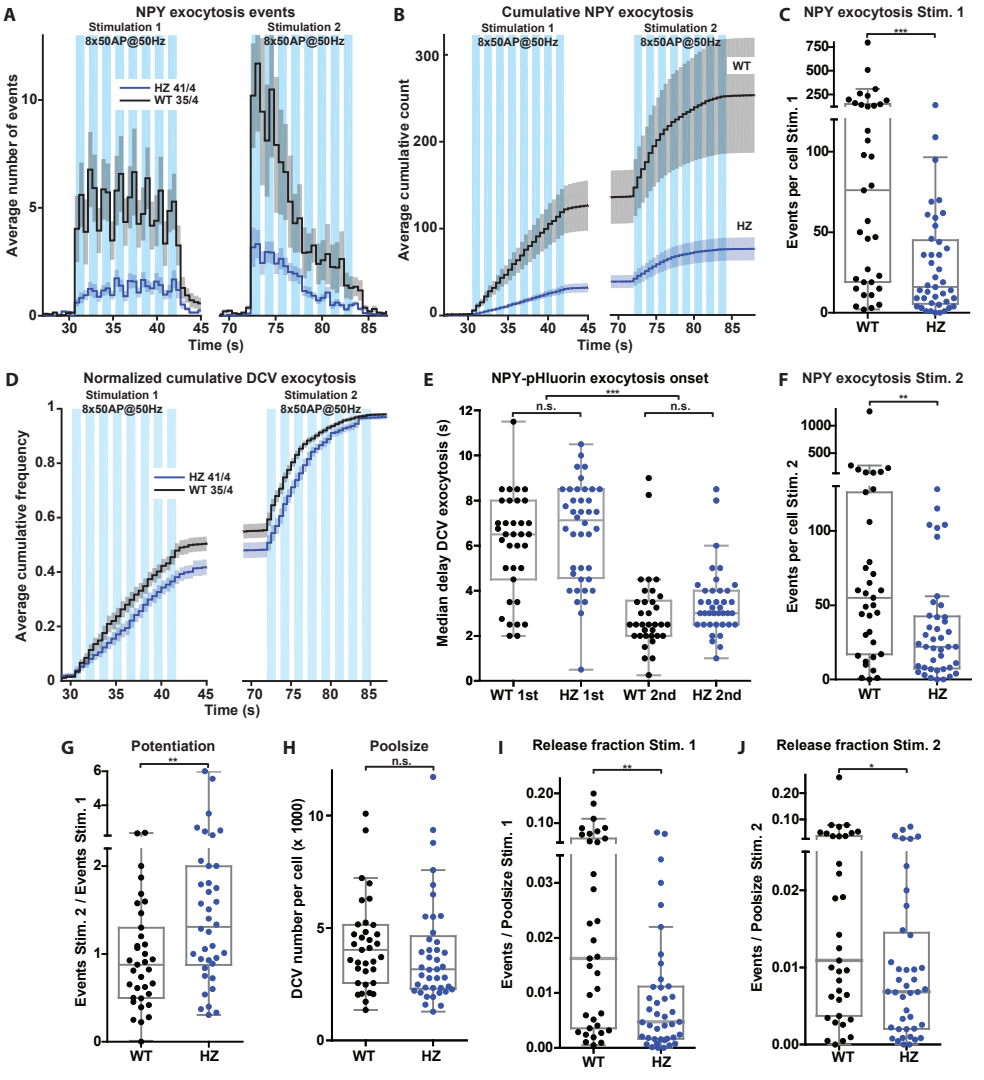

Figure 4: Munc18-1 heterozygous inactivation reduces exocytosis of NPY-pHluorin labeled DCVs. (**A**) The histogram shows the average number of DCV exocytosis events for *Munc18-1* WT (black) and HZ (blue) neurons that were infected with NPY-pHluorin (sample size is indicated as n/N). The blue bars indicate the two stimulation paradigms (8 times 50 action potentials at 50 Hz). Error bars are SEM. (**B**) Cumulative representation of the data in A. Error bars are SEM. (**C**) The Tukey/scatter plot shows that the number of DCV exocytosis events per cell during the first train-stimulation is decreased in *Munc18-1* HZ neurons. Mann Whitney-U test: *** $p < 0.001$. In this experiment, *Munc18-1* WT neurons had higher absolute numbers of DCV exocytosis compared to those in Fig. 3. (**D**) Normalized cumulative representation of the data in A. Error bars are SEM. (**E**) The Tukey/scatter plot shows the median delay of DCV exocytosis events, relative to the start of each train-stimulation, for *Munc18-1* WT and HZ neurons. The delay within each train-stimulation is similar between *Munc18-1* WT and HZ neurons. During the second train-stimulation, in both WT and HZ neurons, the median delay of exocytosis is decreased compared with the first stimulation. Kruskal-Wallis with Dunn's correction: *** $p < 0.001$, n.s. = non-significant. (**F**) The Tukey/scatter plot shows that the number of DCV exocytosis events per cell during the second train-stimulation is decreased in *Munc18-1* HZ neurons. Mann Whitney-U test: ** $p < 0.01$. (**G**) The Tukey/scatter plot shows that the ratio of the number of exocytosis events between the second and first train-stimulation (potentiation) is higher in *Munc18-1* HZ neurons. Mann Whitney-U test: ** $p < 0.01$. (**H**) The Tukey/scatter plot shows that *Munc18-1* WT and HZ neurons have a similar total pool of DCVs, as revealed by NH_4 application. Mann Whitney-U test: n.s. = non-significant. (**I**) The Tukey/scatter plot shows that the number of DCV exocytosis events normalized by the total pool (indicated as release fraction) was decreased

in *Munc18-1* HZ neurons during the first train-stimulation. Mann Whitney-U test: ** p < 0.01. (**J**) The Tukey/scatter plot shows that the number of DCV exocytosis events normalized by the total pool (indicated as release fraction) was decreased in *Munc18-1* HZ neurons during the second train-stimulation. Mann Whitney-U test: * p < 0.01

protein level decreased DCV exocytosis substantially, independent of DCV cargo, with a relatively stronger effect during the first stimulation.

Discussion

Here we report that MUNC18-1 is essential for DCV exocytosis in hippocampal neurons. Live imaging of fluorescent reporters showed that *Munc18-1* inactivation abolished neuropeptide release. Expression of paralogs MUNC18-2 or MUNC18-3 did restore cell viability but not DCV exocytosis. Furthermore, *Munc18-1* HZ inactivation impaired DCV exocytosis. Hence, neurons critically and selectively depend on MUNC18-1 for DCV exocytosis.

We previously showed that neurotransmitter secretion critically depends on MUNC18-1 (Verhage et al., 2000). Our current data demonstrates that this is also true for neuropeptide secretion (Figs. 1, 2). SVs and DCVs share many other components of their exocytosis machinery (van de Bospoort et al., 2012; Cao et al., 2013; Südhof, 2013; Farina et al., 2015; Shimojo et al., 2015; Arora et al., 2017; Persoon et al., 2019; Hoogstraaten et al., 2020), however, several properties are strikingly different. DCVs require a much higher number of action potentials to trigger exocytosis and fuse with a much longer delay after the start of stimulation (Zucker, 1973; Rosenmund et al., 1993; Murthy et al., 1997; Persoon et al., 2018). Additionally, while SV exocytosis is generally confined to specialized presynaptic release sites (active zones), DCVs exocytosis frequently occurs at non-synaptic locations (Südhof and Rizo, 2011; van de Bospoort et al., 2012; Persoon et al., 2018) and synaptic DCV exocytosis may be outside the active zone. It is puzzling that the only mechanistic difference for the final stages of either pathways is the critical requirement of RAB3A in DCV but not SV exocytosis (Schlüter et al., 2004, 2006; Persoon et al., 2018). This seems insufficient to explain the strikingly different properties of the two pathways.

Endogenous expression of *Munc18-2* and *Munc18-3* is insufficient to support neuronal viability, synaptic transmission or DCV exocytosis in *Munc18-1 null* neurons (Fig. 1; Santos et al., 2017; Verhage et al., 2000). Overexpression of MUNC18-2 or MUNC18-3 in *Munc18-1 null* neurons compensates for the absence of MUNC18-1 and restores viability, but does not support synaptic transmission or DCV exocytosis (Fig. 2; He et al., 2017; Santos et al., 2017;). Hence, MUNC18-1 is the only MUNC18 paralog capable of supporting neuropeptide and neurotransmitter release in mouse CNS neurons. Likewise, only one SM-protein (MUNC18-2) mediates secretion from several blood cell types (Côte et al., 2009; Hackmann et al., 2013; Gutierrez et al., 2018; Cardenas et al., 2019), and different MUNC18 paralogs support distinct phases of secretion in the pancreas and lung (Oh and Thurmond, 2009; Oh et al., 2012; Lam et al., 2013; Jaramillo et al., 2019). Conversely, overexpression of MUNC18-2 in *Munc18-1 null* chromaffin cells partly rescues DCV exocytosis (Gulyás-Kovács et al., 2007). Hence, with few exceptions, SM-proteins have highly specialized roles in different forms of regulated secretion, with little or no redundancy among its paralogs. In contrast, the (unknown) function of MUNC18-1 in neuronal viability (Santos et al., 2017) as well as its role in regulating

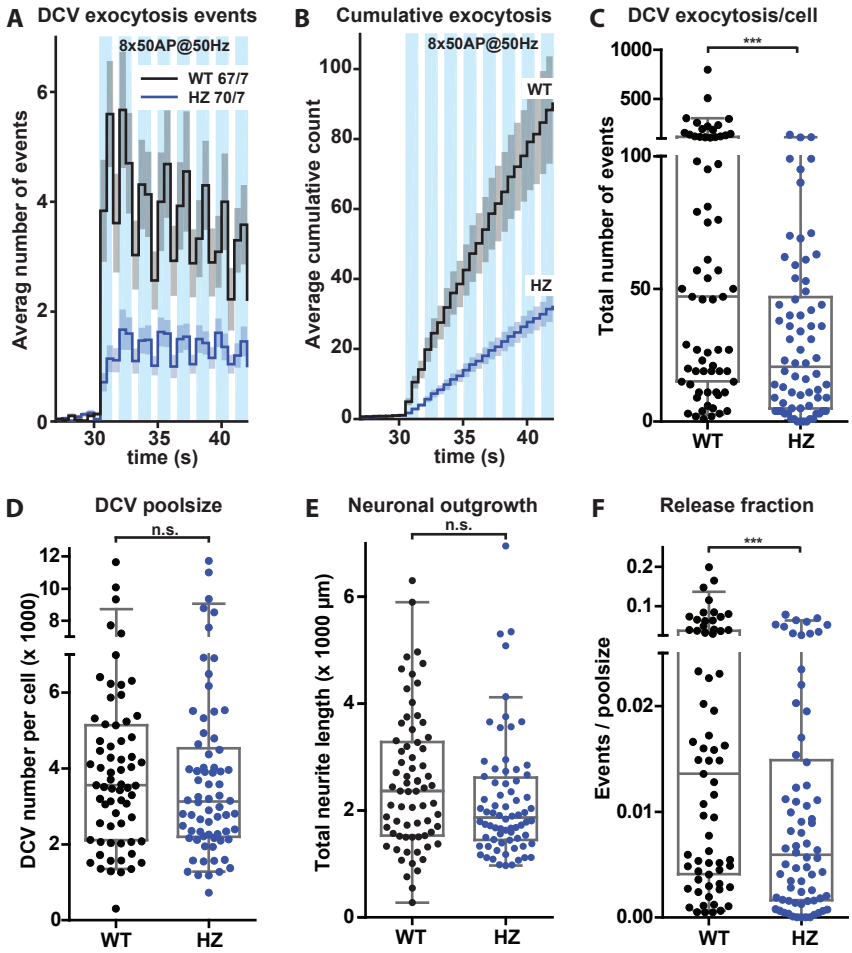

Figure 5: Meta-analysis: Munc18-1 heterozygous inactivation reduces DCV exocytosis. (**A**) The histogram shows the average number of DCV exocytosis events of *Munc18-1* WT (black) and HZ (blue) neurons infected with NPY-pHluorin (sample size is indicated as n/N), during the first 8 bursts of high-frequency train-stimulation (Combined meta-analysis of data sets from figs. 3 & 4). Error bars are SEM. (**B**) Cumulative representation of the data in A. Error bars are SEM. (**C**) The Tukey/scatter plot shows that the number of DCV exocytosis events is decreased in *Munc18-1* HZ neurons during the first 8 bursts of high-frequency train-stimulation. Mann Whitney-U test: *** $p < 0.001$. (**D**) The Tukey/scatter plot shows the total number of DCVs for *Munc18-1* WT and HZ neurons, revealed by NH_4^+ superfusion. Mann Whitney-U test: n.s. = non-significant. (**E**) The Tukey/scatter plot shows the total neurite length of *Munc18-1* WT and HZ neurons. Mann Whitney-U test: n.s. = non-significant. (**F**) The Tukey/scatter plot shows that the number of DCV exocytosis events normalized by the poolsize (indicated as release fraction) is reduced in *Munc18-1* HZ neurons during the first 8 bursts of high-frequency train-stimulation. Mann Whitney-U test: $p < 0.001$

the actin cytoskeleton (Pons-Vizcarra et al., 2019), show ample redundancy among SM-proteins.

We previously showed synaptic assembly of the brain and cortical layering in the absence of synaptic transmission in *Munc18-1 null* mice (Verhage et al., 2000). Our current data suggest that in *Munc18-1 null* brains, secretion of neuropeptides, neurotrophic factors and axon guidance molecules from DCVs may be defective as well, implying that synaptic assembly and cortical layering do not require both secretory pathways. However, we cannot exclude that other, MUNC18-1 independent, secretion pathways may play a

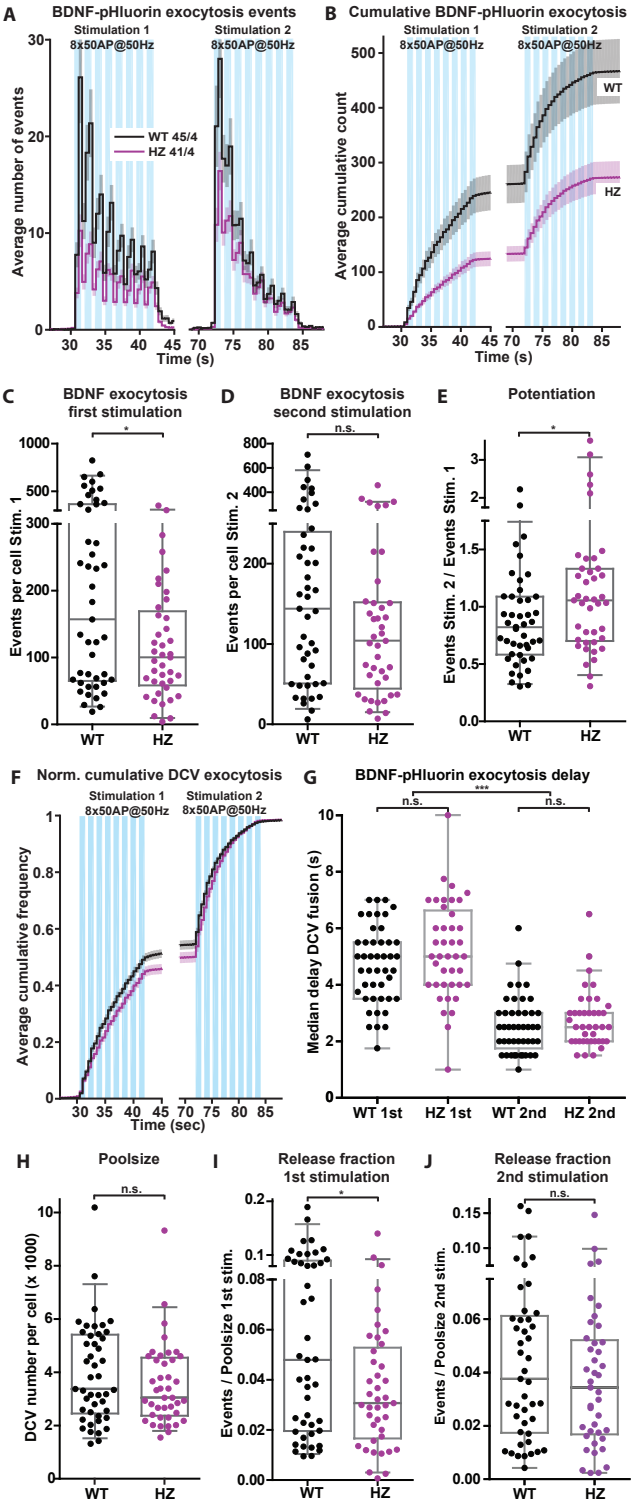

Figure 6: Heterozygous inactivation of *Munc18-1* reduces exocytosis of BDNF-pHluorin labeled DCVs. (A) The histogram shows the average number of DCV exocytosis events for *Munc18-1* WT (black) and HZ (magenta) neurons infected with BDNF-pHluorin (sample size is indicated as n/N). The blue bars indicate the two stimulation paradigms (8 times 50 action potentials at 50 Hz). Error bars are SEM. (**B**) Cumulative representation of the data in A. Error bars are SEM. (**C**) The Tukey/scatter plot shows that the total number of DCV exocytosis events during the first train-stimulation is decreased in *Munc18-1* HZ neurons. Mann Whitney-U test: * $p < 0.05$. (**D**) The Tukey/scatter plot shows the total number of DCV exocytosis events during the second train-stimulation for *Munc18-1* WT and HZ neurons. Mann Whitney-U test: n.s. = non-significant. (**E**) The Tukey/scatter plot shows that the ratio of the number of exocytosis events between the second and first train-stimulation (potentiation) is higher in *Munc18-1* HZ neurons. Mann Whitney-u test: * $p < 0.05$. (**F**) Normalized cumulative representation of the data in A. Error bars are SEM. (**G**) The Tukey/scatter plot shows the median delay of BDNF-pHluorin labeled DCV exocytosis events relative to the start of each train-stimulation for *Munc18-1* WT and HZ neurons. The delay within each train-stimulation is similar between *Munc18-1* WT and HZ neurons. In both WT and HZ neurons, the median delay of exocytosis is decreased during the second train-stimulation compared with the first. Kruskal-Wallis with Dunn's correction: *** $p < 0.001$, n.s. = non-significant. (**H**) The Tukey/scatter plot shows that the total pool of DCVs per cell, revealed by NH_4 application, is similar for *Munc18-1* WT and HZ neurons. Mann Whitney-U test: ns = non-significant. (**I**) The Tukey/scatter plot shows that the number of DCV exocytosis events normalized by the total pool (indicated as release fraction) is decreased in *Munc18-1* HZ neurons during the first train-stimulation. Mann Whitney-U test: * $p < 0.05$. (**J**) The Tukey/scatter plot shows the number of DCV exocytosis events normalized by the total pool (indicated as release fraction) for *Munc18-1* WT and HZ neurons during the second train-stimulation. Mann Whitney-U test: n.s. = non-significant.

role during early brain development. Furthermore, one study recently challenged the conclusion that MUNC18-1 is dispensable for cortical layering of the brain, using more transient interference with MUNC18-1 expression in a small fraction of developing neurons (Hamada et al., 2017). Such a role in brain development may be supported by DCV exocytosis, e.g. by BDNF release (Schwartz et al., 1997; Borghesani et al., 2002; Medina et al., 2004; Zhou et al., 2007). Neuropeptide/neurotrophin signaling is also associated with at least two other aspects of brain development. First, NPY and BDNF promote neural stem cell proliferation and differentiation during development (Hansel et al., 2001; Zhang et al., 2011; Chen et al., 2013). Second, BDNF signaling promotes layer-specific branching of callosal axons *in vivo* (Shimojo et al., 2015) and self-amplifying BDNF signaling underlies axonal differentiation and growth *in vitro* (Cheng et al., 2011). Therefore, it seems plausible that neuropeptides/neurotrophins are released during early brain development in *Munc18-1 null* mice, potentially via constitutive secretion.

BDNF-pHluorin and NPY-pHluorin label a largely overlapping population of DCVs (De Wit et al., 2009; Persoon et al., 2018), but NPY-pHluorin exocytosis events in WT neurons occurred 50% less frequently than BDNF-pHluorin events upon the same stimulation (Figs. 4, 6). Numbers of NPY- or BDNF-pHluorin labeled DCVs were similar (Figs. 4, 6). NPY is inhibits synaptic transmission (Raposinho et al., 1999; Tschenett et al., 2003), while BDNF stimulates spontaneous and evoked synaptic transmission (Collin et al., 2001; Tartaglia et al., 2001; Tyler and Pozzo-Miller, 2001; Shinoda et al., 2014). Our data suggest that NPY and BDNF exert a similar effect on DCV exocytosis.

We observed a different effect size between two data sets obtained with NPY-pHluorin (Figs. 3 and 4), possibly due to differences in culture conditions (supplements, coatings). However, meta-analysis on both data-sets shows clearly reduced DCV exocytosis upon HZ *Munc18-1* inactivation (Fig. 5). To confirm this conclusion with an independent line of evidence, we used DCV exocytosis marker BDNF-pHluorin, and also observed reduced DCV exocytosis in *Munc18-1* HZ neurons (Fig. 6). Hence, HZ *Munc18-1* inactivation reduces DCV exocytosis almost proportionally, by 36% - 56% (Fig. 6 and 4 respectively), while protein levels are 50% reduced (Verhage et al., 2000; Toonen et al., 2005, 2006b; Lee et al., 2019). In contrast, HZ *Munc18-1* inactivation barely affected chromaffin cell secretion, even though docking was ~3-fold reduced (Toonen et al., 2006a), and hippocampal synapses from *Munc18-1* HZ mice had a normal first evoked response (Toonen et al., 2006b). This suggests that DCV exocytosis is generally more vulnerable to reduced MUNC18-1 protein levels than other regulated secretion pathways. However, specific synapses in the brains of *Munc18-1* HZ mice did show substantial impairments, a 40% reduction in synaptic transmission in synapses between neocortical neurons and striatal fast spiking interneurons (Miyamoto et al., 2019) and 45% in synapses between PV interneurons and pyramidal neurons (Chen et al., 2020).

Normal MUNC18-1 expression levels are especially required during the high initial rate of DCV exocytosis, which is ~5 times higher than in later phases (Fig. 3; Arora et al., 2017; Persoon et al., 2018, 2019; Hoogstraaten et al., 2020). In contrast, *Munc18-1* HZ chromaffin cells and synapses showed the largest effects during later phases of release (Toonen et al., 2006a, 2006b; Miyamoto et al., 2019), albeit using different stimulation paradigms. It is tempting to speculate that the MUNC18-1-dependent rate-limiting step in the secretory pathway (probably docking/priming and setting up *trans*-SNARE-complexes) has already taken place prior to the onset of stimulation in chromaffin cells and synapses, while for neuronal DCVs this occurs after the onset. Such a scenario may help to explain why neuronal DCV exocytosis is so much slower than SV exocytosis and

why the initial secretion response in synapses and chromaffin cells is hardly affected by reduced MUNC18-1 expression.

In dual train-stimulated neurons (2 episodes of 8 x 50 AP), NPY- and BDNF-pHluorin exocytosis events were accelerated at the onset of the second stimulation compared to the first (Figs. 4, 6). To our knowledge, such an acceleration of neuronal DCV exocytosis has not been reported before. *Munc18-1* HZ inactivation did not affect this acceleration (Figs. 4, 6). Hence, normal MUNC18-1 expression levels are not required for the acceleration of DCV exocytosis during a second train-stimulation. However, neurons with a reduced MUNC18-1 level, but not wildtype neurons, show potentiation of DCV exocytosis during the second train-stimulation (Figs. 4, 6). Potentiation of DCV exocytosis during dual stimulation has also been observed in (wildtype) *Drosophila* neuromuscular junctions, where ER-mediated calcium release elevates neuropeptide release via CaMKII during a second stimulation episode (Shakiryanova et al., 2007). However, mouse neuronal DCV exocytosis is normal in the absence of both alpha and beta CaMKII (Moro et al., 2020), suggesting that a possible potentiation mechanism does not depend on CaMKII in mouse neurons.

This study shows that neuronal DCV exocytosis is particularly vulnerable to reduced MUNC18-1 expression levels. This finding may be relevant for *STXBP1* syndrome, which is caused by mutations in the human *STXBP1* gene (encoding for MUNC18-1) and characterized by developmental delay, intellectual disability, often epilepsy, motor abnormalities and sometimes also autistic traits (Saitsu et al., 2008; Stamberger et al., 2016; Abramov et al., 2020). Haploinsufficiency, due to impaired MUNC18-1/STXBP1 protein stability and consequently reduced cellular levels, is considered to explain the disease in most cases (Guiberson et al., 2018; Kovačević et al., 2018; Verhage and Sørensen, 2020). *Munc18-1* HZ mice recapitulate the major hallmarks of STXBP1 syndrome (Kovačević et al., 2018; Miyamoto et al., 2019; Chen et al., 2020). Impaired neuropeptide secretion may contribute, in addition to reduced synaptic transmission, to the behavioral and neurodevelopmental phenotypes in *Munc18-1* HZ mice and the pathogenesis of STXBP1 syndrome.

Methods

Animals

Animal housing and breeding was in line with institutional and Dutch governmental guidelines and all procedures were approved by the ethical committee of the VU University/VU Medical Center (license number: DEC-FGA 11-03 and AVD112002017824). Munc18-1$^{lox/lox}$ mice (Heeroma et al., 2004) and *Munc18-1* null mice (Munc18-1 KO) (Verhage et al., 2000; Toonen et al., 2006b) were generated as described before. To obtain Munc18-1 conditional knock-out (cKO) primary cultures, Munc18-1$^{lox/lox}$ mice were time-mated and P1 pups were used for dissection of the hippocampi. For Munc18-1 WT, Munc18-1 KO and Munc18-1 HZ primary cultures, Munc18-1 HZ mice were time-mated and E18 pups were collected via caesarean section, after which they were used for dissection of the hippocampi. All pups were genotyped prior to culturing and were of unknown sex.

Neuron culture

Preparation of dissociated hippocampal neuron cultures was performed as reported before (De Wit et al., 2009; Farina et al., 2015). In brief, isolated hippocampi were digested with 0.25% trypsin (Life Technologies) for 20 min at 37°C in Hanks' balanced salt solution (Sigma) with 10mM HEPES (Life Technologies). After 3x washing and trituration, 1,000-2,000 neurons were plated per well onto pre-grown glia micro-islands. These were generated by stamping agarose coated 18mm glass coverslips with a solution of 0.5mg/ml poly-D-lysine (Sigma), 3.5 mg/ml rat tail collagen (BD Biosciences) and 17mM acetic acid onto which 6.000 rat glia were plated (Mennerick et al., 1995; Wierda et al., 2007).

Viruses

All constructs were generated with sequence verification, cloned into a pLenti vector containing a Synapsin promotor. To obtain Munc18-1 cKO and control neurons, Cre recombinase and defective Cre (deltaCre) (Kaeser et al., 2011; Persoon et al., 2019) were delivered into Munc18-1$^{lox/lox}$ neurons via lenti-virus particles at DIV 8. Imaging was performed at DIV15, when synaptic transmission was absent (Fig S1), but before neuronal degeneration occurred. Lentiviral NPY-mCherry was used as a marker for neuropeptide release as reported before (van de Bospoort et al., 2012; Persoon et al., 2018) and Synaptophysin-pHluorin as a marker for synaptic transmission (Granseth et al., 2006).

To rescue Munc18-1 KO neurons with the paralogs MUNC18-1, -2 or -3, we used previously described MUNC18-1, -2 and -3 plasmids (Toonen et al., 2006b; He et al., 2017; Santos et al., 2017) with Cre-EGFP co-expressed via a T2A cleavage-peptide sequence. Cre-EGFP fluorescence is confined to the nucleus and therefore does not preclude pHluorin-based DCV exocytosis analysis. Munc18-1 KO neurons were infected with these paralogs at DIV0 to ensure neuronal survival and viral concentrations were adjusted until similar survival rates were observed between conditions. For Munc18-1 KO rescue experiments and Munc18-1 HZ experiments, NPY-pHluorin and BDNF-pHluorin were used as described before (De Wit et al., 2009; van de Bospoort et al., 2012; Farina et al., 2015; Persoon et al., 2018, 2019).

Western blot

Munc18-1 null (KO) neurons were infected at DIV0 with Munc18-1, -2 or -3 containing lentiviral particles and harvested by scraping in ice-cold PBS at DIV14. Samples were centrifuged (12,000 rpm, 5 min.) and lysed in Laemmni sample buffer containing 2% SDS (VWR chemicals, M107), 10% glycerol (Merck, 818709), 0.26M β-mercaptoethanol (Sigma, M3148), 60mMTris-HCl (Serva, 37180) pH 6.8, and 0.01% Bromophenol blue (Applichem, A3640). E18 brains from *Munc18-1* KO and WT littermate and the spleen from an E18 WT embryo were triturated in ice-cold PBS prior to lysis in Laemmni sample buffer. Lysates were separated on 8% SDS-polyacrylamide gels. Proteins were transferred overnight at 150mA and 4°C via wet-blot transfer. Blocking was done with 2% BSA (Acros Organics, 268131000) in PBS with 0.1% Tween20 for 4h at RT. Blots were incubated with polyconal Munc18-1 (SySy 116 003; Cijsouw et.al., 2014; 1:1000), Munc18-2 (SySy 116 102; 1:500) or Munc18-3 (Sigma HPA027255; 1:500) antibodies. Mouse monoclonal γ-Tubulin antibody (Sigma; T5326; 1:1000) was used as control for total protein levels. After washing with PBS + 0.1% Tween20, the blots were incubated with secondary antibodies (Goat anti-mouse or anti-rabbit alkaline

phosphatase-conjugated secondary antibodies (1:10000; Jackson) in PBS with 2% BSA and 0.1% Tween20 for 45 min. at 4°C. After washing, blots were incubated with Atto-Phos substrate for 5 min, scanned on a Fujifilm FLA-5000 Reader and analyzed with ImageJ software.

Live imaging

All live imaging experiments were performed between DIV 14 and 18 at room temperature (RT; 21-26°C). We used a custom-built set-up including an inverted microscope (IX81; Olympus) with an MT20 light source (Olympus), the appropriate filter sets (Semrock, Rochester, NY), a 40x oil objective (NA 1.3), an EM charge-coupled device camera (EMCCD; C9100-02; Hamamatsu Photonics, Japan) and Xcellence RT imaging software (Olympus). Electrical stimulation was delivered by parallel platinum electrodes placed around the glia-island, conducting 30 mA, 1 ms pulses controlled by a Master 8 system (AMPI, Germany) and a stimulus generator (A385RC, World Precision Instruments, Germany). 16 or 8 trains of 50 AP were generated at 50 Hz with 0.5s interval after 30 seconds of baseline recording. Imaging acquisition rate was 2Hz.

Coverslips were perfused with Tyrode's solution (2 mM CaCl2, 2.5 mM KCl, 119 mM NaCl, 2 mM MgCl2, 30 mM glucose and 25 mM HEPES, pH 7.4). pHluorin-based DCV exocytosis assays ended with a 10-seconds NH_4^+ perfusion (Tyrode's with 50mM NH_4Cl, replacing 50mM NaCl), delivered via a gravity flow system with a capillary placed above the neuron, to de-quench pHluorin in all DCVs.

Analysis

In ImageJ (NIH), 2x2 pixel regions were placed on NPY-mCherry DCV exocytosis events and 3x3 pixel regions were placed on NPY- or BDNF-pHluorin events. The ROI intensity measures were loaded into a custom written MATLAB (Mathworks) script for semi-automatic analysis, where each was plotted as change in fluorescence (DF) compared to baseline fluorescence (F0, average fluorescence during the first 10 frames). An exocytosis event was detected when DF was at least 2 standard deviations below or above F0 for respectively NPY-mCherry and NPY/BDNF-pHluorin labeled DCVs. Somatic events were excluded because of high background signal. Histograms and cumulative plots were generated in MATLAB. Further analysis including statistical tests and generation of Tukey/scatter plots was conducted in GraphPad Prism. The onset delay in DCV exocytosis was calculated for each neuron by subtracting the time point of the start of the simulation from the time point where 50% of the events have occurred.

To calculate the neurite length and total number of DCVs (poolsize) per neuron, the highest-intensity frame during NH_4 perfusion was taken for pHluorin based assays and further analyzed using the MATLAB program SynD (Schmitz et al., 2011; van de Bospoort et al., 2012). Parameters were optimized for detection of DCVs and the number of detected DCVs was adjusted for intensity by dividing by the mode intensity.

Experimental design and Statistical Analysis

Statistical analysis was performed in GraphPad Prism (summarized in Table 1 which also includes experimental design and full GraphPad Prism output in Fig. 1-2). Shapiro-Wilk normality test was used to test for normal distributions and Levene's to test for homogeneity of variances. In all data sets at least one group was not normally distributed. Therefore, a Mann Whitney-U test for data with two conditions and multiple

comparisons were tested using a Kruskal-Wallis test followed by a Dunn's multiple comparisons post hoc test.

Table 1: Statistical analysis summary and experimental design. The conditions, values, sample sizes, p-values and statistical test are represented for each measurement. n = number of independent experiments (number of cells), n.s. = non-significant, p values were calculated in GraphPad Prism

Measurement	Condition	Value (mean ± SEMs)	n	p value	Statistical test (Test value)
DCV exocytosis per cell Figure 1J	Wild-type *Munc18-1 null (*conditional)	41.4 ± 24.9 0.462 ± 0.877	4(21) 4(13)	** p = 0.0024	Mann Whitney test (53.5
Neurite length Figure 2D	*Munc18-1 null* (1) + MUNC18-1 (2) + MUNC18-2 (3) + MUNC18-3	 2377 ± 160.4 2480 ± 245.1 2720 ± 324.2	 4(38) 4(39) 4(37)	n.s.: 1 versus 2, 1 versus 3, 2 versus 3	Kruskal-Wallis with Dunn's correction (0.040)
DCV exocytosis per cell Figure 2G	*Munc18-1 null* (1) + MUNC18-1 (2) + MUNC18-2 (3) + MUNC18-3	 62.1 ± 10.6 7.05 ± 4.01 0.24 ± 0.09	 4(38) 4(39) 4(37)	n.s.: 2 versus 3 *** p < 0.001: 1 versus 2, 1 versus 3	Kruskal-Wallis with Dunn's correction (65.8)
DCV poolsize Figure 2H	*Munc18-1 null* (1) + MUNC18-1 (2) + MUNC18-2 (3) + MUNC18-3	 3971 ± 327.7 3595 ± 522.0 4381 ± 558.4	 4(38) 4(39) 4(37)	n.s.: 1 versus 2, 1 versus 3, 2 versus 3	Kruskal-Wallis with Dunn's correction (2.15)
Release fraction Figure 2I	*Munc18-1 null* (1) + MUNC18-1 (2) + MUNC18-2 (3) + MUNC18-3	 0.0191 ± 0.0039 0.0030 ± 0.0019 0.000 ± 0.000	 4(38) 4(39) 4(37)	n.s.: 2 versus 3 *** p < 0.001: 1 versus 2, 1 versus 3	Kruskal-Wallis with Dunn's correction (65.3)
Early DCV exocytosis Figure 3D	Wild-type *Munc18-1* HZ	0.238 ± 0.032 0.117 ± 0.026	3(30) 3(26)	** p = 0.0069	Mann Whitney test (225.5)
DCV exocytosis per cell Figure 3E	Wild-type *Munc18-1* HZ	79.1 ± 15.7 57.2 ± 8.9	3(30) 3(26)	n.s. p = 0.502	Mann Whitney test (336.5)
DCV poolsize Figure 3F	Wild-type *Munc18-1* HZ	3642 ± 411.6 3528 ± 432.2	3(30) 3(26)	n.s. p = 0.702	Mann Whitney test (471)

Release fraction Figure 3G	Wild-type *Munc18-1* HZ	0.0306 ± 0.0070 0.0255 ± 0.0058	3(30) 3(26)	n.s. p = 0.598	Mann Whitney test (437)
DCV exocytosis delay Figure 3H	Wild-type *Munc18-1* HZ	8.1 ± 0.9 10.6 ± 0.8	3(30) 3(26)	* p = 0.0438	Mann Whitney test (427)
DCV exocytosis Stim. 1 Figure 4C	Wild-type *Munc18-1* HZ	118 ± 26.9 29.5 ± 5.00	4(35) 4(41)	*** p = 0.0003	Mann Whitney test (366.5)
DCV exocytosis delay Figure 4E	(1) WT 1st stim (2) HZ 1st stim (3) WT 2nd stim (4) HZ 2nd stim	6.0 ± 0.38 6.6 ± 0.36 3.0 ± 0.30 3.5 ± 0.24	4(35) 4(40) 4(35) 4(39)	n.s.: 1 versus 2, 3 versus 4 *** p < 0.001: 1 versus 3, 2 versus 4	Kruskal-Wallis with Dunn's correction (58.8)
DCV exocytosis Stim. 2 Figure 4F	Wild-type *Munc18-1* HZ	105 ± 35.7 33.9 ± 5.44	4(35) 4(41)	** p = 0.0028	Mann Whitney test (430.5)
Potentiation Figure 4G	Wild-type *Munc18-1* HZ	0.97 ± 0.10 1.60 ± 0.20	4(35) 4(41)	** p = 0.0077	Mann Whitney test (423)
Poolsize Figure 4H	Wild-type *Munc18-1* HZ	4224 ± 339 3888 ± 360	4(35) 4(41)	n.s. p = 0.223	Mann Whitney test (600)
Release fraction Stim. 1 Figure 4I	Wild type *Munc18-1* HZ	0.0348 ± 0.0079 0.0104 ± 0.0024	4(35) 4(41)	** p = 0.0028	Mann Whitney test (430)
Release fraction Stim. 2 Figure 4J	Wild type *Munc18-1* HZ	0.0284 ± 0.0078 0.0120 ± 0.0024	4(35) 4(41)	* p = 0.0416	Mann Whitney test (521.5)
DCV exocytosis meta-analysis Figure 5C	Wild type *Munc18-1* HZ	86.7 ± 15.5 31.5 ± 3.88	7(67) 7(70)	*** p = 0.0006	Mann Whitney test (1551)
DCV poolsize meta-analysis Figure 5D	Wild type *Munc18-1* HZ	3946 ± 265.0 3739 ± 275.2	7(67) 7(70)	n.s. p = 0.338	Mann Whitney test (2122)
Neurite length Figure 5E	Wild type *Munc18-1* HZ	2525 ± 152.6 2185 ± 134.3	7(70) 7(72)	n.s. p = 0.0631	Mann Whitney test (2064)
Release fraction Figure 5F	Wild type *Munc18-1* HZ	0.0284 ± 0.0049 0.0129 ± 0.0022	7(67) 7(70)	** p = 0.0039	Mann Whitney test (1675)

BDNF-pHluorin exocytosis Stim. 1 Figure 6C	Wild type *Munc18-1* HZ	233 ± 31.0 118 ± 13.2	4(45) 4(41)	* p = 0.0230	Mann Whitney test (659)
BDNF-pHluorin exocytosis Stim. 2 Figure 6D	Wild type *Munc18-1* HZ	182 ± 24.0 127 ± 16.3	4(45) 4(41)	n.s. p = 0.1336	Mann Whitney test (748.5)
Potentiation BDNF-pHluorin Figure 6E	Wild type *Munc18-1* HZ	0.878 ± 0.061 1.175 ± 0.108	4(45) 4(41)	* p = 0.0300	Mann Whitney test (671)
BDNF-pHluorin exocytosis delay Figure 6G	(1) WT 1st Stim. (2) HZ 1st Stim. (3) WT 2nd Stim. (4) HZ 2nd Stim.	4.7 ± 0.2 5.2 ± 0.3 2.5 ± 0.1 2.8 ± 0.2	4(45) 4(41) 4(45) 4(40)	n.s.: 1 versus 2, 3 versus 4 *** p < 0.001: 1 versus 3, 2 versus 4	Kruskal-Wallis with Dunn's correction (83)
DCV poolsize BDNF-pHluorin Figure 6H	Wild type *Munc18-1* HZ	3947 ± 275.1 3514 ± 236.7	4(45) 4(41)	n.s. p = 0.2895	Mann Whitney test (669.5)
BDNF-pHluorin release fraction Stim. 1 Figure 6I	Wild type *Munc18-1* HZ	0.0586 ± 0.0066 0.0372 ± 0.0043	4(45) 4(41)	* p = 0.0449	Mann Whitney test (690)
BDNF-pHluorin release fraction Stim. 2 Figure 6J	Wild type *Munc18-1* HZ	0.0466 ± 0.0055 0.0383 ± 0.0046	4(45) 4(41)	n.s. p = 0.3920	Mann Whitney test (823)

Acknowledgements

The authors thank Robbert Zalm for cloning and producing viral particles, Lisa Laan and Desiree Schut for producing glia island cultures and providing primary culture assistance, Joke Wortel for organizing the animal breeding, Joost Hoetjes for genotyping, Jurjen Broeke for technical support, Ingrid Saarloos for Western blots and members of the CNCR DCV team for discussions and helpful input. This work is supported by an ERC Advanced Grant (322966) of the European Union (to MV).

Author contributions

D.C.P., M.F., R.F.T. and M.V. designed the experiments. D.C.P. performed all pHluorin-based live imaging assays and analyzed these data. S.A and M.F. performed the cherry-based live imaging experiment and designed figure 1 & S1. D.C.P., R.F.T and M.V. designed figures and wrote the manuscript with input from all authors.

Conflict of interest

The authors declare that they have no conflict of interest.

Supplemental information

Movies 1, 2 (Puntman et al., 2021)

References

Aalto MK, Ronne H, Keranen S (1993) Yeast syntaxins Sso1p and Sso2p belong to a family of related membrane proteins that function in vesicular transport. EMBO J 12:4095–4104 DOI: 10.1002/j.1460-2075.1993.tb06093.x.

Abramov D, Guiberson NGL, Burré J (2020) STXBP1 encephalopathies: Clinical spectrum, disease mechanisms, and therapeutic strategies. J Neurochem:1–14 DOI: 10.1111/jnc.15120.

André T, Classen J, Brenner P, Betts MJ, Dörr B, Kreye S, Zuidinga B, Meijer M, Russell RB, Verhage M, Söllner TH (2020) The Interaction of Munc18-1 Helix 11 and 12 with the Central Region of the VAMP2 SNARE Motif Is Essential for SNARE Templating and Synaptic Transmission. eNeuro 7:1–15 DOI: 10.1523/ENEURO.0278-20.2020.

Arora S, Saarloos I, Kooistra R, van de Bospoort R, Verhage M, Toonen RF (2017) SNAP-25 gene family members differentially support secretory vesicle fusion. J Cell Sci 130:1877–1889 DOI: 10.1242/jcs.201889.

Bin N-R, Jung CH, Piggott C, Sugita S (2013) Crucial role of the hydrophobic pocket region of Munc18 protein in mast cell degranulation. Proc Natl Acad Sci U S A 110:4610–4615 DOI: 10.1073/pnas.1214887110.

Borghesani PR, Peyrin JM, Klein R, Rubin J, Carter AR, Schwartz PM, Luster A, Corfas G, Sergal RA (2002) BDNF stimulates migration of cerebellar granule cells. Development 129:1435–1442.

Burkhardt P, Hattendorf DA, Weis WI, Fasshauer D (2008) Munc18a controls SNARE assembly through its interaction with the syntaxin N-peptide. EMBO J 27:923–933 DOI: 10.1038/emboj.2008.37.

Cao P, Yang X, Südhof TC (2013) Complexin activates exocytosis of distinct secretory vesicles controlled by different synaptotagmins. J Neurosci 33:1714–1727 DOI: 10.1523/JNEUROSCI.4087-12.2013.

Cardenas EI, Gonzalez R, Breaux K, Da Q, Gutierrez BA, Ramos MA, Cardenas RA, Burns AR, Rumbaut RE, Adachi R (2019) Munc18-2, but not Munc18-1 or Munc18-3, regulates platelet exocytosis, hemostasis, and thrombosis. J Biol Chem 294:4784–4792 DOI: 10.1074/jbc.RA118.006922.

Chen BY, Wang X, Wang ZY, Wang YZ, Chen LW, Luo ZJ (2013) Brain-derived neurotrophic factor stimulates proliferation and differentiation of neural stem cells, possibly by triggering the Wnt/β-catenin signaling pathway. J Neurosci Res 91:30–41 DOI: 10.1002/jnr.23138.

Chen W, Cai Z-L, Chao ES, Chen H, Longley CM, Hao S, Chao H-T, Kim JH, Messier JE, Zoghbi HY, Tang J, Swann JW, Xue M (2020) Stxbp1/Munc18-1 haploinsufficiency impairs inhibition and mediates key neurological features of STXBP1 encephalopathy. Elife 9:1–33 DOI: 10.7554/eLife.48705.

Cheng PL, Song AH, Wong YH, Wang S, Zhang X, Poo MM (2011) Self-amplifying autocrine actions of BDNF in axon development. Proc Natl Acad Sci U S A 108:18430–18435 DOI: 10.1073/pnas.1115907108.

Collin C, Vicario-Abejon C, Rubio ME, Wenthold RJ, McKay RDG, Segal M (2001) Neurotrophins act at presynaptic terminals to activate synapses among cultured hippocampal neurons. Eur J Neurosci 13:1273–1282 DOI: 10.1046/j.0953-816X.2001.01500.x.

Comeras LB, Herzog H, Tasan RO (2019) Neuropeptides at the crossroad of fear and hunger: a special focus on neuropeptide Y. Ann N Y Acad Sci:nyas.14179 DOI: 10.1111/nyas.14179.

Côte M et al. (2009) Munc18-2 deficiency causes familial hemophagocytic lymphohistiocytosis type 5 and impairs cytotoxic granule exocytosis in patient NK cells. J Clin Invest 119:3765–3773 DOI: 10.1172/JCI40732.

Cropper EC, Jing J, Vilim FS, Weiss KR (2018) Peptide Cotransmitters as Dynamic, Intrinsic Modulators of Network Activity. Front Neural Circuits 12:1–7 DOI: 10.3389/fncir.2018.00078.

de Wit H, Walter AM, Milosevic I, Gulyás-Kovács A, Riedel D, Sørensen JB, Verhage M (2009) Synaptotagmin-1 Docks Secretory Vesicles to Syntaxin-1/SNAP-25 Acceptor Complexes. Cell 138:935–946 DOI: 10.1016/j.cell.2009.07.027.

De Wit J, Toonen RF, Verhage M (2009) Matrix-Dependent Local Retention of Secretory Vesicle Cargo in Cortical Neurons. J Neurosci 29:23–37 DOI: 10.1523/JNEUROSCI.3931-08.2009.

Dulubova I, Khvotchev M, Liu S, Huryeva I, Südhof TC, Rizo J (2007) Munc18-1 binds directly to the neuronal SNARE complex. PNAS 104:2697–2702 DOI: 10.1073/pnas.0611318104.

Farina M et al. (2015) CAPS-1 promotes fusion competence of stationary dense-core vesicles in presynaptic terminals of mammalian neurons. Elife 4:393–422 DOI: 10.7554/eLife.05438.

Granseth B, Odermatt B, Royle SJJ, Lagnado L (2006) Clathrin-Mediated Endocytosis Is the Dominant Mechanism of Vesicle Retrieval at Hippocampal Synapses. Neuron 51:773–786 DOI: 10.1016/j.neuron.2006.08.029.

Guiberson NGL, Pineda A, Abramov D, Kharel P, Carnazza KE, Wragg RT, Dittman JS, Burré J (2018) Mechanism-based rescue of Munc18-1 dysfunction in varied encephalopathies by chemical chaperones. Nat Commun 9:3986 DOI: 10.1038/s41467-018-06507-4.

Gulyás-Kovács A, De Wit H, Milosevic I, Kochubey O, Toonen R, Klingauf J, Verhage M, Sørensen JB (2007) Munc18-1: Sequential Interactions with the Fusion Machinery Stimulate Vesicle Docking and Priming. J Neurosci 27:8676–8686 DOI: 10.1523/JNEUROSCI.0658-07.2007.

Gutierrez BA, Chavez MA, Rodarte AI, Ramos M, Dominguez A, Petrova Y, Davalos AJ, Costa RM, Elizondo R, Tuvim MJ, Dickey BF, Burns AR, Heidelberger R, Adachi R (2018) Munc18-2, but not Munc18-1 or Munc18-3, controls compound and single-vesicle regulated exocytosis in mast cells. J Biol Chem 19:7148-7159 DOI: 10.1074/jbc.RA118.002455.

Hackmann Y, Graham SC, Ehl S, Höning S, Lehmberg K, Aricò M, Owen DJ, Griffiths GM (2013) Syntaxin binding mechanism and disease-causing mutations in Munc18-2. Proc Natl Acad Sci U S A 110:E4482-91 DOI: 10.1073/pnas.1313474110.

Hamada N, Iwamoto I, Tabata H, Nagata KI (2017) MUNC18-1 gene abnormalities are involved in neurodevelopmental disorders through defective cortical architecture during brain development. Acta Neuropathol Commun 5:92 DOI: 10.1186/s40478-017-0498-5.

Hansel DE, Eipper BA, Ronnett G V. (2001) Neuropeptide Y functions as a neuroproliferative factor. Nature 410:940–944 DOI: 10.1038/35073601.

He E, Wierda K, Van Westen R, Broeke JH, Toonen RF, Cornelisse LN, Verhage M (2017) Munc13-1 and Munc18-1 together prevent NSF-dependent de-priming of synaptic vesicles. Nat Commun 8:15915 DOI: 10.1186/s40478-017-0498-5.

Heeroma JH, Roelandse M, Wierda K, Van Aerde KI, Toonen RFG, Hensbroek RA, Brussaard A, Matus A, Verhage M (2004) Trophic support delays but not prevent cell-intrinsic degeneration of neurons deficient for munc18-1. Eur J Neurosci 20:623–634 DOI: 10.1111/j.1460-9568.2004.03503.x.

Hoogstraaten RI, Keimpema L Van, Toonen RF, Verhage M (2020) Tetanus insensitive VAMP2 differentially restores synaptic and dense core vesicle fusion in tetanus neurotoxin treated neurons. Sci Rep 10:10913 DOI: 10.1038/s41598-020-67988-2.

Jahn R, Scheller RH (2006) SNAREs - Engines for membrane fusion. Nat Rev Mol Cell Biol 7:631–643 DOI: 10.1038/nrm2002.

Jaramillo AM, Piccotti L, Velasco W V., Delgado ASH, Azzegagh Z, Chung F, Nazeer U, Farooq J, Brenner J, Parker-Thornburg J, Scott BL, Evans CM, Adachi R, Burns AR, Kreda SM, Tuvim MJ, Dickey BF (2019) Different Munc18 proteins mediate baseline and stimulated airway mucin secretion. JCI Insight 4:6 DOI: 10.1172/jci.insight.124815.

Jiao J, He M, Port SA, Baker RW, Xu Y, Qu H, Xiong Y, Wang Y, Jin H, Eisemann TJ, Hughson FM, Zhang Y (2018) Munc18-1 catalyzes neuronal SNARE assembly by templating SNARE association. Elife 7: e41771 DOI: 10.7554/eLife.41771.

Kaeser PS, Deng L, Wang Y, Dulubova I, Liu X, Rizo J, Südhof TC (2011) RIM proteins tether Ca2+ channels to presynaptic active zones via a direct PDZ-domain interaction. Cell 144:282–295 DOI: 10.1016/j.cell.2010.12.029.

Kaeser PS, Regehr WG (2014) Molecular mechanisms for synchronous, asynchronous, and spontaneous neurotransmitter release. Annu Rev Physiol 76:333–363 DOI: 10.1146/annurev-physiol-021113-170338.

Kauppi M, Wohlfahrt G, Olkkonen VM (2002) Analysis of the Munc18b-syntaxin binding interface. Use of a mutant Munc18b to dissect the functions of syntaxins 2 and 3. J Biol Chem 277:43973–43979 DOI: 10.1074/jbc.M208315200.

Korteweg N, Maia AS, Thompson B, Roubos EW, Burbach JPH, Verhage M (2005) The role of Munc18-1 in docking and exocytosis of peptide hormone vesicles in the anterior pituitary. Biol Cell 97:445–455 DOI: 10.1042/BC20040101.

Kovačević J, Maroteaux G, Schut D, Loos M, Dubey M, Pitsch J, Remmelink E, Koopmans B, Crowley J, Cornelisse LN, Sullivan PF, Schoch S, Toonen RF, Stiedl O, Verhage M (2018) Protein instability, haploinsufficiency, and cortical hyper-excitability underlie STXBP1 encephalopathy. Brain 141:1350–1374 DOI: 10.1093/brain/awy046.

Lam PPL, Ohno M, Dolai S, He Y, Qin T, Liang T, Zhu D, Kang Y, Liu Y, Kauppi M, Xie L, Wan WCY, Sugita S, Olkkonen VM, Takahashi N, Kasai H, Gaisano HY (2013) Munc18b Is a Major Mediator of Insulin Exocytosis in Rat Pancreatic b-Cells. Diabetes 62:2416–2428 DOI: 10.2337/db12-1380.

Lee Y Il, Kim YG, Pyeon HJ, Ahn JC, Logan S, Orock A, Joo KM, Lőrincz A, Deák F (2019) Dysregulation of the SNARE-binding protein Munc18-1 impairs BDNF secretion and synaptic neurotransmission: a novel interventional target to protect the aging brain. GeroScience 41:109–123 DOI: 10.1007/s11357-019-00067-1.

Medina DL, Sciarretta C, Calella AM, Von Bohlen Und Halbach O, Unsicker K, Minichiello L (2004) TrkB regulates neocortex formation through the Shc/PLCγ-mediated control of neuronal migration. EMBO J 23:3803–3814 DOI: 10.1038/sj.emboj.7600399.

Meijer M, Dörr B, Lammertse HC, Blithikioti C, Weering JR, Toonen RF, Söllner TH, Verhage M (2018) Tyrosine phosphorylation of Munc18-1 inhibits synaptic transmission by preventing SNARE assembly . EMBO J 37:300–320 DOI: 10.15252/embj.201796484.

Mennerick S, Que J, Benz A, Zorumski CF (1995) Passive and Synaptic Properties of Hippocampal Neurons Grown in Microcultures and in Mass Cultures. J NEUROPHYSIOIOGY 73:320-332 DOI: 10.1152/jn.1995.73.1.320.

Miranda M, Morici JF, Zanoni MB, Bekinschtein P (2019) Brain-Derived Neurotrophic Factor: A Key Molecule for Memory in the Healthy and the Pathological Brain. Front Cell Neurosci 13:363 DOI: 10.3389/fncel.2019.00363.

Misura KM, Scheller RH, Weis WI (2000) Three-dimensional structure of the neuronal-Sec1-syntaxin 1a complex. Nature 404:355–362 DOI: 10.1038/35006120.

Miyamoto H, Tatsukawa T, Shimohata A, Yamagata T, Suzuki T, Amano K, Mazaki E, Raveau M, Ogiwara I, Oba-Asaka A, Hensch TK, Itohara S, Sakimura K, Kobayashi K, Kobayashi K, Yamakawa K (2019) Impaired cortico-striatal excitatory transmission triggers epilepsy. Nat Commun 10:1917 DOI: 10.1038/s41467-019-09954-9.

Moro A, Woerden GM Van, Toonen RF, Verhage M (2020) CaMKII controls neuromodulation via neuropeptide gene expression and axonal targeting of neuropeptide vesicles. PLOS Biol 18(8): e3000826 DOI: 10.1371/journal.pbio.3000826.

Murthy VN, Sejnowski TJ, Stevens CF (1997) Heterogeneous release properties of visualized individual hippocampal synapses. Neuron 18:599–612 DOI: 10.1016/S0896-6273(00)80301-3.

Novick P, Ferro S, Schekman R (1981) Order of events in the yeast secretory pathway. Cell 25:461–469 DOI: 10.1016/0092-8674(81)90064-7.

Novick P, Field C, Schekman R (1980) Identification of 23 Complementation Groups Required for Post-translational Events in the Yeast Secretory Pathway. Cell 21:205–221 DOI: 10.1016/0092-8674(80)90128-2.

Novick P, Schekman R (1979) Secretion and cell-surface growth are blocked in a temperature-sensitive mutant of Saccharomyces cerevisiae. PNAS 76:1858–1862 DOI: 10.1073/pnas.76.4.1858.

Oh E, Kalwat MA, Kim MJ, Verhage M, Thurmond DC (2012) Munc18-1 regulates first-phase insulin release by promoting granule docking to multiple syntaxin isoforms. J Biol Chem 287:25821–25833 DOI: 10.1074/jbc.M112.361501.

Oh E, Thurmond DC (2009) Munc18c depletion selectively impairs the sustained phase of insulin release. Diabetes 58:1165–1174 DOI: 10.2337/db08-1059.

Parisotto D, Pfau M, Scheutzow A, Wild K, Mayer MP, Malsam J, Sinning I, Söllner TH (2014) An extended helical conformation in domain 3a of Munc18-1 provides a template for SNARE (soluble N-Ethylmaleimidesensitive factor attachment protein receptor) complex assembly. J Biol Chem 289:9639–9650 DOI: 10.1074/jbc.M113.514273.

Persoon CM, Hoogstraaten RI, Nassal JP, van Weering JRT, Kaeser PS, Toonen RF, Verhage M (2019) The RAB3-RIM Pathway Is Essential for the Release of Neuromodulators. Neuron 104:1065-1080.e12 DOI: 10.1016/j.neuron.2019.09.015.

Persoon CM, Moro A, Nassal JP, Farina M, Broeke JH, Arora S, Dominguez N, van Weering JR, Toonen RF, Verhage M (2018) Pool size estimations for dense-core vesicles in mammalian CNS neurons. EMBO J 37:e99672 DOI: 10.15252/embj.201899672.

Pons-Vizcarra M, Kurps J, Tawfik B, Sørensen JB, van Weering JRT, Verhage M (2019) MUNC18-1 regulates submembrane F-actin network, independently of syntaxin1 targeting, via hydrophobicity in β-sheet 10. J Cell Sci:jcs. 132:234674 DOI: 10.1242/jcs.234674.

Protopopov V, Govindan B, Novick P, Gerst JE (1993) Homologs of the synaptobrevin/VAMP family of synaptic vesicle proteins function on the late secretory pathway in S. cerevisiae. Cell 74:855–861 DOI: 10.1016/0092-8674(93)90465-3.

Raposinho PD, Broqua P, Pierroz DD, Hayward A, Dumont Y, Quirion R, Junien JL, Aubert ML (1999) Evidence that the inhibition of luteinizing hormone secretion exerted by central administration of neuropeptide Y (NPY) in the rat is predominantly mediated by the NPY-Y5 receptor subtype. Endocrinology 140:4046–4055 DOI: 10.1210/endo.140.9.6985.

Rosenmund C, Clements JD, Westbrook GL (1993) Nonuniform probability of glutamate release at a hippocampal synapse. Science 262:754–757 DOI: 10.1126/science.7901909.

Saitsu H, Kato M, Mizuguchi T, Hamada K, Osaka H, Tohyama J, Uruno K, Kumada S, Nishiyama K, Nishimura A, Okada I, Yoshimura Y, Hirai SI, Kumada T, Hayasaka K, Fukuda A, Ogata K, Matsumoto N (2008) De novo mutations in the gene encoding STXBP1 (MUNC18-1) cause early infantile epileptic encephalopathy. Nat Genet 40:782–788 DOI: 10.1038/ng.150.

Santos TC, Wierda K, Broeke JH, Toonen RF, Verhage M (2017) Early Golgi Abnormalities and Neurodegeneration upon Loss of Presynaptic Proteins Munc18-1, Syntaxin-1, or SNAP-25. J Neurosci 37(17):4525–4539 DOI: 10.1523/JNEUROSCI.3352-16.2017.

Schlüter OM, Basu J, Südhof TC, Rosenmund C (2006) Rab3 superprimes synaptic vesicles for release: Implications for short-term synaptic plasticity. J Neurosci 26(4):1239–1246 DOI: 10.1523/JNEUROSCI.3553-05.2006.

Schlüter OM, Schmitz F, Jahn R, Rosenmund C, Südhof TC (2004) A complete genetic analysis of neuronal Rab3 function. J Neurosci 24(29):6629–6637 DOI: 10.1523/JNEUROSCI.1610-04.2004.

Schmitz SK, Hjorth JJJ, Joemai RMS, Wijntjes R, Eijgenraam S, de Bruijn P, Georgiou C, de Jong APH, van Ooyen A, Verhage M, Cornelisse LN, Toonen RF, Veldkamp W (2011) Automated analysis of neuronal morphology, synapse number and synaptic recruitment. J Neurosci Methods 195:185–193 DOI: 10.1016/j.jneumeth.2010.12.011.

Schwartz PM, Borghesani PR, Levy RL, Pomeroy SL, Segal RA (1997) Abnormal cerebellar development and foliation in BDNF(-/-) mice reveals a role for neurotrophins in CNS patterning. Neuron 19:269–281 DOI: 10.1016/S0896-6273(00)80938-1.

Shakiryanova D, Klose MK, Zhou Y, Gu T, Deitcher DL, Atwood HL, Hewes RS, Levitan ES (2007) Cellular/Molecular Presynaptic Ryanodine Receptor-Activated Calmodulin Kinase II Increases Vesicle Mobility and Potentiates Neuropeptide Release. J Neurosci 27:7799–7806 DOI: 10.1523/JNEUROSCI.1879-07.2007.

Shimojo M, Courchet J, Pieraut S, Torabi-Rander N, Sando R, Polleux F, Maximov A (2015) SNAREs Controlling Vesicular Release of BDNF and Development of Callosal Axons. Cell Rep 11:1054–1066 DOI: 10.1016/j.celrep.2015.04.032.

Shinoda Y, Ahmed S, Ramachandran B, Bharat V, Brockelt D, Altas B, Dean C (2014) BDNF enhances spontaneous and activity-dependent neurotransmitter release at excitatory terminals but not at inhibitory terminals in hippocampal neurons. Front Synaptic Neurosci 6(27):1–12 DOI: 10.3389/fnsyn.2014.00027.

Sitarska E, Xu J, Park S, Liu X, Quade B, Stepien K, Sugita K, Brautigam CA, Sugita S, Rizo J (2017) Autoinhibition of munc18-1 modulates synaptobrevin binding and helps to enable munc13-dependent regulation of membrane fusion. Elife 6:e24278 DOI: 10.7554/eLife.24278.

Stamberger H, Nikanorova M, Accorsi P, Angriman M, Benkel-herrenbrueck I, Capovilla G, Erasmus CE, Fannemel M, Giordano L, Helbig KL, Maier O, Phalin J (2016) A neurodevelopmental disorder including epilepsy. Neurology 86:954–962 DOI: 10.1212/WNL.0000000000002457.

Südhof TC (2013) Neurotransmitter Release: The Last Millisecond in the Life of a Synaptic Vesicle. Neuron 80:675–690 DOI: 10.1016/j.neuron.2013.10.022.

Südhof TC, Rizo J (2011) Synaptic vesicle exocytosis. Cold Spring Harb Perspect Biol 3:a005637 DOI: 10.1101/cshperspect.a005637.

Südhof TC, Rothman JE (2009) Membrane fusion: Grappling with SNARE and SM proteins. Science (80-) 323:474–477 DOI: 10.1126/science.1161748.

Tamori Y, Kawanishi M, Niki T, Shinoda H, Araki S, Okazawa H, Kasuga M (1998) Inhibition of insulin-induced GLUT4 translocation by Munc18c through interaction with syntaxin4 in 3T3-L1 adipocytes. J Biol Chem 273:19740–19746 DOI: 10.1074/jbc.273.31.19740.

Tartaglia N, Du J, Tyler WJ, Neale E, Pozzo-Miller L, Lu B (2001) Protein Synthesis-dependent and -independent Regulation of Hippocampal Synapses by Brain-derived Neurotrophic Factor. J Biol Chem 276:37585–37593 DOI: 10.1074/jbc.M101683200.

Thurmond DC, Ceresa BP, Okada S, Elmendorf JS, Coker K, Pessin JE (1998) Regulation of insulin-stimulated GLUT4 translocation by Munc18c in 3T3L1 adipocytes. J Biol Chem 273:33876–33883 DOI: 10.1074/jbc.273.50.33876.

Thurmond DC, Kanzaki M, Khan a H, Pessin JE (2000) Munc18c function is required for insulin-stimulated plasma membrane fusion of GLUT4 and insulin-responsive amino peptidase storage vesicles. Mol Cell Biol 20:379–388 DOI: 10.1128/MCB.20.1.379-388.2000.

Toonen RF, Kochubey O, de Wit H, Gulyas-Kovacs A, Konijnenburg B, Sørensen JB, Klingauf J, Verhage M (2006a) Dissecting docking and tethering of secretory vesicles at the target membrane. EMBO J 25:3725-3737 DOI: 10.1038/sj.emboj.7601256.

Toonen RF, de Vries KJ, Zalm R, Südhof TC, Verhage M (2005) Munc18-1 stabilizes syntaxin 1, but is not essential for syntaxin 1 targeting and SNARE complex formation. J Neurochem 93:1393–1400 DOI: 10.1111/j.1471-4159.2005.03128.x.

Toonen RF, Verhage M (2003) Vesicle trafficking: Pleasure and pain from SM genes. Trends Cell Biol 13:177–186 DOI: 10.1016/S0962-8924(03)00031-X.

Toonen RF, Verhage M (2007) Munc18-1 in secretion: lonely Munc joins SNARE team and takes control. Trends Neurosci 30:564–572 DOI: 10.1016/j.tins.2007.08.008.

Toonen RF, Wierda K, Sons MS, de Wit H, Cornelisse LN, Brussaard A, Plomp JJ, Verhage M (2006b) Munc18-1 expression levels control synapse recovery by regulating readily releasable pool size. Proc Natl Acad Sci 103:18332–18337 DOI: 10.1073/pnas.0608507103.

Tschenett A, Singewald N, Carli M, Balducci C, Salchner P, Vezzani A, Herzog H, Sperk G (2003) Reduced anxiety and improved stress coping ability in mice lacking NPY-Y2 receptors. Eur J Neurosci 18:143–148 DOI: 10.1046/j.1460-9568.2003.02725.x.

Tyler WJ, Pozzo-Miller LD (2001) BDNF enhances quantal neurotransmitter release and increases the number of docked vesicles at the active zones of hippocampal excitatory synapses. J Neurosci 21:4249–4258 DOI: 10.1523/jneurosci.21-12-04249.2001.

van de Bospoort R, Farina M, Schmitz SK, de Jong A, de Wit H, Verhage M, Toonen RF (2012) Munc13 controls the location and efficiency of dense-core vesicle release in neurons. J Cell Biol 199:883–891 DOI: 10.1083/jcb.201208024.

Verhage M, Maia AS, Plomp JJ, Brussaard AB, Heeroma JH, Vermeer H, Toonen RF, Hammer RE, van den Berg TK, Missler M, Geuze HJ, Südhof TC (2000) Synaptic Assembly of the Brain in the Absence of Neurotransmitter Secretion. Science 287:864–869 DOI: 10.1126/science.287.5454.864.

Verhage M, Sørensen JB (2020) SNAREopathies: Diversity in Mechanisms and Symptoms. Neuron Available at: https://doi.org/10.1016/j.neuron.2020.05.036 DOI: 10.1016/j.neuron.2020.05.036.

Voets T, Toonen RF, Brian EC, de Wit H, Moser T, Rettig J, Südhof TC, Neher E, Verhage M (2001) Munc18-1 Promotes Large Dense-Core Vesicle Docking. Neuron 31:581–592 DOI: 10.1016/S0896-6273(01)00391-9.

Wang S, Li Y, Gong J, Ye S, Yang X, Zhang R, Ma C (2019) Munc18 and Munc13 serve as a functional template to orchestrate neuronal SNARE complex assembly. Nat Commun 10:69 DOI: 10.1038/s41467-018-08028-6.

Wierda KDB, Toonen RFG, de Wit H, Brussaard AB, Verhage M (2007) Interdependence of PKC-Dependent and PKC-Independent Pathways for Presynaptic Plasticity. Neuron 54:275–290 DOI: 10.1016/j.neuron.2007.04.001.

Yue F et al. (2014) A comparative encyclopedia of DNA elements in the mouse genome. Nature 515:355–364 DOI: 10.1038/nature13992.

Zeisel A, M̂oz-Manchado AB, Codeluppi S, Lönnerberg P, Manno G La, Juréus A, Marques S, Munguba H, He L, Betsholtz C, Rolny C, Castelo-Branco G, Hjerling-Leffler J, Linnarsson S (2015) Cell types in the mouse cortex and hippocampus revealed by single-cell RNA-seq. Science 347:1138–1142 DOI: 10.1126/science.aaa1934.

Zhang Q, Liu G, Wu Y, Sha H, Zhang P, Jia J (2011) BDNF promotes EGF-induced proliferation and migration of human fetal neural stem/progenitor cells via the PI3K/Akt pathway. Molecules 16:10146–10156 DOI: 10.3390/molecules161210146.

Zhou P, Porcionatto M, Pilapil M, Chen Y, Choi Y, Tolias KF, Bikoff JB, Hong EJ, Greenberg ME, Segal RA (2007) Polarized Signaling Endosomes Coordinate BDNF-Induced Chemotaxis of Cerebellar Precursors. Neuron 55:53–68 DOI: 10.1016/j.neuron.2007.05.030.

Zucker RS (1973) Changes in the statistics of transmitter release during facilitation. J Physiol 229:787–810 DOI: 10.1113/jphysiol.1973.sp010167.Verhage M, Maia AS, Plomp JJ, Brussaard AB, Heeroma JH, Vermeer H, Toonen RF, Hammer RE, van den Berg TK, Missler M, Geuze HJ, Südhof TC (2000) Synaptic Assembly of the Brain in the Absence of Neurotransmitter Secretion. Science 287:864–869 DOI: 10.1126/science.287.5454.864.

Verhage M, Sørensen JB (2020) SNAREopathies: Diversity in Mechanisms and Symptoms. Neuron Available at: https://doi.org/10.1016/j.neuron.2020.05.036 DOI: 10.1016/j.neuron.2020.05.036.

Voets T, Toonen RF, Brian EC, de Wit H, Moser T, Rettig J, Südhof TC, Neher E, Verhage M (2001) Munc18-1 Promotes Large Dense-Core Vesicle Docking. Neuron 31:581–592 DOI: 10.1016/S0896-6273(01)00391-9.

Wang S, Li Y, Gong J, Ye S, Yang X, Zhang R, Ma C (2019) Munc18 and Munc13 serve as a functional template to orchestrate neuronal SNARE complex assembly. Nat Commun 10:69 DOI: 10.1038/s41467-018-08028-6.

Wierda KDB, Toonen RFG, de Wit H, Brussaard AB, Verhage M (2007) Interdependence of PKC-Dependent and PKC-Independent Pathways for Presynaptic Plasticity. Neuron 54:275–290 DOI: 10.1016/j.neuron.2007.04.001.

Yue F et al. (2014) A comparative encyclopedia of DNA elements in the mouse genome. Nature 515:355–364 DOI: 10.1038/nature13992.

Zeisel A, M̂oz-Manchado AB, Codeluppi S, Lönnerberg P, Manno G La, Juréus A, Marques S, Munguba H, He L, Betsholtz C, Rolny C, Castelo-Branco G, Hjerling-Leffler J, Linnarsson S (2015) Cell types in the mouse cortex and hippocampus revealed by single-cell RNA-seq. Science 347:1138–1142 DOI: 10.1126/science.aaa1934.

Zhang Q, Liu G, Wu Y, Sha H, Zhang P, Jia J (2011) BDNF promotes EGF-induced proliferation and migration of human fetal neural stem/progenitor cells via the PI3K/Akt pathway. Molecules 16:10146–10156 DOI: 10.3390/molecules161210146.

Zhou P, Porcionatto M, Pilapil M, Chen Y, Choi Y, Tolias KF, Bikoff JB, Hong EJ, Greenberg ME, Segal RA (2007) Polarized Signaling Endosomes Coordinate BDNF-Induced Chemotaxis of Cerebellar Precursors. Neuron 55:53–68 DOI: 10.1016/j.neuron.2007.05.030.

Zucker RS (1973) Changes in the statistics of transmitter release during facilitation. J Physiol 229:787–810 DOI: 10.1113/jphysiol.1973.sp010167.

Chapter 3

STXBP1 is essential for DCV exocytosis in human iNeurons

Daniël C. Puntman, Ganna Balugara, Annemiek van Berkel, Anushka Nair, Ruud F. Toonen, Matthijs Verhage

Abstract

Mutations in the STXBP1 gene are the cause of STXBP1-syndrome, characterized by developmental delay and intellectual disability. Haploinsufficiency is suggested to be the main pathogenic mechanism underlying this disease, which alters synaptic transmission to various extents. We used CRISPR/Cas9 gene-editing to introduce STXBP1 mutations in human isogenic induced pluripotent stem cells (iPSCs), differentiated via NGN2 expression into glutamatergic neurons (iNeurons) and infected these with dense core vesicle (DCV) exocytosis marker NPY-pHluorin to assess neuropeptide secretion. Live imaging during high-frequency train-stimulation revealed that DCV exocytosis in STXBP1 null mutant (KO) iNeurons was abolished. An iPSC clone carrying a heterozygous D207G mutation showed reduced DCV exocytosis and decreased total STXBP1 protein levels. Conversely, clones carrying a heterozygous null or S241 frameshift mutation in STXBP1 showed no affected DCV exocytosis and STXBP1 protein levels compared to control. Hence, STXBP1 is essential for DCV exocytosis in human neurons and these data suggest that some patient mutations may affect DCV exocytosis via reduced STXBP1 protein levels.

Introduction

Mutations in genes required for synaptic vesicle (SV) exocytosis are causal to neurodevelopmental, neurological and psychiatric diseases (For reviews see: Waites and Garner, 2011; Cortès-Saladelafont et al., 2018; Bonnycastle et al., 2020). These include the genes coding for SNARE proteins Syntaxin-1, SNAP25 and VAMP2, and assessor protein MUNC18-1, which together are part of the core machinery responsible for neurotransmitter secretion (For a review see: Verhage and Sørensen, 2020). However, the function of these proteins is not limited to synaptic transmission, as MUNC18-1 is not only essential for SV exocytosis, but also for neuropeptide secretion and neuronal survival (Chapter 2; Verhage et al., 2000; Bouwman et al., 2004; Heeroma et al., 2004; Santos et al., 2017; Puntman et al., 2021). Studies on these genes are mainly performed in mice, which may recapitulate some of the disease phenotypes. However, genetic background and behavior differ significantly between mice and patients. New cellular models such as human induced pluripotent stem cell (iPSC)-derived neurons (from here on referred to as iNeurons) enable to study these genes and diseases on a human genetic background (Ichida and Kiskinis, 2015).

Patients carrying mutations in STXBP1 typically have neurodevelopmental delay, intellectual disability, often epilepsy and sometimes autistic features, in a disease we termed STXBP1-syndrome (Saitsu et al., 2008; Hamdan et al., 2011; Gburek-Augustat et al., 2016; Verhage and Sørensen, 2020). Analysis on several heterozygous missense mutations revealed instability and impaired syntaxin binding of the resulting protein (Saitsu et al., 2008). In line with that, expression of MUNC18-1 carrying STXBP1-syndrome associated mutations in mice reduced MUNC18-1 protein levels (Kovačević et al., 2018). Therefore, haploinsufficiency is considered causal for STXBP1-syndrome. Additionally, STXBP1-syndrome mutations may cause aggregation of the mutated and possibly even the WT protein (Guiberson et al., 2018). Due to these features, heterozygous (HZ) *Munc18-1 null* mutation is often used in mice to mimic disease conditions, as it decreases MUNC18-1 protein expression by ~50% (Verhage et al., 2000; Toonen et al., 2005, 2006; Lee et al., 2019). Indeed, mice carrying a HZ null mutation in STXBP1 display similar cognitive, behavioral and neurodevelopmental features as STXBP1-syndrome patients, and show similar spike-wave discharges (SWDs) measured via EEG and epileptic-like phenotypes (Ohtahara and Yamatogi, 2006; Kovačević et al., 2018; Miyamoto et al., 2019; Chen et al., 2020).

We showed in Chapter 2 that *Munc18-1* HZ mouse neurons also have defects in neuropeptide secretion. Due to the properties of neuropeptides, with broad functions in amongst others stress, mood, appetite, hunger, learning and memory (for reviews see: Tschenett et al., 2003; Arora and Anubhuti, 2006; Cropper et al., 2018; Comeras et al., 2019; Miranda et al., 2019) and their association with several neurological and psychiatric diseases (for reviews see: Werner and Coveñas, 2010; Nagahara and Tuszynski, 2011; Griebel and Holsboer, 2012; Nestor et al., 2019), alterations in neuropeptide secretion may also contribute to the symptoms of STXBP1-syndrome. Currently, many brain diseases are also being studied in human iNeurons. One of these studies showed that reducing STXBP1 protein levels with only ~35% via heterozygous (HZ) null mutation resulted in severely decreased EPSC size and miniature EPSC

frequency (Patzke et al., 2015), suggesting that STXBP1 is also important for synaptic transmission in human neurons. However, given the essential role of MUNC18-1 in mouse DCV exocytosis (Chapter 2), neuropeptide secretion may be an important factor in understanding STXBP1 syndrome.

The aim of this chapter is to test whether the role of MUNC18-1 in DCV exocytosis generalizes to human neurons and if heterozygous STXBP1-syndrome-causing mutations affect neuropeptide secretion. For this, human NGN2-differentiated iNeurons carrying specific mutations in STXBP1 on an isogenic background were infected with DCV exocytosis marker NPY-pHluorin and analyzed using live cell imaging. *STXBP1* KO (null; knock-out) abolished DCV exocytosis in these neurons, while high-frequency train-stimulation robustly elicited DCV exocytosis in control iNeurons. An iNeuron clone carrying the patient mutation D207G (aspartic acid to glycine) resulted in decreased DCV exocytosis, while a clone carrying patient mutation S241fs (frame-shift at Serine 241) or HZ (heterozygous null) mutation did not limit NPY-pHluorin labeled DCV exocytosis events. In addition, STXBP1 protein levels were measured via immunocytochemistry (ICC) and Western-Blot, revealing a decrease in D207G mutated neurons but no robust reduction for the other mutations. We conclude that STXBP1 is essential in human neurons for DCV exocytosis and some STXBP1-syndrome patient mutations may affect neuropeptide secretion.

Results

DCV exocytosis is abolished in human iPSC-derived *STXBP1* KO neurons

To test the role of MUNC18-1 in neuropeptide secretion in human neurons, we used Crispr-Cas9 gene-editing in human iPSCs to generate *STXBP1* KO and isogenic control iNeurons. iPSC clones were quality controlled, differentiated using forced NGN2 expression (Zhang et al., 2013) and plated at single cell density on glia micro-islands. After 6 weeks in vitro (WIV6), *STXBP1* KO neurons had normal dendritic arborization and number of synapses compared to control neurons, while STXBP1 immunofluorescence was absent (Fig. 1A). To assess DCV exocytosis, neurons were infected with NPY-pHluorin 7 days prior to imaging. DCV exocytosis events, marked as NPY-pHluorin dequenching events, were visible during two episodes of high-frequency train-stimulation (8 x 50AP at 50Hz) with 30s interval in control neurons, but not in *STXBP1* KO neurons at WIV6 (Fig. 1B,C). Further analysis of these DCV exocytosis events showed that the duration of events in human control iNeurons was much shorter than in mouse WT neurons (Fig. S1A). In control human iNeurons, a median of 90 DCV exocytosis events per cell was detected with large cell to cell variability, but DCV exocytosis was abolished in all *STXBP1* KO neurons (Fig. 1D). To address whether this effect was due to an absence of DCVs or incapability of DCV exocytosis, the number of DCVs per cell (DCV poolsize) was quantified during NH_4 perfusion, which dequenches all pHluorin in acidic compartments. The DCV poolsize was similar in *STXBP1* KO and control iNeurons, suggesting normal DCV biogenesis (Fig. 1E). These data show that STXBP1 is essential for DCV exocytosis in human iPSC-derived neurons.

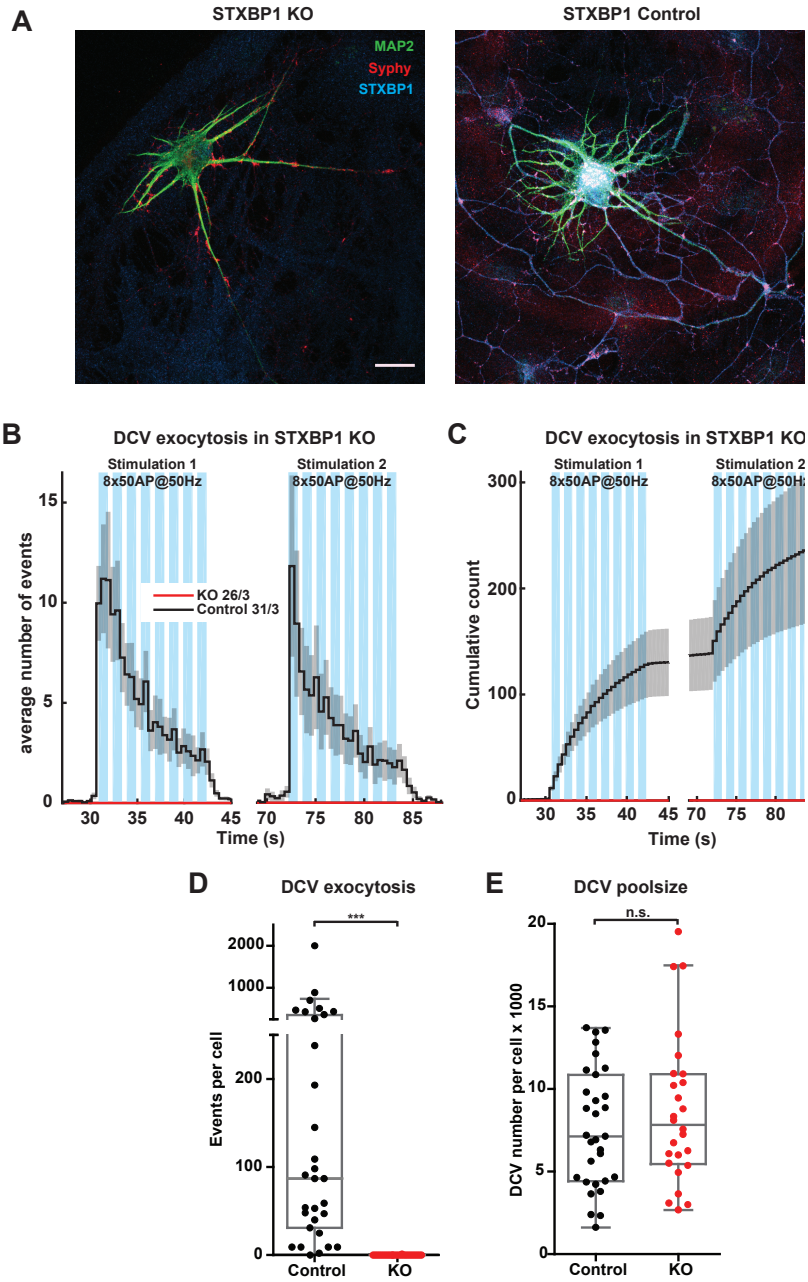

Figure 1. DCV exocytosis is abolished in STXBP1 KO neurons. (**A**) NGN2-differentiated iPSC-derived human neurons (iNeurons) with Cripr-Cas9 mediated STXBP1 KO or isogenic control both show dendritic arborization and synaptic assembly. However, STXBP1 immunofluorescence is absent in STXBP1 KO neurons. Immunofluorescence is shown for MAP2 (green), Synaptophysin (Syphy; red), STXBP1 (MUNC18-1 antibody; blue). Scale bar = 25µm (**B**) To test if DCV exocytosis depends on STXBP1, NPY-pHluorin as a DCV exocytosis marker was expressed in autaptic cultures of STXBP1 control and STXBP1 KO iNeurons and live imaging was performed at DIV42-47 in standard tyrodes imaging solution. In 3 independent cultures, 26 KO and 31 control cells were analyzed. In the histogram, the average number of events is visualized per condition (control: black; STXBP1 KO: red) over time. The blue bars

indicate the train-stimulations (2 episodes of 8 trains including 50 action potentials at 50Hz). Error bars are SEM. (**C**) Cumulative representation of data in (B). Error bars are SEM. (**D**) Tukey/scatter plot showing the total number of NPY-pHluorin exocytosis events per neuron. (E) Tukey/scatter plot showing the total number of NPY-pHluorin puncta per neuron during ammonium perfusion, which was precisely applied to each neuron via a barrel.

DCV exocytosis is decreased in D207G iNeuron clones, but unaffected in *STXBP1* HZ or S241fs clones

To test whether neuropeptide secretion is affected in cellular models of STXBP1-syndrome, we quantified NPY-pHluorin labeled DCV exocytosis events in NGN2-differentiated human iNeurons harboring Crispr-Cas9 gene-edited mutations. A heterozygous null mutation (HZ) was used to generate neurons with reduced STXBP1 expression, which is considered causal for STXBP1-syndrome (Stamberger et al., 2016; Kovačević et al., 2018). Additionally, two STXBP1-syndrome patient mutations were introduced: a frameshift mutation at S241 (S241fs) and missense mutation D207G. All mutated iPSC lines and an isogenic control line were sequence verified and passed quality control, differentiated into neurons using NGN2-induction and grown as single neurons for 6 WIV on glia micro-islands. iNeurons from each CRISPR clone showed NPY-pHluorin dequenching events during both episodes of high-frequency train-stimulation (8x 50AP @ 50Hz with 30s interval), although this was absent in a large subgroup of D207G iNeurons (Fig. 2A,B). Quantification of these events showed that DCV exocytosis was significantly reduced in iNeurons carrying a D207G mutation compared to WT, HZ or S241fs iNeurons (Fig. 2C). The total number of DCVs revealed by NH_4 was not affected by any mutation, except that S241fs mutated neurons had a slightly reduced DCV poolsize compared with WT or D207G neurons (Fig. 2D). Resequencing of the WT control line revealed a 400 bp deletion in the STXBP1 gene, effectively deleting one STXBP1 allele. Therefore, the WT control should be considered as a *STXBP1* HZ genotype. These data show that the iNeurons harboring a D207G mutation in STXBP1 had severely reduced DCV exocytosis, but that *STXBP1* HZ or S241fs mutation did not result in an effect on DCV exocytosis compared to control. However, due to STXBP1 heterozygosity in the WT control line, we cannot determine whether *STXBP1* HZ or 241fs mutation have an effect on DCV exocytosis.

STXBP1 protein levels are reduced in D207G mutated neurons

To test if the effect of the D207G mutation on neuropeptide secretion may be due to reduced STXBP1 protein levels or due to a specific functional change in the protein, STXBP1 protein levels in iPSC-derived neurons from each clone were assessed in two experiments. First, immunohistochemistry was performed on sister cultures of the cultures that were used for the live DCV exocytosis assay in Figure 2. Immunostaining for MAP2 and MUNC18-1 showed that STXBP1 was present predominantly in axons in all genotypes to a similar extent, except for a large subgroup of D207G iNeurons where STXBP1 immunofluorescence was absent (Fig. 3A,B). Dendritic and somatic STXBP1 levels followed the same trend (Fig. S1B,C). Second, differentiated neurons from each clone and from a *STXBP1* KO clone as negative control were cultured in parallel on POL-coated 6-wells plates and lysed at WIV6 for Western-Blot analysis. Here, no STXBP1 detection was observed in lysates from *STXBP1* KO iNeurons, while STXBP1 was

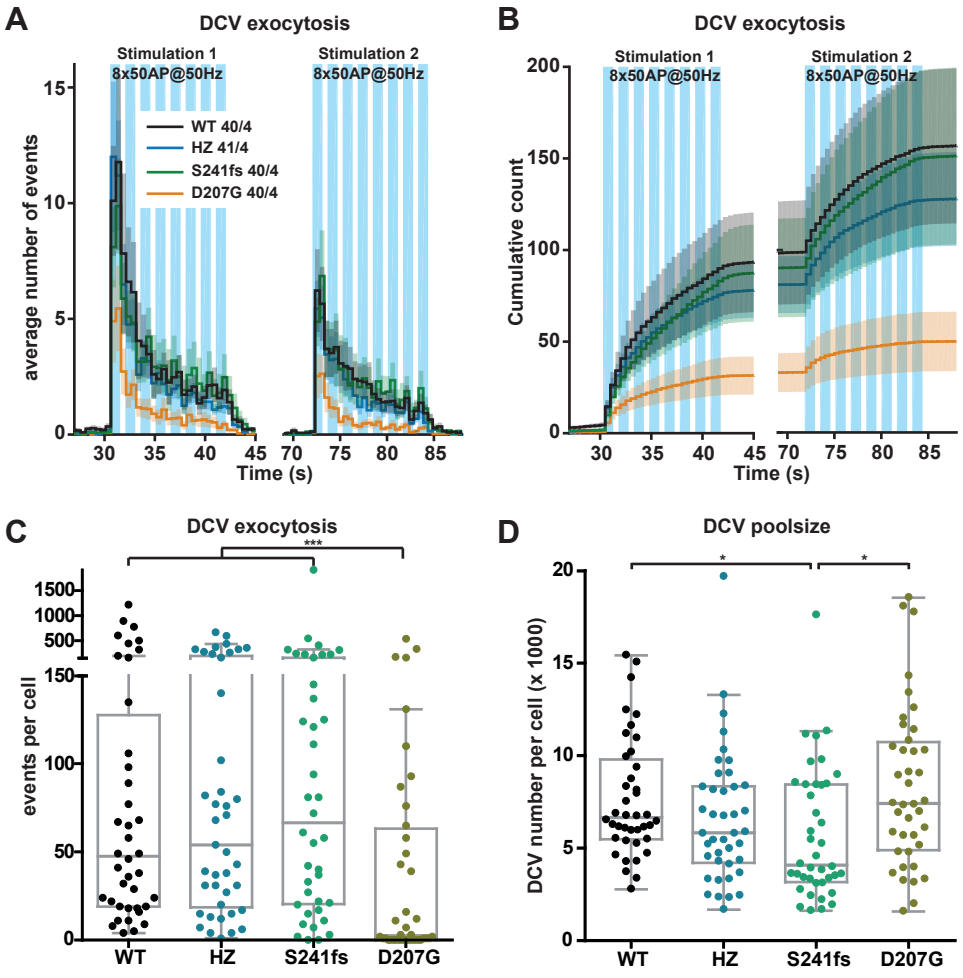

Figure 2. DCV exocytosis is unaffected by STXBP1 HZ mutation, but decreased by D207G missense mutation. (**A**) To test if decreased STXBP1 expression or STXBP1 syndrome patient mutations affect DCV exocytosis, Crispr-cas9 mediated mutations were generated in human iPSCs from isogenetic background, which were NGN2-induced to iNeurons, resulting in heterozygous null (Official cell line: NGN2-SS241_A2_23 in BioniC13 (HZ)), S241frameshift (SS241; Official cell line: NGN2-SS241_E11_33 in BioniC13 (HZ mutation)) or D207G missense (Official cell line: NGN2-SD207G_F7 in BioniC13 (HZ mutation)) mutations and a control (Official cell line: NGN2-SD207G_F8 in BioniC13 (WT)). In these neurons, NPY-pHluorin was expressed to enable live imaging at DIV41 of DCV exocytosis, performed in standard tyrodes imaging solution. In 4 independent cultures, 40 WT, SS241 or D207G and 41 HZ neurons were analyzed. In the histogram, the average number of events is visualized per condition (STXBP1 WT: black; STXBP1 HZ: blue; STXBP1 HZ SS241: green; STXBP1 HZ D207G: orange) over time. The blue bars indicate the train-stimulations (2 episodes of 8 trains including 50 action potentials at 50Hz). Error bars are SEM. (**B**) Cumulative representation of data in (A). Error bars are SEM. (**C**) Tukey/scatter plot showing the total number of NPY-pHluorin exocytosis events per neuron. (**D**) Tukey/scatter plot showing the total number of NPY-pHluorin puncta per neuron during ammonium perfusion, which was precisely applied to each neuron via a barrel.

detected in *STXBP1* HZ, D207G, S241 and control lysates (Fig. 3C,D, S1D). These findings show that many neurons derived from the D207G clone have no detectable STXBP1 protein levels, while clones carrying *STXBP1* HZ or S241fs mutations have more similar STXBP1 protein levels to control iNeurons.

Table 1. Variation of DCV exocytosis in mouse and human neurons

Measurement	Mouse	Human	Source
SEM/Average NPY-mCherry exocytosis	0.204	0.178	(Emperador Melero et al., 2017)
SEM/Average NPY-pHluorin exocytosis	0.227-0.229		(Puntman et al., 2021)
SEM/Average NPY-pHluorin exocytosis		0.231-0.280	Chapter 3, Fig. 1-2
SEM/Average BDNF-pHluorin exocytosis	0.168		(Moro et al., 2020)

Values are SEM divided by the Average of the fraction of DCV exocytosis, this fraction was calculated as the number of DCV exocytosis events divided by the total DCV pool in each neuron.

STXBP1 protein levels are reduced in D207G mutated neurons

To compare the variation in DCV exocytosis between mouse and human neurons between different studies, from each study the fraction of DCV exocytosis (defined as the number of WT DCV exocytosis events divided by the total number of DCVs visualized by the fluorescent marker in each cell) was extracted and the variation was expressed as the SEM divided by the mean (Table 1). We included data from this chapter, from chapter 2 (Puntman et al., 2021), from a study comparing human embryonic stem cell derived neurons with mouse neurons (Emperador Melero et al., 2017) and from a mouse neuron study (Moro et al., 2020). Variations of normalized DCV exocytosis in mouse neuron studies were between 0.168 and 0.229, while in human neuron studies these variations were between 0.178 and 0.280. Hence, the variation in DCV exocytosis between neurons is comparable between mouse and human neurons.

Discussion

The aim of this study was to test the role of STXBP1 in human DCV exocytosis and to assess whether disease-causing mutations in STXBP1 affect neuropeptide secretion. NPY-pHluorin labeled DCV exocytosis events were absent in *STXBP1* KO human iNeurons during high-frequency train-stimulation, while the same stimulation readily triggered NPY-pHluorin exocytosis events in control iNeurons. iNeurons carrying a HZ D207G missense patient mutation in STXBP1 also showed reduced NPY-pHluorin marked DCV exocytosis compared to control iNeurons and a majority of these neurons showed an absence of STXBP1 staining via immunofluorescence, while all control neurons were positive for STXBP1. Conversely, iNeurons carrying a HZ null mutation or a HZ S241 frameshift mutation in STXBP1 showed no reduction in NPY-pHluorin labeled DCV exocytosis events and no decreased STXBP1 protein levels on immunohistochemistry or Western Blot. Hence, STXBP1 is essential for DCV exocytosis in human neurons and some STXBP1-syndrome-causing mutations may reduce STXBP1 protein levels and hamper neuropeptide secretion.

Here, we assessed for the first time DCV exocytosis in NGN2-differentiated iPSC-derived human neurons. DCV exocytosis events were readily triggered by a high-frequency

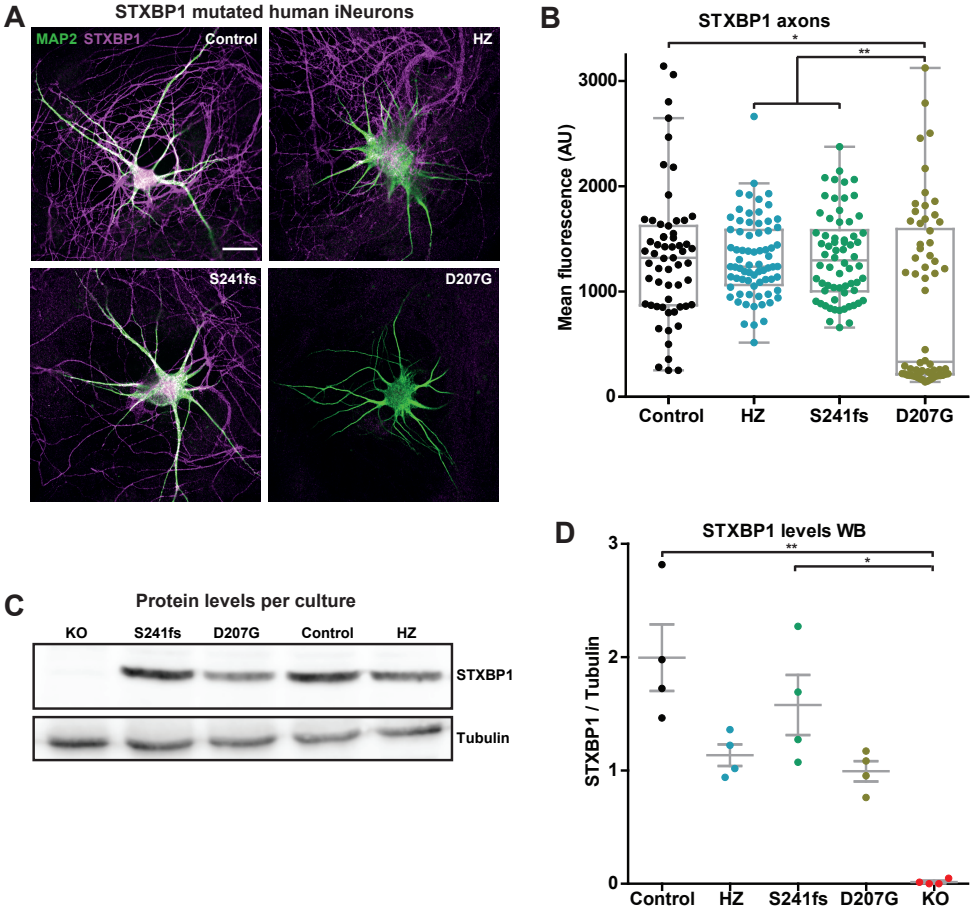

Figure 3. STXBP1 protein levels are reduced in iNeurons with D207G mutation. (**A**) To assess if STXBP1 expression is affected by the Crispr-Cas9 mediated mutations, immunocytochemistry was performed on sister coverslips of the neurons shown in Figure 2. MAP2 shows dendritic morphology (green) and STXBP1 immunofluorescence is predominantly located in axons (MUNC18-1 antibody; magenta). (**B**) The Tukey/scatter plot shows quantification of the average STXBP1 immunofluorescence in the axons of each iNeuron, which is decreased in D207G mutated neurons. ** = $p < 0.01$, * = $p < 0.05$, other comparisons are non-significant ($p > 0.05$). (**C**) Typical example of STXBP1 and Tubulin protein levels. For this experiment, the same iNeurons were mass-cultured in parallel on POL-coated 6-wells plates for 5-6 weeks, to asses STXBP1 expression with an independent technique. In addition, STXBP1 KO iNeurons were taken along as a negative control. Lysates of these cells were run on SDS-PAGE and immunoblotted for STXBP1 and Tubulin as a loading control. (**D**) STXBP1 levels normalized to Tubulin measured from Western-Blot from 4 independent cultures of IPSC-derived human neurons from STXBP1 Control, HZ, S241fs, D207G and KO Crispr-Cas9 clones. ** = $p < 0.01$, * = $p < 0.05$, Kruskal Wallis test with Dunn's multiple comparisons, non-indicated comparisons were non-significant ($p > 0.05$).

train-stimulation, with highest exocytosis levels during the start of the stimulation and a rapid decline as the stimulation continued (Fig. 1). This is a similar pattern as we observed before in mouse neurons with NPY-pHluorin (Chapter 2, 4; Arora et al., 2017; Emperador-Melero et al., 2018; Persoon et al., 2018, 2019; Hoogstraaten et al., 2020; Moro et al., 2020). Also, cell to cell variation in the total number of DCV exocytosis events was comparable to variation in mouse DIV14-18 neurons (Table 1). Therefore, despite that NGN2 induction of iNeurons is considered to create a

more homogeneous cell population compared to primary mouse neurons that have large diversity, this apparently does not result in more homogeneous DCV exocytosis. Whether these similar degrees of variation have common causes or are mediated via different parameters remains to be tested. A previous study from our lab compared NPY-mCherry secretion from iNeurons (iPSCs from neuroepithelial stem cells, differentiated with purmorphamine and valproic acid) with cultured mouse hippocampal neurons and found a similar exocytosis pattern throughout high-frequency burst-stimulation (Emperador Melero et al., 2017). These findings show that DCV exocytosis is robustly triggered by high-frequency train-stimulation in human iNeurons, in a similar way as was observed before in mouse neurons. Therefore, human iNeurons are a suitable model to study DCV exocytosis, but due to the large cell to cell variation in secretion that was also found in mouse neurons, large sample sizes are required.

Using Crispr-Cas9 gene-edited *STXBP1* KO iNeurons, we show that STXBP1 is essential for DCV exocytosis in human neurons. DCV exocytosis was abolished in *STXBP1* KO neurons, while the total number of DCVs was unaffected (Fig. 1), suggesting normal DCV biogenesis. In addition, STXBP1 protein was absent on Western Blot, confirming the KO genotype (Fig. 3). *Munc18-1 null* mutation in mice triggers neuronal degeneration *in vivo* and in primary cultures (Verhage et al., 2000; Bouwman et al., 2004; Heeroma et al., 2004; Santos et al., 2017). In contrast, human *STXBP1* KO iNeurons were viable (Fig. 1). Therefore, while the role of MUNC18-1 in neuronal secretion is likely the same between mouse and human, its role in maintaining neuronal viability may differ. One possible explanation is that human iNeurons express other MUNC18 paralogs to sustain viability. Overexpression of MUNC18-2 or -3 in mouse neurons rescues neuronal viability (Chapter 2; He et al., 2017; Santos et al., 2017). Comparison of single-cell RNA sequencing databases for human and mouse cortical areas shows that both have high expression of Munc18-1/STXBP1 (Tasic et al., 2018; Hodge et al., 2019; Yao et al., 2020). However, mouse neurons also express Munc18-2 in many neuron types, albeit at much lower levels compared with STXBP1. In comparison, human neurons generally do not express STXBP2, but have moderate STXBP3 expression in several neuron types. These findings suggest that STXBP3 expression may alleviate the neuronal death phenotype of STXBP1/*Munc18-1 null* neurons. Immunocytochemistry showed that iNeurons with a D207G mutation in *STXBP1* had reduced STXBP1 protein levels due to a large subgroup without STXBP1 immunofluorescence (Fig. 3). On Western-Blot, this effect was less clearly visible (Fig. 3). The substantial decrease in STXBP1 protein levels in at least a large subset of D207G iNeurons could be causal for the lack of DCV exocytosis in a large subset of D207G iNeurons. This bifurcation of STXBP1 levels and DCV exocytosis in D207G iNeurons suggests that perhaps these iNeurons derived from the D207G clone are in fact a mixture of WT and homozygous D207G mutation. This would explain why a subpopulation contains no STXBP1 staining and hampered DCV exocytosis, while other iNeurons appear similar to control neurons. If this is the case, the homozygous mutation would have a drastic effect on STXBP1 levels and DCV exocytosis, creating effectively a STXBP1 KO phenocopy. Future studies including an extra quality control of the D207G clone and testing sister clones for STXBP1 levels and DCV exocytosis should reveal whether D207G HZ mutation affects DCV exocytosis via protein haploinsufficiency.

Protein levels measured via immunocytochemistry and Western Blot showed similar STXBP1 protein levels in *STXBP1* HZ, S241fs and control iNeurons (Fig. 3). In addition to this absence of an effect on STXBP1 protein levels in S241fs and *STXBP1* HZ iNeurons, DCV exocytosis from these neurons was also similar to control iNeurons (Fig. 2). In contrast, a previous study on human *STXBP1* HZ iNeurons showed a small but significant decrease in STXBP1 protein levels on Western-Blot (Patzke et al., 2015), while *Munc18-1* HZ mouse neurons have ~50% lower MUNC18-1 levels (Verhage et al., 2000; Toonen et al., 2006; Kovačević et al., 2018; Miyamoto et al., 2019; Chen et al., 2020). Furthermore, introduction of MUNC18-1 with patient mutations in mouse *Munc18-1* HZ neurons also resulted in decreased MUNC18-1 levels on Western-Blot (Kovačević et al., 2018) and mutated MUNC18-1 proteins were shown to aggregate and affect WT MUNC18-1 protein in a prion-like fashion, leading to substantially decreased MUNC18-1 protein levels (Guiberson et al., 2018). Therefore, it seems unlikely that *STXBP1* HZ null and S241fs mutations have no influence on STXBP1 protein levels in human iNeurons. An explanation for this lack of effect comes from resequencing of the control clone, which revealed a 400bp deletion in one of the STXBP1 alleles that escaped detection in our initial quality control. This effectively rendered this clone STXBP1 heterozygous, and probably fully explains the lack effect on STXBP1 levels and DCV exocytosis in *STXBP1* HZ and S241fs iNeurons. Future experiments including non-mutated isogenic control iNeurons will reveal whether S241fs or *STXBP1* HZ mutation hamper DCV exocytosis due to haploinsufficiency.

Altogether, in systems with decreased STXBP1 or MUNC18-1 protein levels, or STXBP1 patient mutations, both synaptic transmission and DCV exocytosis are affected albeit to a different extent. Synaptic transmission is specifically reduced in *Munc18-1* HZ mice for some inhibitory and excitatory synapse types, but unaffected in others (Toonen et al., 2006; Miyamoto et al., 2019; Chen et al., 2020). *Munc18-1* HZ mutation in mouse primary cultures did not affect first evoked EPSC amplitude or miniature EPSC frequency, while the same mutation in human iPSCs substantially reduced both (Toonen et al., 2006; Patzke et al., 2015). Expressing MUNC18-1 carrying STXBP1-syndrome patient mutations in primary mouse *Munc18-1 null* neurons decreased EPSC amplitude and miniature EPSC frequency for some mutations, but these effects were not observed when the same proteins were expressed on a *Munc18-1* HZ background (Kovačević et al., 2018). As both patients and *Munc18-1* HZ mice have similar and severe symptoms including epilepsy and behavioral or cognitive impairments (Ohtahara and Yamatogi, 2006; Kovačević et al., 2018; Miyamoto et al., 2019; Chen et al., 2020), it is striking that the synaptic phenotypes are so variable. Due to the important functions of neuropeptides in repressing synaptic activity (in case of NPY) (Tschenett et al., 2003), and in learning and memory via synaptic plasticity (in case of BDNF) (Kesslak et al., 1998; Mizuno et al., 2000; Cirulli et al., 2004; Bekinschtein et al., 2007; Heldt et al., 2007), both of which are highly relevant factors in STXBP1-syndrome, it may be more likely that impaired neuropeptide secretion also contributes to these phenotypes.

Methods

CRISPR/Cas9 mediated mutations

To generate isogenic iPSCs carrying *STXBP1* KO, HZ, S241fs or D207G mutations, CRISPR/Cas9 mediated gene editing as used in a BioniC13 iPSC line (BIONI010-C-13), which carries an NGN2 cassette in its safe harbor locus. For CRISPR/Cas9, guideRNA TATAGGCATCGAGCTTGTCC, which targets c.620(A) was used to generate the D207G mutation and TCATGGAGCACAGGGGAGCT was used for the other mutations, which targets c.721(T). For generating the D207G mutation iPSC line, a specific repair template was used: AGACTTACCTCCCCCATTGTTGGATCATCAGCTTTATAGGCATCAAGCT TGCCCTGAATTAGCTGAGCCAGCAGGGCATTGTCCTTGTATTCCCTGACAA. The isogenic iPSC lines hereby generated included homozygous mutations SS241_C11 (KO-10) and SS241_D9 (KO+1T), and heterozygous mutations SS241_A2_23 (HZ-10), SS241_E11_33 (HZ+1T) and D207G_F7. All lines passed quality control consisting of sequencing.

Gene editing via RNP-nucleofection

In preparation, a 24-wells plate and two 6cm dishes are coated with matrigel for 1hr at RT (room temperature) and 1hr prior to nucleofection, medium is changed to E8+ RI. The CRISPR mix consists of 1,2µl sgRNA 100µM (120pmol final concentration), 1,7µl Cas9 protein 62µM (103pmol final concentration) and 0.9µl PBS (or 2.1µl without ssODN) and requires 15m incubation at RT. Next, a single cell suspension is made from 200k BioniC13 iPSCs. This requires 1x washing with PBS, incubation with accutase (300µl per well of a 6-wells plate) for 5-8m at 37°C and resuspension of the cells in 3ml E8. Next 200,000 cells were collected for each reaction in a falcon tube, which was filled up with PBS and centrifuged for 5m at 1,000 rpm (rounds per minute). Nucleofection mix was prepared by adding 1.2µl ssODN (single-stranded oligonucleotides) to the CRISPR mix (total volume 5µl) and mixing with 16.2µl Primary P3 Cell Suspension and 3.6µl Supplement. For nucleofection, supernatant was removed and iPSC pellet was resuspended in 25µl Nucleofection mix and transferred to a nucleofector cuvette, for use in the Lonza machine (program CA137). After nucleofection, cells were mixed in 200µl E8+ RI and plated on a 24-wells plate. After 1 day, medium was replaced by E8 medium without RI. When cells were confluent, half was used for DNA and the rest for passaging.

DNA isolation for pool sequencing was done with 50-100% confluent iPSCs. Cells were incubated for 3-5m in 300µl 1mM EDTA and after removal of EDTA collected in PBS. After centrifuging (5m at 3,000 rpm), pellet was resuspended in QuickExtract Solution (1µl per 1,000 cells; Lucigen; #QE09050), then transferred to PCR tubes, vortexed and incubated for 6m at 65°C, next again vortexed and incubated for 2m at 98°C.

After correct sequencing, cells were used for single cell plating. To do so, cells were 1x washed with PBS and incubated with accutase (300µl per well in 6-wells plate) for 5-8m at 37°C, then resuspended in 3ml E8+ RI. 3,000 – 6,000 cells were plated in 6cm matrigel coated dishes, refreshed after 2 days and colonies were manually picked after 6-8 days into matrigel coated 96-wells plates in E8+ RI. After 2 days incubation, medium

was refreshed each day with E8 until confluency, when wells were double passaged (1 for freezing and 1 for DNA). Passaging was done by first incubating for 3-5m at RT in 100µl 1mM EDTA per well, then removal of EDTA and resuspending cells in 100µl E8+ RI, which was transferred to new matrigel coated 96-wells plates. Freezing of plates was done after incubating in 100µl EDTA for 3-5m at RT by resuspending cells in 100µl cold KSR, transferring this to a new plate on ice and adding 100µl cold KSR with 20% DMSO, after which plates were stored at -80°C. Frozen plates were used for QuickExtract DNA isolation as described above (with adjusted volumes) or for iPSC colony expansion. Colony expansion was done after quickly thawing on 37°C by pipetting one well into 3ml E8+ RI in a falcon tube, which was centrifuged for 5m at 1,000 rpm. Pellet was resuspended in 200µl E8+ RI and put onto matrigel coated 96 or 48 wells plates containing 100µl or 250µl E8+ RI. Plates were washed after 1 day with E8+ RI and subsequently each day with E8, after which cells were passaged.

iPSC-derived human neuron differentiation and culturing

BioniC13 iPSCs were plated on Matrigel coated plates and cultured in TeSR-E8 medium with 0.1% Penicillin/Streptomycin (P/S) in an incubator at 37°C with 5% CO_2. Medium was refreshed daily. When confluent, cells were dissociated using 1 mM EDTA in PBS and re-plated in TeSR-E8 medium supplemented with 5µM ROCK inhibitor. The NGN2 differentiation was described before (Zhang et al., 2013). In short, the NGN2 cassette is doxycycline inducible (Tet-On promotor) and is incorporated in the genomic safe harbor locus of the BioniC13 iPSCs. To induce differentiation, cells were dissociated using accutase and replated in N2 medium (DMEM/F12 medium supplemented with 1% N2 supplement B, 200mM Glutamax, 20% Dextrose and 0.1% P/S and with added SMAD inhibitors (10µM SB431542, 2µM XAV939, 100nM LDN1093189). After 24h incubation, medium was refreshed for another day. Next, medium was changed to N2-supplemented medium with 10% FUDR. The next day, cells were dissociated using accutase and plated with 750 – 1,000 cells per well onto glial micro-islands (For generation of glial micro-islands see methods Chapter 2) for live imaging and immunohistochemistry experiments, and onto POL (Poly-ornithin/Laminin) coated 6-wells plates (250,000 cells per well) for Western-Blot. From here on, cells are maintained in neuronal maintenance medium, consisting of Neurobasal with 20% Dextrose, NEAA, B27, 0.1% Penicillin/Streptomycin, 0.5% Fetal bovine serum, 200mM Glutamax, 10ng/ml BDNF, 10ng/ml CNTF, 10ng/ml GDNF and 2µg/ml Doxycycline hyclate. Medium of micro-island cultures was refreshed 1x per week by replacing 50% of the medium, for POL-plates this was done twice per week.

Immunohistochemistry

For immunohistochemistry, coverslips containing 6-week old iPSC-derived neurons on glia microislands were fixed for 20m in 4% PFA, 3x washed, permeabilized in 0.5% Triton for 5m and blocked (in PBS with 2% normal goat serum and 0.1% Triton). Primary antibody incubation was done overnight at 4°C with polyclonal chicken MAP2 (Abcam, 1:1000), polyclonal rabbit MUNC18-1 (Sigma HPA023483, 1:250) and polyclonal Guinee pig Synaptophysin (SYSY 101004, 1:500) or monoclonal mouse anti SMI321 (Covance, 1:1000) in blocking solution. Secondary antibody incubation after 3x washing in PBS

was done for 1h at RT and coverslips were mounted with Mowiol. Samples were imaged on a confocal laser-scanning microscope (NIKON A1+ with LU4A laser unit) with a 40x (NA 1.3) or 60x (NA 1.4) oil immersion objective and NIS elements software (version 4.60, Nikon).

Viruses

All constructs were generated with sequence verification, cloned into a pLenti vector containing a Synapsin promotor. Lentiviral NPY-pHluorin was used as a marker for DCV exocytosis as reported before and was infected 7 days prior to live-imaging (van de Bospoort *et al.*, 2012; Persoon *et al.*, 2018).

Live cell imaging

Live-cell imaging to asses DCV exocytosis in human iPSC-derived neurons from each clone was done during WIV6 at room temperature (RT; 21-26°C). A custom-built set-up was used including an inverted microscope (IX81; Olympus) with an MT20 light source (Olympus), the appropriate filter sets (Semrock, Rochester, NY), a 40x oil objective (NA 1.3), an EM charge-coupled device camera (EMCCD; C9100-02; Hamamatsu Photonics, Japan) and Xcellence RT imaging software (Olympus). Electrical stimulation was delivered by parallel platinum electrodes placed carefully around each glia micro-island, conducting 30 mA, 1 ms pulses controlled by a Master 8 system (AMPI, Germany) and a stimulus generator (A385RC, World Precision Instruments, Germany). Two episodes of high-frequency train-stimulation were generated including both 8 trains of 50 AP at 50Hz, with the first episode starting after 30s of baseline recording and the second episode starting 30s after the end of the first stimulation episode. Imaging acquisition rate was 2Hz. Coverslips were perfused with Tyrode's solution (2 mM CaCl2, 2.5 mM KCl, 119 mM NaCl, 2 mM MgCl2, 30 mM glucose and 25 mM HEPES, pH 7.4). pHluorin-based DCV exocytosis assays ended with a 10-seconds NH_4^+ perfusion (Tyrode's with 50mM NH_4Cl, replacing 50mM NaCl), delivered via a gravity flow system with a capillary placed above the neuron, to de-quench pHluorin in all DCVs.

Western Blot

Human iPSC-derived neurons from each clone were grown for 5-6 weeks on POL plates befor lysing. Neurons were washed twice in PBS and collected by scraping in 1ml of PBS containing 100x protease inhibitor E-64d (Sigma, E8640). Scraped cells were centrifuged for 5m at 12000 rpm (rounds per minute) and pellets were lysed in 70 µl Laemmli sample buffer containing 2% SDS (VWR chemicals, M107), 10% glycerol (Merck, 818709), 0.26M β-mercaptoethanol (Sigma, M3148), 60mMTris-HCl (Serva, 37180) pH 6.8, and 0.01% Bromophenol blue (Applichem, A3640), homogenized by a 20 gauge needle and vortexed, after which samples were boiled at 100°C for 5 minutes. 10 µl of each sample was loaded and separated on 10% SDS-polyacrylamide gels with 2,2,2-Trichloroethanol using standard SDS-PAGE technique. Proteins were transferred to nitrocellulose membrane 0.2 µm (Bio-Rad #1620112) using Trans-Blot® Turbo™ Transfer System, with High MW protocol (2.5 A, up to 25 V; 10 min). Membranes were blocked with 2% protease-free Bovine Serum Albumin (268131000, ACROS Organics™)

in PBS-0.05% Tween solution for 1 h at room temperature and then incubated with primary antibodies, diluted in the blocking buffer. The following antibodies were used: Monoclonal Mouse Anti- Munc-18 (610336, BD Transduction Laboratories™), overnight at 4°C, followed by 30 minutes incubation at room temperature with IRDye® 680LT Goat anti-Mouse IgG Secondary Antibody (926-68020, LI-COR); Monoclonal Mouse Anti-g-Tubulin (T5326, Sigma-Aldrich), overnight at 4°C, followed by 30 minutes incubation at room temperature with IRDye® 680LT Goat anti-Mouse IgG Secondary Antibody (926-68020, LI-COR). Western blotting images were acquired using with LI-COR Odyssey Fc according to the manufacturer's instructions. Band intensity was calculated using Image Studio™ Software. Stxbp1 protein levels were normalized to g-Tubulin levels.

Analysis

For analysis of NPY-pHluorin labeled DCV exocytosis events, 3x3 pixel regions (Regions of interest; ROIs) were placed manually on NPY-pHluorin dequenching events in ImageJ (NIH). Somatic events were not taken along due to the high background signal. The mean intensity of each ROI was measured and loaded into a custom written MATLAB (Mathworks) script for semi-automatic analysis, in which each measurement was plotted as change in fluorescence (ΔF) per baseline fluorescence (F0, average fluorescence during the first 10 frames). Automatic detection of NPY-pHluorin labeled DCV exocytosis events occurred when ΔF was at least 2 standard deviations above F0. Histograms and cumulative plots were generated in MATLAB. To calculate the total number of DCVs (poolsize) per neuron, the highest-intensity frame during NH_4 perfusion was taken for pHluorin based assays and further analyzed using the MATLAB program SynD (Schmitz *et al.*, 2011; van de Bospoort *et al.*, 2012). Parameters were optimized for detection of DCVs and the number of detected DCVs was adjusted for intensity by dividing by the mode intensity. Analysis of STXBP1 levels from fixed and immunostained samples was done by manually drawing ROIs (3 dendritic ROIs, 2 axonal ROIs and 1 somatic ROI) in ImageJ, of which the average intensities were measured. STXBP1 levels on Western Blot were analyzed by drawing ROIs around the specific bands in ImageJ and measuring total intensity. Data computation was done in Excel, while Tukey/scatter plots and statistics were generated using GraphPad Prism.

Statistics

Statistical analysis was performed in GraphPad Prism. Shapiro-Wilk normality test was used to test for normal distributions and Levene's to test for homogeneity of variances. Due to not normally distributed data, all data with two groups (Fig. 1) were analyzed for significance using Mann Whitney-U tests and data with more than two groups using Kruskal-Wallis tests followed by Dunn's multiple comparisons post hoc tests.

Acknowledgements

The authors thank Robbert Zalm for cloning and producing viral particles, Lisa Laan and Desiree Schut for producing glia island cultures, helping with Crispr-Cas9 gene editing of iPSCs and culturing of iPSCs and iNeurons, Jurjen Broeke for technical support and members of the CNCR DCV team and human neuron team for discussions and helpful input. This work is supported by an ERC Advanced Grant (322966) of the European Union (to MV).

Author contributions

D.C.P., R.F.T. and M.V. designed the experiments. D.C.P. performed all DCV exocytosis live imaging assays and the immunohistochemistry for figure 3 & S1 and analyzed these data. G.B. performed the Western-Blots. A.B. performed the Crispr-Cas9 gene editing of iPSCs. A.N. performed the immunohistochemistry for figure 1. D.C.P., R.F.T. and M.V. designed figures and wrote the manuscript with input from all authors.

References

Arora S, Anubhuti (2006) Role of neuropeptides in appetite regulation and obesity - A review. Neuropeptides 40:375–401.

Arora S, Saarloos I, Kooistra R, van de Bospoort R, Verhage M, Toonen RF (2017) SNAP-25 gene family members differentially support secretory vesicle fusion. J Cell Sci 130:1877–1889.

Bekinschtein P, Cammarota M, Igaz LM, Bevilaqua LRM, Izquierdo I, Medina JH (2007) Persistence of Long-Term Memory Storage Requires a Late Protein Synthesis- and BDNF- Dependent Phase in the Hippocampus. Neuron 53:261–277.

Bonnycastle K, Davenport EC, Cousin MA (2020) Presynaptic dysfunction in neurodevelopmental disorders: Insights from the synaptic vesicle life cycle. J Neurochem:179–207.

Bouwman J, Maia AS, Camoletto PG, Posthuma G, Roubos EW, Oorschot VMJ, Klumperman J, Verhage M (2004) Quantification of synapse formation and maintenance in vivo in the absence of synaptic release. Neuroscience 126:115–126.

Chen W, Cai Z-L, Chao ES, Chen H, Longley CM, Hao S, Chao H-T, Kim JH, Messier JE, Zoghbi HY, Tang J, Swann JW, Xue M (2020) Stxbp1/Munc18-1 haploinsufficiency impairs inhibition and mediates key neurological features of STXBP1 encephalopathy. Elife 9:1–33 DOI: 10.7554/eLife.48705.

Cirulli F, Berry A, Chiarotti F, Alleva E (2004) Intrahippocampal administration of BDNF in adult rats affects short-term behavioral plasticity in the Morris water maze and performance in the elevated plus-maze. Hippocampus 14:802–807.

Comeras LB, Herzog H, Tasan RO (2019) Neuropeptides at the crossroad of fear and hunger: A special focus on neuropeptide y. In: Annals of the New York Academy of Sciences, pp 59–80. John Wiley & Sons, Ltd (10.1111). DOI: 10.1111/nyas.14179.

Cortès-Saladelafont E, Lipstein N, García-Cazorla À (2018) Presynaptic disorders: a clinical and pathophysiological approach focused on the synaptic vesicle. J Inherit Metab Dis 41:1131–1145.

Cropper EC, Jing J, Vilim FS, Weiss KR (2018) Peptide Cotransmitters as Dynamic, Intrinsic Modulators of Network Activity. Front Neural Circuits 12:1–7 DOI: 10.3389/fncir.2018.00078.

Emperador-Melero J, Huson V, van Weering J, Bollmann C, Fischer von Mollard G, Toonen RF, Verhage M (2018) Vti1a/b regulate synaptic vesicle and dense core vesicle secretion via protein sorting at the Golgi. Nat Commun 9 DOI: 10.1038/s41467-018-05699-z.

Emperador Melero J, Nadadhur AG, Schut D, Weering J V, Heine VM, Toonen RF, Verhage M (2017) Differential Maturation of the Two Regulated Secretory Pathways in Human iPSC-Derived Neurons. Stem Cell Reports 8:659–672 DOI: 10.1016/j.stemcr.2017.01.019.

Gburek-Augustat J, Beck-Woedl S, Tzschach A, Bauer P, Schoening M, Riess A (2016) Epilepsy is not a mandatory feature of STXBP1 associated ataxia-tremor-retardation syndrome. Eur J Paediatr Neurol 20:661–665.

Griebel G, Holsboer F (2012) Neuropeptide receptor ligands as drugs for psychiatric diseases: The end of the beginning? Nat Rev Drug Discov 11:462–478.

Guiberson NGL, Pineda A, Abramov D, Kharel P, Carnazza KE, Wragg RT, Dittman JS, Burré J (2018) Mechanism-based rescue of Munc18-1 dysfunction in varied encephalopathies by chemical chaperones. Nat Commun 9.

Hamdan FF, Gauthier J, Dobrzeniecka S, Lortie A, Mottron L, Vanasse M, D'Anjou G, Lacaille JC, Rouleau GA, Michaud JL (2011) Intellectual disability without epilepsy associated with STXBP1 disruption. Eur J Hum Genet 19:607–609.

He E, Wierda K, Van Westen R, Broeke JH, Toonen RF, Cornelisse LN, Verhage M (2017) Munc13-1 and Munc18-1 together prevent NSF-dependent de-priming of synaptic vesicles. Nat Commun 8 DOI: 10.1038/ncomms15915.

Heeroma JH, Roelandse M, Wierda K, Van Aerde KI, Toonen RFG, Hensbroek RA, Brussaard A, Matus A, Verhage M (2004) Trophic support delays but not prevent cell-intrinsic degeneration of neurons deficient for munc18-1. Eur J Neurosci 20:623–634.

Heldt SA, Stanek L, Chhatwal JP, Ressler KJ (2007) Hippocampus-specific deletion of BDNF in adult mice impairs spatial memory and extinction of aversive memories. Mol Psychiatry 12:656–670.

Hodge RD et al. (2019) Conserved cell types with divergent features in human versus mouse cortex. Nature 573:61–68 DOI: 10.1038/s41586-019-1506-7.

Hoogstraaten RI, Keimpema L Van, Toonen RF, Verhage M (2020) Tetanus insensitive VAMP2 differentially restores synaptic and dense core vesicle fusion in tetanus neurotoxin treated neurons. Sci Rep:1–14 DOI: 10.1038/s41598-020-67988-2.

Ichida JK, Kiskinis E (2015) Probing disorders of the nervous system using reprogramming approaches. EMBO J 34:1456–1477.

Kesslak JP, So V, Choi J, Cotman CW, Gomez-Pinilla F (1998) Learning upregulates brain-derived neurotrophic factor messenger ribonucleic acid: A mechanism to facilitate encoding and circuit maintenance? Behav Neurosci 112:1012–1019.

Kovačević J, Maroteaux G, Schut D, Loos M, Dubey M, Pitsch J, Remmelink E, Koopmans B, Crowley J, Cornelisse LN, Sullivan PF, Schoch S, Toonen RF, Stiedl O, Verhage M (2018) Protein instability, haploinsufficiency, and cortical hyper-excitability underlie STXBP1 encephalopathy. Brain 141:1350–1374 DOI: 10.1093/brain/awy046.

Lee Y Il, Kim YG, Pyeon HJ, Ahn JC, Logan S, Orock A, Joo KM, Lőrincz A, Deák F (2019) Dysregulation of the SNARE-binding protein Munc18-1 impairs BDNF secretion and synaptic neurotransmission: a novel interventional target to protect the aging brain. GeroScience 41:109–123.

Miranda M, Morici JF, Zanoni MB, Bekinschtein P (2019) Brain-Derived Neurotrophic Factor: A Key Molecule for Memory in the Healthy and the Pathological Brain. Front Cell Neurosci 13:363.

Miyamoto H, Tatsukawa T, Shimohata A, Yamagata T, Suzuki T, Amano K, Mazaki E, Raveau M, Ogiwara I, Oba-Asaka A, Hensch TK, Itohara S, Sakimura K, Kobayashi K, Kobayashi K, Yamakawa K (2019) Impaired cortico-striatal excitatory transmission triggers epilepsy. Nat Commun 10:1–13 DOI: 10.1038/s41467-019-09954-9.

Mizuno M, Yamada K, Olariu A, Nawa H, Nabeshima T (2000) Involvement of brain-derived neurotrophic factor in spatial memory formation and maintenance in a radial arm maze test in rats. J Neurosci 20:7116–7121.

Moro A, Woerden GMV, Toonen RF, Verhage M (2020) Camkii controls neuromodulation via neuropeptide gene expression and axonal targeting of neuropeptide vesicles. PLoS Biol 18:1–30 DOI: 10.1371/JOURNAL.PBIO.3000826.

Nagahara AH, Tuszynski MH (2011) Potential therapeutic uses of BDNF in neurological and psychiatric disorders. Nat Rev Drug Discov 10:209–219.

Nestor PG, O'Donovan K, Lapp HE, Hasler VC, Boodai SB, Hunter R (2019) Risk and protective effects of serotonin and BDNF genes on stress-related adult psychiatric symptoms. Neurobiol Stress 11:100186.

Ohtahara S, Yamatogi Y (2006) Ohtahara syndrome: With special reference to its developmental aspects for differentiating from early myoclonic encephalopathy. Epilepsy Res 70:58–67.

Patzke C, Han Y, Covy J, Yi F, Maxeiner S, Wernig M, Südhof TC (2015) Analysis of conditional heterozygous STXBP1 mutations in human neurons. J Clin Invest 125:3560–3571 DOI: 10.1172/JCI78612.

Persoon CM, Hoogstraaten RI, Nassal JP, van Weering JRT, Kaeser PS, Toonen RF, Verhage M (2019) The RAB3-RIM Pathway Is Essential for the Release of Neuromodulators. Neuron 104:1065-1080.e12 DOI: 10.1016/j.neuron.2019.09.015.

Persoon CM, Moro A, Nassal JP, Farina M, Broeke JH, Arora S, Dominguez N, Weering JR, Toonen RF, Verhage M (2018) Pool size estimations for dense-core vesicles in mammalian CNS neurons. EMBO J 37:e99672 DOI: 10.1172/JCI78612.

Puntman DC, Arora S, Farina M, Toonen RF, Verhage M (2021) Munc18-1 is essential for neuropeptide secretion in neurons . J Neurosci 41:JN-RM-3150-20 DOI: 10.1523/jneurosci.3150-20.2021.

Saitsu H, Kato M, Mizuguchi T, Hamada K, Osaka H, Tohyama J, Uruno K, Kumada S, Nishiyama K, Nishimura A, Okada I, Yoshimura Y, Hirai SI, Kumada T, Hayasaka K, Fukuda A, Ogata K, Matsumoto N (2008) De novo mutations in the gene encoding STXBP1 (MUNC18-1) cause early infantile epileptic encephalopathy. Nat Genet 40:782–788.

Santos TC, Wierda K, Broeke JH, Toonen RF, Verhage M (2017) Early Golgi Abnormalities and Neurodegeneration upon Loss of Presynaptic Proteins Munc18-1, Syntaxin-1, or SNAP-25. J Neurosci 37:4525–4539 DOI: 10.1523/JNEUROSCI.3352-16.2017.

Stamberger H, Nikanorova M, Accorsi P, Angriman M, Benkel-herrenbrueck I, Capovilla G, Erasmus CE, Fannemel M, Giordano L, Helbig KL, Maier O, Phalin J (2016) A neurodevelopmental disorder including epilepsy. Neurology 86:954–962.

Tasic B et al. (2018) Shared and distinct transcriptomic cell types across neocortical areas. Nature 563:72–78 DOI: 10.1038/s41586-018-0654-5.

Toonen RFG, De Vries KJ, Zalm R, Südhof TC, Verhage M (2005) Munc18-1 stabilizes syntaxin 1, but is not essential for syntaxin 1 targeting and SNARE complex formation. J Neurochem 93:1393–1400.

Toonen RFG, Wierda K, Sons MS, de Wit H, Cornelisse LN, Brussaard A, Plomp JJ, Verhage M (2006) Munc18-1 expression levels control synapse recovery by regulating readily releasable pool size. Proc Natl Acad Sci 103:18332–18337 DOI: 10.1073/pnas.0608507103.

Tschenett A, Singewald N, Carli M, Balducci C, Salchner P, Vezzani A, Herzog H, Sperk G (2003) Reduced anxiety and improved stress coping ability in mice lacking NPY-Y2 receptors. Eur J Neurosci 18:143–148.

Verhage M, Maia AS, Plomp JJ, Brussaard AB, Heeroma JH, Vermeer H, Toonen RF, Hammer RE, van den Berg TK, Missler M, Geuze HJ, Südhof TC (2000) Synaptic Assembly of the Brain in the Absence of Neurotransmitter Secretion. Science (80-) 287:864–869 DOI: 10.1126/science.287.5454.864.

Verhage M, Sørensen JB (2020) SNAREopathies: Diversity in Mechanisms and Symptoms. Neuron 107:22–37 DOI: 10.1016/j.neuron.2020.05.036.

Waites CL, Garner CC (2011) Presynaptic function in health and disease. Trends Neurosci 34:326–337 DOI: 10.1016/j.tins.2011.03.004.

Werner FM, Coveñas R (2010) Classical neurotransmitters and neuropeptides involved in major depression: A review. Int J Neurosci 120:455–470.

Yao Z et al. (2020) A taxonomy of transcriptomic cell types across the isocortex and hippocampal formation Zizhen. bioRxiv.

Zhang Y, Pak CH, Han Y, Ahlenius H, Zhang Z, Chanda S, Marro S, Patzke C, Acuna C, Covy J, Xu W, Yang N, Danko T, Chen L, Wernig M, Südhof TC (2013) Rapid single-step induction of functional neurons from human pluripotent stem cells. Neuron 78:785–798.

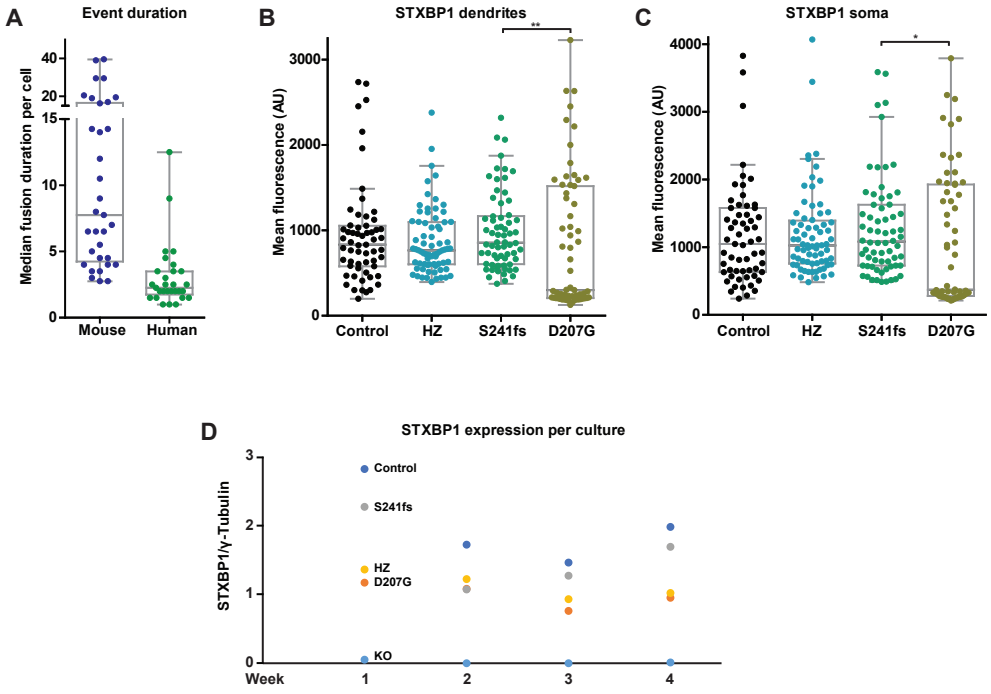

Suppl. Figure 1. DCV exocytosis is unaffected by STXBP1 HZ mutation, but decreased by D207G missense mutation. (**A**) Duration of DCV exocytosis events was measured by calculating the time from the onset until the termination of each NPY-pHluorin dequenching event. Data from human control iNeurons (Fig. 1) was compared with data from mouse WT neurons (Chapter 2, Fig. 4). (**B**) The Tukey/scatter plot shows quantification of the average STXBP1 immunofluorescence in the dendrites. ** = $p < 0.01$, other comparisons are non-significant ($p > 0.05$), Kruskal Wallis test with Dunn's multiple comparisons. (**C**) The Tukey/scatter plot shows quantification of the average STXBP1 immunofluorescence in the soma of each iNeuron. * = $p < 0.05$, other comparisons are non-significant ($p > 0.05$), Kruskal Wallis test with Dunn's multiple comparisons. (**D**) STXBP1 expression values per week on Western-Blot as total intensity of the STXBP1 band divided by the γ-Tubulin band.

3

Chapter 4

MUNC18-2 is not required for neuropeptide, neurotransmitter or GLUT4 secretion in mouse hippocampal neurons

Daniël C. Puntman, Enqi He, Swati Arora, Michael J. Tuvim, Ruud F. Toonen, Matthijs Verhage

Abstract

The role of exocytic Sec1/MUNC18(SM)-proteins MUNC18-2 and -3 in neuronal secretion has not been directly tested. First, mouse brain expression levels of SM-genes were compared *in silico* using a single-cell RNA sequencing dataset. Munc18-3 expression was absent in almost all cortical and hippocampal cells, while Munc18-2 was expressed at a higher level, albeit still much lower than MUNC18-1. Next, we studied the role of MUNC18-2 in different neuronal secretion pathways, using fluorescent exocytosis markers or patch clamp in *Munc18-2* conditional knockout (cKO) or wild-type (WT) mouse neurons. *Munc18-2* cKO did not affect DCV (dense core vesicle) fusion, neuropeptide release or their kinetics. In addition, synaptic transmission was normal. Next, we used GLUT4 (glucose transporter 4) vesicle exocytosis marker GLUT4-pHluorin to visualize GLUT4 insertion in the plasma membrane, which occurred at baseline conditions and increased upon different electrical stimulations. However, *Munc18-2* cKO did not alter the number of GLUT4-pHluorin exocytosis events. We conclude that MUNC18-2 is not required for DCV exocytosis, synaptic transmission or GLUT4 vesicle exocytosis.

Introduction

Exocytic Sec1/Munc18(SM)-proteins are conserved from yeast to *choanoflagellata* and *metazoan* (Burkhardt et al., 2011) and are essential for regulated exocytosis (for a review see: Toonen and Verhage, 2003). Some animals, including *C. elegans* and *D. melanogaster*, express only one exocytic SM-protein (UNC18 in *C. elegans* or Rop in *D. melanogaster*), indicating that only one exocytic SM-protein can be sufficient to support regulated secretion. Two gene duplications gave rise to 3 MUNC18 paralogs in vertebrates, MUNC18-1, -2 and -3, of which the latter two have 62% and 52% homology to MUNC18-1, respectively (For a review see: Toonen and Verhage, 2003). Each of these paralogs supports regulated secretion in various cell types. Mice with genetic null mutations in both alleles of either *Munc18-1, -2* or *-3* do not survive beyond embryonic or fetal stages (Verhage et al., 2000; Oh et al., 2005, 2012; Gutierrez et al., 2018), underlining the essential role of each paralog. Similar to *C. elegans* or *Drosophila*, many mammalian secretion pathways are supported by only one of the paralogs. However, some cell types require multiple MUNC18 paralogs to regulate secretion (Oh and Thurmond, 2009; Oh et al., 2012; Lam et al., 2013; Zhu et al., 2015; Jaramillo et al., 2019).

One cell type in which all three MUNC18 paralogs have a role in secretion, is the pancreatic β-cell. In response to high blood sugar levels, pancreatic β-cells release insulin in a bi-phasic fashion: a short acute phase and a sustained phase of secretion. The first phase is mainly supported by MUNC18-1, while the prolonged phase requires MUNC18-3 (Oh and Thurmond, 2009; Oh et al., 2012). MUNC18-2 supports both phases of insulin release (Lam et al., 2013) and one study suggests that MUNC18-3 may support both phases as well (Zhu et al., 2015). Similarly, mucus secretion from lung epithelial cells requires more than one paralog: basal and stimulated secretion depend on MUNC18-1 and -2 respectively (Jaramillo et al., 2019). These findings show that despite extensive homology, all MUNC18 paralogs support different aspects within the same secretion pathway.

The main regulated secretion pathways in neurons are neurotransmitter secretion from synaptic vesicles (SVs) and neuropeptide secretion from dense core vesicles (DCVs). The most highly expressed paralog in the brain is MUNC18-1, which is essential for both secretion pathways and is additionally required for neuronal survival (Chapter 2; Verhage et al., 2000). Over-expression of paralogs MUNC18-2 or -3 does not compensate for the loss of MUNC18-1 in DCV exocytosis or neurotransmission, but supports neuronal viability (Chapter 2; He et al., 2017; Santos et al., 2017). Although MUNC18-2 and -3 are expressed in the brain (Tellam et al., 1995; Martin-Verdeaux et al., 2002; Imai et al., 2004; Mandic et al., 2011; Kim et al., 2012; Lam et al., 2013; Zhu et al., 2015), their function in neuronal secretion has not been discovered yet.

Other neuronal secretion pathways include regulated exocytosis of AMPA, NMDA or $GABA_A$ receptor containing vesicles at the postsynapse (Derkach et al., 2007; Rao and Finkbeiner, 2007), lysosomal secretion from both axons and dendrites (Padamsey et al., 2017; Ibata et al., 2019) and activity-dependent exocytosis of glucose transporter 4 (GLUT4) vesicles in presynapses. Upon prolonged, substantial firing, refilling of the RRP (readily releasable pool) of SVs is limited by ATP generation via local glycolysis (Ashrafi et al., 2017). Using pHluorin-tagged GLUT4, the authors showed that neurons solve this problem by inserting extra GLUT4 into the presynaptic membrane upon increased synaptic activity. In addition, the authors suggest that GLUT4 exocytosis is cAMP and MUNC13 dependent, but the full exocytic machinery has not been characterized yet, including the role of an exocytic SM-protein.

Since MUNC18-2 and -3 are expressed in the brain, it could be that not all neuronal secretion depends on MUNC18-1, especially since neurons require several secretion pathways to be active simultaneously. In addition, the roles of MUNC18-2 and -3 in synaptic transmission and neuropeptide secretion have only indirectly been assessed in neurons via overexpression in *Munc18-1 null* neurons (Chapter 3; He et al., 2017; Santos et al., 2017). Therefore, the roles of the exocytic SM-proteins MUNC18-2 and -3 in neuronal secretion may have been overlooked.

The aim of this chapter was to assess the role of MUNC18-2 and -3 in neuronal secretion. First, the expression levels of SM-genes in the mouse brain were compared *in silico* using a single-cell RNA sequencing dataset. Subsequently, secretion of neuropeptides, neurotransmitters or GLUT4 was tested in *Munc18-2* cKO and WT mouse neurons. *Munc18-2* cKO did not affect DCV fusion, neuropeptide release or their kinetics. In addition, synaptic transmission was normal. We show using GLUT4-pHluorin, that GLUT4 exocytosis occurs at baseline conditions and increases upon different electrical stimulations. However, conditional *Munc18-2* inactivation did not affect GLUT4-pHluorin exocytosis. We propose that the function of MUNC18-2 in the brain may be in another secretion pathway.

Results

Munc18-1 and -2 are expressed in mouse cortical and hippocampal neurons

To determine SM-gene expression in the brain, transcription of SM genes in 367 mouse cortical and hippocampal cell types was compared by assessing a single-cell RNA sequencing database (Yao et al., 2020). Munc18-1 transcripts were detected at 3-4 fold

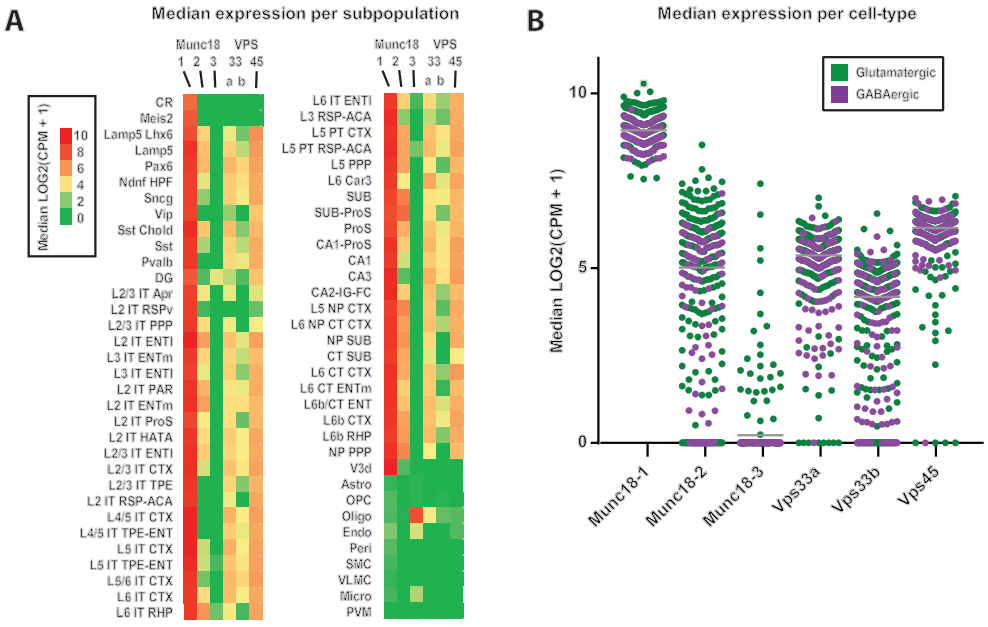

Figure 1. Expression of SM-proteins in mouse neurons. (**A**) Median values of each cell subpopulation were extracted from a single-cell RNA sequencing database of cortical and hippocampal mouse neurons and glia cells (n = 379). The rows represent each subpopulation and the columns the expressed gene of interest. Values are color coded and represented as the LOG2 of CPM +1. CPM = counts per million. (**B**) Scatter plot showing the median mRNA expression levels per SM-gene for each neuron (n = 355) on a logarithmic scale. Neuron types are additionally color coded for glutamatergic (green) and GABAergic (magenta). Grey lines indicate median of the population.

higher level in most cell types than any other SM-gene (Fig. 1A,B). Munc18-2 transcripts were present in a majority of neuronal subtypes and more abundant than Munc18-3 transcripts, which were found in oligodendrocytes and some Dentate-Gyrus neurons, but absent in most cell types. SM genes VPS33a/b & VPS45, which control intracellular membrane trafficking, were also expressed higher than Munc18-3 in most cell types. These findings show that the exocytic SM-gene Munc18-2 is generally expressed in addition to Munc18-1 in most mouse cortical and hippocampal neurons. Therefore, the role of MUNC18-2 in neuronal secretion was further assessed in this chapter.

Munc18-2 is not required for DCV exocytosis

For direct assessment of the role of MUNC18-2 in DCV exocytosis, primary neurons from *Munc18-2*$^{lox/lox}$ mice were infected with Cre-EGFP or inactive ΔCre-EGFP lentiviruses at DIV3 to generate *Munc18-2* cKO (conditional Knock-Out) or WT (wild type) conditions respectively. We generated a specific MUNC18-2 antibody that detected MUNC18-2 expressed in HEK293 cells but not in neuronal lysates (Fig. S1A-C). *Munc18-2* cKO did not affect neuronal viability or morphology (Fig. 2A,B). To evaluate neuropeptide secretion, NPY-pHluorin was used as a DCV exocytosis marker as previously described (Chapter 2; Arora et al., 2017; Dominguez et al., 2018; Emperador-Melero et al., 2018; Farina et al., 2015; Hoogstraaten et al., 2020; Moro et al., 2020; Persoon et al., 2018, 2019) and was infected 4-6 days prior to imaging. At DIV14-18, DCV exocytosis was detected as NPY-pHluorin dequenching events during high-frequency train-stimulation (16x 50AP @ 50Hz) (Fig. S2A,B).

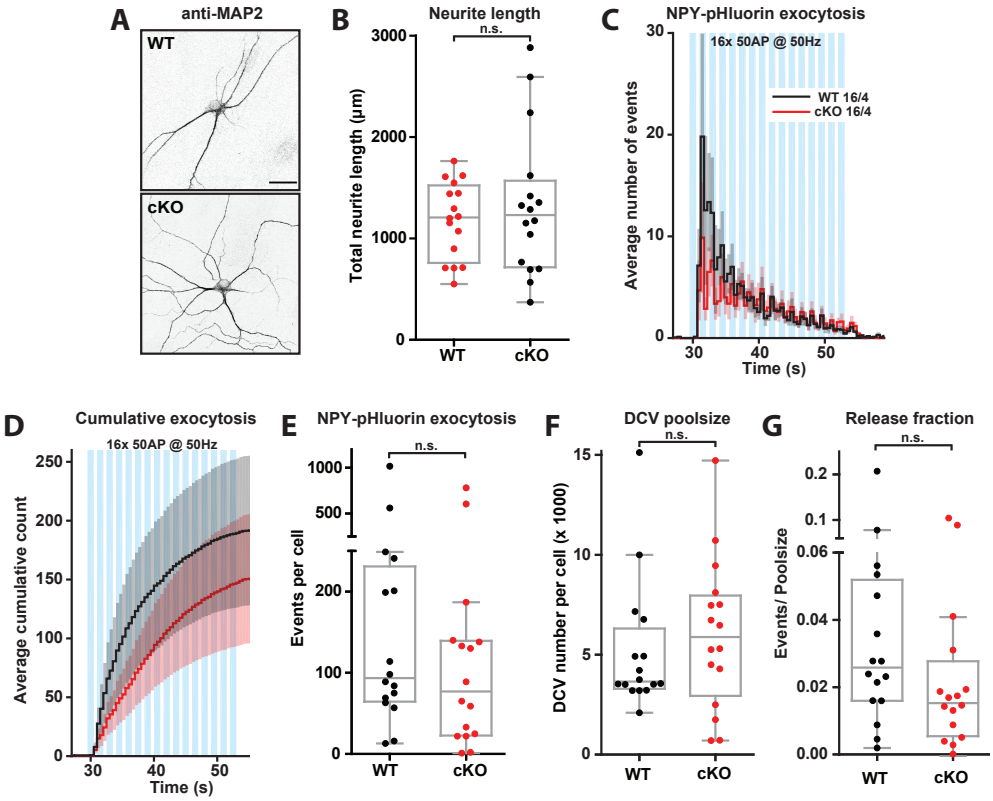

Figure 2. Munc18-2 cKO does not affect DCV exocytosis. (**A**) Typical example of conditional Munc18-2 null (cKO) and WT neurons immunostained with MAP2. Scale bar = 25µm. (**B**) Tukey/scatter plot shows that the total neurite length is similar between Munc18-2 WT and cKO neurons that were infected with NPY-pHluorin and perfused with NH4. (**C**) Histogram showing the average number of NPY-pHluorin labeled DCV exocytosis events during high-frequency train-stimulation (16 x 50 APs at 50Hz) in Munc18-2 WT (black) and cKO (red) neurons. Error bars are SEM. Sample size is indicated per condition as n/N. (**D**) Cumulative representation of C. Error bars are SEM. (**E**) The Tukey/Scatter plot shows that the total number of DCV exocytosis events is not affected by conditional Munc18-2 inactivation. Mann Whitney-U test: n.s. = non-significant. $p > 0.05$. (**F**) The Tukey/scatter plot shows that the total pool of DCVs per cell, revealed by NH4 application, is similar in conditional Munc18-2 null and WT neurons. Mann Whitney-U test: n.s. = non-significant. $p > 0.05$. (**G**) The Tukey/scatter plot shows that the number of DCV exocytosis events per cell normalized to the DCV poolsize is similar between conditional Munc18-2 null and WT neurons. Mann Whitney-U test: n.s. = non-significant. $p > 0.05$.

Munc18-2 cKO did not affect DCV exocytosis upon stimulation (Fig. 2C-E). The total number of DCVs, revealed upon NH_4^+ perfusion, was unaltered (Fig. 2F) and NPY-pHluorin content per vesicle, expressed as the ΔF/F0 (change in fluorescence divided by baseline) of single fusion events was not changed (Fig. S2C). Consequently, the release fraction (number of DCV exocytosis events normalized to total DCV number) was not affected in *Munc18-2* cKO neurons (Fig. 2G). However, *Munc18-2* cKO slightly reduced (during the first 5 seconds of stimulation) and delayed (time between stimulus start and 40% of fusion vents) DCV exocytosis (Fig. S2D-G). Event duration (time between onset and termination of the NPY-pHluorin signal), was not affected by *Munc18-2* cKO (Fig. S2H-J). These data suggest that MUNC18-2 is largely dispensable for DCV exocytosis in mouse hippocampal neurons, perhaps due to its low expression levels.

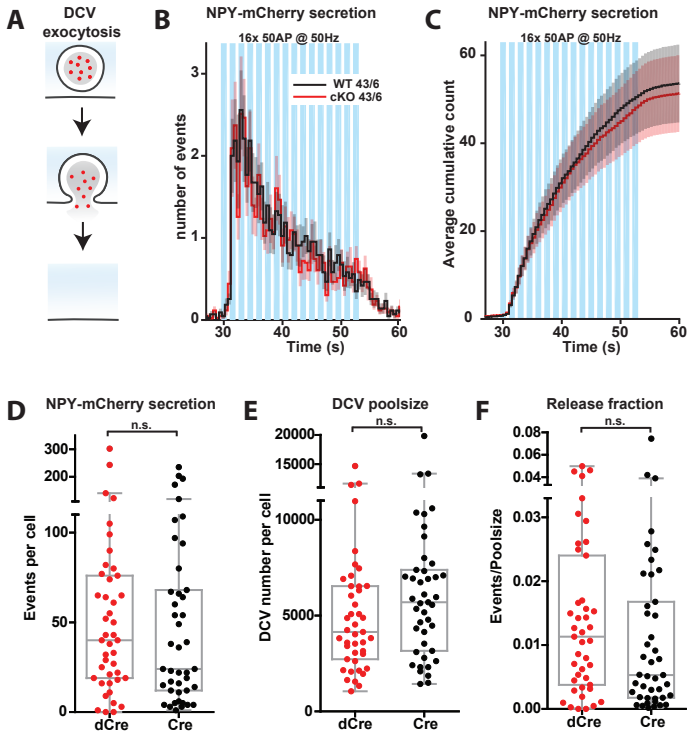

Figure 3. Conditional Munc18-2 inactivation does not affect NPY release. (**A**) Model example of NPY-mCherry exocytosis. (**B**) Histogram showing the average number of NPY-mCherry secretion events during high-frequency train-stimulation (16 x 50 APs at 50Hz) in Munc18-2 WT (black) and cKO (red) neurons. Error bars are SEM. Sample size is indicated per condition as n/N. (**C**) Cumulative representation of B. Error bars are SEM. (**D**) The Tukey/Scatter plot shows that the total number of NPY-mCherry labeled DCV exocytosis events is not affected by conditional Munc18-2 inactivation. Mann Whitney-U test: n.s. = non-significant. $p > 0.05$. (**E**) The Tukey/scatter plot shows that the DCV poolsize per cell (number of NPY-mCherry puncta) is similar in conditional Munc18-2 null and WT neurons. Mann Whitney-U test: n.s. = non-significant. $p > 0.05$. (**F**) The Tukey/scatter plot shows that the number of DCV exocytosis events per cell normalized to the DCV poolsize is similar between conditional Munc18-2 null and WT neurons. Mann Whitney-U test: n.s. = non-significant. $p > 0.05$.

As NPY-pHluorin only marks DCV fusion pore opening, effects on cargo release may remain undetected. Therefore, *Munc18-2* cKO and WT neurons were infected with the DCV exocytosis marker NPY-mCherry. This marker is not quenched at a low pH and reports full cargo release as sudden disappearances of the mCherry signal (Fig. 3A; Chapter 2; van de Bospoort et al., 2012; Emperador-Melero et al., 2018; Farina et al., 2015; Hoogstraaten et al., 2020; Persoon et al., 2018, 2019; De Wit et al., 2009). *Munc18-2* cKO did not disrupt NPY-mCherry secretion from DCVs (Fig. 3B-D). The total number of NPY-mCherry puncta per neuron was not affected by *Munc18-2* inactivation (Fig. 3E) and consequently, the release fraction was also unaffected (Fig. 3F). Hence, MUNC18-2 is not required for neuropeptide secretion.

Co-infection with both NPY-mCherry and NPY-pHluorin enabled quantifying the co-occurrence and delay between fusion pore opening and full cargo release in *Munc18-2* cKO and WT neurons (Fig. S3A). If Munc18-2 has any role in opening or maintaining DCV fusion pores, this should be reflected in these data. In 20% of NPY-pHluorin detected DCV exocytosis events, NPY-mCherry signal disappeared, which was unaffected by *Munc18-2*

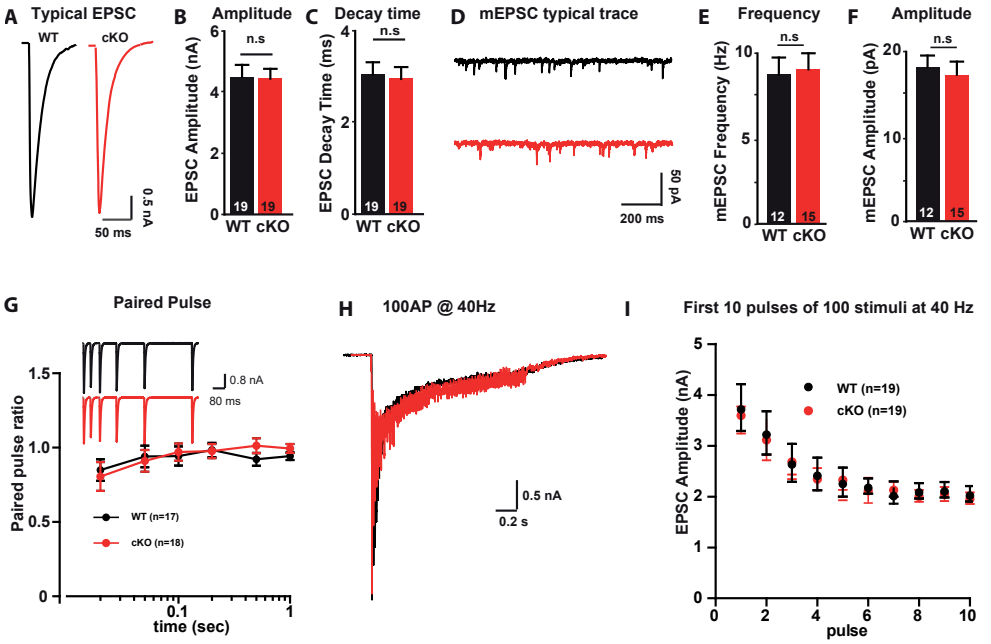

Figure 4. Munc18-2 cKO does not affect synaptic transmission. (**A, B, C**) sample traces (**A**), quantification of evoked EPSCs (**B**), and decay time of EPSCs (**C**) in control or Munc18-2 null neurons. (**D-F**) sample traces of miniature EPSC (**D**), and quantification of frequency (**E**) and amplitudes (**F**) in control or Munc18-2 null neurons. (**G**) Sample trace and quantification of paired pulse ratio (PPR). (**H**) Sample trace of EPSC size depression during repetitive stimulation (100 pulses) at 40Hz in control or Munc18-2 null neurons. (**I**) Quantification of first 10 EPSCs during 100 stimuli at 40Hz in control or Munc18-2 null neurons. All data in this figure are means ± SEMs, p value are determined by un-paired T test.

cKO (Fig. S3B). Coincidence of NPY-mCherry disappearance with the termination NPY-pHluorin dequenching events (i.e. chance that a DCV proceeds from fusion pore opening to full cargo release) was also unaltered (Fig. S3C). In addition, the delay between start of NPY-pHluorin signal and NPY-mCherry disappearance was similar between *Munc18-2* cKO and WT neurons (Fig. S3D). Therefore, MUNC18-2 is not required for DCV fusion pore opening or full cargo release.

Munc18-2 is dispensable for synaptic transmission

Munc18-1 null neurons are synaptically silent (Verhage et al., 2000), and MUNC18-2 overexpression in these neurons does not restore normal synaptic transmission (He et al., 2017; Santos et al., 2017). However, a slightly higher evoked response (EPSC amplitude) was observed in MUNC18-2 rescued neurons compared to *Munc18-1 null* neurons rescued with MUNC18-3. Whole cell patch-clamp recordings in conditional *Munc18-2* cKO neurons showed unaltered evoked EPSCs (excitatory postsynaptic currents) (Fig. 4A-C), miniature EPSC frequency or amplitude compared to control (Fig. 4D-F). In addition, paired pulse ratio and EPSC depression during repetitive stimulation were not affected (Fig. 4G-I). We conclude that MUNC18-2 is dispensable for synaptic transmission.

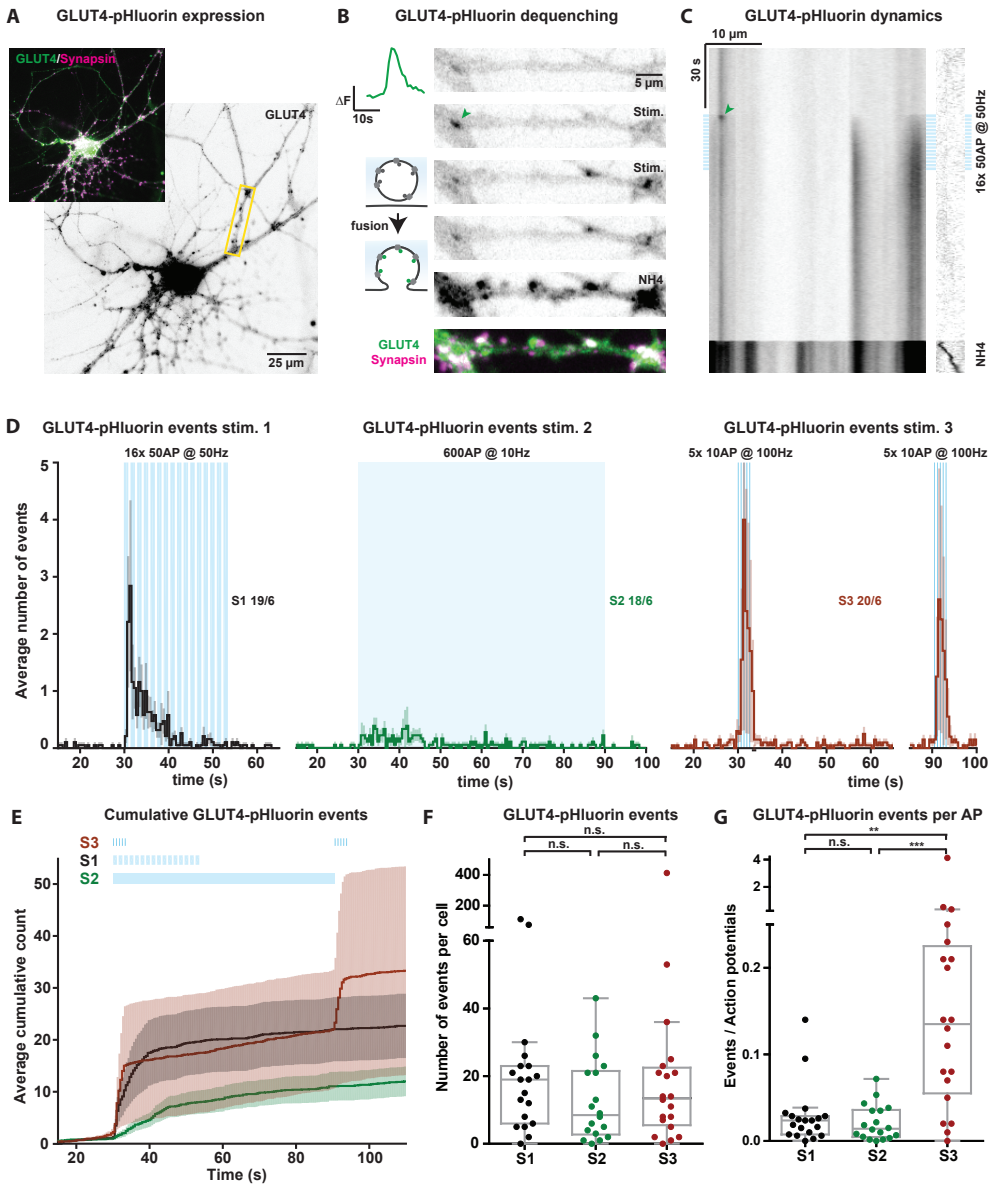

Figure 5: GLUT4-pHluorin marks exocytosis both during basal and stimulation conditions. (**A**) A still frame from fluorescent live imaging shows synapsin-mCherry (magenta) and GLUT4-pHluorin (green) and an enlargement (grayscale) of the latter. GLUT4-pHluorin is visualized using NH4+ perfusion, which dequenches pHluorin in acidic compartments. The neurite stretch indicated by yellow is further analyzed in B and C. (**B**) Left top shows a typical trace of a GLUT4-pHluorin exocytosis event and left below a model showing a GLUT4-pHluorin labeled vesicle quenched at the low pH inside the vesicle, and de-quenched during a exocytosis event or NH4+ application as vesicular pH rises. Right: the still frames show a neurite stretch before, during and after stimulation, and during NH4+ perfusion. The green arrow indicates de event of the typical trace. Below GLUT4-pHluorin during NH4+ perfusion (green) is shown together with synapsin-mCherry (magenta), showing colocalization. (**C**) The kymograph shows the neurite stretch of B over time, visualizing GLUT4-pHluorin de-quenching during stimulation, as well as de-quenching caused by NH4+ (depicted by green-shading at the bottom). The green arrowhead indicates the same exocytosis event as in B. High-frequency train-stimulation is indicated with blue bars. (**D**) The histogram shows the average number of GLUT4-pHluorin dequenching events during each stimulation, which were given to different neurons on the same

coverslip. The blue bars indicate the stimulation paradigms. The sample size is indicated for each condition as N/n. Error bars are SEM. (**E**) Cumulative representation of the data in D. Error bars are SEM. (**F**) The Tukey/scatter plot shows that the total number of GLUT4-pHluorin events per cell is similar between stimulation paradigms. Kruskal-Wallis with Dunn's correction: n.s. = non-significant, $p > 0.05$. (**G**) The Tukey/scatter plot shows that the number of evoked GLUT4-pHluorin dequenching events per action potential is higher for stimulation 3 than stimulations 1 or 2. Kruskal-Wallis with Dunn's correction: n.s. = non-significant, $p > 0.05$, ** = $p < 0.01$, *** = $p < 0.001$.

GLUT4-pHluorin shows exocytosis both during basal and stimulation conditions

To further explore the role of MUNC18-2 in the brain, we tested the insertion GLUT4 into the synaptic plasma membrane (Ashrafi et al., 2017), using GLUT4-pHluorin. Infection of WT neurons grown on glia micro-islands with lentiviral GLUT4-pHluorin resulted in presence of the recombinant protein in acidic compartments that unquenched upon NH_4^+ perfusion (Fig. 5A). GLUT4-pHluorin dequenching events were also observed during electrical stimulation, as abrupt increases in fluorescence confined to small areas (Fig. 5B,C). In addition, gradual persistent increases were observed during stimulation and sometimes moving GLUT4-pHluorin puncta were observed (Fig. 5C). Three stimulation paradigms were tested: high-frequency train-stimulation (Stimulation 1), 600AP at 10Hz stimulation as described in Ashrafi *et. al.,* (2017) (Stimulation 2), and a short burst-stimulation including two episodes of train-stimulation with 5 bursts of 10APs at 100Hz (repeated after 60 seconds; Stimulation 3) based on natural firing patterns in the hippocampus (Klausberger et al., 2004). All stimulations triggered GLUT4-pHluorin dequenching, albeit with a high variability between neurons (Fig. 5D-F). Additionally, many events occurred during basal conditions (Fig. 5D). As the stimulation paradigms included different numbers of action potentials (APs), for each neuron, the number of GLUT4-pHluorin events was divided by the number of APs. Stimulation 3 triggered more GLUT4 dequenching events per AP than the other stimulation paradigms (Fig. 5G). These findings show that GLUT4 exocytosis occurs both during basal and stimulation conditions, and that different stimulation patterns trigger exocytosis of GLUT4 containing vesicles with a different efficiency.

Munc18-2 is not required for GLUT4 exocytosis

To test if MUNC18-2 is required for activity-induced GLUT4 exocytosis, *Munc18-2* cKO and WT neurons were infected with GLUT4-pHluorin and imaged at DIV14-18. To trigger GLUT4 vesicle exocytosis, two high-frequency train-stimulations were applied (each 8 trains of 50AP at 50Hz with 30s interval between the blocks), similar to previous DCV exocytosis experiments (Chapter 2, Figs 3 & 4). *Munc18-2* inactivation did not hamper stimulated or basal GLUT4-pHluorin labeled GLUT4 vesicle exocytosis (Fig. 6A-C). The second train-stimulation triggered less GLUT4 exocytosis events than the first, similar in WT and KO (Fig. 6A,B). In addition, estimation of the total GLUT4-pHluorin vesicle pool showed no difference between *Munc18-2* cKO and WT neurons (Fig. 6D) and consequently the number of GLUT4-pHluorin events normalized to the poolsize was also unaltered (Fig. 6E). These data indicate that MUNC18-2 is not required for GLUT4 exocytosis.

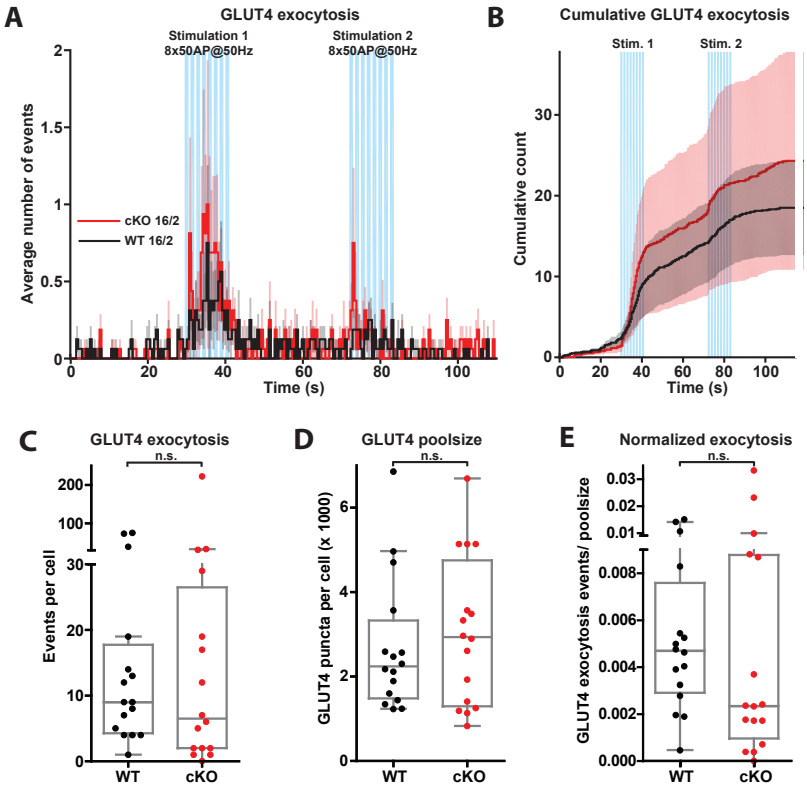

Figure 6. Munc18-2 cKO does not affect GLUT4 vesicle exocytosis. (**A**) Histogram showing the average number of GLUT4-pHluorin marked exocytosis events during two episodes of high-frequency train-stimulation (2 episodes of 8 bursts of 50 APs at 50Hz) in conditional Munc18-2 WT (black) and cKO (red) neurons. Error bars are SEM. Sample size is indicated per condition as n/N. (**B**) Cumulative representation of A. Error bars are SEM. (**C**) The Tukey/Scatter plot shows that the total number of GLUT4-pHluorin labeled exocytosis events is not affected by conditional Munc18-2 inactivation. Mann Whitney-U test: n.s. = non-significant. $p > 0.05$ (**D**) The Tukey/scatter plot shows that the GLUT4 vesicle poolsize per cell (number of GLUT4-pHluorin puncta revealed during NH4 perfusion) is similar in conditional Munc18-2 null and WT neurons. Mann Whitney-U test: n.s. = non-significant. $p > 0.05$. (**E**) The Tukey/scatter plot shows that the number of GLUT4-pHluorin events per cell normalized to the poolsize is similar between conditional Munc18-2 null and WT neurons. Mann Whitney-U test: n.s. = non-significant. $p > 0.05$.

Discussion

The aim of this chapter was to assess the role of the exocytic SM-proteins MUNC18-2 and MUNC18-3 in neuronal secretion pathways. While Munc18-3 expression is below the detection limit in most mouse cortical and hippocampal cells, Munc18-2 is more generally expressed. Therefore, we tested the role of MUNC18-2 in mouse hippocampal neurons. Most aspects of DCV exocytosis were not affected upon *Munc18-2* cKO, including kinetics, opening of the fusion pore and full cargo release from the vesicle. However, DCV exocytosis was slightly delayed in *Munc18-2* cKO neurons. Whole cell patch clamp recordings revealed that *Munc18-2* cKO did not affect synaptic transmission. Next, we used GLUT4-pHluorin to test GLUT4 insertion into the plasma membrane, which occurred both during basal and stimulated conditions. However, *Munc18-2* cKO did not

disrupt GLUT4 vesicle exocytosis. These data indicate that Munc18-2 is not involved in these 3 secretory routes.

Expression of SM-proteins in the mouse brain

Munc18-1 is expressed 3- to 4-fold higher than other SM-genes in nearly all cortical and hippocampal mouse neurons (Fig. 1; Yao et al., 2020). This is well in line with its essential function in neuronal secretion (Chapter 2; Verhage et al., 2000). In addition, Munc18-2 mRNA was also robustly expressed in many mouse cortical and hippocampal neuron types, reaching levels of a similar order of magnitude as mRNA from SM-genes VPS33a/b and VPS45 (Fig. 1; Yao et al., 2020). Conversely, Munc18-3 transcripts were absent in most of these neurons. This suggests a potential function of MUNC18-2 in neuronal secretion. However, other studies using RT-PCR or Western-blot show varying results on Munc18-2 or -3 expression in rodent brains (Tellam et al., 1995; Martin-Verdeaux et al., 2002; Imai et al., 2004; Mandic et al., 2011; Kim et al., 2012; Lam et al., 2013; Zhu et al., 2015). Many of these studies do not detect Munc18-2 in the brain, and we also did not detect MUNC18-2 on Western-blot (Fig. S1). These findings suggest that MUNC18-2 protein levels in the brain are low. This discrepancy between RNA levels and protein levels may be explained by the low sensitivity of Western-Blot compared to single-cell RNA sequencing, but it could also be that protein levels of MUNC18-2 are actually much lower than RNA levels, as RNA and protein levels not always correlate (Gry et al., 2009).

GLUT4 exocytosis occurs during basal conditions and is triggered by electrical stimulation

GLUT4-pHluorin was present as a (partly mobile) punctate pattern throughout the neurons, often but not always colocalizing with presynapse marker synapsin (Fig. 5). A similar pattern was reported before for endogenous and overexpressed GLUT4 (Ashrafi et al., 2017), suggesting correct targeting of GLUT4-pHluorin. Both during basal conditions and several electrical stimulation paradigms, we detected GLUT4-pHluorin exocytosis events, suggesting that GLUT4 secretion is both constitutive and regulated. This is different from DCV exocytosis, which generally have much less spontaneous events, but multiple factors more stimulus-evoked events (Fig. 1; Chapter 2)(De Wit et al., 2009; Arora et al., 2017; Van Keimpema et al., 2017; Dominguez et al., 2018; Persoon et al., 2018, 2019; Hoogstraaten et al., 2020; Puntman et al., 2021) .

A short high-frequency stimulation (2 episodes of 5 bursts with 10AP at 100Hz each) was per AP most effective in triggering GLUT4 exocytosis, while 600 APs at 10Hz or 16 bursts of 50 APs at 50Hz triggered relatively fewer events (Fig. 5). For each stimulation, multiple APs occurred before GLUT4 exocytosis was triggered. Similarly, DCV exocytosis cannot be triggered by a single AP and requires high-frequency burst-firing (Persoon et al., 2018). Conversely, SVs already fuse upon a single AP (Watanabe et al., 2013), suggesting that neurotransmitter secretion is more sensitive than neuropeptide or GLUT4 secretion to electrical stimulation. Short high-frequency firing naturally occurs in some hippocampal neurons (Kandel and Spencer, 1961; Buzsáki et al., 1996; Klausberger et al., 2004). Therefore, GLUT4 insertion into the presynaptic membrane may be adapted to best respond to these natural firing patterns. In addition, this type of stimulation also triggers cyclic AMP signaling, (Nguyen and Kandel, 1997), which stimulates DCV and SV exocytosis in *C. elegans* (Steuer Costa et al., 2017). Together, these findings suggest that GLUT4 may be constitutive and regulated secreted, and that

exocytosis is most efficiently triggered by high-frequency burst firing which naturally occurs in the hippocampus.

MUNC18-2 may be involved in a different neuronal secretion pathway

Conditional bi-allelic inactivation of *Munc18-2* in mouse hippocampal neurons does not affect neuropeptide secretion, synaptic transmission or GLUT4 insertion into the presynaptic plasma membrane (Fig. 2-4, 6). Conversely, DCV exocytosis was slightly delayed in *Munc18-2* cKO neurons, but fusion pore formation, full cargo release and kinetics were all unaltered (Fig. 2,3,S2,S3). These data suggest that MUNC18-2 is not involved in synaptic transmission, DCV exocytosis or GLUT4 translocation. Alternatively, a dominant role for MUNC18-1 is more likely. MUNC18-1 has high expression levels in the CNS and *Munc18-1* knock-out in mice completely silences synaptic transmission and additionally causes neuronal degeneration (Verhage et al., 2000; Bouwman et al., 2004; Heeroma et al., 2004; Santos et al., 2017; Yao et al., 2020). Over-expression of paralogs MUNC18-2 or -3 in *Munc18-1 null* neurons rescues neuronal viability, while not supporting normal evoked EPSCs (He et al., 2017; Santos et al., 2017). However, the inability of MUNC18-2 to support normal EPSCs in *Munc18-1 null* neurons was not due to defective tethering/docking or priming, but rather because MUNC18-2 was unable to prevent NSF-dependent de-priming (He et al., 2017). These findings suggest that MUNC18-2 could still have a role in docking or priming of SVs or other vesicles. However, the lack of a DCV, SV or GLUT4 exocytosis phenotype in *Munc18-2 cKO* neurons in our current data (Fig. 1-4, 6) suggests that endogenous expression of MUNC18-1 is probably sufficient to fulfill these roles.

A potential role for MUNC18-2 in neurons was suggested before by the finding that bi-allelic mutations in STXBP2 (Syntaxin binding protein 2, human gene encoding MUNC18-2), that cause FHL4 including immune deficiency, blood coagulation defects and enteropathy, were also associated with neurological defects in a few patients (Meeths et al., 2010; Deiva et al., 2012; Hackmann et al., 2013). However, whether these symptoms arose via a direct effect on neurons, or via indirect effects via glial cells, CSF or blood vessels, remains unclear. It is striking that despite robust mRNA expression of Munc18-2 in many mouse CNS neurons, no function for MUNC18-2 in neuronal secretion has been found. Two scenarios for a possible role of MUNC18-2 in the brain are here explored.

Firstly, MUNC18-2 function in neurons may be limited to a few subtypes, which precludes detection of an effect on secretion by gene inactivation in primary cultures from the whole hippocampus. Typically, these neuron cultures contain several different neuron types (Williams et al., 2011). Furthermore, Munc18-2 mRNA was only found in a subset of hippocampal neurons (Fig. 1; Yao et al., 2020). However, MUNC18-2 over-expression in *Munc18-1 null* neurons partially or fully restored docking, priming and recovery after 40Hz stimulation (He et al., 2017; Santos et al., 2017). This may suggest a more general function in all neurons, but could still be limited by neuron-type differences in MUNC18-2 expression.

A second explanation may be more reasonable: Perhaps MUNC18-2 is required for a different secretion pathway than neuropeptides, neurotransmitters or GLUT4. Other neuronal regulated secretion pathways include AMPA, NMDA and $GABA_A$ receptor exocytosis and lysosomal secretion. Some evidence on AMPAR/NMDAR-membrane insertion suggests a role of MUNC18-1 herein (Duan et al., 2020), but direct evidence is lacking. AMPAR and NMDAR trafficking is essential for normal synaptic transmission

and plasticity (For reviews see: Rao and Finkbeiner, 2007; Choquet, 2018; Groc and Choquet, 2020). Therefore, the complete lack of an electrophysiological phenotype in *Munc18-2* cKO neurons (Fig. 4) suggests that MUNC18-2 is not required for basal AMPAR or NMDAR vesicle exocytosis. The underlying mechanisms for lysosomal exocytosis are also uncharacterized, making this a second candidate for a possible function of Munc18-2. Lysosomal secretion supports synaptic plasticity by secretion of ECM (extracellular matrix) modulating enzymes and synaptic organizer cbln1 (Padamsey et al., 2017; Ibata et al., 2019). A potential role for MUNC18-2 in the exocytosis of lysosomes is plausible, given the robust RNA expression levels of Munc18-2 in many neurons and the variety of parallel functioning exocytosis pathways.

Methods

Animals

Animal housing and breeding was in line with institutional and Dutch governmental guidelines and all procedures were approved by the ethical committee of the VU University/ VU Medical Center (license number: DEC-FGA 11-03 and AVD112002017824). Munc18-1$^{lox/lox}$ mice (Heeroma *et al.*, 2004) were generated as described before. To obtain Munc18-2 conditional knock-out (cKO) primary cultures, Munc18-2$^{lox/lox}$ mice (a kind gift of Michael J. Tuvim, published as: Jaramillo et al., 2019) were time-mated and P1 pups were used for dissection of the hippocampi. For WT primary cultures, Munc18-1 HZ mice (Verhage et al., 2000; Toonen et al., 2006) were time-mated and E18 pups were collected via caesarean section, after which they were used for dissection of the hippocampi. All pups were genotyped prior to culturing.

Neuron culture

Preparation of dissociated hippocampal neuron cultures was performed as reported before (De Wit, Toonen and Verhage, 2009; Farina *et al.*, 2015). In brief, isolated hippocampi were digested with 0.25% trypsin (Life Technologies) for 20 min at 37°C in Hanks' balanced salt solution (Sigma) with 10mM HEPES (Life Technologies). After 3x washing and trituration, 1,000-2,000 neurons were plated per well onto pre-grown glia micro-islands. These were generated by stamping agarose coated 18mm glass coverslips with a solution of 0.5mg/ml poly-D-lysine (Sigma), 3.5 mg/ml rat tail collagen (BD Biosciences) and 17mM acetic acid onto which 6.000 rat glia were plated (Mennerick *et al.*, 1995; Wierda *et al.*, 2007).

Viruses

All constructs were generated with sequence verification, cloned into a pLenti vector containing a Synapsin promotor. For Western-blot, classical Munc18-1 KO neurons were rescued at DIV0 with a GFP-Munc18-2 lentivirus to ensure neuronal survival and expression of a GFP-MUNC18-2 fusion protein that runs higher on Western-Blot than WT MUNC18-2. Additionally, HEK cells infected with Munc18-1, Munc18-2 or Munc18-3 lentiviruses were used as positive control.

To obtain conditional Munc18-2 *null* and WT neurons, Cre recombinase and defective Cre (deltaCre) (Kaeser *et al.*, 2011; Persoon *et al.*, 2019) were delivered into Munc18-2$^{lox/lox}$ neurons via lenti-virus particles at DIV0. Lentiviral NPY-pHluorin and NPY-mCherry were used as markers for DCV exocytosis as reported before (van de Bospoort *et al.*, 2012; Persoon *et al.*, 2018). GLUT4-pHluorin as a marker for GLUT4 vesicle exocytosis was also delivered via lentiviral particles, 6 days prior to imaging at DIV14-18.

Western-Blot

Neurons were infected at DIV0 and grown until DIV14-18. Lysates were collected by cell-scraping or tituration of tissue in PBS on ice. Samples were centrifuged (5 min. at 12000 rpm) and homogenized in Laemmli sample buffer containing 2% SDS (VWR chemicals, M107), 10% glycerol (Merck, 818709), 0.26M β-mercaptoethanol (Sigma, M3148), 60mMTris-HCl (Serva, 37180) pH 6.8, and 0.01% Bromophenol blue (Applichem, A3640). Samples were separated on 8% SDS-polyacrylamide gels using standard SDS-PAGE technique. Proteins were transferred overnight at 150mA and 4°C via wet-blot transfer. Blocking was done with 2% BSA (Acros Organics, 268131000) in PBS with 0.1% Tween20 for 4h at RT. Primary antibodies included monoclonal mouse alpha-Tubulin (1:10000; SySy), monoclonal mouse Actin (1:10000; Chemicon), polyclonal rabbit MUNC18-2 (1:1000; kind gift from Ulrich Blank; published as Martin-Verdeaux et al., 2003). The other MUNC18-2 antibody was newly generated (1:500; SySy 116 102) by immunizing 2 rabbits (8750 and 8751) against same peptides (500-510: SDPAPVPSSQA and 432-458: QSYSSLIRNLEQLGGTVTNSAGSGTSS). Additionally, these bleeds were purified using a peptide consisting of amino acids 500-510 of the MUNC18-2 mouse protein. After washing with PBS-0.1%Tween20, the blots were incubated with secondary antibodies (Goat anti-mouse or anti-rabbit alkaline phosphatase-conjugated secondary antibodies (1:10000; Jackson) in 2% BSA-PBS-0.1%Tween20 for 45min. at 4°C. After washing, blots were incubated with Atto-Phos substrate for 5 min, and scanned on a Fujifilm FLA-5000 Reader.

Live imaging

All live imaging experiments were performed between DIV 14 and 18 at room temperature (RT; 21-26°C). We used a custom-built set-up including an inverted microscope (IX81; Olympus) with an MT20 light source (Olympus), the appropriate filter sets (Semrock, Rochester, NY), a 40x oil objective (NA 1.3), an EM charge-coupled device camera (EMCCD; C9100-02; Hamamatsu Photonics, Japan) and Xcellence RT imaging software (Olympus). Electrical stimulation was delivered by parallel platinum electrodes placed around the glia-island, conducting 30 mA, 1 ms pulses controlled by a Master 8 system (AMPI, Germany) and a stimulus generator (A385RC, World Precision Instruments, Germany). 16 or 8 trains of 50 AP were generated at 50 Hz, or 5 trains of 10 AP at 100HZ, with 0.5s interval after 30 seconds of baseline recording. The 600 AP at 10Hz were generated in a similar way. Imaging acquisition rate was 2Hz. Coverslips were perfused with Tyrode's solution (2 mM CaCl2, 2.5 mM KCl, 119 mM NaCl, 2 mM MgCl2, 30 mM glucose and 25 mM HEPES, pH 7.4). pHluorin-based DCV exocytosis assays ended with a 10-seconds NH_4^+ perfusion (Tyrode's with 50mM NH_4Cl, replacing 50mM NaCl), delivered via a gravity flow system with a capillary placed above the neuron, to de-quench pHluorin in all DCVs.

Electrophysiology

Whole-cell recordings were performed using an Axopatch 200B amplifier (Molecular Devices) at room temperature. Digidata 1440 and Clampex 10.0 (Molecular Devices) were used for data acquisition. The external solution contained (in mM): 140 NaCl, 2.4 KCl, 4 $MgCl_2$, 4 $CaCl_2$, 10 HEPES, and 10 glucoses (pH 7.30, 300 mOsmol). Patch-pipette solution contained (in mM): 125 K^+–gluconic acid, 10 NaCl, 4.6 $MgCl_2$, 15 creatine phosphate, 10 U/ml phosphocreatine kinase, and 1 EGTA (pH 7.30). Only cells with an access resistance of <10 MΩ and leak current of <300 pA were accepted for analysis. The series-resistance for recording was compensated to 60%. All analyses were performed using Clampfit 10.2, MiniAnalysis (Synaptosoft) and custom software routines in Matlab R2017a. In action potential induced EPSCs the stimulation artifact was removed and interpolated using cubic interpolation

Analysis

Analysis of SM-gene mRNA levels in cortical and hippocampal mouse neurons was done via assessment of the Transcriptomics Explorer of the Allen brain atlas (available on: https://celltypes.brain-map.org/rnaseq/mouse_ctx-hip_smart-seq), which was based on a single-cell RNA sequencing data set (Methods provided via: Yao et al., 2020).

Analysis of DCV and GLUT4 exocytosis was done in ImageJ (NIH). 2x2 Pixel regions were placed on NPY-mCherry DCV exocytosis events and 3x3 pixel regions were placed on NPY- or BDNF-pHluorin, or GLUT4-pHluorin events. The ROI intensity measures were loaded into a custom written MATLAB (Mathworks) script for semi-automatic analysis, where each was plotted as change in fluorescence (DF) compared to baseline fluorescence (F0, average fluorescence during the first 10 frames). An exocytosis event was detected when DF was at least 2 standard deviations below or above F0 for respectively NPY-mCherry and NPY/BDNF-pHluorin labeled DCVs. For GLUT4-pHluorin events a lower DF of at least 1 SD was used as cut-off. Somatic events were excluded because of high background signal. Histograms and cumulative plots were generated in MATLAB. Further analysis including statistical tests and generation of Tukey/scatter plots was conducted in GraphPad Prism.

The onset delay in DCV exocytosis was calculated for each neuron by subtracting the time point of the start of the simulation from the time point where 50% of the events have occurred. In neurons that were stimulated twice, only the events within each stimulation block were taken along. The duration of NPY-pHluorin dequenching events was calculated by taking for each event the onset of the event (the time point when DF was at least 2 standard deviations above F0) and subtracting this from the termination of the event (the time point when DF returned to baseline). This disappearance of NPY-pHluorin signal (termination) could reflect 2 physiological events: (i) NPY-pHluorin is released into the extracellular space, or (ii) NPY-pHluorin remains in the DCV, but the fusion pore has closed and the DCV reacidifies, requenching NPY-pHluorin.

To calculate the neurite length and total number of DCVs (poolsize) per neuron, the highest-intensity frame during NH_4 perfusion was taken for pHluorin based assays and further analyzed using the MATLAB program SynD (Schmitz *et al.*, 2011; van de Bospoort *et al.*, 2012). Parameters were optimized for detection of DCVs and the number of detected DCVs was adjusted for intensity by dividing by the mode intensity.

For comparing NPY-pHluorin and NPY-mCherry marked exocytosis from the same vesicle, neurons infected with both markers were analyzed as above, with placing regions on NPY-pHluorin marked events. The ROIs were measured not only for NPY-pHluorin but also NPY-mCherry signal and further analyzed as above. Fusion pore opening is marked by a fluorescent increase due to NPY-pHluorin dequenching, while full cargo release is indicated by disappearance of both the NPY-pHluorin and NPY-mCherry signal. Events that lacked one of the two markers were not taken along. After semi-automatic analysis including carefully marking the onset and termination of DCV exocytosis events, for each ROI these time points were compared between NPY-pHluorin and NPY-mCherry. Many ROIs contained both an NPY-pHluorin as an NPY-mCherry event (Fig. S3B), but in only a subset of events the disappearance of both NPY-pHluorin and NPY-mCherry coincided (Fig. S3C), indicating that these fluorescent proteins marked the same vesicle. For measurements on the delay between fusion pore opening and full cargo release (Fig. S3D), only the latter events were taken along.

Statistics

Statistical analysis was performed in GraphPad Prism. Shapiro-Wilk normality test was used to test for normal distributions and Levene's to test for homogeneity of variances. For normally distributed data sets with two experimental groups Student's t-tests were performed, for not normally distributed data with two groups, Mann Whitney-U tests were done. The data with more than 2 groups was not normally distributed, so a Kruskal-Wallis test was done, followed by a Dunn's multiple comparisons post hoc test.

Acknowledgements

The authors thank Robbert Zalm for cloning and producing viral particles, Lisa Laan and Desiree Schut for producing glia island cultures and providing primary culture assistance, Joke Wortel for organizing the animal breeding, Joost Hoetjes for genotyping, Jurjen Broeke for technical support, Ingrid Saarloos for Western blots and members of the CNCR DCV team for discussions and helpful input. This work is supported by an ERC Advanced Grant (322966) of the European Union (to MV).

Author contributions

D.C.P., S.A., R.F.T. and M.V. designed the experiments. D.C.P. performed all -mCherry- or pHluorin-based live imaging assays and analyzed these data. E.H. performed the electrophysiology experiment and designed figure 4. M.J.T. provided the *Munc18-2*$^{lox/lox}$ mice. D.C.P., R.F.T and M.V. designed figures and wrote the manuscript with input from all authors.

References

Arora S, Saarloos I, Kooistra R, van de Bospoort R, Verhage M, Toonen RF (2017) SNAP-25 gene family members differentially support secretory vesicle fusion. J Cell Sci 130:1877–1889 DOI: 10.1242/jcs.201889.

Ashrafi G, Wu Z, Farrell RJ, Ryan TA (2017) GLUT4 Mobilization Supports Energetic Demands of Active Synapses. Neuron 93:606-615.e3 DOI: 10.1016/J.NEURON.2016.12.020.

Bouwman J, Maia AS, Camoletto PG, Posthuma G, Roubos EW, Oorschot VMJ, Klumperman J, Verhage M (2004) Quantification of synapse formation and maintenance in vivo in the absence of synaptic release. Neuroscience 126:115–126.

Burkhardt P, Stegmann CM, Cooper B, Kloepper TH, Imig C, Varoqueaux F, Wahl MC, Fasshauer D (2011) Primordial neurosecretory apparatus identified in the choanoflagellate Monosiga brevicollis. Proc Natl Acad Sci U S A 108:15264–15269.

Buzsáki G, Penttonen M, Nádasdy Z, Bragin A (1996) Pattern and inhibition-dependent invasion of pyramidal cell dendrites by fast spikes in the hippocampus in vivo. Proc Natl Acad Sci U S A 93:9921–9925.

Choquet D (2018) Linking nanoscale dynamics of AMPA receptor organization to plasticity of excitatory synapses and learning. J Neurosci 38:9318–9329.

De Wit J, Toonen RF, Verhage M (2009) Matrix-Dependent Local Retention of Secretory Vesicle Cargo in Cortical Neurons. J Neurosci 29:23–37.

Deiva K, Mahlaoui N, Beaudonnet F, De Saint Basile G, Caridade G, Moshous D, Mikaeloff Y, Blanche S, Fischer A, Tardieu M (2012) CNS involvement at the onset of primary hemophagocytic lymphohistiocytosis. Neurology 78:1150–1156.

Derkach VA, Oh MC, Guire ES, Soderling TR (2007) Regulatory mechanisms of AMPA receptors in synaptic plasticity. Nat Rev Neurosci 8:101–113.

Dominguez N, van Weering JRT, Borges R, Toonen RFG, Verhage M (2018) Dense-core vesicle biogenesis and exocytosis in neurons lacking chromogranins A and B. J Neurochem 144:241–254.

Duan XL, Guo Z, He YT, Li YX, Liu YN, Bai HH, Li HL, Hu XD, Suo ZW (2020) SNAP25/syntaxin4/VAMP2/Munc18-1 Complexes in Spinal Dorsal Horn Contributed to Inflammatory Pain. Neuroscience 429:203–212 DOI: /10.1016/j.neuroscience.2020.01.003.

Emperador-Melero J, Huson V, van Weering J, Bollmann C, Fischer von Mollard G, Toonen RF, Verhage M (2018) Vti1a/b regulate synaptic vesicle and dense core vesicle secretion via protein sorting at the Golgi. Nat Commun 9 DOI: 10.1038/s41467-018-05699-z.

Farina M et al. (2015) CAPS-1 promotes fusion competence of stationary dense-core vesicles in presynaptic terminals of mammalian neurons. Elife 4:393–422 DOI: 10.7554/eLife.05438.

Groc L, Choquet D (2020) Linking glutamate receptor movements and synapse function. Science (80-) 368.

Gry M, Rimini R, Strömberg S, Asplund A, Pontén F, Uhlén M, Nilsson P (2009) Correlations between RNA and protein expression profiles in 23 human cell lines. BMC Genomics 10:1–14.

Gutierrez BA, Chavez MA, Rodarte AI, Ramos MA, Dominguez A, Petrova Y, Davalos AJ, Costa RM, Elizondo R, Tuvim MJ, Dickey BF, Burns AR, Heidelberger R, Adachi R (2018) Munc18-2, but not Munc18-1 or Munc18-3, controls compound and single-vesicle–regulated exocytosis in mast cells. J Biol Chem 293:7148–7159.

Hackmann Y, Graham SC, Ehl S, Höning S, Lehmberg K, Aricó M, Owen DJ, Griffiths GM (2013) Syntaxin binding mechanism and disease-causing mutations in Munc18-2. Proc Natl Acad Sci U S A 110:E4482-91.

He E, Wierda K, Van Westen R, Broeke JH, Toonen RF, Cornelisse LN, Verhage M (2017) Munc13-1 and Munc18-1 together prevent NSF-dependent de-priming of synaptic vesicles. Nat Commun 8 DOI: 10.1038/ncomms15915.

Heeroma JH, Roelandse M, Wierda K, Van Aerde KI, Toonen RFG, Hensbroek RA, Brussaard A, Matus A, Verhage M (2004) Trophic support delays but not prevent cell-intrinsic degeneration of neurons deficient for munc18-1. Eur J Neurosci 20:623–634.

Hoogstraaten RI, Keimpema L Van, Toonen RF, Verhage M (2020) Tetanus insensitive VAMP2 differentially restores synaptic and dense core vesicle fusion in tetanus neurotoxin treated neurons. Sci Rep:1–14.

Ibata K, Kono M, Narumi S, Motohashi J, Kakegawa W, Kohda K, Yuzaki M (2019) Activity-Dependent Secretion of Synaptic Organizer Cbln1 from Lysosomes in Granule Cell Axons. Neuron:1–15 DOI: 10.1016/j.neuron.2019.03.044.

Imai A, Nashida T, Shimomura H (2004) Roles of Munc18-3 in amylase release from rat parotid acinar cells. Arch Biochem Biophys 422:175–182.

Jaramillo AM, Piccotti L, Velasco W V., Delgado ASH, Azzegagh Z, Chung F, Nazeer U, Farooq J, Brenner J, Parker-Thornburg J, Scott BL, Evans CM, Adachi R, Burns AR, Kreda SM, Tuvim MJ, Dickey BF (2019) Different Munc18 proteins mediate baseline and stimulated airway mucin secretion. JCI Insight 4.

Kandel ER, Spencer WA (1961) Electrophysiology of Hippocampal Neurons II. After-Potentials and Repetitive Firing. Potentials 23:243–259.

Kim K, Petrova YM, Scott BL, Nigam R, Agrawal A, Evans CM, Azzegagh Z, Gomez A, Rodarte EM, Olkkonen VM, Bagirzadeh R, Piccotti L, Ren B, Yoon J, McNew JA, Adachi R, Tuvim MJ, Dickey BF (2012) Munc18b is an essential gene in mice whose expression is limiting for secretion by airway epithelial and mast cells. Biochem J 446:383–394.

Klausberger T, Márton LF, Baude A, David J, Roberts B, Magill PJ, Somogyi P (2004) Spike timing of dendrite-targeting bistratified cells during hippocampal network oscillations in vivo. Nat Neurosci 7 DOI: 10.1038/nn1159.

Lam PPL, Ohno M, Dolai S, He Y, Qin T, Liang T, Zhu D, Kang Y, Liu Y, Kauppi M, Xie L, Wan WCY, Bin NR, Sugita S, Olkkonen VM, Takahashi N, Kasai H, Gaisano HY (2013) Munc18b is a major mediator of insulin exocytosis in rat pancreatic b-Cells. Diabetes 62:2416–2428.

Mandic SA, Skelin M, Johansson JU, Rupnik MS, Berggren P-O, Bark C (2011) Munc18-1 and Munc18-2 proteins modulate beta-cell Ca2+ sensitivity and kinetics of insulin exocytosis differently. J Biol Chem 286:28026–28040.

Martin-Verdeaux S, Pombo I, Iannascoli B, Roa M, Varin-Blank N, Rivera J, Blank U (2002) Evidence of a role for Munc18-2 and microtubules in mast cell granule exocytosis. J Cell Sci 116:325–334.

Martin-Verdeaux S, Pombo I, Iannascoli B, Roa M, Varin-Blank N, Rivera J, Blank U (2003) Evidence of a role for Munc18-2 and microtubules in mast cell granule exocytosis. J Cell Sci 116:325–334.

Meeths M, Entesarian M, Al-Herz W, Chiang SCC, Wood SM, Al-Ateeqi W, Almazan F, Boelens JJ, Hasle H, Ifversen M, Lund B, Merlijn Van Den Berg J, Gustafsson B, Hjelmqvist H, Nordenskjö M, Bryceson YT, Henter J-I (2010) Spectrum of clinical presentations in familial hemophagocytic lymphohistiocytosis type 5 patients with mutations in STXBP2. Blood 116:2635–2643.

Moro A, Woerden GMV, Toonen RF, Verhage M (2020) Camkii controls neuromodulation via neuropeptide gene expression and axonal targeting of neuropeptide vesicles. PLoS Biol 18:1–30 DOI: 10.1371/journal.pbio.3000826.

Nguyen P V., Kandel ER (1997) Brief Θ-burst stimulation induces a transcription-dependent late phase of LTP requiring cAMP in area CA1 of the mouse hippocampus. Learn Mem 4:230–243.

Oh E, Kalwat MA, Kim MJ, Verhage M, Thurmond DC (2012) Munc18-1 regulates first-phase insulin release by promoting granule docking to multiple syntaxin isoforms. J Biol Chem 287:25821–25833.

Oh E, Spurlin BA, Pessin JE, Thurmond DC (2005) Munc18c heterozygous knockout mice display increased susceptibility for severe glucose intolerance. Diabetes 54:638–647.

Oh E, Thurmond DC (2009) Munc18c depletion selectively impairs the sustained phase of insulin release. Diabetes 58:1165–1174.

Padamsey Z, McGuinness L, Bardo SJ, Reinhart M, Tong R, Hedegaard A, Hart ML, Emptage NJ (2017) Activity-Dependent Exocytosis of Lysosomes Regulates the Structural Plasticity of Dendritic Spines. Neuron 93:132–146 DOI: 10.1016/j.neuron.2016.11.013.

Persoon CM, Hoogstraaten RI, Nassal JP, van Weering JRT, Kaeser PS, Toonen RF, Verhage M (2019) The RAB3-RIM Pathway Is Essential for the Release of Neuromodulators. Neuron 104:1065-1080.e12 DOI: 10.1016/j.neuron.2019.09.015.

Persoon CM, Moro A, Nassal JP, Farina M, Broeke JH, Arora S, Dominguez N, Weering JR, Toonen RF, Verhage M (2018) Pool size estimations for dense-core vesicles in mammalian CNS neurons. EMBO J 37:e99672 DOI: 10.15252/embj.201899672.

Puntman DC, Arora S, Farina M, Toonen RF, Verhage M (2021) Munc18-1 is essential for neuropeptide secretion in neurons . J Neurosci 41:JN-RM-3150-20.

Rao VR, Finkbeiner S (2007) NMDA and AMPA receptors: old channels, new tricks. Trends Neurosci 30:284–291.

Santos TC, Wierda K, Broeke JH, Toonen RF, Verhage M (2017) Early Golgi Abnormalities and Neurodegeneration upon Loss of Presynaptic Proteins Munc18-1, Syntaxin-1, or SNAP-25. J Neurosci 37:4525–4539.

Steuer Costa W, Yu S chieh, Liewald JF, Gottschalk A (2017) Fast cAMP Modulation of Neurotransmission via Neuropeptide Signals and Vesicle Loading. Curr Biol 27:495–507.

Tellam JT, McIntosh S, James DE (1995) Molecular identification of two novel Munc-18 isoforms expressed in non-neuronal tissues. J Biol Chem 270:5857–5863.

Toonen RFG, Verhage M (2003) Vesicle trafficking: Pleasure and pain from SM genes. Trends Cell Biol 13:177–186.

Toonen RFG, Wierda K, Sons MS, de Wit H, Cornelisse LN, Brussaard A, Plomp JJ, Verhage M (2006) Munc18-1 expression levels control synapse recovery by regulating readily releasable pool size. Proc Natl Acad Sci 103:18332–18337.

van de Bospoort R, Farina M, Schmitz SK, de Jong A, de Wit H, Verhage M, Toonen RF (2012) Munc13 controls the location and efficiency of dense-core vesicle release in neurons. J Cell Biol 199:883–891.

Van Keimpema L, Kooistra R, Toonen RF, Verhage M (2017) CAPS-1 requires its C2, PH, MHD1 and DCV domains for dense core vesicle exocytosis in mammalian CNS neurons. Sci Rep 7.

Verhage M, Maia AS, Plomp JJ, Brussaard AB, Heeroma JH, Vermeer H, Toonen RF, Hammer RE, van den Berg TK, Missler M, Geuze HJ, Südhof TC (2000) Synaptic Assembly of the Brain in the Absence of Neurotransmitter Secretion. Science (80-) 287:864–869 DOI: 10.1126/science.287.5454.864.

Watanabe S, Rost BR, Camacho-Pérez M, Davis MW, Söhl-Kielczynski B, Rosenmund C, Jorgensen EM (2013) Ultrafast endocytosis at mouse hippocampal synapses. Nature 504:242–247 DOI: 10.1038/nature12809.

Williams ME, Wilke SA, Daggett A, Davis E, Otto S, Ravi D, Ripley B, Bushong EA, Ellisman MH, Klein G, Ghosh A (2011) Cadherin-9 regulates synapse-specific differentiation in the developing hippocampus. Neuron 71:640–655 DOI: 10.1016/j.neuron.2011.06.019.

Yao Z et al. (2020) A taxonomy of transcriptomic cell types across the isocortex and hippocampal formation Zizhen. bioRxiv.

Zhu D, Xie L, Karimian N, Liang T, Kang Y, Huang Y-C, Gaisano HY (2015) Munc18c mediates exocytosis of pre-docked and newcomer insulin granules underlying biphasic glucose stimulated insulin secretion in human pancreatic beta-cells. Mol Metab 4:418–426.

Supplementary information

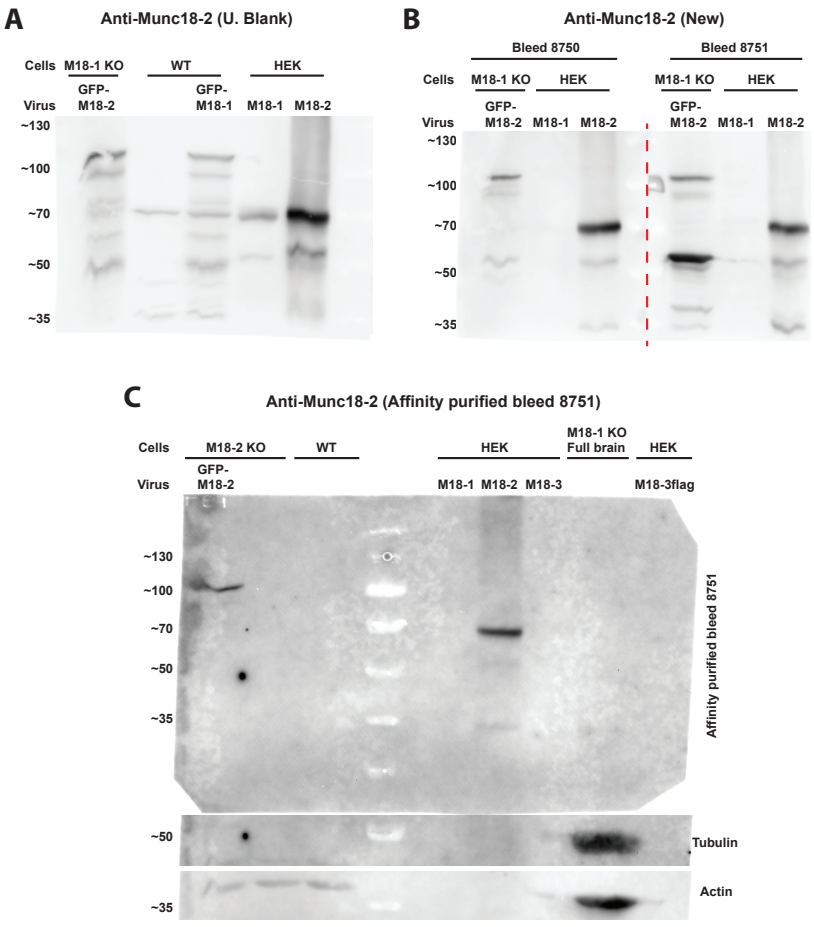

Figure S1. A newly generated antibody for MUNC18-2 is specific but does not detect MUNC18-2 in mouse WT neurons. (**A**) A MUNC18-2 antibody kindly provided by U. Blank recognizes MUNC18-2, but also MUNC18-1. Lysates are from left to right: Cultured Munc18-1 null neurons infected with GFP-Munc18-2 (lane 1); Cultured WT neurons that were uninfected (lane 2) or infected with GFP-Munc18-1 (lane 3), HEK cells infected with Munc18-1 (lane 4) or Munc18-2 (lane 5). (**B**) Two newly generated polyclonal rabbit antibodies (bleeds from 2 separate rabbits) against Munc18-2 shows specific recognition of Munc18-2, but not Munc18-1. Lysates are: Cultured Munc18-1 null neurons infected with GFP-Munc18-2 (lane 1 & 5); HEK cells infected with Munc18-1 (lane 2 & 6) or Munc18-2 (lane 3 & 7); marker (lane 4). The blot was cut at the dotted line prior to antibody incubation. (**C**) An affinity purified bleed of rabbit 8751 shows specific recognition of MUNC18-2, but not MUNC18-1 or -3. In addition it does not detect MUNC18-2 in WT or Munc18-1 null neurons. Lysates are: Cultured conditional Munc18-2 null neurons infected with GFP-Munc18-2 (lane 1) or uninfected (lane 2); Cultured WT neurons (lane 3); marker (lane 4); HEK cells infected with Munc18-1 (lane 5), Munc18-2 (lane 6) or Munc18-3 (lane 7); Brain lysate of E18 Munc18-1 null mouse (lane 8); HEK cells infected with Munc18-2-FLAG. Below, the same blot was incubated with Tubulin, or actin antibodies to indicate differences in loading.

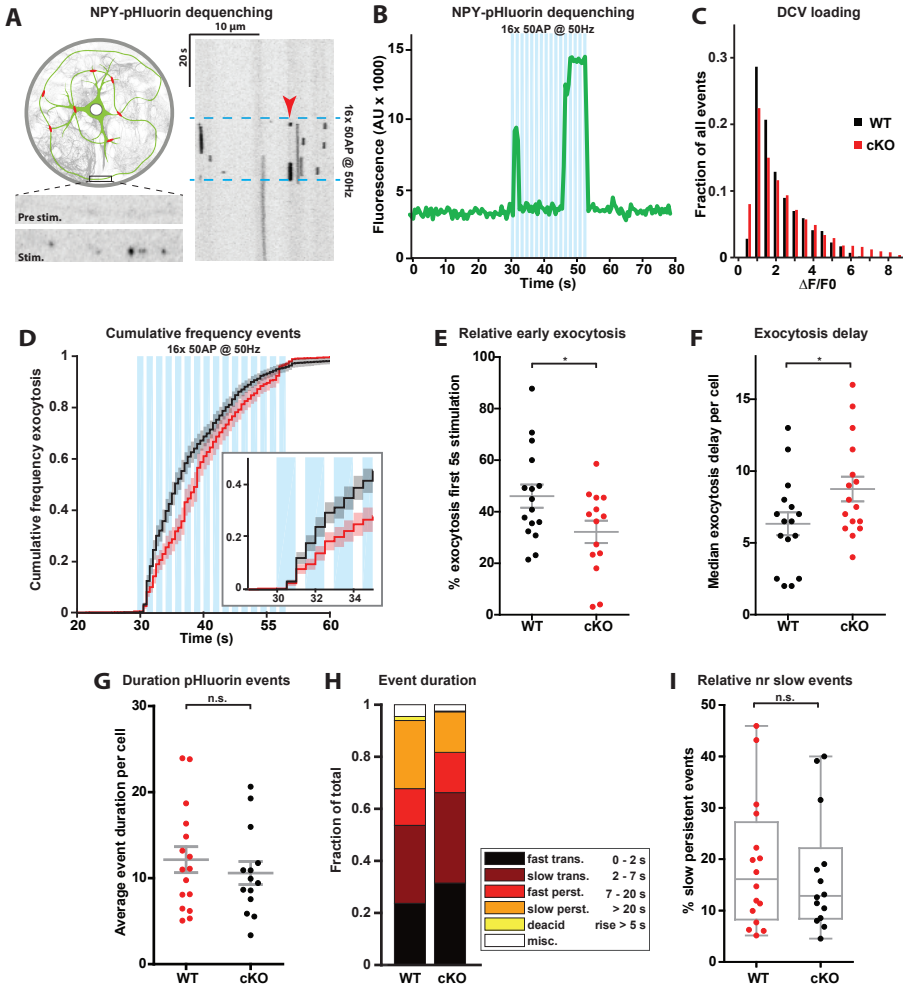

Figure S2. Conditional Munc18-2 inactivation affects some properties of DCV exocytosis. (**A**) A single neuron (green) with synapses (red) on a glia micro-island is represented in the schematic figure. Below, still frames of an axonal stretch before and during high-frequency train-stimulation (16 x 50AP at 50Hz, between dashed blue lines) reveals NPY-pHluorin dequenching events as puncta. On the right, the same axonal stretch is visualized through time in a kymograph, where DCV exocytosis events are visible as dequenching events. The event indicated by the red arrowhead is analyzed in B. (**B**) The event of A is here analyzed and the fluorescence is plotted through time. The blue bars indicate the high-frequency train-stimulation. (**C**) DCV loading in *Munc18-2 WT* (black) and *cKO* (red) is here visualized in a frequency distribution: The x-axis shows the change in fluorescence of the DCV exocytosis events divided by baseline fluorescence and distributed in bins, the y-axis represents the relative frequency. (**D**) Cumulative frequency of DCV exocytosis in conditional *Munc18-2 WT* (black) and *null* (red) neurons. Insert is zoom-in on the first 5 seconds of stimulation. Error bars are SEM. (**E**) The scatter plot shows that the relative number of DCV exocytosis events during the first 5 seconds of stimulation compared with the total number of events per cell is decreased in conditional *Munc18-2 null* neurons. Error bars indicate means and SEM. Student's t-test: * = $p < 0.05$. (**F**) The scatter plot shows that the median delay of DCV exocytosis events is larger in conditional *Munc18-2 null* neurons, indicating that the moment when 50% of the events have occurred is later in these cells. Error bars indicate means and SEM. Student's t-test: * = $p < 0.05$. (**G**) The scatter plot shows that the average duration of DCV exocytosis events is similar between conditional *Munc18-2 WT* and *null* neurons. Error bars indicate means and SEM. Student's t-test: * = $p < 0.05$. (**H**) The distribution shows the relative fraction of each group of event durations which are depicted on the right. (**I**) The Tukey/scatter plot shows that the percentage of slow persistent events (orange group in H) is similar between *Munc18-2 WT* and *cKO* neurons. Mann Whitney-U test: n.s. = non-significant. $p > 0.05$.

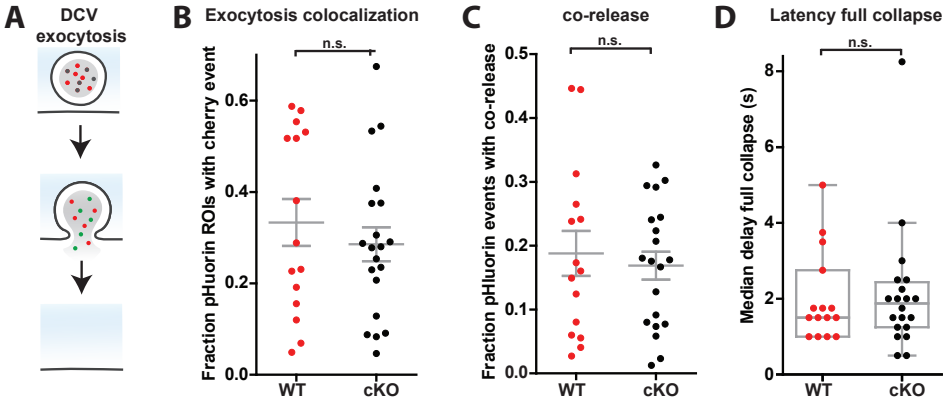

Figure S3. *Munc18-2 cKO* does not affect DCV full cargo release or fusion pore stability. (**A**) Model example of DCV exocytosis labeled with both NPY-mCherry and NPY-pHluorin. (**B**) The scatter plot shows that the fraction of NPY-pHluorin labeled DCV exocytosis events that also have an NPY-mCherry release event in the same region of interest (ROI) is similar for conditional *Munc18-2 WT* and *null* neurons. Stimulation paradigm was the same as in Figure 2 and 3. Error bars indicate means and SEM. Student's t-test: n.s. = $p > 0.05$. (**C**) The scatter plot shows that the fraction of NPY-pHluorin events in which the termination of the pHluorin signal coincided with disappearance of the NPY-mCherry signal is similar for *Munc18-2 WT* and *cKO* neurons. Error bars indicate means and SEM. Student's t-test: n.s. = $p > 0.05$. (**D**) The Tukey/scatter plot shows that the median delay between appearance of the NPY-pHluorin signal and disappearance of the NPY-mCherry signal is similar in *Munc18-2 WT* and *cKO* neurons. Mann Whitney-U test: n.s. = $p > 0.05$.

Chapter 5

Visualizing DCV biogenesis

Daniël C. Puntman, Jolijn ten Bos, Ruud F. Toonen, Matthijs Verhage

Abstract

The biogenesis of dense-core vesicles (DCVs) is an essential aspect of neuropeptide secretion, but is poorly understood. We used primary mouse hippocampal neurons to test methods for tracking newly generated DCVs over time. Here we show that the fluorescent SNAPtag binding compound SNAP-SiR specifically labeled DCVs in NPY-SNAPtag expressing neurons. However, labeling was sparse and immunostaining for NPY revealed immunolabeled NPY-SNAPtag puncta throughout the neurons that were not labeled with SNAP-SiR. SNAP-SiR also labeled the Golgi, but did not accumulate there. As an alternative approach, we tested doxycycline induced expression of NPY-pHluorin. The first labeled DCVs were detected after 6 hours and much higher numbers from 18 hours onwards. However, we observed large variation in the number of NPY-pHluorin puncta between neurons. This number of puncta correlated only partly with the viral load. Therefore, we conclude that DCV production depends on cell-intrinsic properties and may be affected by neuronal activity. Furthermore, these findings suggest that genetically induced DCV cargo expression is a promising technique to study DCV biogenesis and maturation in the future, while SNAP-SiR labeling of neuronal DCVs is not sensitive enough.

Introduction

Major improvements on the understanding of DCV exocytosis mechanisms have revealed much of its molecular machinery. However, upstream processes such as DCV biogenesis and maturation are relatively unexplored territory. The current principles of DCV biogenesis and maturation mainly come from non-neuronal secretory cells. During biogenesis, secretory cargo is synthesized at the endoplasmic reticulum (ER), travels through the Golgi and is sorted into distinct vesicles at the trans-Golgi network (TGN) (for reviews see: Kim et al., 2006; Dikeakos and Reudelhuber, 2007; Zanetti et al., 2012; Brandizzi and Barlowe, 2013). After budding from the TGN, DCVs are considered immature and undergo a maturation process, which includes increasing luminal acidity and calcium concentration, improving core crystallization and cargo processing (For reviews on DCV pH, biogenesis and maturation see: Wu et al., 2001; Kim et al., 2006; Bonnemaison et al., 2013). In addition, DCVs may increase in size via homotypic fusion, which was shown by *in vitro* experiments (Urbé et al., 1998; Wendler et al., 2001; Ahras et al., 2006; Du et al., 2016). Another suggested maturation process is referred to as sorting by retention, by which unwanted cargo is removed by clathrin/Arf1/GGA- and possibly VAMP4-dependent fission and sorted back towards the Golgi or different organelles (Barr and Huttner, 1996; Chen and Shields, 1996; Dittié et al., 1996; Austin et al., 2000; Puertollano et al., 2001; Hinners et al., 2003; Kakhlon et al., 2006; Asensio et al., 2010; Sirkis et al., 2013).

Genetic interference with processes upstream of DCV exocytosis, including DCV biogenesis, maturation or trafficking often impacts neuropeptide secretion. Deletion of Vti1a/b in mice disrupts secretory cargo sorting at the Golgi, which severely impairs DCV biogenesis, and consequently neuropeptide secretion (Emperador-Melero et al., 2018). In *Rab2* mutant *C. elegans* neurons, DCV cargos are missorted to the endolysosomal

pathway (Edwards et al., 2009), suggesting that RAB2 mediates retention of DCV cargo during DCV maturation. Furthermore, *Rab2 null* mutation in *Drosophila* reduces bidirectional axonal transport of DCVs, endosomes and lysosomes, thereby also limiting neuropeptide secretion (Lund et al., 2020). In mouse hippocampal neurons, loss of CaMKII resulted in decreased DCV biogenesis, which in turn reduced neuropeptide secretion (Moro et al., 2020). This was due to CaMKII acting in a feedback loop where neuropeptide secretion is coupled to expression of DCV cargo and axonal targeting of DCVs (Moro et al., 2020). These studies point out the requirement for several genes to maintain the DCV population and support neuropeptide secretion, but so far only little insight is gained in the underlying mechanisms.

Many basic questions on DCV biogenesis, maturation and lifetime remain unanswered. For example, it is unclear at what speed DCV biogenesis occurs and how many DCVs are generated per unit of time. One study showed that production of DCVs may be dynamically regulated, as neuronal silencing via the sodium-channel blocker tetrodoxin (TTX) caused synaptic accumulation of DCVs (Tao et al., 2018). In addition, it is unknown whether newly generated DCVs are immediately ready for exocytosis, or whether they require time to mature and become fusogenic. In PC12 cells, young secretory granules are preferentially exocytosed (Tsuboi et al., 2010) and insulin secretion in β-cells more often comes from newcomer granules than stably docked vesicles (Gaisano, 2014). This suggests that secretory granules (SGs) in these cells quickly become fusion competent, but gradually lose fusion competence over time. In neurons, DCV exocytosis efficiency is only 6% or less, even during intense high-frequency stimulation (van Keimpema et al., 2017; Dominguez et al., 2018; Emperador-Melero et al., 2018; Persoon et al., 2018; Moro et al., 2020; Puntman et al., 2021; Westen et al., 2021), suggesting that many DCVs may not fuse for a long time after their biogenesis. Whether these DCVs may remain fusogenic for a long while, or are recycled in time is unknown.

A few techniques have the potential to monitor a population of newly generated vesicles over time via a pulse-chase principle. One technique includes genetically controlled expression of fluorescent cargo proteins, which is limited to a temporal resolution of multiple hours due to the delay between genetic induction and cargo delivery. Another approach is expression of fluorescent timer proteins as DCV cargo, which was used to show that young DCVs underwent more often exocytosis than older DCVs in PC12 cells (Tsuboi et al., 2010). However, slow, stochastic color switching limits the temporal resolution. Finally, a promising technique is SNAP-Cell, which was used in beta-cells to block and stain insulin granules by incubation with membrane permeable blockers or fluorophores that covalently bind to SNAP-tags (Ivanova et al., 2013). The authors labeled distinct vesicle populations through time, which were physically separated. In addition, this technique allowed for following insulin granules up to the moment of their degradation (Hoboth et al., 2015).

The aim of this chapter is to test methodology to study DCV biogenesis and lifetime. We used mouse hippocampal neurons grown on glia micro-islands to test two strategies: live-labeling techniques using SNAP-Cell methodology and temporally controlled expression of fluorescent DCV cargos. We show that SNAP-SiR labeled the Golgi, but not was not trapped there and that SNAP-SiR specifically labeled DCVs, albeit with low efficiency. Parallel testing of genetically controlled DCV cargo expression showed that termination of the expression was hampered due to leakiness of the tamoxifen inducible Cre construct. Doxycycline-induced expression of NPY-pHluorin showed the first labeled DCVs detected after 6 hours and much higher numbers from 18 hours onwards. A typical neuron produced roughly 55 DCVs per hour during the highest

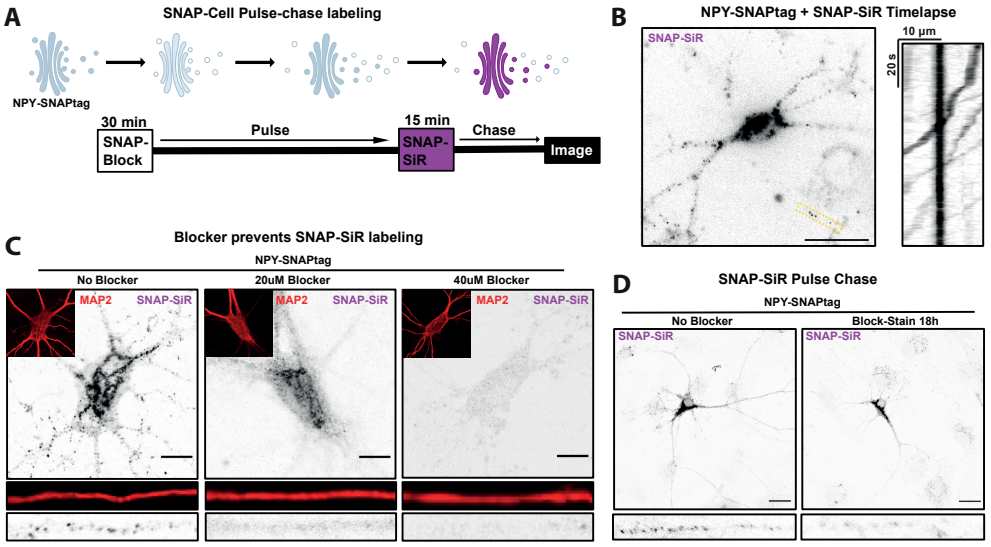

Figure 1. SNAP-Cell Pulse-chase labeling. (**A**) Model of SNAP-Cell live pulse-chase labeling visualizing the Golgi and vesicles. On the left, before blocking (30m of SNAP-Block), NPY-SNAPtag is stably expressed and present in the Golgi and vesicles. After blocking, NPY-SNAPtag is unavailable for staining, but new NPY-SNAPtag expression slowly fills-up the Golgi and DCVs. After staining (15m of SNAP-SiR), all NPY-SNAPtag fusion proteins that were generated after blocking will be stained with SNAP-SiR (magenta). The duration of the pulse is defined by the time between blocking and staining, while the duration of the chase depends on the time between staining and imaging or fixation. (**B**) Left, still frame of a timelapse from a primary mouse hippocampal neuron cultured on a glia micro-island, that was infected with NPY-SNAPtag and live-stained with SNAP-SiR (without blocker). Scale bar is 25µm. Right, kymograph of the axonal stretch selected by yellow in the still frame shows mobile SNAP-SiR puncta. Distance is visualized in x and time in y. (**C**) Primary neurons were infected with NPY-SNAPtag and after adding 0µM (left), 20µM (middle) or 40µM (right) SNAP-Block, live-stained with SNAP-SiR and fixated. Immunostaining for MAP2 marks dendrites and neurons were analyzed via Confocal imaging. Blocking with 20µM prevented the punctate and partly Golgi staining seen when no blocker was added, 40µM prevented all staining. Scalebar is 10µm. (**D**) Primary neurons were labeled with SNAP-SiR either without blocking, or 18 hours after blocking. Typically, no clear punctate staining was visible by staining 18 hours after blocking. Scale bar is 10µm.

increase in DCVs. However, the number of newly generated DCVs varied substantially between neurons and could not be attributed to differences in viral load. Therefore, we propose that the DCV biogenesis rate depends on cell-intrinsic properties.

Results

SNAP-Cell allows sparse labelling of DCVs

In order to visualize populations of newly generated DCVs over time, we implemented the SNAP-Cell system (Ivanova et al., 2013). With this technique, pulse-chase labeling of newly generated SNAPtag-fusion proteins is achieved by first incubating with a blocking compound (SNAP-Block) and later at variable time intervals (pulse) with a fluorescent compound (SNAP-SiR), both of which bind covalently to the SNAPtag (Fig. 1A). In order to pulse-chase label DCVs, NPY-SNAPtag or BDNF-SNAPtag cDNA was delivered via lentiviral particles to mouse hippocampal neurons grown on glia micro-

island cultures and after 6 days coverslips were incubated in medium containing SNAP-Block, washed and followed by a waiting step (18h) in SNAP-SiR containing medium. SNAP-SiR labeling in non-blocked neurons resulted in dense staining in the cell soma and sparse staining of mobile puncta in the neurites (Figure 1B). In neurons that were blocked with a high concentration of SNAP-Block (40µM) directly prior to incubation with SNAP-SiR, no SNAP-SiR staining was observed (Fig. 1C). In neurons that were blocked with a lower concentration (20µM), neurite staining was also not observed, but somatic staining was still detected (Fig. 1C). Since the lower blocker concentration was sufficient in preventing punctate staining (DCVs), this was used for further experiments. To acquire high time resolution within a pulse-chase experiment, the time between blocking and staining (pulse) should optimally be as short as possible. However, even upon 18 hours between blocking and staining, little to no punctate pattern was visible (Fig. 1D). We conclude that SNAP-SiR labels overexpressed SNAPtags in neurons, which can be blocked using SNAP-Block, but recovery from blocking is slow or incomplete.

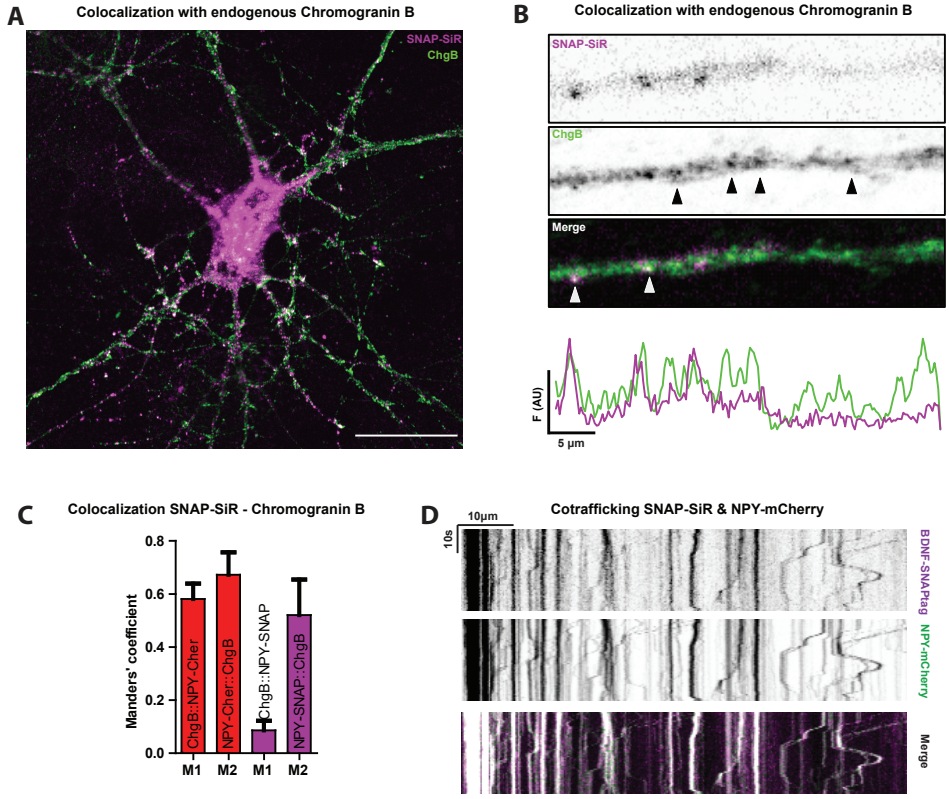

Figure 2. SNAP-Cell labels DCVs. (**A**) NPY-SNAPtag expressing neuron was live-stained with SNAP-SiR (magenta), fixed and immunostained for Chromogranin B (green). Scalebar is 25µm. (**B**) Zoom-in on a neurite shows that some SNAP-SiR puncta overlap with Chromogranin B puncta. (**C**) Neurons infected with NPY-SNAPtag and live-stained with SNAP-Sir (magenta; n = 6), or infected with NPY-mCherry , were fixed and immunostained for Chromogranin B. SNAP-SiR stained NPY-SNAPtag overlapped with Chromogranin B to the same extend as NPY-mCherry (red; n = 4), but vice versa Chromogranin B overlapped less with SNAP-SiR than with NPY-mCherry. (**D**) Kymograph from a time-lapse of a neuron infected with BDNF-SNAPtag and NPY-mCherry, and live-stained with SNAP-SiR, shows cotrafficking.

To find out if SNAP-SiR live-labeling of NPY-SNAPtag infected neurons labels DCVs, neurons were fixed and immunostained for Chromogranin B as an endogenous DCV marker as was reported before (Fig. 2A; Persoon et al., 2018). SNAP-SiR puncta colocalized with Chromogranin B, to the same extent as the canonical DCV marker NPY-mCherry, but vice versa Chromogranin B puncta did not colocalize with SNAP-SiR (Fig. 2A-C). In addition, neurons infected with BDNF-SNAPtag and DCV marker NPY-mCherry, and stained with SNAP-SiR showed often co-trafficking of SNAP-SiR puncta with NPY-mCherry (Fig. 2D). In conclusion, SNAP-SiR labeling in NPY-SNAPtag or BDNF-SNAPtag infected neurons specifically labels DCVs, albeit with a low efficiency, as many DCVs remain unlabeled.

SNAP-tag fusion proteins are depleted from the Golgi

To test if inefficient labeling of DCVs by SNAP-SiR in NPY-SNAPtag expressing neurons was due to limited NPY-SNAPtag expression in DCVs or due to reduced SNAP-SiR staining of the NPY-SNAPtag fusion proteins, neurons were fixed and immunostained for NPY. All neurons showed a bright punctate immunostaining for NPY (which is normally expressed in only 10% of the neurons), while SNAP-SiR staining was largely limited to the soma (Fig. 3A). Hence, SNAPtags are efficiently expressed and packaged in DCVs, but inefficiently labeled with SNAP-SiR.

Next, the time between SNAP-SiR staining and fixation was increased, to address whether SNAP-SiR labeled cargo left the Golgi network. Immunostaining with GM130 was used to label the Golgi. SNAP-SiR in neurons fixed directly after staining showed Golgi and punctate staining, while neurons fixed 24 hours after SNAP-SiR staining showed no Golgi fluorescence, but also no punctate staining outside the Golgi (Fig. 3B). To give an expression to the extend in which SNAP-SiR left the Golgi we divided SNAP-SiR neurite fluorescence by SNAP-SiR Golgi fluorescence, which showed SNAP-SiR Golgi exit in all neurons (Fig. 3C). These findings show that SNAP-SiR not efficiently labels all NPY-SNAPtags, even though SNAP-SiR does not accumulate in the Golgi.

Cellular variability of induced DCV cargo expression

In parallel to the SNAP-Cell system, a genetically controlled pulse-chase method was tested. To control both induction and termination of DCV cargo expression, first a combination of two constructs was tested: TRE-loxp-BDNF-mCherry-loxp and ERT-Cre. The BDNF-mCherry construct was designed so that its expression is induced by doxycycline, while the presence of Cre (whose expression is induced by tamoxifen) terminates BDNF expression by recombination via the loxp sites. In neurons that were not infected with Cre-ERT, BDNF-mCherry expression was induced by doxycycline and present in a punctate pattern (Fig. S1A,B). However, BDNF-mCherry did not express in Cre-ERT infected neurons, even when tamoxifen was not yet added to induce expression of Cre-ERT (Fig. S1C), suggesting that some Cre is expressed even without the presence of tamoxifen. Hence, BDNF-mCherry expression is induced by doxycycline, but prematurely terminated by Cre due to leakiness of the Cre construct.

To determine the DCV production rate, genetically induced expression of a cargo protein is sufficient and does not require termination. Therefore, a doxycycline inducible NPY-pHluorin construct was infected in mouse hippocampal neurons grown on glia micro-islands (Fig. 4A). To determine the relevant time range for the experiment, coverslips were fixed at 0, 6 or 18 hours after inducing NPY-pHluorin expression and whole coverslips were analyzed by confocal imaging for expression (Fig. 4B). After 6-18 hours,

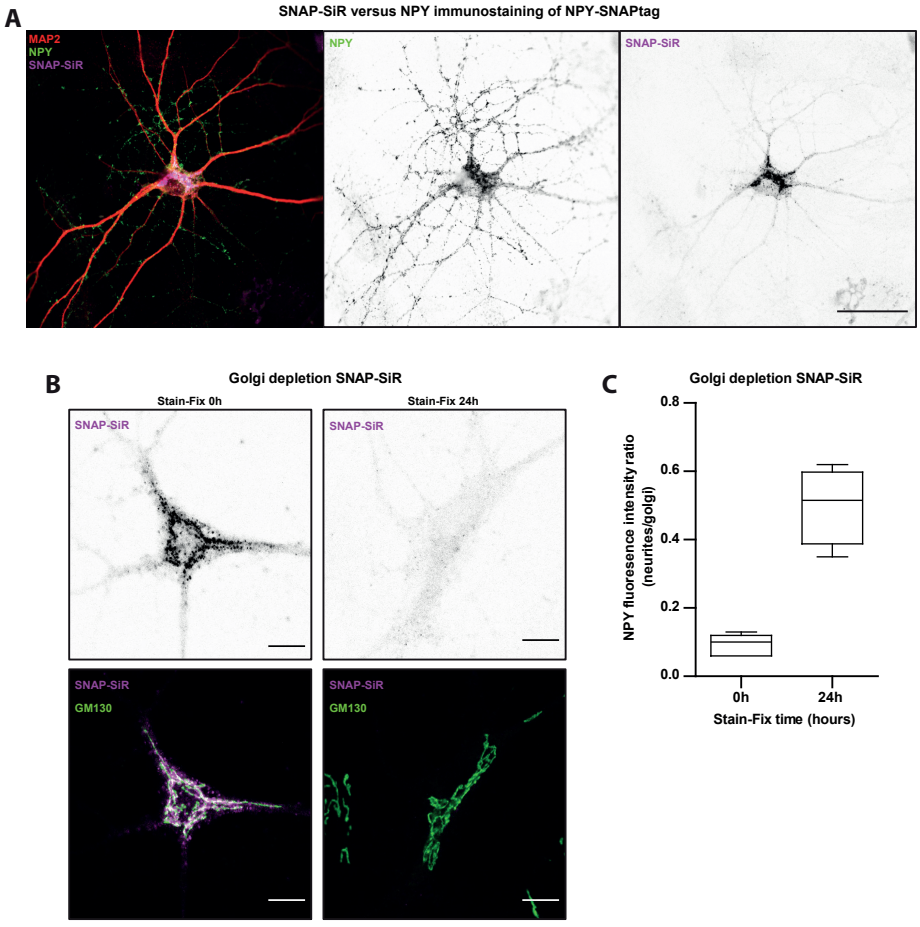

Figure 3. SNAP-SiR labels NPY-SNAPtag inefficient but does not accumulate at the Golgi. (**A**) Typical image: neurons infected with NPY-SNAPtag, live-stained with SNAP-SiR (magenta) and after fixation immunostained for NPY (green) and MAP2 (red) show a punctate NPY immunostaining, but often no clear SNAP-SiR punctate staining. Scale bar is 25µm. (**B**) Neurons infected with NPY-SNAPtag and live-stained with SNAP-SiR (magenta) that are directly fixed, and afterwards immunostained for GM130 (green) to mark the Golgi, show dense staining of SNAP-SiR in the golgi, but neurons that were fixed 24 hours after live-staining showed no SNAP-SiR staining in the Golgi. Scale bar is 10µm. (**C**) In the same neurons as in B, SNAP-SiR fluorescence in the neurites divided by fluorescence in the golgi was increased in neurons fixated 24 hours after live-labeling due to Golgi clearance.

more than 90% of the cells showed increased fluorescence, indicating they were infected (Fig. 4C). After 6 hours only a few (5%) neurons had neurite NPY-pHluorin expression and after 18 hours this increased to 36% (Fig. 4C). In conclusion, doxycycline-induced NPY-pHluorin expression in DCVs occurs only in a subset of the neurons within our timeframe.

Most DCVs are generated 6-18 hours after induction, with large variety between neurons

To monitor whether viral infection efficiency may explain the neuron to neuron variation in DCV cargo expression, we next used a TRE-Cre-mCherry-T2A-NPY-pHluorin

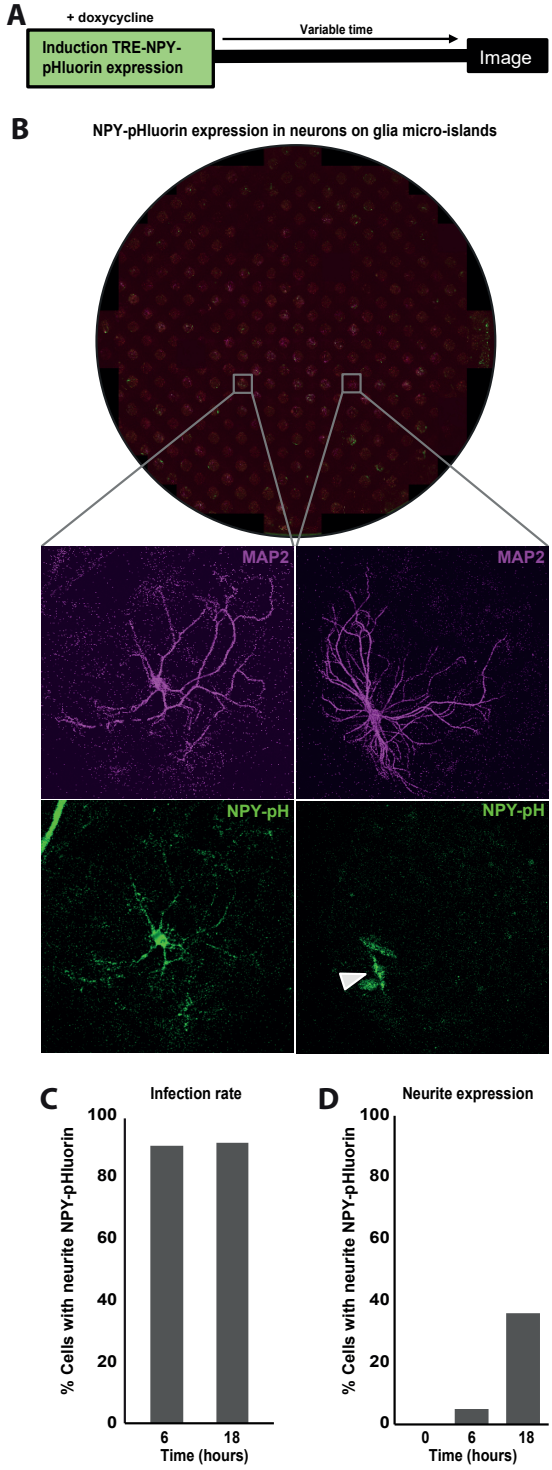

Figure 4. Induced DCV cargo expression is variably visible in neurites after 18 hours. (**A**) Neurons were infected with TRE-NPY-pHluorin lentiviral particles, of which the expression was induced by adding doxycycline. After a variable time, coverslips were fixated, immunostained and imaged by confocal. (**B**) Confocal image (fixed 18h after inducing NPY-pHluorin expression) of a whole coverslip containing glia micro-islands on which mouse hippocampal neurons were grown. Zooms show immunostaining for MAP2 (magenta) and NPY-pHluorin (green). (**C**) On each coverslip, most neurons fixed 6 or 18 hours after live-staining showed somatic NPY-pHluorin fluorescence, while only a subset showed NPY-pH fluorescence in the neurites (left). (**D**) On coverslips fixated 6 hours after live-staining, 5% of the neurons had NPY-pHluorin expression in the neurites, and on coverslips fixated 18 hours after live-labeling, 36% of the neurons showed neurite NPY-pHluorin expression.

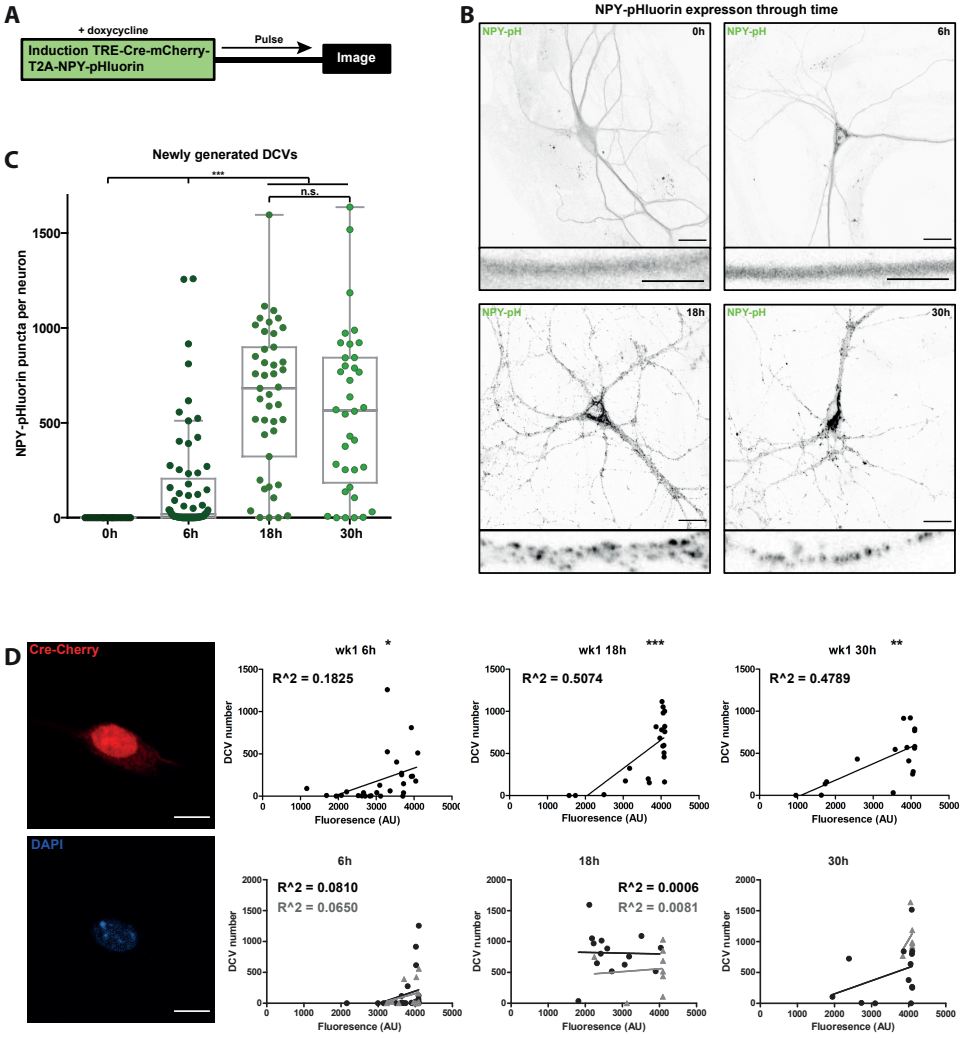

Figure 5. DCV production is variable from neuron to neuron. (**A**) Neurons were infected with TRE-Cre-mCherry-T2A-NPY-pHluorin lentiviral particles, of which the expression was induced by adding doxycycline. After a variable time, coverslips were fixated, immunostained and imaged by confocal. (**B**) NPY-pHluorin fluorescence 0h, 6h, 18h or 30h after doxycycline induction measured by confocal. Scale bar = 10µm. Inserts are zoomed in on dendrites, scale bar = 5µm. (**C**) Tukey/scatter plot showing the number of NPY-pHluorin puncta per neuron for each fixation time point. Median numbers of puncta are 0 (0h), 19 (6h), 682 (18h), 565 (30h). *** = $p < 0.001$, Kruskal-Wallis with Dunn's multiple comparisons test. (**D**) Infected neurons show Cre-Cherry fluorescence in the nucleus, which colocalizes with DAPI (left). Due to the T2A sequence, Cre-Cherry is expressed equally to NPY-pHluorin and is used as a measure for viral load. The graphs on the right show for each fixation time point, for three independent experiments, the number of NPY-pHluorin puncta (DCV number) on the y-axis and the Cre-Cherry fluorescence on the x-axis. In experiment 1 (top) a significant correlation was found for each time point. * = $p < 0.05$, ** = $p < 0.01$, *** = $p < 0.001$, Pearsons correlation coefficient. In experiment 2 and 3 (bottom) no significant correlations were found on each time point.

construct. Due to the T2A part, a self-cleaving peptide, this construct expresses Cre-mCherry and NPY-pHluorin, both of which are induced by doxycycline (Fig. 5A). In neurons fixed at 0, 6, 18 or 30 hours after induction with doxycycline, DCV production was assessed by measuring the total number of NPY-pHluorin puncta. At 6 hours after

induction, some neurons showed punctate NPY-pHluorin in soma and neurites (up to 1250 puncta), while most neurons showed no puncta (Fig. 5B,C). After 18 to 30 hours the majority of neurons had NPY-pHluorin positive puncta, again with high variability (0 – 1637 fluorescent puncta per neuron) (Fig. 5B,C). Following the variety detected earlier (Figure 3C), during all time points except 0 hours, between 0 and 1637 NPY-pHluorin puncta were detected, reflecting different DCV production rates between neurons (Figure 4C). On average, DCV production increased from approximately 3 puncta per hour during the first 6 hours (i.e. in between 0 hours and 6 hours), to approximately 55 NPY-pHluorin puncta per hour between 6 and 18 hours after induction. To assess whether the variability in DCV biogenesis rates could be explained by variations in viral load, nuclear Cre-mCherry intensities were measured in the same neurons (Fig. 5D). DCV numbers correlated with Cre-mCherry expression levels in week 1, but not in week 2 and 3, indicating that at least some variation of DCV biogenesis is explained by viral load (Fig. 5E,F). However, still a large part of the variation in NPY-pHluorin puncta remains unexplained by the viral load, suggesting that this variation may be cell-intrinsic.

Discussion

The aim of this study was to test experimental paradigms that enable tracing of a population of newly generated DCVs over time. We showed that SNAP-SiR applied to NPY-SNAPtag expressing neurons labeled the Golgi and sparsely labelled DCVs, while labeling was prevented by *a priori* incubation with SNAP-Blocker. However, even 18 hours after blocking, SNAP-SiR labeling of DCVs was absent. In addition, SNAP-SiR staining without blocker only sparsely labeled DCVs, even though immunostaining revealed punctate expression of NPY-SNAPtag throughout the neurons. SNAP-SiR did not accumulate in the Golgi, as it was cleared from the Golgi within 24 hours after staining. Furthermore, a genetic approach was tested with doxycycline inducible NPY-pHluorin. A few neurons already showed many NPY-pHluorin puncta 6 hours after induction, while the majority from 18 hours onwards. Approximately 55 DCVs per hour were generated between 6 and 18 hours after inducing NPY-pHluorin expression. Neurons showed substantial variation in DCV biogenesis, which only in part could be explained by differences in viral load.

SNAP-Cell sparsely, but inefficiently labels DCVs

We chose SNAP-Cell to achieve the highest temporal resolution in labeling newly generated DCVs. However, SNAP-SiR staining of NPY-SNAPtag was only sparse and inefficient. NPY immunostaining showed that NPY-SNAPtag efficiently expressed into a punctate pattern in all neurons, which was inefficiently stained by SNAP-SiR (Fig. 3). The few puncta positive for SNAP-SiR were mobile, showed co-trafficking with a live DCV marker, and largely colocalized with Chromogranin B, indicating DCV labeling (Fig. 1-2). Mobile vesicles labeled with SNAP-Cell were shown before with Insulin-SNAP in β-cells (Hoboth et al., 2015), but to our knowledge, colocalization with an endogenous protein was never tested. Hence, our data show specific SNAP-SiR labeling of an organelle, albeit with low efficiency. In addition, old (30h) SNAP-Cell labeled Insulin granules were found more mobile than young ones (5h) and EM revealed that they appeared to end-up in multigranular bodies (Hoboth et al., 2015). Since we performed

a long 18h pulse and imaged directly after (no chase), our observed SNAP-SiR puncta represented 0h – 18h old vesicles and are not clearly comparable to the old or young insulin granules. Therefore, the labeled DCVs in our study form a group of vesicles with large age range, while despite this large range, only few of the DCVs present in each neuron were labeled.

Other SNAP-SiR staining was largely limited to the Golgi and was cleared from the Golgi 24 hours after staining (Fig. 3), suggesting that Golgi accumulation does not explain the sparse DCV staining. SNAP-Blocker in high concentration prevented all SNAP-SiR staining and in lower concentration it prevented peripherous SNAP-SiR staining (Fig. 1). However, even 18 hours after blocking, staining with SNAP-SiR was weak (Fig. 1). Two explanations for this lack of staining might be possible. (1) SNAP-tags may be readily cleaved off after newly formed DCVs have budded off the Golgi. This would render the SNAP-tags susceptible for degrading and/or trafficking to other pathways. Studies in *C. elegans* showed with soluble DCV cargoes that part of the immature DCV content could be trafficked to other pathways (Edwards et al., 2009; Ailion et al., 2014). In addition, between the SNAP and NPY peptide, there may possible cleavage sites (Brakch et al., 2002). (2) Quickly after DCV biogenesis, the cargo of the newly formed DCVs may already crystallize, with the SNAP-tags becoming inaccessible for the SNAP-Cell compounds. However, evidence for this is still lacking. Both of these explanations could also explain the low SNAP-SiR staining in non-blocked cells. Nonetheless, following a newly generated pool of DCVs through time seemed at this point impossible using the SNAP-Cell system.

Generation of new DCVs

For genetically controlled pulse-chase labeling, termination of the pulse (determining/starting the chase) was not possible, probably due to expression of Cre-ERT already in absence of tamoxifen (Fig. S1). Tamoxifen inducible Cre is a widespread method for condition-dependent recombination of loxp sites and such a leakiness is rare with genomically integrated Cre-ERT (Danielian et al., 1998; Valny et al., 2016). However, Cre-ERT delivered via lentiviral particles may produce such a high copy number, that the chances of leaking Cre became high enough to induce recombination in all infected neurons.

Doxycycline induced NPY-pHluorin expression varied extensively between neurons, with some already showing a punctate pattern after 6 hours, and most neurons having NPY-pHluorin labeled DCVs after 18 or 30 hours (Fig. 4-5). Between 6 and 18 hours after induction, a typical neuron produced 55 DCVs per hour. However, whether *in vivo* DCV production rates with endogenously expressed neuropeptides are similar remains unknown. Extrapolating from such a production speed would mean that neurons require 25 - 327 hours to produce their entire pool of DCVs, but only 1,5 to 20 hours to replenish the poolsize of DCVs that is typically released (<6%) during high-frequency stimulation (Persoon et al., 2018; Moro et al., 2020). Therefore, DCV biogenesis may be a slow process that takes hours to days, to replenish the full or relevant DCV pool. Although neuropeptide expression may be highly dynamic (Nawa et al., 1993; Kim et al., 2005; Moss et al., 2008), other factors might limit how quickly now mature DCVs are formed. For example in PC12 cells, neuroendocrine polypeptide 7B2 interacts with the pro form of prohormone cleavage enzyme PC2, thereby protecting proPC2 from prematurely be cleaved and thus also protecting prohormones to be processed too early in the pathway (Braks and Martens, 1994). Therefore, even though neuropeptide expression could change rapidly, the process of DCV biogenesis and maturation is highly controlled and

probably requires a certain minimum time until mature DCVs are present after inducing the process.

Variation of DCV production speeds

As early as 6 hours after inducing NPY-pHluorin expression, some neurons were filled with fluorescent puncta, while most were still empty (Fig. 3). This suggests that DCV biogenesis may be switched off in a majority of the neurons. In addition, the number of newly labeled DCVs per neuron varied substantially between neurons at 18 and 30 hours after induction. This variation in DCV production is larger than the typical variation in DCV pool sizes measured with Chromogranin B immunofluorescence in fixed neurons, or with NPY-pHluorin in live neurons (Persoon et al., 2018; Puntman et al., 2021) and could only partly be explained by differences in viral load (Fig. 5). Therefore, the variation in DCV biogenesis speed may have a cell-intrinsic origin.

One explanation could be that DCV production speed varies between different neuronal cell-types. Differences in DCV numbers between neuronal subtypes were observed between hippocampal and striatal neurons (Persoon et al., 2018), suggesting that they also require different DCV production rates to maintain their population. Furthermore, many different neuropeptide genes are expressed in the brain, with each neuronal cell-type expressing a subset of these neuropeptides (Smith et al., 2019). Possibly, some neuropeptides have a different secretion efficiency, therefore requiring faster replenishment via DCV biogenesis. In favor of this, BDNF secretion is typically higher than NPY secretion in primary neurons triggered by the same number of action potentials (Puntman et al., 2021). In addition, neuron to neuron differences in gene expression of DCV cargo proteins (Yao et al., 2020) may be a limiting factor for the biogenesis of the DCVs simply by providing the content. Furthermore, specific neuropeptides might differ in their affinity for sorting receptors or their ability to self-aggregate. However, this is currently unknown. Therefore, neuronal subtype specific differences in the speed of DCV biogenesis are likely to occur.

A second explanation for the variation in DCV production rate could be changes over time in the demand to generate new DCVs. In PC12 cells and pancreatic beta-cells, young or newcomer vesicles have a higher release probability (Duncan et al., 2003; For a review on newcomer insulin granule exocytosis see: Gaisano, 2014), suggesting that fast refilling of the young granule pool may be required during or after secretion episodes. If such a preference for young DCVs also exists in neurons, the state of neuronal activity may control the rate of DCV biogenesis. Dynamic changes in neuropeptide gene expression are for example linked to neuropeptide secretion via a feedback loop involving CaMKII (Moro et al., 2020). A different link between neuronal activity and DCV production may be homeostatic plasticity. Silencing neurons with TTX for two days increased synaptic numbers of DCVs (Tao et al., 2018), perhaps via generation of new DCVs. We propose that the speed of neuronal DCV biogenesis depends on cell-intrinsic properties such as neuropeptide expression or neuronal activity.

Methods

Animals

Wild-type C57BL/6 mice embryos were used at embryonic day (E) 18.5 for dissociated neuron cultures. The embryos were obtained by caesarean section of pregnant female mice. Wistar rat pups were sacrificed at postnatal day 0 (P0) for glia micro-island cultures (Meijer *et al.*, 2012). All experiments were conducted according to Dutch governmental guidelines.

Primary Neuronal Cultures

In order to create dissociated neuron cultures, hippocampi were isolated from E18.5 C57BL/6 mice. Hippocampi were dissected in Hanks' balanced salt solution (Sigma) and digested in 0.25% trypsin (GIBCO) in Hanks-HEPES for 20 minutes at 37°C. Dissociated neurons were plated at a density of 1500 cells/well in 12 wells plates containing 18 mm glass coverslips coated with micro-islands of rat glia in order to optain single cell neuron cultures as previously described (Meijer et al., 2012) and cultured in Neurobasal medium (Invitrogen) supplemented with 2% B-27 (GIBCO), 1.8% HEPES (GIBCO), 0.25% glutamax (GIBCO) and 0.1% Penicillin-Streptomycin (GIBCO). Micro-islands were generated by plating isolated rat glia on UV-sterilized agarose-coated and etched glass co-verslips that were stamped with a 0.1mg/ml poly-ᴅ-lysine (Sigma) and 0.2mg/ml rat tail colla-gen solution (BD Biosciences).

Constructs

For live labelling pulse-chase experiments, DCV cargo NPY and BDNF were separately fused to a SNAP-tag and put under a synapsin promotor, resulting in syn-NPY-SNAPtag and syn-BDNF-SNAPtag. syn-NPY-Cherry was described before (De Wit et al., 2009; van de Bospoort et al., 2012). For the DCV production assay, NPY was labelled with a pH-sensitive fluophore (pHluorin). NPY-pHluorin (NPY-pH) was driven by a doxycycline-inducible promoter (TRE) by substituting the synapsin promotor of a previously manufactured NPY-pH construct (van de Bospoort *et al.*, 2012) with the TRE promotor, resulting in TRE-NPY-pHluorin. For genetic pulse-chase experiments, Cre-Cherry was fused to T2A and NPY-pH, and driven by a TRE promotor, resulting in TRE-Cre-Cherry-T2A-NPY-pH.

Lentiviral Infection

After 7 days in vitro (DIV), primary hippocampal cells were infected with lentiviral particles expressing one of the earlier described constructs. For the live labelling pulse-chase experi-ment with NPY, cells were infected with either Syn-NPY-SNAPtag or Syn-NPY-Cherry. Addi-tionally, for the live labelling pulse-chase experiment with BDNF, cells were infected with Syn-BDNF-SNAPtag. For the genetic pulse-chase assay cells were infected with TRE-LoxP-BDNF-Cherry-LoxP or with TRE-LoxP-BDNF-Cherry-LoxP and ERT-Cre. In order to perform the DCV production assay cells were infected with TRE-NPY-pHluorin.

Live Labelling Pulse-Chase system

To block all synthesized and available SNAP-tags, primary neuronal DIV14 cultures were incubated in 75µl prewarmed blocking solution, which contained 20µM or 40µM SNAP-

Cell® Block (New England Biolabs) in culture medium, on parafilm for 30 minutes at 37°C with a CO2-concentration of 5%. After consecutive washes of 5 and 15 minutes in prewarmed and conditioned culture medium in 12 wells plates, cells were incubated for 0 or 18 hours at 37°C and 5% CO2. Subsequently, live staining was performed by incubating cells in 75µl prewarmed staining solution (0.3µM SNAP-Cell® 647-SiR (New England BioLabs) in supplemented Neu-robasal medium) on parafilm, for 15 minutes at 37°C and 5% CO2. Thereafter, cells were washed for 2 times 5 minutes in prewarmed, conditioned and supplemented Neurobasal me-dium in 12 wells plates at 37°C and 5% CO2. Lastly, cells were fixed in 3.7% paraformaldehyde (PFA) in 1X phosphate buffered saline (PBS) for 20 minutes at room temperature (RT).

Genetic pulse-chase system

For the genetic pulse-chase system cells infected with TRE-LoxP-BDNF-Cherry-LoxP were exposed to 2 ug/ml doxycycline (Sigma) at DIV8. Cells infected with both TRE-LoxP-BDNF-Cherry-LoxP and ERT-Cre were exposed to 2 ug/ml doxycycline and 3 ug/ml tamoxifen at DIV8. After 5 days the cells were fixed in 3.7% PFA in 1X PBS for 20 minutes at RT.

DCV production assay

Primary neuronal cultures were infected at DIV7 as described earlier (see section "Lentiviral Infection"). At DIV 14, 2 µg/ml doxycycline (Sigma) was administered to the culture medium of infected primary neuronal cultures. Either after 0 hours, 6 hours, 18 hours or 30 hours, the cells were fixed in 3.7% PFA in 1X PBS for 20 minutes at RT.

Immunocytochemistry

Fixed primary neuronal cultures were washed 3 times in 1X PBS and permeabilized in 0.5%Tri-ton-100X (Fisher Chemical) in 1X PBS for 5 minutes at RT. Subsequently, non-specific binding was prevented by incubating the cells in blocking solution that contained 2% normal goat se-rum (NGS) (GIBCO) and 0.1% Triton-100X in 1X PBS for 1 hour at RT. Thereafter, cells were incubated with 25 µl primary antibody solution (primary antibodies, 2% NGS and 0.1%Triton-100X in 1X PBS) per coverslip, at 4°C overnight with coverslips facing down. Primary antibodies were the following are listed in resource table. Cells were washed 3 times in 1x PBS and briefly blocked in blocking solution for 1 minute at RT. Subsequently, cells were incubated with secondary antibody solution (secondary antibodies, 2% NGS and 0.1%Triton-100X in 1X PBS) for 1 hour at RT. When applicable, DAPI (1:1000) was added to the secondary antibody dilution. Secondary antibodies are listed in the resource table. After several washes in 1x PBS, coverslips were mounted on microscopy slides with Mowiol 4-88 (Sigma).

Image Acquisition

Fixed coverslips containing glia micro-islands with cultured primary neurons were examined using the confocal A1 microscope (Nikon) with the 40x oil immersion objective to create high magnification images. Gain and laser power were kept constant within experiments. All images were acquired at 1024x1024 pixels. Coverslip overview images for the DCV production rate assay were obtained by stitching images that were acquired using the Nikon Ti-E Eclipse mi-croscope (Nikon) with the 10x air objective.

Image analysis

Colocalization assay

Images were analysed using the JACoP plugin in ImageJ (Bolte and Cordelières, 2006). First a mask was created using MAP2 staining. Threshold for puncta detection in the JACoP plugin was determined on initial puncta intensity. Colocalization was measured by determination of the Manders' coefficient between either the SNAP-SiR or the Cherry signal and ChgB. As n=1 no statistical analysis was performed.

Golgi intensity measurements

SNAP-SiR intensity within a Golgi-mask was measured in ImageJ. A mask was created using GM130 staining. As n<2 no statistical analysis was performed.

DCV production assay

For the quantification of the coverslip overviews, NPY-pH signal was examined and cells were grouped as neurite-positive or neurite-negative and counted by eye. Infection efficiency was determined by counting the number of cells that showed NPY-pH staining in the cell soma compared to cells that did not show NPY-pH staining.

For the DCV production assay with the viral load control, the SynJ plugin was used in ImageJ. SynJ is an adapted version of SynD (Schmitz *et al.*, 2011), developed for use in ImageJ (by Alessandro Moro). The program was used to detect neurites in the MAP2 channel, and puncta in the NPY-pH channel. In quantifying DCV number per cell, the threshold for puncta detection was optimized per cell in order to detect all present puncta. Shapiro-Wilk was used to test for normality and the Kruskal-Wallis test together with Dunn's multiple comparisons post hoc analysis was used to test whether DCV number differed significantly between the measured time points.

Quantifications of the viral load control were performed by measuring the Cre-Cherry signal intensity within a nuclear mask, which was based on DAPI stainings. DCV number was measured as described above. Linear regression between DCV number and Cre-Cherry signal intensity was tested using the Simple Linear Regression analysis.

Statistics

Statistical analysis was performed in GraphPad Prism. Shapiro-Wilk normality test was used to test for normal distributions and Levene's to test for homogeneity of variances. For normally distributed data sets with two experimental groups Student's t-tests were performed, for not normally distributed data with two groups, Mann Whitney-U tests were done. The data with more than 2 groups was not normally distributed, so a Kruskal-Wallis test was done, followed by a Dunn's multiple comparisons post hoc test.

Acknowledgements

The authors thank Robbert Zalm for cloning and producing viral particles, Lisa Laan and Desiree Schut for producing glia island cultures and providing primary culture assistance, Joke Wortel for organizing the animal breeding, Joost Hoetjes for genotyping, Jurjen Broeke for technical support and members of the CNCR DCV team for discussions and helpful input. This work is supported by an ERC Advanced Grant (322966) of the European Union (to MV).

Author contributions

D.C.P., J.B., R.F.T. and M.V. designed the experiments. D.C.P., and J.B. performed all experiments, analysis and designed the figures. D.C.P., J.B., R.F.T. and M.V. wrote the manuscript with input from all authors.

References

Ahras M, Otto GP, Tooze SA (2006) Synaptotagmin IV is necessary for the maturation of secretory granules in PC12 cells. J Cell Biol 173:241–251.

Ailion M, Hannemann M, Dalton S, Pappas A, Watanabe S, Hegermann J, Liu Q, Han HF, Gu M, Goulding MQ, Sasidharan N, Schuske K, Hullett P, Eimer S, Jorgensen EM (2014) Two Rab2 interactors regulate dense-core vesicle maturation. Neuron 82:167–180.

Asensio CS, Sirkis DW, Edwards RH (2010) RNAi screen identifies a role for adaptor protein AP-3 in sorting to the regulated secretory pathway. J Cell Biol 191:1173–1187.

Austin C, Hinners I, Tooze SA (2000) Direct and GTP-dependent interaction of ADP-ribosylation factor 1 with clathrin adaptor protein AP-1 on immature secretory granules. J Biol Chem 275:21862–21869.

Barr FA, Huttner WB (1996) A role for ADP-ribosylation factor 1, but not cop 1, in secretory vesicle biogenesis from the trans-Golgi network. FEBS Lett 384:65–70.

Bonnemaison ML, Eipper BA, Mains RE (2013) Role of adaptor proteins in secretory granule biogenesis and maturation. Front Endocrinol (Lausanne) 4:1–17.

Brakch N, Allemandou F, Cavadas C, Grouzmann E, Brunner HR (2002) Dibasic cleavage site is required for sorting to the regulated secretory pathway for both pro- and neuropeptide Y. J ofNeurochemistry 81:1166–1175.

Braks JAM, Martens GJM (1994) 7B2 is a neuroendocrine chaperone that transiently interacts with prohormone convertase PC2 in the secretory pathway. Cell 78:263–273.

Brandizzi F, Barlowe C (2013) Organization of the ER-Golgi interface for membrane traffic control. Nat Rev Mol Cell Biol 14:382–392.

Chen YG, Shields D (1996) ADP-ribosylation factor-1 stimulates formation of nascent secretory vesicles from the trans-Golgi network of endocrine cells. J Biol Chem 271:5297–5300.

Danielian PS, Muccino D, Rowitch DH, Michael SK, McMahon AP (1998) Modification of gene activity in mouse embryos in utero by a tamoxifen-inducible form of Cre recombinase. Curr Biol 8:1323–1326.

De Wit J, Toonen RF, Verhage M (2009) Matrix-Dependent Local Retention of Secretory Vesicle Cargo in Cortical Neurons. J Neurosci 29:23–37.

Dikeakos JD, Reudelhuber TL (2007) Sending proteins to dense core secretory granules: Still a lot to sort out. J Cell Biol 177:191–196.

Dittié AS, Hajibagheri N, Tooze SA (1996) The AP-1 adaptor complex binds to immature secretory granules from PC12 cells, and is regulated by ADP-ribosylation factor. J Cell Biol 132:523–536.

Dominguez N, van Weering JRT, Borges R, Toonen RFG, Verhage M (2018) Dense-core vesicle biogenesis and exocytosis in neurons lacking chromogranins A and B. J Neurochem 144:241–254.

Du W, Zhou M, Zhao W, Cheng D, Wang L, Lu J, Song E, Feng W, Xue Y, Xu P, Xu T (2016) HID-1 is required for homotypic fusion of immature secretory granules during maturation. Elife 5:1–22.

Duncan RR, Greaves J, Wiegand UK, Matskevich I, Bodammer G, Apps DK, Shipston MJ, Chow RH (2003) Functional and spatial segregation of secretory vesicle pools according to vesicle age. Nature 422:176–180.

Edwards SL, Charlie NK, Richmond JE, Hegermann J, Eimer S, Miller KG (2009) Impaired dense core vesicle maturation in Caenorhabditis elegans mutants lacking Rab2. J Cell Biol 186:881–895.

Emperador-Melero J, Huson V, van Weering J, Bollmann C, Fischer von Mollard G, Toonen RF, Verhage M (2018) Vti1a/b regulate synaptic vesicle and dense core vesicle secretion via protein sorting at the Golgi. Nat Commun 9 DOI: 10.1038/s41467-018-05699-z.

Gaisano HY (2014) Here come the newcomer granules, better late than never. Trends Endocrinol Metab 25:381–388.

Hinners I, Wendler F, Fei H, Thomas L, Thomas G, Tooze SA (2003) AP-1 recruitment to VAMP4 is modulated by phosphorylation-dependent binding of PACS-1. EMBO Rep 4:1182–1189.

Hoboth P, Müller A, Ivanova A, Mziaut H, Dehghany J, Sönmez A, Lachnit M, Meyer-Hermann M, Kalaidzidis Y, Solimena M (2015) Aged insulin granules display reduced microtubule-dependent mobility and are disposed within actin-positive multigranular bodies. Proc Natl Acad Sci U S A 112:E667-76 DOI: 10.1073/pnas.1505858112.

Ivanova A, Kalaidzidis Y, Dirkx R, Sarov M, Gerlach M, Schroth-Diez B, Müller A, Liu Y, Andree C, Mulligan B, Münster C, Kurth T, Bickle M, Speier S, Anastassiadis K, Solimena M (2013) Age-dependent labeling and imaging of insulin secretory granules. Diabetes 62:3687–3696.

Kakhlon O, Sakya P, Larijani B, Watson R, Tooze SA (2006) GGA function is required for maturation of neuroendocrine secretory granules. EMBO J 25:1590–1602.

Kim RY, Shin SW, Kim BJ, Lee W, Baik JH (2005) Dynamic regulation of hypothalamic neuropeptide gene expression and food intake by melanocortin analogues and reversal with melanocortin-4 receptor antagonist. Biochem Biophys Res Commun 329:1178–1185.

Kim T, Gondré-Lewis MC, Arnaoutova I, Loh YP (2006) Dense-core secretory granule biogenesis. Physiology 21:124–133.

Lund VK, Lycas MD, Schack A, Andersen RC, Gether U (2020) Rab2 drives axonal transport of dense core vesicles and lysosomal organelles. BioRxiv: https://doi.org/10.1101/2020.06.03.131672.

Meijer M, Burkhardt P, De Wit H, Toonen RF, Fasshauer D, Verhage M (2012) Munc18-1 mutations that strongly impair SNARE-complex binding support normal synaptic transmission.

Moro A, Woerden GMV, Toonen RF, Verhage M (2020) Camkii controls neuromodulation via neuropeptide gene expression and axonal targeting of neuropeptide vesicles. PLoS Biol 18:1–30 DOI: 10.1371/journal.pbio.3000826.

Moss A, Ingram R, Koch S, Theodorou A, Low L, Baccei M, Hathway GJ, Costigan M, Salton SR, Fitzgerald M (2008) Origins, actions and dynamic expression patterns of the neuropeptide VGF in rat peripheral and central sensory neurones following peripheral nerve injury. Mol Pain 4:1–12.

Nawa H, Bessho Y, Carnahan J, Nakanishi S, Mizuno K (1993) Regulation of neuropeptide expression in cultured cerebral cortical neurons by brain-derived neurotrophic factor. J Neurochem 60:772–775.

Persoon CM, Moro A, Nassal JP, Farina M, Broeke JH, Arora S, Dominguez N, Weering JR, Toonen RF, Verhage M (2018) Pool size estimations for dense-core vesicles in mammalian CNS neurons. EMBO J 37:e99672 DOI: 10.15252/embj.201899672.

Puertollano R, Randazzo PA, Presley JF, Hartnell LM, Bonifacino JS (2001) The GGAs Promote ARF-Dependent Recruitment of Clathrin to the TGN coats containing GGAs, however, remains to be eluci- dated. The domain organization of the GGAs may hold clues. Cell 105:93–102.

Puntman DC, Arora S, Farina M, Toonen RF, Verhage M (2021) Munc18-1 is essential for neuropeptide secretion in neurons . J Neurosci 41:JN-RM-3150-20 DOI: 10.1523/jneurosci.3150-20.2021.

Sirkis DW, Edwards RH, Asensio CS, Chandy K, Chow R (2013) Widespread Dysregulation of Peptide Hormone Release in Mice Lacking Adaptor Protein AP-3 Marks MS, ed. PLoS Genet 9:e1003812.

Smith SJ, Smbül U, Graybuck LT, Collman F, Seshamani S, Gala R, Gliko O, Elabbady L, Miller JA, Bakken TE, Rossier J, Yao Z, Lein E, Zeng H, Tasic B, Hawrylycz M (2019) Single-cell transcriptomic evidence for dense intracortical neuropeptide networks. Elife 8:1–35 DOI: 10.7554/eLife.47889.

Tao C-L, Liu Y-T, Zhou ZH, Lau P-M, Bi G-Q (2018) Accumulation of Dense Core Vesicles in Hippocampal Synapses Following Chronic Inactivity. Front Neuroanat 12 DOI: 10.3389/fnana.2018.00048/full.

Tsuboi T, Kitaguchi T, Karasawa S, Fukuda M, Miyawaki A (2010) Age-dependent Preferential Dense-Core Vesicle Exocytosis in Neuroendocrine Cells Revealed by Newly Developed Monomeric Fluorescent Timer Protein. Mol Biol Cell 21:87–94.

Urbé S, Page LJ, Tooze SA (1998) Homotypic Fusion of Immature Secretory Granules during Maturation in a Cell-free Assay. J Cell Biol 143:1831–1844.

Valny M, Honsa P, Kirdajova D, Kamenik Z, Anderova M (2016) Tamoxifen in the mouse brain: Implications for fate-mapping studies using the tamoxifen-inducible cre-loxP system. Front Cell Neurosci 10:1–12.

van de Bospoort R, Farina M, Schmitz SK, de Jong A, de Wit H, Verhage M, Toonen RF (2012) Munc13 controls the location and efficiency of dense-core vesicle release in neurons. J Cell Biol 199:883–891.

van Keimpema L, Kooistra R, Toonen RF, Verhage M (2017) CAPS-1 requires its C2, PH, MHD1 and DCV domains for dense core vesicle exocytosis in mammalian CNS neurons. Sci Rep 7:10817.

Wendler F, Page LJ, Urbé S, Tooze SA (2001) Homotypic Fusion of Immature Secretory Granules During Maturation Requires Syntaxin 6. J Cell Biol 143:1831–1844.

Westen R Van, Poppinga J, Díez R, Toonen RF, Verhage M (2021) Neuromodulator release in neurons requires two functionally redundant calcium sensors. PNAS 118.

Wu MM, Grabe M, Adams S, Tsien RY, Moore HPH, Machen TE (2001) Mechanisms of pH Regulation in the Regulated Secretory Pathway. J Biol Chem 276:33027–33035.

Yao Z et al. (2020) A taxonomy of transcriptomic cell types across the isocortex and hippocampal formation Zizhen. bioRxiv.

Zanetti G, Pahuja KB, Studer S, Shim S, Schekman R (2012) Erratum: COPII and the regulation of protein sorting in mammals (Nature Cell Biology (2012) 14 (20-28)). Nat Cell Biol 14:221.

Supplementary figure legends

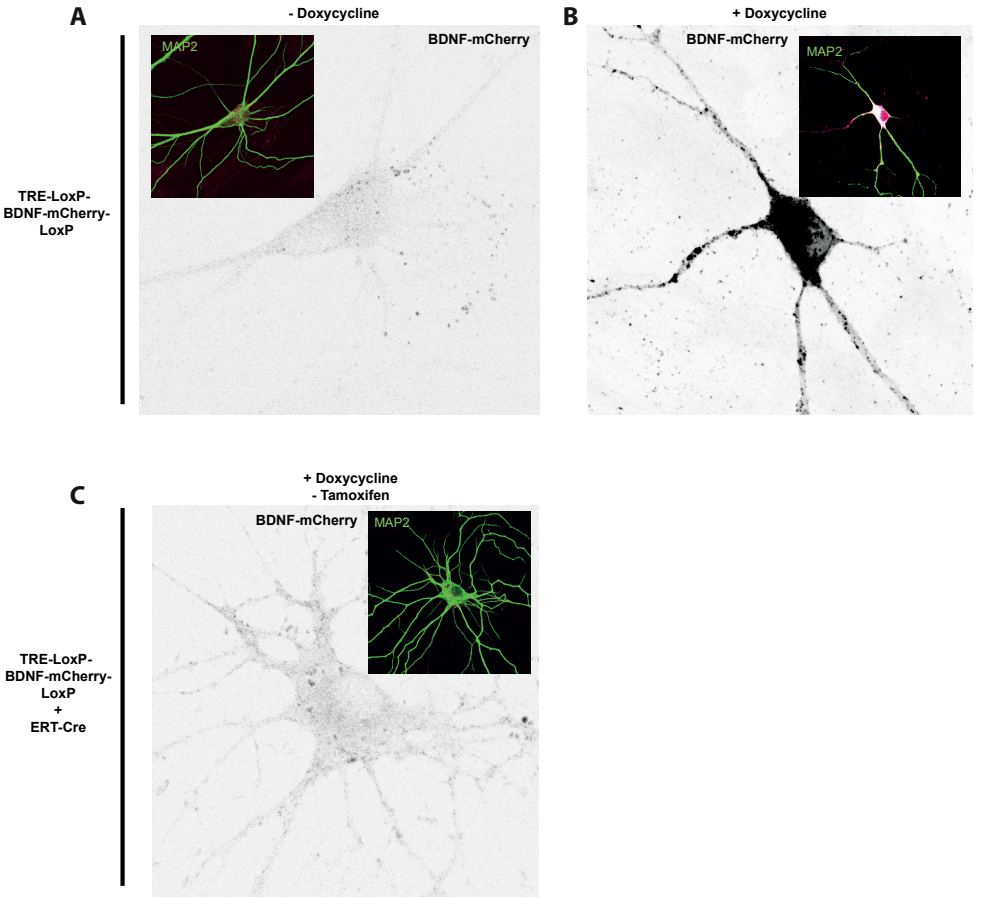

Supplemental Figure 1. Genetically induced termination of the pulse via ERT-Cre is precluded by leaky Cre expression. (**A**) Neurons that were infected with TRE-LoxP-BDNF-mCherry-LoxP showed no BDNF-mCherry fluorescence. (**B**) Neurons infected with TRE-LoxP-BDNF-mCherry-LoxP and incubated with doxycycline showed punctate BDNF-mCherry fluorescence. (**C**) Neurons infected with TRE-LoxP-BDNF-mCherry-LoxP and ERT-Cre showed no BDNF-mCherry fluorescence after doxycyclien induction in absence of ERT-Cre induction by tamoxifen.


5

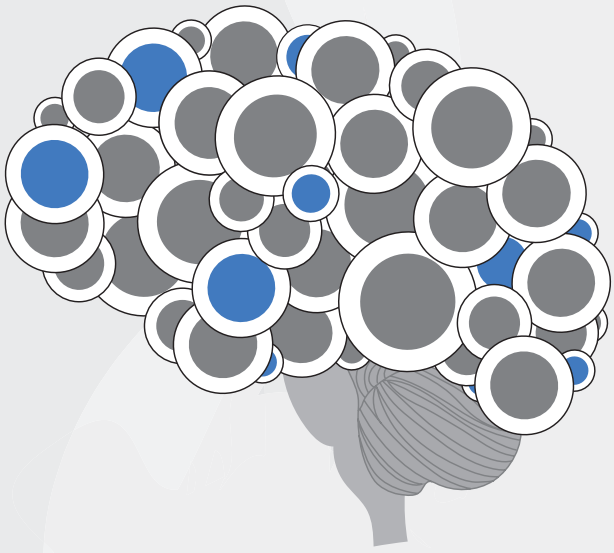

Chapter 6

Summary & Discussion

6.1 Summary of the chapters

The general aim of this thesis was to reveal the role of SM-proteins in neuronal secretion, and in particular, neuropeptide secretion from DCVs. Neuropeptide signaling occurs throughout the brain, with each neuron having its own subset of neuropeptides and receptors. This signaling network is important for many brain functions including memory, sleep, appetite and fear. Although the molecular determinants of neurotransmission are well described, including the essential role of SM-protein MUNC18-1, it has remained unclear which SM-protein is required for DCV exocytosis. We identified MUNC18-1 as the SM-protein for DCV exocytosis and showed that STXBP1 has the same role in human iNeurons. Additionally, we found evidence that reduced MUNC18-1/STXBP1 expression decreases DCV exocytosis, implicating neuropeptide secretion defects in STXBP1 syndrome. In search of a role of MUNC18-2 in neuronal secretion, we found that MUNC18-2 is not required for SV, DCV or GLUT4 exocytosis in mammalian neurons. Finally, because the upstream mechanisms required for DCV exocytosis are less well understood, we tested methods to investigate DCV biogenesis and maturation.

We started with searching for the SM-protein required for mammalian DCV exocytosis. In **Chapter 2,** we identified MUNC18-1 as the essential SM-protein for neuropeptide secretion in primary mouse neurons, while MUNC18-2 and -3 did not support DCV exocytosis in absence of MUNC18-1. In addition, we showed that the reduced expression levels of MUNC18-1 in *Munc18-1* HZ neurons led to a decrease in DCV exocytosis. This suggests that the neurodevelopmental, behavioral and cognitive deficits that *Munc18-1* HZ mice display may be in part due to defects in neuropeptide secretion and that this provides a possible additional disease mechanism in STXBP1 syndrome. In **Chapter 3,** we tested DCV exocytosis in human iNeurons, which was readily visible as NPY-pHluorin dequenching events upon high-frequency train-stimulation, similar to previous experiments in mouse CNS neurons. We showed that STXBP1 in human iNeurons is essential for DCV exocytosis. In addition, we found that a STXBP1 syndrome patient mutation generated with Crispr-Cas9 reduced STXBP1 protein levels and hampered DCV exocytosis. Therefore, it is plausible that defective neuropeptide secretion caused by mutations in STXBP1 contributes to the neurodevelopmental, cognitive, psychiatric and neurological symptoms in STXBP1 syndrome.

In **Chapter 4,** we tested the role of MUNC18-2 in neuronal secretion. We used conditional knock-out in primary mouse neurons to show that MUNC18-2 is not required for DCV exocytosis, or any property of DCV exocytosis including opening of the fusion pore and full collapse of the vesicle. Furthermore, we tested GLUT4 exocytosis marker GLUT4-pHluorin and observed GLUT4 exocytosis events during basal conditions and increased exocytosis upon high-frequency stimulation. A stimulation similar to natural burst-firing was most effective in triggering GLUT4 exocytosis. Next, we showed that MUNC18-2 is not required for basal or stimulated GLUT4 exocytosis.

In search of upstream mechanisms important for DCV exocytosis, we explored tools to visualize DCV biogenesis and maturation in **Chapter 5**. Here, we tested DCV labeling with SNAP-Cell, which only sparsely labeled DCVs. In parallel, we tested a genetic pulse-chase strategy by doxycycline-induced expression of DCV cargo NPY-pHluorin. Induction of NPY-pHluorin led to a highly variable number of labeled DCVs in primary mouse neurons, which could not be explained by viral load and thus suggests that individual neurons possess different DCV biogenesis rates.

6.2 Requirements for secretion

Neuronal secretion machinery

We found that MUNC18-1 is essential for neuropeptide secretion from mouse and human neurons (Chapter 2, 3; Puntman et al., 2021), in addition to its role in synaptic transmission (Verhage et al., 2000; Patzke et al., 2015). Previously, SNAP25 and VAMP2 were also found to support both types of secretion (Schoch et al., 2001; Washbourne et al., 2002; Delgado-Martínez et al., 2007; Zimmermann et al., 2014; Shimojo et al., 2015; Arora et al., 2017; Hoogstraaten et al., 2020). Therefore, it seems that the core SNARE/assessor proteins syntaxin 1-SNAP25-VAMP2 and MUNC18-1 in mammals that have genetic and functional homologs in yeast, are essential for both SV and DCV exocytosis by docking and priming of secretory vesicles. However, the role of a syntaxin in DCV exocytosis has not yet directly been studied yet. Our findings add to the similarity of exocytosis machineries between SVs and DCVs. It is striking that despite these similarities, SVs and DCVs are triggered with highly different efficiency by the same stimulations.

In addition to the core SNARE/assessor protein complex, the other essential module for DCV exocytosis is the RIM-RAB3/27-MUNC13 complex, which may serve as a mammalian substitute/homolog for the yeast exocyst complex herein (Bowser et al., 1992; TerBush and Novick, 1995; TerBush et al., 1996; Guo et al., 1999; Persoon et al., 2019). Similarly, RIM and MUNC13 are also required for neurotransmitter secretion, while RAB3 is not essential (Augustin et al., 1999; Schlüter et al., 2004, 2006; Kaeser et al., 2011, 2012; van de Bospoort et al., 2012; Persoon et al., 2019). Hence, RAB2 is essential for neuropeptide secretion, but not for synaptic transmission. Other important components for secretion shared between SVs and DCVs, include calcium sensors synaptotagmin-1 and -7 (Geppert et al., 1994; Banerjee et al., 2020; Westen et al., 2021) and calcium-dependent priming factor CAPS (Renden et al., 2001; Jockusch et al., 2007; Hammarlund et al., 2008; Farina et al., 2015; Van Keimpema et al., 2017), while calcium sensor DOC2A/B, which regulates spontaneous and asynchronous neurotransmitter secretion (Groffen et al., 2010; Yao et al., 2011), is not required for DCV exocytosis (Westen et al., 2021). Our finding that MUNC18-1 is essential for mammalian DCV exocytosis adds to the high similarity between the core machineries of neuropeptide and neurotransmitter secretion, which up to now only clearly differ in their requirement of RAB3 and perhaps DOC2.

Triggers for secretion

In chemical frequency coding, neurons secrete different substances depending on their firing frequency. We tested several stimulation patterns for DCV and GLUT4 exocytosis (Chapter 2-4), which consisted of prolonged, repeated versions of burst firing that naturally occur in some hippocampal neurons (Kandel and Spencer, 1961; Buzsáki et al., 1996; Klausberger et al., 2004). During high-frequency train-stimulation, exocytosis peaked during the first two trains and rapidly declined afterwards (Chapters 2-4; Puntman et al., 2021). This was also evident for DCV exocytosis in other studies from our lab (Farina et al., 2015; Arora et al., 2017; Emperador Melero et al., 2017; van Keimpema et al., 2017; Dominguez et al., 2018; Emperador-Melero et al., 2018; Persoon et al., 2018, 2019; Hoogstraaten et al., 2020; Moro et al., 2020; Westen et al., 2021) and similar patterns were found using other high frequency stimulations (Matsuda et al.,

2009) in mouse neurons, or in *Drosophila* neuromuscular junctions. In addition, GLUT4 exocytosis was immediately triggered by a stimulation that mimics natural burst firing and had a lower, delayed response to 10 Hz stimulation (Chapter 4), similar to what was previously observed upon 10 Hz (Ashrafi et al., 2017). However, time resolution was insufficient to distinguish GLUT4 exocytosis during the different APs of the natural burst firing. These secretion patterns are strikingly different from SV exocytosis, which peaks immediately upon the first action potential of 10-100 Hz stimulations and quickly (in 3-20 AP) depresses afterwards (He et al., 2017; Yin et al., 2018; Meijer et al., 2019). Therefore, both GLUT4 vesicles and DCVs have a delayed and lower response to electrical stimulations compared with SVs. Furthermore, having more neurotransmission during low-frequency firing or the start of high-frequency firing, and more neuropeptide secretion during prolonged high-frequency firing may result in chemical frequency coding towards receiving neurons.

The basis for different responses of DCVs, GLUT4 and SVs to the same simulation patterns may be in how their exocytosis is linked to presynaptic signaling pathways. Release-ready SVs are thought to be coupled to presynaptic calcium channels and are therefore subject to local high calcium concentrations during neuronal activity (Sheng et al., 1998). DCVs may not be coupled to these calcium channels, and are mostly found outside of the SV cluster adjacent to the AZ (Verhage et al., 1991; Persoon et al., 2018), while this is unknown for GLUT4 vesicles as their subcellular localization has not been systematically studied on EM. This larger distance to calcium channels may explain the decreased sensitivity of DCVs to stimulations compared with SVs. Another source of calcium comes from internal calcium stores, especially from the ER via local calcium channels (For reviews on internal calcium release see: Berridge, 1998; Brini et al., 2014). DCV exocytosis may be triggered by calcium release from the ER (Balkowiec and Katz, 2002; Kolarow et al., 2007; Shakiryanova et al., 2007; Wong et al., 2009). However, ionomycin induced calcium influx from intra- and extracellular sources is not very effective to trigger DCV exocytosis compared with KCl superfusion or repeated burst stimulation (Persoon et al., 2018), suggesting that membrane depolarization may stimulate DCV exocytosis in addition to calcium, also partly in a calcium-independent manner. Nonetheless, DCVs share most of their exocytosis machinery with SVs, including calcium sensors, and it has been shown before that their exocytosis is triggered by calcium (Gärtner and Staiger, 2002; Matsuda et al., 2009). Therefore, calcium is a trigger for both DCV and SV exocytosis, but DCVs may have less sensitivity for calcium.

In addition to calcium, other signaling pathways may stimulate exocytosis. In *C. elegans*, cAMP was found as a calcium independent trigger for both DCV and SV exocytosis (Shakiryanova et al., 2011; Steuer Costa et al., 2017). Conversely, *C. elegans pkc-1* mutants had deficient DCV exocytosis but unaffected neurotransmission (Sieburth et al., 2007), suggesting that the DAG-PKC pathway may specifically support or trigger DCV exocytosis in nematodes. A calcium independent trigger for GLUT4 exocytosis could be AMP kinase, since AICAR (5-Aminoimidazole-4-carboxamide ribonucleotide, an AMP analog that stimulates AMP kinase activity) readily elevated plasma membrane localization of GLUT4-pHluorin (Ashrafi et al., 2017). These data suggest that signaling pathways such as DAG-PKC and AMP kinase may support the differential exocytosis of respectively DCVs and GLUT4 vesicles compared with SVs. Taken together, high frequency burst stimulation seems most effective in triggering DCV/GLUT4 exocytosis, probably largely in a calcium dependent way, supporting chemical frequency coding.

Recovery of neuropeptide secretion

In *Munc18-1* HZ mouse neurons, a potentiation effect was observed when a second high-frequency train-stimulation was administered 30s after a first stimulation (Chapter 2; Puntman et al., 2021). This potentiation effect was absent in WT mouse neurons and in human iNeurons when the total number of DCV exocytosis were compared between the first and second stimulation (Chapter 2-3). Nonetheless, in both mouse and human neurons, the number of DCV exocytosis events quickly decayed after peaking during the first few bursts of the first stimulation episode, while DCV exocytosis numbers peaked again to the same levels at the first bursts of the second stimulation episode 30s later (Chapter 2, 3; Moro et al., 2020; Puntman et al., 2021). This suggests that in both mouse and human neurons, a 30s pause between bursts of stimulations restores the releasable DCV pool, or potentiates DCV exocytosis of an incompletely restored pool. We also observed a similar effect with this dual stimulation pattern for GLUT4-pHluorin exocytosis in mouse WT neurons (Chapter 4). At much faster timescale, a 40Hz stimulation caused synaptic rundown of neurotransmitter secretion, with depressed EPSC amplitude, which was readily restored after a few seconds (He et al., 2017). This different timescale may be due to rapid replenishment of the SV RRP via ultrafast or bulk endocytosis (Clayton et al., 2008; Watanabe et al., 2013), while replenishing of the releasable DCV pool does not involve endocytosis.

Mechanisms to elevate DCV exocytosis during a second burst-stimulation may include (i) arrival or capture of new DCVs at presynaptic release zones (replenishment of the DCV pool), (ii) docking/priming of DCVs that were already present, or (iii) modification of the efficiency of the last steps of exocytosis (potentiation). (i) Activity dependent regulation of the presynaptic presence of DCVs was shown before in mammalian neurons when 2-day neuronal silencing via TTX to induce homeostatic plasticity resulted in an increase in presynaptic DCVs (Tao et al., 2018). Vice versa, K^+-induced membrane depolarization increased DCV localization to presynapses (Frischknecht et al., 2008) and immobilized moving DCVs (Bharat et al., 2017), suggesting that also increased neuronal firing may recruit DCVs to axonal/presynaptic release sites. In *Drosophila* neuromuscular boutons, stimulation induced neuropeptide secretion was followed by refilling of the boutons with DCVs via capture (Shakiryanova et al., 2006; Bulgari et al., 2014, 2017; Cavolo et al., 2016). In mammalian dendrites, DCV recruitment to spines is regulated by Liprin-α/TANC2 in a calcium dependent manner (Stucchi et al., 2018). These data point at activity dependent recruitment of DCVs to release zones, either during activity or after loss of DCVs due to secretion.

(ii) Whether docking/priming of DCVs may be elevated during recovery after burst stimulation has not been described yet. Very few DCVs are found docked at all times (Verhage et al., 1991; Lysakowski et al., 1999; van de Bospoort et al., 2012; Persoon et al., 2018), suggesting that DCV docking/priming may be a transient process occurring immediately prior to exocytosis. Therefore, this seems an unlikely mechanism to explain the recovery/potentiation in DCV exocytosis at the start of the second train-stimulation. However, the last steps of exocytosis may occur more efficiently during the second train-stimulation via a potentiation mechanism. A first candidate for such a potentiation mechanism may be CaMKII, whose activation is required for post-tetanic potentiation of neuropeptide release in *C. elegans* (Shakiryanova et al., 2007). However, CaMKII does not regulate potentiation of DCV exocytosis in mammalian neurons (Moro et al., 2020). Therefore, CaMKII independent signaling pathways are more likely candidates to regulate potentiation. These may include cAMP, since this stimulates both SV and DCV exocytosis (Shakiryanova et al., 2011; Steuer Costa et al., 2017), or DAG-

PKC signaling (Sieburth et al., 2007). These findings suggest that a recovery of 30s after high-frequency burst-firing restores normal neuropeptide release by refilling the local DCV pool and/or potentiating DCV exocytosis.

Secretory vesicles: production on demand

We detected newly generated DCVs at several time-points after inducing expression of DCV marker NPY-pHluorin and observed large variation in DCV production from neuron to neuron (Chapter 5). One explanation for this variation could be that DCV production speed depends on the neuronal subtype, since many subtypes are present within primary hippocampal neuron cultures (Mynlieff, 1999). Indeed, the DCV pool strongly correlated with neuronal size (Persoon et al., 2018), suggesting that DCV production depends on the neuronal subtype. Alternatively, DCV biogenesis may be highly regulated, in that way causing the high variation in DCV production between neurons. We have shown that the amount of neuropeptide secretion may be linked to the number of DCVs that are present in each neuron (Chapter 2-3; Dominguez et al., 2018; Emperador-Melero et al., 2018; Persoon et al., 2018; Moro et al., 2020; Puntman et al., 2021). Therefore, regulating DCV biogenesis may be a powerful way of modulating neuropeptide secretion. In favor of this hypothesis, accumulation of DCVs in presynapses was observed in neurons that were inactivated via TTX for 2 days, which induces homeostatic plasticity, (Tao et al., 2018).

In β-cells, glucose stimulated depletion of the insulin granule pool rapidly induces insulin granule biogenesis (Guest et al., 1989; Alarcon et al., 1993; Martin et al., 1994; Trogden et al., 2019), serving as a produce on demand mechanism. In immune cells, extracellular cytokines trigger SG production (Paul et al., 1994), also indicating upregulation of SG biogenesis in conditions where their secretion may be elevated. Therefore, in non-neuronal secretory cells, a produce on-demand system may regulate SG biogenesis that can be triggered by extracellular cues or a depletion of granules. In neurons, such a mechanism would aid in sustaining neuropeptide secretion. Two modes of regulating this seem logical: (i) The DCV pool may be refilled after losing DCVs via exocytosis during neuronal activity, either by boosting DCV biogenesis after heavy activity or by sensing the loss of DCVs, triggering DCV biogenesis. (ii) Alternatively, neurons may anticipate DCV loss by refilling the DCV pool already during neuronal activity. For both options, neurons either have to link their state of activity to DCV biogenesis, or have to sense DCV loss.

In hippocampal neurons, CaMKII depletion or phosphomutation reduces DCV numbers by decreasing neuropeptide expression (Moro et al., 2020). In addition, CaMKII is required for ectopic BDNF-induced production of BDNF via pCREB. This suggests that DCV biogenesis could be directly regulated by controlling the expression of DCV content via the BDNF-TrkB-CaMKII pathway, which therefore links neuropeptide secretion to DCV biogenesis. Furthermore, NPY triggers Gonadotropin Releasing Hormone (GnRH) production in GT1-7 neurons by activating cAMP via several NPY receptors (Dhillon et al., 2009). In this way, loss of DCVs could be sensed via autocrine neuropeptide signaling, leading to DCV biogenesis. In addition, neighboring neuronal (burst) activity may also induce DCV biogenesis, since secreted neuropeptides are not limited to only targeting the neuron of origin. Together, these data suggest that neuronal DCV biogenesis is highly regulated, either by neuronal activity in order to replenish DCVs after secretion, or prior to secretion.

6.3 Role of SM-proteins in all membrane fusion steps

Exocytic SM-proteins help recruiting vesicles to the plasma membrane and set-up the SNARE complexes for vesicle to plasma membrane fusion. SM-proteins for internal membrane trafficking act in a similar way, but then by recruiting two membranes of internal organelles. We now describe the essential role of MUNC18-1 in the two major neuronal secretion pathways, neurotransmitter and neuropeptide secretion, while MUNC18-2 and -3 are dispensable (Chapter 2-4; Verhage et al., 2000; He et al., 2017; Santos et al., 2017).

Functional redundancy between exocytic SM-proteins

MUNC18-2 or -3 do not support DCV exocytosis in *Munc18-1 null* neurons (Chapter 2; Puntman et al., 2021). Similarly, overexpression of MUNC18-2 or -3 in *Munc18-1 null* neurons did not restore synaptic transmission (He et al., 2017; Santos et al., 2017) and synaptic transmission was unaffected in *Munc18-2 null* neurons (Chapter 2; Puntman et al., 2021). Therefore, MUNC18-1 appears the only exocytic SM-protein required for the final steps of neuropeptide and neurotransmitter secretion. However, MUNC18-2 overexpression in *Munc18-1 null* mouse neurons rescued priming and largely rescued docking of SVs (He et al., 2017), suggesting it may contribute to these aspects of vesicular exocytosis in WT neurons that have sufficient MUNC18-2 expression levels, if these neurons exist. Conversely, MUNC18-1 prevents NSF-dependent depriming of SVs, which could not be rescued with MUNC18-2 (He et al., 2017). Whether this type of depriming may be a factor in DCV exocytosis is currently not known. Observations in chromaffin cells suggest that the syntaxin binding and docking function of MUNC18-1 is also supported by MUNC18-2 (Gulyás-Kovács et al., 2007). In other cell-types that have more robust co-expression of multiple MUNC18 paralogs (*i.e.* pancreatic β-cells and lung epithelial cells), parallel roles of MUNC18 paralogs within the same secretion pathway have been observed (Oh and Thurmond, 2009; Kim et al., 2012; Oh et al., 2012; Lam et al., 2013; Zhu et al., 2015; Jaramillo et al., 2019). These findings suggest that MUNC18-2 may support neuronal secretion if expression levels are high enough. However, MUNC18-2 and -3 are only moderately, if at all, expressed in most mouse CNS neurons (Chapter 4; Tellam et al., 1995; Martin-Verdeaux et al., 2002; Imai et al., 2004; Mandic et al., 2011; Kim et al., 2012; Lam et al., 2013; Zhu et al., 2015b; Yao et al., 2020). Therefore, (native) MUNC18-2 or -3 seem to be irrelevant for DCV exocytosis, at least in neurons studied here.

Despite the differences between MUNC18-1, -2 and -3 in supporting neuronal secretion, neuronal viability is restored upon expression of any MUNC18 paralog in mouse *Munc18-1 null* neurons (Chapter 2; He et al., 2017; Santos et al., 2017). Since *Munc18-1 null* neurons survive if MUNC18-2 or -3 are overexpressed, but are unable to perform synaptic transmission or neuropeptide secretion, it is unlikely that a lack of neurotransmitter or neuropeptide secretion is the cause of neuronal death in *Munc18-1 null* neurons. Although neuronal survival could be prolonged for a few days via administration of BDNF or insulin, neurons still died after several days in culture (Heeroma et al., 2004), supporting the hypothesis that neuronal death is not caused by a lack of neurotrophin secretion from DCVs. Taken together, these data suggest that the MUNC18 paralogs are redundant in their support of neuronal health upon sufficient expression, but often play different roles in the final steps of secretion.

We did not study the role of the non-exocytic SM-proteins in DCV exocytosis or biogenesis. However, since the MUNC18 paralogs are exocytic, and VPS33, 45 and/or Sly1 are limited to internal membrane trafficking, it is plausible that the latter SM-proteins control certain aspects of the DCV secretory pathway (e.g., biogenesis or maturation). For example, Sly1 supports ER to Golgi trafficking in yeast and human cell lines (Peng and Gallwitz, 2002; Nogueira et al., 2014) and Golgi to ER trafficking in mammalian cell lines (Laufman et al., 2009). This could be important for DCV biogenesis; however, it is unclear whether it functions in the same steps as are required for neuropeptide trafficking via COPII vesicles. There is some direct evidence for a role of VPS33 in SG biogenesis/maturation. In megakaryocytes and platelets, VPS33B is required for the biogenesis of alpha-granules (Lo et al., 2005). Furthermore, in HeLa cells VPS33B is required for endosomal to lysosomal fusion (Galmes et al., 2015). Interestingly, Sly1 and VPS33 in yeast protect SNARE complexes from disassembly by SEC18, similar to MUNC18-1 preventing NSF-dependent depriming of synaptic vesicles in mammalian neurons (Lobingier et al., 2014; He et al., 2017). VPS45 is also associated with endocytic trafficking. In yeast, VPS45 binds the N-terminus of Tlg2p (homolog of mammalian syntaxin 16) in an open conformation, facilitating membrane fusion. In mammals, VPS45 is required for endocytic trafficking together with syntaxin 16 (Rahajeng et al., 2010) by fusion of early endosomes (Frey et al., 2021). Due to the proposed link between DCV biogenesis/maturation and the endolysosomal pathway, VPS45 may directly or indirectly take part in the upstream steps of DCV exocytosis. Taken together, SM-proteins VPS33a/b, VPS45 and Sly1 may have important roles in supporting DCV biogenesis, by supporting membrane trafficking from and to the Golgi, while DCV exocytosis is supported uniquely by the exocytic SM-protein MUNC18-1.

6.4 DCV exocytosis in mice versus human neurons

DCV exocytosis dynamics in mouse and human neurons

In Chapter 3, we quantified DCV exocytosis in NGN2-differentiated human iPSCs (iNeurons). Two episodes of high-frequency train-stimulation readily elicited DCV exocytosis, which peaked during the first two trains of both stimulation episodes and quickly decayed after, suggesting replenishment of the releasable DCV pool or potentiation of DCV exocytosis. We observed a similar pattern before in primary mouse hippocampal neurons using the same stimulation paradigm (Chapter 2; Moro et al., 2020; Puntman et al., 2021) and using a single episode of 16 trains (Chapter 2, 4; Farina et al., 2015; Arora et al., 2017; van Keimpema et al., 2017; Dominguez et al., 2018; Emperador-Melero et al., 2018; Persoon et al., 2018, 2019; Hoogstraaten et al., 2020; Puntman et al., 2021). This suggests that DCV fusion dynamics are similar between mice and humans. Furthermore, we found similar total numbers of DCV exocytosis events for primary mouse neurons and human iNeurons for each stimulation and the DCV pool sizes were comparable (Chapters 2-4). This was also found before when human neurons derived from neuroepithelial stem cells were compared with primary mouse neurons (Emperador Melero et al., 2017). These parallels between mouse and human neuronal DCV exocytosis may be explained by having largely the same expression of exocytic proteins (Hodge et al., 2019; Yao et al., 2020).

Interestingly, DCV fusion event duration was much shorter in human iNeurons compared to primary mouse hippocampal neurons (Chapter 3). This shorter duration may be due to (i) an increased number of kiss-and-run events, (ii) faster opening of the fusion pore (i.e. faster/increased full collapse), or (iii) increased diffusion after full collapse due to different properties of the ECM. There is currently no evidence supporting differences in the number of kiss-and-run events or timing of fusion pore opening between human and mouse neurons. However, some differences in ECM composition between human iNeuron cultures and primary mouse neuron cultures have been found (Fietz et al., 2012), suggesting that ECM properties might differ and lead to differential diffusion after DCV full collapse in mouse and human neurons. Nonetheless, most properties of DCV exocytosis are similar between human iNeurons and primary mouse CNS neurons in culture, suggesting that human iNeurons are a suitable model system for research on neuropeptide release.

Human *STXBP1 null* iNeurons do not degenerate

Although the roles of MUNC18-1 in primary mouse neurons and STXBP1 in human iNeurons are similar, with an essential role in neuropeptide secretion, neuronal viability is only affected in mouse neurons lacking MUNC18-1/STXBP1. Mouse neurons lacking MUNC18-1 do not survive beyond DIV4 in culture (Heeroma et al., 2004) and degenerate *in vivo* (Verhage et al., 2000). However, human *STXBP1 null* iNeurons survived through 6 weeks of culture, without showing signs of stress or degeneration (Chapter 3). Comparing mRNA levels in scRNA sequencing data-bases indicates that human neurons may express more STXBP3 than mouse neurons (Hodge et al., 2019; Yao et al., 2020), which may compensate for the loss of STXBP1 and support cell viability.

6.5 Roles of SM genes in human diseases

STXBP2 is essential for secretion in several non-neuronal cell-types

We showed that conditional *Munc18-2 null* in mouse neurons did not alter total numbers of DCVs, DCV exocytosis, synaptic transmission or GLUT4 exocytosis (Chapter 4). This suggests that MUNC18-2 is not required for neuronal secretion. Conversely, some neurological defects were reported in two FHL4 patients, suggesting a function of STXBP2 in the brain. Mutations in STXBP2 causal for FHL4 are mainly found at the syntaxin 11 binding groove region (zur Stadt et al., 2009). Therefore, the interaction between STXBP2 and syntaxin 11 appears essential for the function of STXBP2 in many cell types. STXBP2 and syntaxin-11 expression levels in the human brain are very low, if not absent (Hodge et al., 2019), suggesting that FHL4 causing mutations probably do not affect neuronal secretion. In line with FHL4 disease symptoms, MUNC18-2 has major roles in secretion from immune cells and blood platelets, and intestinal development (Gutierrez et al., 2018; Mosa et al., 2018; Cardenas et al., 2019). Conversely, although roles for MUNC18-2 in lung mucus secretion (Kim et al., 2012; Jaramillo et al., 2019) and insulin secretion (Lam et al., 2013) have been reported, FHL4 symptoms related to these functions are unknown. Possibly, FHL4 immunodeficiency, bleedings and enteropathy may be of such severity that other symptoms are often overlooked. Together, these findings indicate an important role for STXBP2 in secretion from many non-neuronal cell types.

MUNC18-1 availability affects DCV exocytosis in mouse and human neurons in STXBP1 syndrome

In *Munc18-1* HZ primary mouse neurons, which have ~50% reduced MUNC18-1 expression (Verhage et al., 2000; Toonen et al., 2005, 2006; Lee et al., 2019), DCV exocytosis was decreased compared to WT neurons (Chapter 2; Puntman et al., 2021). In Chapter 3, we showed that only D207G mutant human iNeurons had severely reduced STXBP1 levels and defective DCV exocytosis. Therefore, MUNC18-1/STXBP1 levels may be rate-limiting for DCV exocytosis in both mouse and human neurons. Similarly, neurotransmission is hampered in *Munc18-1* HZ mouse and also human synapses, albeit with variable severity (Toonen et al., 2006; Patzke et al., 2015; Miyamoto et al., 2019; Chen et al., 2020). Therefore, both DCV and SV exocytosis follow the haploinsufficiency principle, suggesting that decreased STXBP1 protein levels cause STXBP1 syndrome symptoms.

Local availability of MUNC18-1 may change during neuronal activity changes (Cijsouw et al., 2014). MUNC18-1 associates with mGLUR4 subunits of presynaptic metabotropic glutamate receptors, and may dissociate upon elevated calcium (Nakajima et al., 2009; Ramos et al., 2012). Nanoclusters of MUNC18-1 and mGLUR4 have been visualized by super resolution microscopy (Siddig et al., 2020). Similarly, upon action potentials, synaptic MUNC18-1 dissociates and disperses into the axon, only to return afterwards to elevate synaptic MUNC18-1 levels (Cijsouw et al., 2014). These findings suggest regulation of MUNC18-1 availability, with small concentration differences being required for proper network regulation. Since DCV exocytosis and synaptic transmission appear sensitive to MUNC18-1 levels in both mouse and human neurons, this type of regulating MUNC18-1 availability may impact these secretion pathways during the course of neuronal activity changes. We propose that if MUNC18-1 levels are decreased, such as in STXBP1 syndrome, this regulation may be compromised, having effects on synaptic transmission, neuropeptide secretion and neuronal network activity.

6.6 Future directions

With MUNC18-1 added to the core components of the DCV exocytosis machinery, many, if not most proteins important for neuropeptide secretion have been identified. However, several fundamental questions remain unanswered. For example, why do DCVs require such an extensive trigger compared to SVs in order to secrete and why is their release probability so low? Do DCVs dock and prime during, or already prior to neuronal activity? Furthermore, does the role of MUNC18-1 in inhibiting NSF-dependent depriming of SVs also extend to DCVs? Despite all these remaining questions about the last steps of DCV exocytosis, the upstream steps required for neuropeptide secretion have remained more elusive.

Following DCVs over time

Fundamental questions about DCV biogenesis and maturation include: What upstream steps are required to generate DCVs and make them fusion-competent? We made the first steps by measuring DCV production in single neurons, and saw large inter-neuronal variability (Chapter 5). Perhaps DCV biogenesis is highly regulated, depending on neuronal activity status. Future experiments should focus on building this picture:

How many DCVs are made per time-unit and what parameters (neuron type, activity status) influence this? After that additional questions can be answered: (1) Are newly generated DCVs able to undergo exocytosis with the same probability as older DCVs? (2) Is there a time window when newly generated DCVs will be most likely to undergo exocytosis? (3) What happens to old DCVs that have not released their content? We tested SNAP-Cell with the goal to answer these questions, but the labeling was not efficient enough (Chapter 5). If the time window for DCV biogenesis and maturation is not short and strict, a genetic pulse-chase with time-locked expression of DCV markers may be sufficient to answer many of the above questions.

Finding the SM-protein that mediates lysosomal exocytosis

Since we only tested primary mouse hippocampal neurons, a role for MUNC18-2 or -3 in secretion from other neurons cannot be ruled out completely. A next step could be isolation of Munc18-2/3 expressing neurons to test if SV/DCV exocytosis in these cells also exclusively depends on MUNC18-1. Furthermore, we only tested a few secretion pathways. One recently discovered neuronal secretion pathway is lysosomal exocytosis, which modulates the extracellular matrix, synaptic plasticity and dendritic morphology (Padamsey et al., 2017; Ibata et al., 2019). Both papers showed detection of single lysosomal exocytosis events, but the exocytic machinery for lysosomal secretion remains unidentified. A future experiment could focus on finding the SM-protein responsible for lysosomal fusion, taking the first step in identifying the exocytosis machinery.

Search for compounds that may alleviate STXBP1 syndrome symptoms

While testing the effect of STXBP1 syndrome mutations on DCV exocytosis in human iNeurons, we found one mutation (D207G) that decreased DCV exocytosis compared to control. However, post hoc sequencing revealed that the control was effectively HZ for STXBP1. Therefore, it is still possible that STXBP1 HZ or S241fs mutations show an impact on DCV exocytosis compared with human iNeurons containing two wildtype STXBP1 alleles. This experiment should be repeated in the future with a bona fide WT control. Based on the mouse experiments and effect of STXBP1 expression levels, we hypothesize that STXBP1 HZ and S241fs iNeurons will have decreased DCV exocytosis compared to control. In addition, it would be interesting to verify the decreased DCV exocytosis and STXBP1 protein levels phenotype of D207G iNeurons. It has remained elusive why STXBP1 protein levels were so low in D207G mutated neurons, but perhaps it was due to a mixed culture of WT and homozygous D207G mutated iNeurons. Additional experiments including RNA sequencing and proteomics, as well as repeating the experiments in D207G mutated patient iNeurons may further pinpoint why STXBP1 protein levels are declined. Our findings suggest that neuropeptide secretion may be an important factor in the neurodevelopmental, neurological and psychiatric symptoms of STXBP1 syndrome, and opens an interesting palette of possible treatments via neuropeptide receptors, of which most are G-protein coupled receptors that could be targeted via specific agonist or antagonist drugs to alleviate lack of neuropeptide signaling. Additionally, chemical chaperones may restore specific STXBP1 syndrome phenotypes by chaperoning syntaxin 1 (Guiberson et al., 2018; Abramov et al., 2021). Therefore, both symptom relieving therapies as well as mechanism-based ones could prove useful in tackling this syndrome.

Disentangling neuropeptide and neurotransmitter secretion in STXBP1 syndrome for therapy

Due to a highly similar release machinery between SVs and DCVs, it may be difficult to disentangle the symptoms caused by hampered synaptic transmission or defective neuropeptide secretion in synaptopathies. In addition, synaptic transmission and neuropeptide secretion are intimately coupled, via the modulating effects of neuropeptides on neurotransmission, and the state of neuronal activity determining how much DCV exocytosis occurs. RAB3 QDKO mice may provide answers, since their neurons are unable to secrete neuropeptides but still have largely intact neurotransmission. Disentangling which symptoms have a basis in defective synaptic transmission and which have a neuropeptide signaling based cause, may provide useful in treating these diseases. Specific drugs are able to inhibit or promote synaptic transmission via targeting neurotransmitter receptors, while others could mimic neuropeptide action by targeting G-protein coupled receptors. Of course, fixing the genetic cause of the disease may be the best option, but if this is not possible, a balanced approach targeting neurotransmission and neuropeptide signaling may help. In addition, many neurodevelopmental, psychiatric or neurological diseases do not have a single genetic cause, highlighting the need for an integral approach to alleviate the symptoms, rather than gene therapy. Hopefully, further understanding of how the roles of neurotransmission and neuropeptide signaling are intertwined to bring about neuronal communication will bring us further towards finding these integral drug-based cures.

Future research on the role of SM-proteins in neuronal secretion

As described above, research on neuronal SM-proteins is not finished. Munc18-2, and to a lesser extend Munc18-3 RNA expression in specific mouse neurons suggests that they may perform a function in neuronal secretion. In human neurons, Munc18-3 RNA was detected, suggesting that not Munc18-2, but Munc18-3 may have an additional role next to Munc18-1 in the human brain. Several other exocytic systems could still be researched, such as lysosomal secretion. MUNC18-1 may still be the main candidate for these types of exocytosis, as it is robustly expressed in each neuron, while MUNC18-2 and -3 only in some. SM-proteins for internal membrane trafficking (Sly1, VPS33a/b and VPS45) may have key roles in DCV biogenesis. Several lines of evidence point towards a link between DCV maturation/biogenesis and the endocytic pathway, of which the latter depends on VPS33/45, while Golgi defects were seen for mutations in all these SM-genes. Future experiments using inducible knock-outs of these genes, in combination with molecular replacement of WT and mutated proteins, may reveal their role in managing the route of DCV cargo towards their secretory sites. In these studies, pHluorin based DCV cargo may provide answers about the role of these genes in managing DCV acidity and exocytosis, while any fluorescent DCV cargo in combination with labeling specific neuronal organelles will provide knowledge about whether these genes help generating DCVs and retaining their cargo up until secretion. Additionally, these experiments may lay bare the connections that the DCV biogenesis/exocytosis pathway has with other pathways, for example by removal of unwanted cargo towards the endolysosomal system. All in all, for most types of membrane fusion, the question is not whether, but which SM-protein is involved to set-up the SNARE complexes to drive the fusion reaction.

References

Abramov D, Guiberson NGL, Daab A, Na Y, Petsko GA, Sharma M, Burré J (2021) Targeted stabilization of Munc18-1 function via pharmacological chaperones. EMBO Mol Med 13:1–18.

Alarcon C, Lincoln B, Rhodes CJ (1993) The biosynthesis of the subtilisin-related proprotein convertase PC3, but not that of the PC2 convertase, is regulated by glucose in parallel to proinsulin biosynthesis in rat pancreatic islets. J Biol Chem 268:4276–4280.

Arora S, Saarloos I, Kooistra R, van de Bospoort R, Verhage M, Toonen RF (2017) SNAP-25 gene family members differentially support secretory vesicle fusion. J Cell Sci 130:1877–1889.

Ashrafi G, Wu Z, Farrell RJ, Ryan TA (2017) GLUT4 Mobilization Supports Energetic Demands of Active Synapses. Neuron 93:606-615.e3 DOI: 10.1016/J.NEURON.2016.12.020.

Augustin I, Rosenmund C, Südhof TC, Brose N (1999) Munc13-1 is essential for fusion competence of glutamatergic synaptic vesicles. Nature 400:457–461.

Balkowiec A, Katz DM (2002) Cellular mechanisms regulating activity-dependent release of native brain-derived neurotrophic factor from hippocampal neurons. J Neurosci 22:10399–10407.

Banerjee A, Lee J, Nemcova P, Liu C, Kaeser PS (2020) Synaptotagmin-1 is the Ca2+ sensor for fast striatal dopamine release. Elife 9:1–16.

Berridge MJ (1998) Neuronal Calcium Signaling Review. NeuronNeuron 21:13–26.

Bharat V, Siebrecht M, Burk K, Ahmed S, Reissner C, Kohansal-Nodehi M, Steubler V, Zweckstetter M, Ting JT, Dean C (2017) Capture of Dense Core Vesicles at Synapses by JNK-Dependent Phosphorylation of Synaptotagmin-4. Cell Rep 21:2118–2133.

Bowser R, Muller H, Govindan B, Novick P (1992) Sec8p and Sec15p are components of a plasma membrane-associated 19.5S particle that may function downstream of Sec4p to control exocytosis. J Cell Biol 118:1041–1056.

Brini M, Calì T, Ottolini D, Carafoli E (2014) Neuronal calcium signaling: Function and dysfunction. Cell Mol Life Sci 71:2787–2814.

Bulgari D, Deitcher DL, Levitan ES (2017) Loss of Huntingtin stimulates capture of retrograde dense-core vesicles to increase synaptic neuropeptide stores.

Bulgari D, Zhou C, Hewes RS, Deitcher DL, Levitan ES (2014) Vesicle capture, not delivery, scales up neuropeptide storage in neuroendocrine terminals. Proc Natl Acad Sci U S A 111:3597–3601.

Buzsáki G, Penttonen M, Nádasdy Z, Bragin A (1996) Pattern and inhibition-dependent invasion of pyramidal cell dendrites by fast spikes in the hippocampus in vivo. Proc Natl Acad Sci U S A 93:9921–9925.

Cardenas EI, Gonzalez R, Breaux K, Da Q, Gutierrez BA, Ramos MA, Cardenas RA, Burns AR, Rumbaut RE, Adachi R (2019) Munc18-2, but not Munc18-1 or Munc18-3, regulates platelet exocytosis, hemostasis, and thrombosis. J Biol Chem 294:4784–4792.

Cavolo SL, Bulgari D, Deitcher DL, Levitan ES (2016) Activity Induces Fmr1-Sensitive Synaptic Capture of Anterograde Circulating Neuropeptide Vesicles. J Neurosci 36:11781–11787.

Chen W, Cai Z-L, Chao ES, Chen H, Longley CM, Hao S, Chao H-T, Kim JH, Messier JE, Zoghbi HY, Tang J, Swann JW, Xue M (2020) Stxbp1/Munc18-1 haploinsufficiency impairs inhibition and mediates key neurological features of STXBP1 encephalopathy. Elife 9:1–33 DOI: 10.7554/eLife.48705.

Cijsouw T, Weber JP, Broeke JH, Broek JAC, Schut D, Kroon T, Saarloos I, Verhage M, Toonen RF (2014) Munc18-1 redistributes in nerve terminals in an activity- and PKC-dependent manner. J Cell Biol 204:759–775.

Clayton EL, Evans GJO, Cousin MA (2008) Bulk synaptic vesicle endocytosis is rapidly triggered during strong stimulation. J Neurosci 28:6627–6632.

Delgado-Martínez I, Nehring RB, Sørensen JB (2007) Differential abilities of SNAP-25 homologs to support neuronal function. J Neurosci 27:9380–9391.

Dhillon SS, Gingerich S, Belsham DD (2009) Regulatory Peptides Neuropeptide Y induces gonadotropin-releasing hormone gene expression directly and through conditioned medium from mHypoE-38 NPY neurons. Regul Pept 156:96–103.

Dominguez N, van Weering JRT, Borges R, Toonen RFG, Verhage M (2018) Dense-core vesicle biogenesis and exocytosis in neurons lacking chromogranins A and B. J Neurochem 144:241–254.

Emperador-Melero J, Huson V, van Weering J, Bollmann C, Fischer von Mollard G, Toonen RF, Verhage M (2018) Vti1a/b regulate synaptic vesicle and dense core vesicle secretion via protein sorting at the Golgi. Nat Commun 9 DOI: 10.1038/s41467-018-05699-z.

Emperador Melero J, Nadadhur AG, Schut D, Weering J V, Heine VM, Toonen RF, Verhage M (2017) Differential Maturation of the Two Regulated Secretory Pathways in Human iPSC-Derived Neurons. Stem Cell Reports 8:659–672 DOI: 10.1016/j.stemcr.2017.01.019.

Farina M et al. (2015) CAPS-1 promotes fusion competence of stationary dense-core vesicles in presynaptic terminals of mammalian neurons. Elife 4:393–422.

Fietz SA, Lachmann R, Brandl H, Kircher M, Samusik N, Schroder R, Lakshmanaperumal N, Henry I, Vogt J, Riehn A, Distler W, Nitsch R, Enard W, Paäbo S, Huttner WB (2012) Transcriptomes of germinal zones of human and mouse fetal neocortex suggest a role of extracellular matrix in progenitor self-renewal. Proc Natl Acad Sci U S A 109:11836–11841.

Frey L, Ziętara N, Łyszkiewicz M, Marquardt B, Mizoguchi Y, Linder MI, Liu Y, Giesert F, Wurst W, Dahlhoff M, Schneider MR, Wolf E, Somech R, Klein C (2021) Mammalian VPS45 orchestrates trafficking through the endosomal system. Blood 137:1932–1944.

Frischknecht R, Fejtova A, Viesti M, Stephan A, Sonderegger P (2008) Activity-induced synaptic capture and exocytosis of the neuronal serine protease neurotrypsin. J Neurosci 28:1568–1579.

Galmes R, ten Brink C, Oorschot V, Veenendaal T, Jonker C, van der Sluijs P, Klumperman J (2015) Vps33B is required for delivery of endocytosed cargo to lysosomes. Traffic 16:1288–1305.

Gärtner A, Staiger V (2002) Neurotrophin secretion from hippocampal neurons evoked by long-term-potentiation-inducing electrical stimulation patterns. Proc Natl Acad Sci U S A 99:6386–6391.

Geppert M, Goda Y, Hammer RE, Li C, Rosahl TW, Stevens CF, Südhof TC (1994) Synaptotagmin I: A major Ca2+ sensor for transmitter release at a central synapse. Cell 79:717–727.

Groffen AJ, Takai Y, Borst JG, Brose N (2010) Doc2b is a high-affinity Ca2+ sensor for spontaneous neurotransmitter release. Science (80-) 328:690.

Guest PC, Rhodes CJ, Hutton JC (1989) Regulation of the biosynthesis of insulin-secretory-granule proteins. Co-ordinate translational control is exerted on some, but not all, granule matrix constituents. Biochem J 257:431–437.

Guiberson NGL, Pineda A, Abramov D, Kharel P, Carnazza KE, Wragg RT, Dittman JS, Burré J (2018) Mechanism-based rescue of Munc18-1 dysfunction in varied encephalopathies by chemical chaperones. Nat Commun 9.

Gulyás-Kovács A, De Wit H, Milosevic I, Kochubey O, Toonen R, Klingauf J, Verhage M, Sørensen JB (2007) Munc18-1: Sequential interactions with the fusion machinery stimulate vesicle docking and priming. J Neurosci 27:8676–8686.

Guo W, Roth D, Walch-Solimena C, Novick P (1999) The exocyst is an effector for Sec4P, targeting secretory vesicles to sites of exocytosis. EMBO J 18:1071–1080.

Gutierrez BA, Chavez MA, Rodarte AI, Ramos M, Dominguez A, Petrova Y, Davalos AJ, Costa RM, Elizondo R, Tuvim MJ, Dickey BF, Burns AR, Heidelberger R, Adachi R (2018) Munc18-2, but not Munc18-1 or Munc18-3, controls compound and single-vesicle regulated exocytosis in mast cells. J Biol Chem:jbc.RA118.002455 DOI: 10.1074/jbc.RA118.002455.

Hammarlund M, Watanabe S, Schuske K, Jorgensen EM (2008) CAPS and syntaxin dock dense core vesicles to the plasma membrane in neurons. J Cell Biol 180:483–491.

He E, Wierda K, Van Westen R, Broeke JH, Toonen RF, Cornelisse LN, Verhage M (2017) Munc13-1 and Munc18-1 together prevent NSF-dependent de-priming of synaptic vesicles. Nat Commun 8 DOI: 10.1038/ncomms15915.

Heeroma JH, Roelandse M, Wierda K, Van Aerde KI, Toonen RFG, Hensbroek RA, Brussaard A, Matus A, Verhage M (2004) Trophic support delays but not prevent cell-intrinsic degeneration of neurons deficient for munc18-1. Eur J Neurosci 20:623–634.

Hodge RD et al. (2019) Conserved cell types with divergent features in human versus mouse cortex. Nature 573:61–68.

Hoogstraaten RI, Keimpema L Van, Toonen RF, Verhage M (2020) Tetanus insensitive VAMP2 differentially restores synaptic and dense core vesicle fusion in tetanus neurotoxin treated neurons. Sci Rep:1–14 DOI: 10.1038/s41598-020-67988-2.

Ibata K, Kono M, Narumi S, Motohashi J, Kakegawa W, Kohda K, Yuzaki M (2019) Activity-Dependent Secretion of Synaptic Organizer Cbln1 from Lysosomes in Granule Cell Axons. Neuron:1–15.

Imai A, Nashida T, Shimomura H (2004) Roles of Munc18-3 in amylase release from rat parotid acinar cells. Arch Biochem Biophys 422:175–182.

Jaramillo AM, Piccotti L, Velasco W V., Delgado ASH, Azzegagh Z, Chung F, Nazeer U, Farooq J, Brenner J, Parker-Thornburg J, Scott BL, Evans CM, Adachi R, Burns AR, Kreda SM, Tuvim MJ, Dickey BF (2019) Different Munc18 proteins mediate baseline and stimulated airway mucin secretion. JCI Insight 4.

Jockusch WJ, Speidel D, Sigler A, Sørensen JB, Varoqueaux F, Rhee JS, Brose N (2007) CAPS-1 and CAPS-2 Are Essential Synaptic Vesicle Priming Proteins. Cell 131:796–808.

Kaeser PS, Deng L, Fan M, Südhof TC (2012) RIM genes differentially contribute to organizing presynaptic release sites. Proc Natl Acad Sci U S A 109:11830–11835.

Kaeser PS, Deng L, Wang Y, Dulubova I, Liu X, Rizo J, Südhof TC (2011) RIM proteins tether Ca2+ channels to presynaptic active zones via a direct PDZ-domain interaction. Cell 144:282–295.

Kandel ER, Spencer WA (1961) Electrophysiology of Hippocampal Neurons II. After-Potentials and Repetitive Firing. Potentials 23:243–259.

Kim K, Petrova YM, Scott BL, Nigam R, Agrawal A, Evans CM, Azzegagh Z, Gomez A, Rodarte EM, Olkkonen VM, Bagirzadeh R, Piccotti L, Ren B, Yoon J, McNew JA, Adachi R, Tuvim MJ, Dickey BF (2012) Munc18b is an essential gene in mice whose expression is limiting for secretion by airway epithelial and mast cells. Biochem J 446:383–394.

Klausberger T, Márton LF, Baude A, David J, Roberts B, Magill PJ, Somogyi P (2004) Spike timing of dendrite-targeting bistratified cells during hippocampal network oscillations in vivo. Nat Neurosci 7.

Kolarow R, Brigadski T, Lessmann V (2007) Postsynaptic secretion of BDNF and NT-3 from hippocampal neurons depends on calcium-calmodulin kinase II signaling and proceeds via delayed fusion pore opening. J Neurosci 27:10350–10364.

Lam PPL, Ohno M, Dolai S, He Y, Qin T, Liang T, Zhu D, Kang Y, Liu Y, Kauppi M, Xie L, Wan WCY, Bin NR, Sugita S, Olkkonen VM, Takahashi N, Kasai H, Gaisano HY (2013) Munc18b is a major mediator of insulin exocytosis in rat pancreatic b-Cells. Diabetes 62:2416–2428.

Laufman O, Kedan A, Hong W, Lev S (2009) Direct interaction between the COG complex and the SM protein, Sly1, is required for Golgi SNARE pairing. EMBO J 28:2006–2017.

Lee Y Il, Kim YG, Pyeon HJ, Ahn JC, Logan S, Orock A, Joo KM, Lőrincz A, Deák F (2019) Dysregulation of the SNARE-binding protein Munc18-1 impairs BDNF secretion and synaptic neurotransmission: a novel interventional target to protect the aging brain. GeroScience 41:109–123.

Lo B, Li L, Gissen P, Christensen H, McKiernan PJ, Ye C, Abdelhaleem M, Hayes JA, Williams MD, Chitayat D, Kahr WHA (2005) Requirement of VPS33B, a member of the Sec1/Munc18 protein family, in megakaryocyte and platelet α-granule biogenesis. Blood 106:4159–4166.

Lobingier BT, Nickerson DP, Lo SY, Merz AJ (2014) SM proteins Sly1 and Vps33 co-assemble with Sec17 and SNARE complexes to oppose SNARE disassembly by Sec18. Elife 2014:1–22.

Lysakowski A, Figueras H, Price SD, Peng YY (1999) Dense-cored vesicles, smooth endoplasmic reticulum, and mitochondria are closely associated with non-specialized parts of plasma membrane of nerve terminals: Implications for exocytosis and calcium buffering by intraterminal organelles. J Comp Neurol 403:378–390.

Mandic SA, Skelin M, Johansson JU, Rupnik MS, Berggren P-O, Bark C (2011) Munc18-1 and Munc18-2 proteins modulate beta-cell Ca2+ sensitivity and kinetics of insulin exocytosis differently. J Biol Chem 286:28026–28040.

Martin-Verdeaux S, Pombo I, Iannascoli B, Roa M, Varin-Blank N, Rivera J, Blank U (2002) Evidence of a role for Munc18-2 and microtubules in mast cell granule exocytosis. J Cell Sci 116:325–334.

Martin SK, Carroll R, Benig M, Steiner DF (1994) Regulation by glucose of the biosynthesis of PC2, PC3 and proinsulin in (ob/ob) mouse Islets of Langerhans. FEBS Lett 356:279–282.

Matsuda N, Lu H, Fukata Y, Noritake J, Gao H, Mukherjee S, Nemoto T, Fukata M, Poo M -m. (2009) Differential Activity-Dependent Secretion of Brain-Derived Neurotrophic Factor from Axon and Dendrite. J Neurosci 29:14185–14198.

Meijer M, Rehbach K, Brunner JW, Classen JA, Lammertse HCA, van Linge LA, Schut D, Krutenko T, Hebisch M, Cornelisse LN, Sullivan PF, Peitz M, Toonen RF, Brüstle O, Verhage M (2019) A Single-Cell Model for Synaptic Transmission and Plasticity in Human iPSC-Derived Neurons. Cell Rep 27:2199-2211.e6.

Miyamoto H, Tatsukawa T, Shimohata A, Yamagata T, Suzuki T, Amano K, Mazaki E, Raveau M, Ogiwara I, Oba-Asaka A, Hensch TK, Itohara S, Sakimura K, Kobayashi K, Kobayashi K, Yamakawa K (2019) Impaired cortico-striatal excitatory transmission triggers epilepsy. Nat Commun 10:1–13.

Moro A, Woerden GMV, Toonen RF, Verhage M (2020) Camkii controls neuromodulation via neuropeptide gene expression and axonal targeting of neuropeptide vesicles. PLoS Biol 18:1–30 DOI: 10.1371/journal.pbio.3000826.

Mosa MH, Nicolle O, Maschalidi S, Sepulveda FE, Bidaud-Meynard A, Menche C, Michels BE, Michaux G, de Saint Basile G, Farin HF (2018) Dynamic formation of microvillus inclusions during enterocyte differentiation in Munc18-2 deficient intestinal organoids. Cell Mol Gastroenterol Hepatol 6:477-493.e1.

Mynlieff M (1999) Identification of different putative neuronal subtypes in cultures of the superior region of the hippocampus using electrophysiological parameters. Neuroscience 93:479–486.

Nakajima Y, Mochida S, Okawa K, Nakanishi S (2009) Ca2+-dependent release of Munc18-1 from presynaptic mGluRs in short-term facilitation. Proc Natl Acad Sci U S A 106:18385–18389.

Nogueira C, Erlmann P, Villeneuve J, Santos AJM, Martinez-Alonso E, Martínez-Menárguez JÁ, Malhotra V (2014) SLY1 and syntaxin 18 specify a distinct pathway for procollagen VII export from the endoplasmic reticulum. Elife 2014:1–22.

Oh E, Kalwat MA, Kim MJ, Verhage M, Thurmond DC (2012) Munc18-1 regulates first-phase insulin release by promoting granule docking to multiple syntaxin isoforms. J Biol Chem 287:25821–25833.

Oh E, Thurmond DC (2009) Munc18c depletion selectively impairs the sustained phase of insulin release. Diabetes 58:1165–1174.

Padamsey Z, McGuinness L, Bardo SJ, Reinhart M, Tong R, Hedegaard A, Hart ML, Emptage NJ (2017) Activity-Dependent Exocytosis of Lysosomes Regulates the Structural Plasticity of Dendritic Spines. Neuron 93:132–146.

Patzke C, Han Y, Covy J, Yi F, Maxeiner S, Wernig M, Südhof TC (2015) Analysis of conditional heterozygous STXBP1 mutations in human neurons. J Clin Invest 125:3560–3571.

Paul CC, Ackerman SJ, Mahrer S, Tolbert M, Dvorak AM, Baumann MA (1994) Cytokine induction of granule protein synthesis in an eosinophil-inducible human myeloid cell line, AML14. J Leukoc Biol 56:74–79.

Peng R, Gallwitz D (2002) Sly1 protein bound to Golgi syntaxin Sed5p allows assembly and contributes to specificity of SNARE fusion complexes. J Cell Biol 157:645–655.

Persoon CM, Hoogstraaten RI, Nassal JP, van Weering JRT, Kaeser PS, Toonen RF, Verhage M (2019) The RAB3-RIM Pathway Is Essential for the Release of Neuromodulators. Neuron 104:1065-1080.e12 DOI: 10.1016/j.neuron.2019.09.015.

Persoon CM, Moro A, Nassal JP, Farina M, Broeke JH, Arora S, Dominguez N, Weering JR, Toonen RF, Verhage M (2018) Pool size estimations for dense-core vesicles in mammalian CNS neurons. EMBO J 37:e99672 DOI: 10.15252/embj.201899672.

Puntman DC, Arora S, Farina M, Toonen RF, Verhage M (2021) Munc18-1 is essential for neuropeptide secretion in neurons . J Neurosci 41:JN-RM-3150-20.

Rahajeng J, Caplan S, Naslavsky N (2010) Common and distinct roles for the binding partners Rabenosyn-5 and Vps45 in the regulation of endocytic trafficking in mammalian cells. Exp Cell Res 316:859–874.

Ramos C, Chardonnet S, Marchand CH, Decottignies P, Ango F, Daniel H, Le Maréchal P (2012) Native presynaptic metabotropic glutamate receptor 4 (mGluR4) interacts with exocytosis proteins in rat cerebellum. J Biol Chem 287:20176–20186.

Renden R, Berwin B, Davis W, Ann K, Chin CT, Kreber R, Ganetzky B, Martin TFJ, Broadie K (2001) Drosophila CAPS is an essential gene that regulates dense-core vesicle release and synaptic vesicle fusion. Neuron 31:421–437.

Santos TC, Wierda K, Broeke JH, Toonen RF, Verhage M (2017) Early Golgi Abnormalities and Neurodegeneration upon Loss of Presynaptic Proteins Munc18-1, Syntaxin-1, or SNAP-25. J Neurosci 37:4525–4539 Available at: http://www.jneurosci.org/content/jneuro/37/17/4525.full.pdf [Accessed June 7, 2017].

Schlüter OM, Basu J, Südhof TC, Rosenmund C (2006) Rab3 superprimes synaptic vesicles for release: Implications for short-term synaptic plasticity. J Neurosci 26:1239–1246.

Schlüter OM, Schmitz F, Jahn R, Rosenmund C, Südhof TC (2004) A complete genetic analysis of neuronal Rab3 function. J Neurosci 24:6629–6637.

Schoch S, Deák F, Königstorfer A, Mozhayeva M, Sara Y, Südhof TC, Kavalali ET (2001) SNARE function analyzed in synaptobrevin/VAMP knockout mice. Science (80-) 294:1117–1122.

Shakiryanova D, Klose MK, Zhou Y, Gu T, Deitcher DL, Atwood HL, Hewes RS, Levitan ES (2007) Presynaptic ryanodine receptor-activated calmodulin kinase II increases vesicle mobility and potentiates neuropeptide release. J Neurosci 27:7799–7806.

Shakiryanova D, Tully A, Levitan ES (2006) Activity-dependent synaptic capture of transiting peptidergic vesicles. Nat Neurosci 9:896–900.

Shakiryanova D, Zettel GM, Gu T, Hewes RS, Levitan ES (2011) Synaptic neuropeptide release induced by octopamine without Ca2+ entry into the nerve terminal. Proc Natl Acad Sci U S A 108:4477–4481.

Sheng ZH, Westenbroek RE, Catterall WA (1998) Physical link and functional coupling of presynaptic calcium channels and the synaptic vesicle docking/fusion machinery. J Bioenerg Biomembr 30:335–345.

Shimojo M, Courchet J, Pieraut S, Torabi-Rander N, Sando R, Polleux F, Maximov A (2015) SNAREs Controlling Vesicular Release of BDNF and Development of Callosal Axons. Cell Rep 11:1054–1066 DOI: 10.1016/j.celrep.2015.04.032.

Siddig S, Aufmkolk S, Doose S, Jobin ML, Werner C, Sauer M, Calebiro D (2020) Super-resolution imaging reveals the nanoscale organization of metabotropic glutamate receptors at presynaptic active zones. In: Science Advances.

Sieburth D, Madison JM, Kaplan JM (2007) PKC-1 regulates secretion of neuropeptides. Nat Neurosci 10:49–57.

Steuer Costa W, Yu S chieh, Liewald JF, Gottschalk A (2017) Fast cAMP Modulation of Neurotransmission via Neuropeptide Signals and Vesicle Loading. Curr Biol 27:495–507.

Stucchi R, Plucińska G, Hummel JJA, Zahavi EE, Guerra San Juan I, Klykov O, Scheltema RA, Altelaar AFM, Hoogenraad CC (2018) Regulation of KIF1A-Driven Dense Core Vesicle Transport: Ca 2+ /CaM Controls DCV Binding and Liprin-α/TANC2 Recruits DCVs to Postsynaptic Sites. Cell Rep 24:685–700.

Tao C-L, Liu Y-T, Zhou ZH, Lau P-M, Bi G-Q (2018) Accumulation of Dense Core Vesicles in Hippocampal Synapses Following Chronic Inactivity. Front Neuroanat 12.

Tellam JT, McIntosh S, James DE (1995) Molecular identification of two novel Munc-18 isoforms expressed in non-neuronal tissues. J Biol Chem 270:5857–5863.

TerBush DR, Maurice T, Roth D, Novick P (1996) The Exocyst is a multiprotein complex required for exocytosis in Saccharomyces cerevisiae. EMBO J 15:6483–6494.

TerBush DR, Novick (1995) Sec6, Sec8, and Secl5 Are Components of a Multisubunit Complex Which Localizes to Small Bud Tips in Saccharomyces cerevisiae. J Cell Biol 130:299–312.

Toonen RFG, De Vries KJ, Zalm R, Südhof TC, Verhage M (2005) Munc18-1 stabilizes syntaxin 1, but is not essential for syntaxin 1 targeting and SNARE complex formation. J Neurochem 93:1393–1400.

Toonen RFG, Wierda K, Sons MS, de Wit H, Cornelisse LN, Brussaard A, Plomp JJ, Verhage M (2006) Munc18-1 expression levels control synapse recovery by regulating readily releasable pool size. Proc Natl Acad Sci 103:18332–18337.

Trogden KP, Zhu X, Lee JS, Wright CVE, Gu G, Kaverina I (2019) Regulation of Glucose-Dependent Golgi-Derived Microtubules by cAMP/EPAC2 Promotes Secretory Vesicle Biogenesis in Pancreatic β Cells. Curr Biol 29:2339-2350.e5.

van de Bospoort R, Farina M, Schmitz SK, de Jong A, de Wit H, Verhage M, Toonen RF (2012) Munc13 controls the location and efficiency of dense-core vesicle release in neurons. J Cell Biol 199:883–891.

van Keimpema L, Kooistra R, Toonen RF, Verhage M (2017) CAPS-1 requires its C2, PH, MHD1 and DCV domains for dense core vesicle exocytosis in mammalian CNS neurons. Sci Rep 7:10817.

Van Keimpema L, Kooistra R, Toonen RF, Verhage M (2017) CAPS-1 requires its C2, PH, MHD1 and DCV domains for dense core vesicle exocytosis in mammalian CNS neurons. Sci Rep 7.

Verhage M, Maia AS, Plomp JJ, Brussaard AB, Heeroma JH, Vermeer H, Toonen RF, Hammer RE, van den Berg TK, Missler M, Geuze HJ, Südhof TC (2000) Synaptic Assembly of the Brain in the Absence of Neurotransmitter Secretion. Science (80-) 287:864–869.

Verhage M, McMahon HT, Ghijsen WEJM, Boomsma F, Scholten G, Wiegant VM, Nicholls DG (1991) Differential release of amino acids, neuropeptides, and catecholamines from isolated nerve terminals. Neuron 6:517–524.

Washbourne P, Thompson PM, Carta M, Costa ET, Mathews JR, Lopez-Benditó G, Molnár Z, Becher MW, Valenzuela CF, Partridge LD, Wilson MC (2002) Genetic ablation of the t-SNARE SNAP-25 distinguishes mechanisms of neuroexocytosis. Nat Neurosci 5:19–26.

Watanabe S, Rost BR, Camacho-Pérez M, Davis MW, Söhl-Kielczynski B, Rosenmund C, Jorgensen EM (2013) Ultrafast endocytosis at mouse hippocampal synapses. Nature 504:242–247.

Westen R Van, Poppinga J, Díez R, Toonen RF, Verhage M (2021) Neuromodulator release in neurons requires two functionally redundant calcium sensors. PNAS 118.

Wong MY, Shakiryanova D, Levitan ES (2009) Presynaptic ryanodine receptor-CamKII signaling is required for activity-dependent capture of transiting vesicles. J Mol Neurosci 37:146–150.

Yao J, Gaffaney JD, Kwon SE, Chapman ER (2011) Doc2 is a Ca2+ sensor required for asynchronous neurotransmitter release. Cell 147:666–677.

Yao Z et al. (2020) A taxonomy of transcriptomic cell types across the isocortex and hippocampal formation Zizhen. bioRxiv.

Yin L, Zheng R, Ke W, He Q, Zhang Y, Li J, Wang B, Mi Z, Long Y sheng, Rasch MJ, Li T, Luan G, Shu Y (2018) Autapses enhance bursting and coincidence detection in neocortical pyramidal cells. Nat Commun 9:1–12 DOI: 10.1038/s41467-018-07317-4.

Zhu D, Xie L, Karimian N, Liang T, Kang Y, Huang Y-C, Gaisano HY (2015) Munc18c mediates exocytosis of pre-docked and newcomer insulin granules underlying biphasic glucose stimulated insulin secretion in human pancreatic beta-cells. Mol Metab 4:418–426.

Zimmermann J, Trimbuch T, Rosenmund C (2014) Synaptobrevin 1 mediates vesicle priming and evoked release in a subpopulation of hippocampal neurons. J Neurophysiol 112:1559–1565.

zur Stadt U, Rohr J, Seifert W, Koch F, Grieve S, Pagel J, Strauß J, Kasper B, Nürnberg G, Becker C, Maul-Pavicic A, Beutel K, Janka G, Griffiths G, Ehl S, Hennies HC (2009) Familial Hemophagocytic Lymphohistiocytosis Type 5 (FHL-5) Is Caused by Mutations in Munc18-2 and Impaired Binding to Syntaxin 11. Am J Hum Genet 85:482–492.

Addendum

Nederlandse Samenvatting

In ons brein lopen continu informatiestromen. Om onze ademhaling en hartslag te reguleren, om te bewegen, te plannen, te voelen en te denken. Om dit te kunnen regelen moet elke hersencel informatie van andere cellen ontvangen en deze zelf weer doorsturen naar andere hersencellen. Dat gebeurt door middel van signaalstoffen, die via een trucje naar buiten moeten worden gebracht. Hersencellen zijn namelijk omgeven door een vetlaagje (het *plasma membraan*), wat een fysieke en elektrische barrière vormt. Om informatie van de ene naar de andere hersencel te krijgen, worden signaalstoffen in blaasjes met een zelfde soort vetlaagje gestopt, zodat deze signaalstoffen buiten de cel komen als het blaasje fuseert met het plasma membraan (*exocytose*). Vervolgens kunnen andere hersencellen deze chemische signalen oppikken met hun receptoren. Dit gebeurt erg snel en gecontroleerd in *synapsen* (speciale contactpunten tussen twee hersencellen), waar signaalstoffen genaamd *neurotransmitters* binnen $1/50^{e}$ van een seconde een boodschap van de ene naar de andere hersencel kunnen krijgen. Door de snelheid van deze *synaptische transmissie* zijn we in staat om snel te denken en te reageren.

Daarbovenop zijn er ook andere signalen die erg belangrijk zijn voor een gezonde functie van het brein. Juist door het optimaal reguleren van de hierboven genoemde *synaptische transmissie*, is verfijning van de werking van het brein mogelijk, en worden daarbij processen als geheugen, eetlust, het circadiaanse ritme en emoties gereguleerd. Een belangrijke groep signaalstoffen die hiervoor verantwoordelijk zijn, zijn *neuropeptiden*. Dit zijn erg kleine eiwitten die veel lijken op de hormonen die op andere plekken in ons lichaam afgegeven worden. Deze *neuropeptiden* worden centraal in elke hersencel aangemaakt en in blaasjes gestopt. Om zoveel mogelijk neuropeptiden per blaasje kwijt te kunnen worden ze zo dicht op elkaar verpakt, dat binnen elk blaasje een soort kristalachtige structuur van signaalstoffen ontstaat, die onder een elektronenmicroscoop te zien is als een donkere kern (vandaar de naam: *Dense Core Vesicles,* afgekort *DCVs*). Wanneer deze *neuropeptiden* afgegeven worden door fusie van de blaasjes, kunnen ze de activiteit van meerdere zenuwcellen en *synapsen* verhogen of verlagen.

Hoewel we inmiddels goed weten welke eiwitten het proces van *neurotransmitter* afgifte aansturen, is dit minder bekend voor *neuropeptiden*. Binnen ons lab zijn we aan het uitpuzzelen welke van de eiwitten die belangrijk zijn voor *neurotransmitter* afgifte (en dus *synaptische transmissie*), dezelfde functie hebben voor de afgifte van *neuropeptiden*. Eén essentieel eiwit voor *synaptische transmissie* en voor het overleven van zenuwcellen is *SM (Sec1/MUNC18)* eiwit *MUNC18-1*. Ondanks deze belangrijke functie was tot nog toe de rol van dit eiwit in *neuropeptide* afgifte onbekend. In dit proefschrift focus ik daarom op de vraag of *MUNC18-1*, of een ander *SM eiwit*, belangrijk is voor *neuropeptide* afgifte. Daarnaast vraag ik me af of deze eiwitten eventueel andere functies hebben in het brein, en test ik mijn bevindingen in humane hersencellen. Tot slot test ik methoden die onderzoek moeten vergemakkelijken naar hoe neuropeptide blaasjes gemaakt worden in hersencellen: een proces wat we nog maar erg beperkt begrijpen.

In **hoofdstuk 1** wordt bestaande informatie herzien en beoordeeld, om zo te beschrijven hoe hersencellen met elkaar communiceren, hoe ze *neuropeptide* blaasjes (*DCVs*)

maken, welke eiwitten belangrijk zijn om deze *DCVs* met het plasma membraan te fuseren om de neuropeptiden af te geven, en worden de bekende functies van *MUNC18-1* en vergelijkbare eiwitten geïntroduceerd.

De doelstelling voor **hoofdstuk 2** is om te vinden welk *MUNC18* eiwit belangrijk is voor de afgifte van neuropeptiden door hersencellen. Hiervoor hebben we in levende hersencellen van muizen neuropeptiden aangekleurd, zodat we *DCV exocytose* live kunnen volgen. We vinden hier dat in hersencellen waarin het *Munc18-1* gen is uitgeschakeld, waardoor er geen *MUNC18-1* eiwit meer aanwezig is, er ook geen *DCV exocytose* plaatsvindt. Dit gebrek aan *neuropeptide* afgifte kan worden ''gered'' door het toevoegen van *Munc18-1* DNA in deze hersencellen, maar niet door het toevoegen van *Munc18-2* of *Munc18-3* DNA. Dat wijst erop dat *MUNC18-1* essentieel is voor *DCV exocytose* en dat *MUNC18-2* of *MUNC18-3* deze functie niet kunnen overnemen. Bovendien vinden we dat bij uitschakeling van maar één van de allelen van *Munc18-1*, wat resulteert tot een 50% reductie in *MUNC18-1* eiwit, *DCV exocytose* ook verminderd is. Dit suggereert dat in ziektes zoals het *STXBP1-syndroom* (patiënten hebben mutaties in het *STXBP1* gen, de humane versie van *Munc18-1*), waar er onvoldoende *MUNC18-1* eiwitten aanwezig zijn in hersencellen, het mogelijk is dat een defect in neuropeptide afgifte mede oorzaak kan zijn voor de symptomen.

Om hier verder op in te gaan, is de doelstelling voor **hoofdstuk 3** om de bevindingen over de rol van *MUNC18-1* in muizen hersencellen te repliceren in menselijke hersencellen. Deze cellen verkrijgen we door ze te kweken uit stamcellen afkomstig van huidbiopten. Door middel van dezelfde technieken als in hoofdstuk 2 kunnen we *neuropeptide* afgifte (*DCV exocytose*) live volgen. We bevestigen dat *STXBP1* (de humane versie van *MUNC18-1*) ook in humane hersencellen essentieel is voor *DCV exocytose*. Vervolgens creëren we mutaties in deze cellen die ook waren gevonden in patiënten met *STXBP1-syndroom*, of die één allel van STXBP1 uitschakelen, net als we in muizen hebben getest. We vinden in cellen met de mutatie D207G (wat betekent dat in het *STXBP1* eiwit op plek 207 normaal Asparaginezuur zit als aminozuur, maar door deze mutatie er een Glycine zit) een drastische verlaging in zowel de hoeveelheid STXBP1 eiwit, als de hoeveelheid *DCV exocytose* die plaatsvindt. In de andere cellen vinden we daarentegen geen duidelijke afwijkingen. Het lijkt daarom wel mogelijk dat mutaties in STXBP1-syndroom neuropeptide afgifte kunnen aantasten, maar het is duidelijk dat er meer onderzoek is nodig om dit verder te bevestigen.

In **hoofdstuk 4** hebben we getest of *SM* eiwit *MUNC18-2* een rol speelt in de afgifte van verschillende stoffen vanuit muizen hersencellen. Uitschakeling van beide *Munc18-2* allelen heeft geen effect op *DCV* exocytose of *neurotransmitter* afgifte. *MUNC18-2* is daarom niet belangrijk voor *neuropeptide* afgifte of *synaptische transmissie*, en is daarmee dus waarschijnlijk niet belangrijk voor communicatie tussen zenuwcellen. Daarnaast hebben we de *exocytose* van *GLUT4* (Glucose transporter 4) getest, omdat recent bleek dat het plaatsen van het *GLUT4* eiwit in het plasma membraan tijdens zware synaptische activiteit belangrijk is om de glucose levels en daarmee de energie lokaal op peil te houden. We laten hier zien dat *GLUT4* ook in het *plasma membraan* wordt gezet als er geen activiteit is, maar dat dit proces verhoogd wordt tijdens zware activiteit, in lijn met de eerdere bevindingen. Uitschakeling van *Munc18-2* heeft ook geen effect op het verplaatsen van GLUT4 naar het *plasma membraan*. Daarom concluderen we dat *MUNC18-2* tot nog toe geen functie in het brein heeft.

In **Hoofdstuk 5** zoeken we naar methoden om mechanismen te kunnen onderzoeken die vóór de exocytose van DCVs plaatsvinden. Het aanmaken, aanpassen en transporteren

van DCVs is zeker zo belangrijk voor neuropeptide afgifte als de laatste stap in het proces (exocytose). We hebben een techniek gebruikt die *DCVs* aankleurt door middel van een chemische stof die door membranen heen gaat. Deze techniek kleurt alleen niet genoeg *DCVs* aan om te kunnen gebruiken voor vervolgonderzoek. Via een andere techniek kunnen we de expressie van een fluorescente *neuropeptide* aanzetten, om zo de productie van *DCVs* te kunnen volgen. We vinden na een aantal tijdspunten enorme verschillen tussen muizen hersencellen in de hoeveelheid fluorescente *DCVs*, wat aangeeft dat de snelheid waarmee deze cellen *DCVs* aanmaken erg verschilt. Het lijkt erop dat deze verschillen geen technische, maar een cel-intrinsieke oorsprong hebben.

In **hoofdstuk 6** worden de resultaten van de eerdere hoofdstukken samen genomen en vergeleken met de literatuur. Zo geef ik eerst de belangrijkste conclusies uit dit proefschrift. Vervolgens bediscussieer ik hoe deze bevindingen bijdragen aan onze kennis over hoe communicatie tussen hersencellen werkt en probeer ik mijn gevonden resultaten te verklaren door middel van andere publicaties. Tot slot stel ik voor wat voor vervolgonderzoek ten opzichte van de bevindingen in dit proefschrift interessant en belangrijk kan zijn.

Acknowledgements

First of all, a big thank you to all the people I didn't mention here, who helped me in my scientific career or helped me by having fun with.

Matthijs, your ambition and expertise are inspiring! My projects were not always moving with the speed and way that we wished, but despite that, I came to learn that I could always count on you, you had my back whether I realized it or not. Furthermore I admire your eagerness to learn and to adapt your managing style and lab by seriously listening to your employees. I hope many other young scientists will have the opportunity to learn from you. **Ruud**, you're positivity itself! How many times did I come to you in dread over my projects, only to leave with hope and a smile? You have a special way with people that helped a lot of PhD's through dark days. I could always count on you to create some last-minute space in your agenda, or come-up with creative improvisations.

I would like to thank the PI's **Wiep, Niels, Jan, Sander** and **Rik** for helping to create a beautiful atmosphere in the FGA, by your enthusiasm for science, but also for very constructive feedback. Jan, your happy enthusiasm brightens everyone's day. Wiep, your sense for humor and self-assurance makes you a great person to talk to.

Margherita and **Swati**, you did a large effort for the project that I later took over. Many thanks for all that work, it helped me a lot in my progress and getting to a publication. **Enqi, Ganna and Anushka**, thank you for acquiring me some very precious data! **Annemiek**, you were of great help many times, during a few shared projects, by sharing data or protocols and by helping me or taking work out of my hands in the lab. I am proud of you how you multi-tasked between all your projects and did so much excellent science, you're an example in the lab. Thank you for all the fun conversations we had and the sharing. **Jolijn**, many thanks for your efforts during COVID times! You fueled the project with your sharp thinking, working ethics and a bit of (good) stubbornness and you delivered important data. I see a promising career lying at your feet.

Els, like for so many other PhD candidates, you've done so much for me, I could always count on you, thank you! **Rene**, I only met you shortly, but you already were a big help and you seem a great successor of Els.

To the structural and social fundaments of the lab, the technicians: Special thanks to **Desiree** and **Robbie** for always pushing to make the lab run smoother, and to somehow manage to always have solutions. Robbie, I once asked whether you had time to make something for me, while saying no, you did it anyway also promised to anyway do it. How you manage Robbie, and always with such personal flair & friendliness is a mystery to me. Desiree, thank you for all the hard work and help, and transforming into party-Desiree to have a lot of fun with at Fridays and festivals. Thank you **Joke** for running the mouse facility smoothly, for all the fun conversations, and the delicious restaurant recommendations! **Lisa**, I appreciate you for your positive attitude, hard work and talkative personality. Ingrid, I could always count on you for doing or helping with the Western Blots. **Joost**, thank you for all the hard work hidden on the 3rd floor, and for bringing a lot of good atmosphere to the many Friday drinks & festivals. **Jurjen**, I don't know how many times I came to you with questions about a microscope or a script, but

thank you for always being there to solve it!

Thanks **Maaike** for always bringing ''input'' in the office, by insisting on a Friday Techno/dancing sessions, blowing bubbles and providing cute but unsolicited items for my desk. I hope you'll keep the FGA wild for some more years. **Vincent**, I miss our discussions about the most random topics. Your ideas and arguments are as far out of the box as I could wish for and your logic makes you a great scientist. **Javier**, your passion for science is admiring. Your openness and friendliness helped getting a warm welcome in the lab and office. I always looked forward to the Mondays, with the pizza's + series at your place. **Joris**, your righteousness and intellect energized many discussions. You're a warm and chill person to be around. It was such a great weekend to visit your parents in Germany! **Matti**, you're a great buddy to have in the lab. We've shared many good times in breaks, parties and holidays, and also the bad times were better to have together. **Marta**, thank you for the good conversations and sharing. Jian, you're such a friendly person to be around! I often think of you when opening my books: I still have your Chinese bookmark!

Rhodé, it was great having you as TIM2 and coffee buddy. I much appreciated our breaks, where I found what an honest and open person you are. I'm really proud of you how you reignited your PhD career! **Alessandro**, thank you for sharing your expertise and analysis infrastructure with us, you have made a large difference to the whole group! It was fun to share our passion for climbing, although half of the sessions we did together was in a large tree in Coïmbra... **Sonia**, you're such a sweet and happy person. Being part of your wedding with **Axel** and sharing parties with the both of you was the best! I hope you guys will find your way back to the Netherlands. I'm so happy for you that you became parents & I can only imagine you doing a fantastic job. **Kevin**, keep it classy! Thank you for all the random conversations at the parties. **Claudia**, I don't know how you always appear so relaxed, take the time to explain things in a friendly patient way and manage to get so much amazing data. You deserve to get the career you want in science! **Maria**, you're such a heartwarming person. The way you make people feel welcome and how you spread your Catalan (food) culture nicely adds to your character. **Hanna**, you could always brighten my mood with your sarcastic remarks. You came far with your hard work and intellect, and I'm curious where you'll end up. I hope you will 'geniet genoeg'. A big thanks to all the other lab members: **Jorin, Jessica, Ana, Kim, Jessie, Lola, Nikki, Miriam, Andrea, Ula, Irune, Josse, Marieke, Aygul, Lill Eva, Femke, Rocio, Vera, Jovana, Aygul, Jasper, Fiona, Theresa** and **Amparo**, you contributed to a very healthy working atmosphere and good times on the side.

Rein, it's a pleasure having you as my lab- and panini-buddy since our first scientific internship! Thank you for listening to both my serious talks as well as my stupid jokes. You have an easy going nature and the curiosity & resourcefulness you show in your work is admirable.

Philip, you bring me so much depth, empathy and chillness. You're not afraid giving your opinion, but I do feel heard. Thank you for being there for me, from here to Austria and Chicago! It's been beautiful to see the growth you've shown and I'm happy I can share that ride with you. And what a fun we had in Bordeaux!

I thank the **Southpark/Rick&Corona/No jokes just despair** group for all the bad jokes. Thank you **Maurice** for your eternal support: ''Thesis schmesis''. You're great in not taking things too seriously and lightening the mood. Thank you **Flepster**, you also do things! Such as being able to mix serious talk & jokes in a chill way. **Lynn**, we know

each other better for just a short while now, but what a pleasure it has been! Please come back ;)

Arne, you're the most intuitive person I know. Thank you so much for all the support and fun you have given me in that way! You've a way of acting without filter that makes you a lot of fun to be around. ''Huize babyeend'' with you and **Lisa** is an oasis of homely chillness!

Strongrow/kern: Our friendship started with having the same purpose together: Rowing hard & making fun on the way. I'm happy that after all the rowing, surfing and squashing we're still finding new sports and activities to do together! **Joost**, when I started my PhD we still lived at the Hubert Duyfhuysstraat: a place with so many good memories! Your explorativeness and talent for doing your own thing have brought me a lot of chillness and fun times. I'm grateful for all the interesting conversations we have & I feel strong/honored knowing you always have my back. - - This is when my mind switched to Dutch - - **Gijs**, wat bewonderenswaardig hoe je samen jullie eigen bedrijf hebt opgestart en met alles maar even het wiel uitvindt! Jij bent moeilijk bij te houden, dat blijkt wel als ik probeer aan te pikken in je achterwiel. **Justus**, jij brengt jouw eigen stijl en ideëen met je mee: erg verfrissend en iets om trots op te zijn!

Lennart, Sjon, Jesse & Thijs, wat tof om al vanaf de middelbare school vrienden te zijn! We zijn het nog niet verleerd door al onze levensfasen heen en buitenlandse avonturen. Ik kijk er altijd naar uit jullie weer te zien, op naar meer!

Bram, Ellen, Tom, Tanya, Amber en **Jeroen**, jullie laten me welkom en relaxed voelen. Dat ik in februari direct met de COVID-express mee kon naar Putten geeft jullie gastvrijheid maar weer aan. Ook leuk om te merken dat er af en toe naar me geluisterd wordt!

Papa, mama, wat is het fijn om te weten dat ik altijd op jullie terug kan vallen. Jullie stralen jullie trots naar mij uit en dat geeft me veel steun. Jullie hebben me geïnspireerd om mijn interesses te volgen, wat maar even met deze PhD bekroond mag worden! **Meta**, wat fijn om zo'n meelevend, eigenzinnig en grappig zusje te hebben! We kunnen altijd heerlijk praten en lachen. **Freek**, je bent een gezellige sfeermaker met je humor en interesses, ik hoop je nog een keer te verslaan met bollen!

Lieve **Sanne**, wat maken we samen een reis door. Het betekent zo veel voor me om jou aan mijn zijde te hebben! Mijn eigen (mental/emotional/alles)-support human. Het was heel fijn om elkaar te kunnen ondersteunen tijdens onze PhD's. Ik vind het zo mooi en leerzaam om te zien hoe jij dingen aanpakt in je carrière en daarbuiten! Onze behoeftes en interesses sluiten heerlijk op elkaar aan en ik kijk enorm uit naar onze verdere avonturen!